

Practical and continuous luminance distribution measurements for lighting quality

Citation for published version (APA):

Kruisselbrink, T. W. (2020). *Practical and continuous luminance distribution measurements for lighting quality*. Technische Universiteit Eindhoven.

Document status and date:

Published: 08/10/2020

Document Version:

Publisher's PDF, also known as Version of Record (includes final page, issue and volume numbers)

Please check the document version of this publication:

- A submitted manuscript is the version of the article upon submission and before peer-review. There can be important differences between the submitted version and the official published version of record. People interested in the research are advised to contact the author for the final version of the publication, or visit the DOI to the publisher's website.
- The final author version and the galley proof are versions of the publication after peer review.
- The final published version features the final layout of the paper including the volume, issue and page numbers.

[Link to publication](#)

General rights

Copyright and moral rights for the publications made accessible in the public portal are retained by the authors and/or other copyright owners and it is a condition of accessing publications that users recognise and abide by the legal requirements associated with these rights.

- Users may download and print one copy of any publication from the public portal for the purpose of private study or research.
- You may not further distribute the material or use it for any profit-making activity or commercial gain
- You may freely distribute the URL identifying the publication in the public portal.

If the publication is distributed under the terms of Article 25fa of the Dutch Copyright Act, indicated by the "Taverne" license above, please follow below link for the End User Agreement:

www.tue.nl/taverne

Take down policy

If you believe that this document breaches copyright please contact us at:

openaccess@tue.nl

providing details and we will investigate your claim.

Practical and continuous luminance distribution measurements for lighting quality

Thijs Kruisselbrink

The work described in this thesis has been carried out at the Building Lighting group at Eindhoven University of Technology, Department of the Built Environment.

This work is part of the research program “OPTILIGHT: Mathematical Optimizations for Human Centric Lighting” with project number 14671, which is partly financed by the Netherlands Organization for Scientific Research (NWO), and which is conducted in the context of a bilateral cooperation between TU/e and Signify in the Intelligent Lighting Institute (ILI).

A catalogue record is available from the Eindhoven University of Technology library.

ISBN: 978-90-386-5080-7

©Thijs Kruisselbrink

All rights reserved. No part of this document may be reproduced, distributed, or transmitted in any form by any means, including photocopying, recording, or any other electronic or mechanical methods without permission of the author.

Practical and continuous luminance distribution measurements for lighting quality

PROEFSCHRIFT

ter verkrijging van de graad van doctor aan de Technische Universiteit Eindhoven, op gezag van de rector magnificus prof.dr.ir. F.P.T. Baaijens, voor een commissie aangewezen door het College voor Promoties, in het openbaar te verdedigen op donderdag 8 oktober 2020 om 16:00 uur

door

Thijs Willem Kruisselbrink

geboren te Winterswijk

Dit is goedgekeurd door de promotoren en de samenstelling van de promotiecommissie is als volgt:

voorzitter:	prof.dr.ir. T.A.M. Salet
1 ^e promotor:	prof.dr.-Ing A.L.P. Rosemann
2 ^e promotor:	prof.dr.ir. E.J. van Loenen
copromotor(en):	dr.ir. R. Dangol
leden:	prof. W. Osterhaus (Aarhus University) prof.dr. J.L. Scartezzini (École Polytechnique Fédérale de Lausanne)
	dr. T. Özçelebi
adviseur(s):	dr.ir. M.P.J Aarts

Het onderzoek of ontwerp dat in dit proefschrift wordt beschreven is uitgevoerd in overeenstemming met de TU/e Gedragscode Wetenschapsbeoefening.

Summary

A large portion of the Dutch working population spends a significant amount of time in the office environment. Therefore, it is essential that high quality lighting is achieved. However, lighting is often, driven by energy codes and standards, subordinate to the energy consumption, while improving lighting quality can be considered a more efficient strategy as wages represents the majority of cost associated to offices.

Lighting, in general, is a complex phenomenon because it affects users' performance, comfort, alertness, well-being and health in a subtle fashion. Moreover, the holistic concept of lighting quality is one of the least understood aspects in the lighting field and does not have an applicable and comprehensive definition. Our literature review, presented in Chapter 1, showed that lighting quality can be described by seven lighting aspects that vary during the day: quantity, distribution, glare, spectral power distribution, daylight, directionality, and the dynamics of light.

Due to its complexity, there is a trend towards using technology to provide the appropriate lighting. Currently, lighting control systems generally have a limited scope, often focused on energy reduction, and are regularly experienced as annoying. These limitations are mainly due to inadequate sensory input of the lighting control systems. Comprehensive measurements of the lit environment are required for adequate lighting control. Luminance distribution measurement devices seem a suitable tool to monitor lighting quality holistically because it is able to monitor six out of the seven variable lighting aspects in a continuous fashion. Consequently, it was hypothesized that luminance distribution measurement devices can provide adequate sensory input for lighting control systems that aim to provide high quality lighting.

However, the luminance distribution is not easily measured. Currently available luminance distribution measurement devices are costly or cannot capture the fast variations of the sky, let alone suitable for implementation in lighting control systems. Consequently, a low cost luminance distribution measurement device, suitable for integration in lighting control systems, that is able to measure the luminance distribution continuously and autonomously, was developed in Chapter 2. This camera-based system, referred to as **the Bee-Eye**, derives the luminance based on the floating point Red-Green-Blue pixel values originating from High Dynamic Range images. A relative measurement error in the range of 5% to 15% was achieved using the conventional calculation method established in previous research.

To further reduce the measurement error, we aimed to limit the spectral mismatch of the Bee-Eye by including the spectral responsivity of the camera and the spectral power distribution of the light source in the luminance calculation. Two alternative optimization models were developed and validated, in Chapter 3, based on a theoretical model and empirical data. The average measurement error of the Bee-Eye was reduced compared to the conventional method applied in Chapter 2. However, the optimization of the spectral match was limited by the fixed spectral responsivity of the camera.

Due to the relatively low spectral match, induced by the Bee-Eye's fixed spectral responsivity, the expected performance of a range of cameras was assessed in Chapter 4. This showed large variations, and improvements relative to the Bee-Eye, in spectral matches between cameras due to their different spectral responsivities. Moreover, Chapter 4 showed that the spectral power distribution of the light source affected the spectral match as well. Additionally, alternative sensitivities in the visual field of light, such as the melanopic radiance related to the non-visual effects of light, can be approximated using the spectral match optimizations.

The accuracy of the Bee-Eye was deemed adequate for practical applications, such as lighting control systems aiming to provide high quality lighting. However, this requires continuous measurements of the lit environment, which introduces multiple practical issues that need to be considered carefully. Privacy sensitive information, high computational costs and interference with office work should be prevented while continuously measuring the luminance distribution in the office environment. Three practical components were identified that deal with these issues: the spatial resolution, temporal resolution, and the measurement position of the Bee-Eye.

Chapter 5 showed that the spatial resolution of the Bee-Eye, except for glare measurements, can be reduced significantly. The proposed spatial resolution (330 x 440 pixels) limits the privacy sensitive information and computational costs, without compromising the accuracy. Moreover, Chapter 6 showed that it is not essential to measure at the highest temporal resolution, although it is largely dependent on the weather conditions. An interval of 5 minutes generally sufficed. Chapter 7 proposed to position the Bee-Eye at an alternative ceiling-based position, which does not cause interference with the office work, compared to the eye level position (best practice). This ceiling-based position was able to accurately measure surface bound luminance-based metrics using basic commissioning. More complex luminance-based metrics, for instance those mimicking the human field of view, required extensive commissioning.

The feasibility of the Bee-Eye to provide relevant sensory input, in a real office environment, for holistic lighting control was assessed in a combined lab/field study conducted in Chapter 8. This study implemented reduced

spatial and temporal resolutions while using a ceiling-based position. Two identical rooms were subject to continuous lighting quality measurements. One room, the benchmark, was monitored according to the state-of-the-art, while the other room was monitored analogous to a real office environment. The results, measured in the real office environment, showed that not all relevant luminance-based metrics were able to match the benchmark. Distinct systematic errors were introduced due to the alternative, but realistic, measurement setup in the real office environment. Additionally, random errors were introduced due to the presence of a user in the real office environment.

Moreover, to communicate the sensory input measured with the Bee-Eye, integration with actual lighting control systems is required. In Chapter 9, the feasibility of luminance-based lighting control systems was assessed using two alternative systems based on the digital addressable lighting interface. The two lighting control systems were able to control the lighting adequately, using the sensory input of the Bee-Eye. The visual performance was supported and energy reductions were achieved. Nevertheless, The results also showed, analogous to existing lighting control systems utilizing basic photo sensors, that accurate commissioning is essential. However, the spatially resolved sensory input of the Bee-Eye, has a more versatile character allowing alternative and additional types of sensing.

Concluding, the luminance distribution is an excellent means to measure lighting quality but application in real office environments is not straightforward. Nevertheless, it is feasible to monitor the majority of relevant lighting quality aspects with sufficient agreement, to be used as sensory input for lighting control systems. However, for some luminance-based metrics significant errors are introduced, even with careful considerations of the prerequisites. Hence, the first steps towards a lighting control system that provides high quality lighting are made, although the journey is not completed yet. To achieve reliable sensory input, for all relevant lighting quality aspects, further accommodations are required.

Samenvatting

Gemiddeld spendeert de werkende Nederlander een aanzienlijk deel van zijn tijd in het kantoor. Daarom is het van belang dat kantoren beschikken over hoogwaardige verlichting. Echter de kwaliteit van de verlichting is vaak ondergeschikt aan het energie verbruik, dat wordt gestimuleerd door, onder andere, de wetgeving. Terwijl het verbeteren van de verlichtingskwaliteit, en dus de productiviteit, beschouwd kan worden als een efficiëntere strategie omdat de salarissen, over het algemeen, verre weg de meeste kosten met zich mee brengen.

Licht is een complex fenomeen dat, op een subtiele manier, de prestatie, comfort, oplettendheid, welzijn en gezondheid van de mens kan beïnvloeden. Daarnaast is het concept ‘verlichtingskwaliteit’ nog niet volledig doorgrond, het heeft bijvoorbeeld geen toepasbare en alomvattende definitie. Gebaseerd op de literatuur in Hoofdstuk 1, hebben wij gekozen om verlichtingskwaliteit te beschrijven aan de hand van zeven variabele aspecten die relevant zijn voor dit concept. Het gaat hierbij om de aspecten: hoeveelheid van het licht, de verdeling van het licht, de verblinding door het licht, de spectrale compositie van het licht, daglicht, de richting van het licht, en de dynamiek van het licht.

Vanwege deze complexiteit, is er een trend ontstaan om technologie toe te passen om de ruitme op gepaste wijze te verlichten. De bestaande aansturingssystemen hebben echter significante beperkingen doordat deze veelal gefocust zijn op energie besparing, met als gevolg dat deze systemen regelmatig als oncomfortabel worden ervaren. Deze beperkingen worden vaak veroorzaakt door gebrekkige informatie, verworven door de sensoren, die het systeem moeten aansturen. Uitvoerige metingen van de verlichte omgeving zijn noodzakelijk om de benodigde informatie voor de aansturingssystemen te verwerven. Een luminantie camera lijkt een bruikbare oplossing te bieden om de verlichtingskwaliteit te meten, immers zes van de zeven licht aspecten, die zojuist geïntroduceerd zijn, zijn continu meetbaar gebruikmakend van de luminantie verdeling die deze camera's meten. Daarom wordt verwacht dat een luminantie camera de benodigde informatie kan verwerven voor deze complexe aansturingssystemen.

Echter, de technologie achter deze luminantie camera's is niet eenvoudig. Momenteel zijn de beschikbare luminantie camera's kostbaar en niet in staat om de snelle variaties van daglicht te meten. En ze zijn al helemaal niet geschikt voor implementatie in aansturingssystemen. Daarom hebben wij een autonoom camera systeem ontwikkeld in Hoofdstuk 2, gebruikmakend van goedkope componenten, om de luminantie verdeling te meten, dat boven-

dien ook geschikt is voor implementatie in aansturingssystemen. Dit camera systeem, ook wel **de Bee-Eye** genoemd, berekend de luminantie verdeling gebaseerd op de Rood-Groen-Blauw pixel waardes van een High Dynamic Range (NL: Hoog Dynamisch Bereik) afbeelding. Een relatieve meetfout van 5% tot 15% was bereikt, gebruikmakend van de conventionele rekenmethode zoals toegepast in de bestaande literatuur.

Om de meetfout van de Bee-Eye te beperken, hebben wij geprobeerd om de spectrale overeenkomst van de Bee-Eye, met de gevoeligheid van het menselijk oog, te verbeteren. Een alternatieve methode om de luminantie te bepalen was geïntroduceerd gebruikmakende van de camera' spectrale gevoeligheid en van de spectrale compositie van het licht. In Hoofdstuk 3, twee alternatieve modellen waren toegepast, gevalideerd door theoretische modellen en empirische data, om de spectrale overeenkomst te verbeteren. De gemiddelde meetfout van de Bee-Eye was enigszins beperkt ten opzichte van de conventionele methode toegepast in Hoofdstuk 2. Echter de afname van de meetfout wordt gelimiteerd door de specifieke spectrale gevoeligheid van de camera.

Vanwege de relatief lage spectrale overeenkomst, als gevolg van de specifieke spectrale gevoeligheid van de Bee-Eye, was de verwachte prestatie van een aantal alternatieve camera's gemodelleerd in Hoofdstuk 4. Dit resulteerde in grote verschillen, en verbeteringen ten opzichte van de Bee-Eye, in de spectrale overeenkomst omdat de spectrale gevoeligheden van de verschillende camera's afwijkend zijn. Daarnaast kunnen deze modellen gebruikt worden om andere gevoeligheden in zichtbare deel van het spectrum te kwantificeren, zoals de melanopische straling relevant voor de non-visuele effecten van licht.

De nauwkeurigheid van de Bee-Eye wordt voldoende geacht voor praktische applicaties zoals complexe aansturingssystemen die een hoge verlichtingskwaliteit leveren. Echter, de verlichte omgeving moet hiervoor continue gemonitord worden wat een aantal praktische dilemma's met zich mee brengt die zorgvuldig overwogen moeten worden. Privacy gevoelige data, een hoge benodigde reken capaciteit en belemmeringen van kantoor werkzaamheden moeten voorkomen worden tijdens deze continue metingen van de luminantie verdeling. In dit onderzoek, drie praktische componenten waren geïdentificeerd gerelateerd aan deze praktische problemen, namelijk: de resolutie van de High Dynamic Range afbeelding, het meetinterval en de meetpositie van de Bee-Eye.

Hoofdstuk 5 bewees dat de resolutie van de High Dynamic Range afbeeldingen, behalve voor metingen van de verblindingsfactor, beperkt kan worden. De voorgestelde resolutie (330 x 440 pixels) beperkt de privacy gevoelige data en de reken capaciteit zonder te moeten in te leveren op de nauwkeurigheid. Daarnaast toonde Hoofdstuk 6 aan dat het niet noodzakelijk is om te metingen op het hoogste interval te verrichten om relevante resultaten

te verkrijgen. Over het algemeen was een meetinterval van 5 minuten voldoende. Echter, het weer is hierbij in grote lijnen maatgevend. In Hoofdstuk 7 wordt geopperd om de luminantie verdeling te meten vanaf een alternatieve positie, aan het plafond, in plaats van een positie identiek aan het zichtveld van de gebruiker, zodat geen belemmering van de kantoor werkzaamheden veroorzaakt wordt. De alternatieve positie aan het plafond was in staat om relevante oppervlakte gebonden luminantie parameters nauwkeurig te meten met enkel basale inbedrijfstelling. Voor meer complexe parameters was een uitgebreide inbedrijfstelling benodigd.

Om de haalbaarheid van de Bee-Eye als informatievoorziening van een holistische licht aansturingssysteem in een echte kantoor omgeving te testen was een gecombineerde laboratorium/veld studie uitgevoerd in Hoofdstuk 8. In deze studie was een beperkte resolutie en interval toegepast terwijl metingen werden verricht vanaf het plafond. Twee identieke ruimtes werden continue gemonitord door twee Bee-Eye's. De eerste ruimte, die fungeerde als een benchmark, werd gemonitord volgens een best-practice protocol vergelijkbaar met een laboratorium, terwijl de tweede ruimte gemonitord werd zoals in een werkelijke kantoor omgeving. De meetresultaten, verzameld in de kantoor omgeving, suggereerde dat niet alle relevant luminantie parameters overeen kwamen met die van de benchmark. Systematische afwijkingen werden geïntroduceerd door de alternatieve meetopstelling. Daarnaast, werden ook willekeurige afwijkingen geïntroduceerd door de aanwezigheid van een gebruiker.

Om de informatie, verkregen met de Bee-Eye, te communiceren, is integratie met het aansturingssysteem vereist. In Hoofdstuk 9 was de haalbaarheid van een luminantie-gebaseerd aansturingssysteem onderzocht, gebruikmakend van twee alternatieve systemen gebaseerd op de digitale adresseerbare licht interface (DALI). De twee systemen waren in staat het licht adequaat te besturen, gebaseerd op de informatie verworven door de Bee-Eye. Zowel visuele ondersteuning als energie besparingen werden behaald. Daarnaast toonde de resultaten aan dat nauwkeurige inbedrijfsstelling essentieel is, zoals dit ook essentieel is voor huidige aansturingssystemen. Daar komt wel bij dat de Bee-Eye, vergeleken met een standaard lichtsensor, een veelzijdig karakter heeft waardoor meerdere extra metingen, zoals aanwezigheidsdetectie, verricht kunnen worden.

Concluderend, het meten van de luminantie verdeling is een uitermate geschikte methode om het concept verlichtingskwaliteit te duiden. Echter, het toepassen van luminantie camera's, zoals de Bee-Eye, is niet eenvoudig in de praktijk. Het is mogelijk om de meerderheid van relevante licht aspecten met voldoende nauwkeurigheid te meten zodat deze gebruikt kunnen worden als informatievoorziening voor aansturingssystemen. Echter, een aantal aspecten waren niet nauwkeurig meetbaar, zelfs met een grondige overweg-

ing van de randvoorwaarden. Desalniettemin, de eerste stappen naar complexe licht aansturingssystemen, die een hoge verlichtingskwaliteit leveren, zijn gezet, maar deze zoektocht is nog niet voltooid. Bijvoorbeeld, om een betrouwbaar systeem te ontwikkelen, zijn additionele maatregelen benodigd die de huidige beperkingen limiteren.

Contents

1	Introduction	1
1.1	Light in the office environment.....	2
1.2	Controlling the light.....	2
1.3	Lighting quality.....	3
1.4	Direct measurement of lighting quality.....	4
1.5	Indirect measurement of lighting quality.....	6
1.6	A monitoring device for lighting quality.....	18
1.7	Thesis outline.....	19
I	Measuring the luminance distribution	23
2	The Bee-Eye: a practical device to measure the luminance distribution	25
2.1	Introduction.....	26
2.2	Methods and results.....	26
2.3	Discussion.....	39
2.4	Conclusion.....	41
3	Spectral tuning of luminance cameras	43
3.1	Introduction.....	44
3.2	Theoretical model.....	45
3.3	Methodology.....	48
3.4	Results.....	52
3.5	Discussion.....	58
3.6	Conclusion.....	62
4	HDR for luminance and melanopic radiance: cameras and SPDs	63
4.1	Introduction.....	64
4.2	Methodology.....	64
4.3	Results.....	66
4.4	Discussion.....	71
4.5	Conclusion.....	74
II	Recommendations for continuous measurements of the luminance distribution	75
5	The spatial resolution	77
5.1	Introduction.....	78
5.2	Methodology.....	79
5.3	Results.....	86
5.4	Discussion.....	95
5.5	Conclusion.....	99
6	The temporal resolution	101
6.1	Introduction.....	102

Contents

6.2	Methodology.....	103
6.3	Results.....	106
6.4	Discussion.....	111
6.5	Conclusion.....	113
7	Ceiling-based luminance distribution measurements	115
7.1	Introduction.....	116
7.2	Pilot.....	117
7.3	Experimental setup.....	120
7.4	Phase 1.....	125
7.5	Phase 2.....	128
7.6	Discussion.....	134
7.7	Conclusion.....	137
III	Application of the luminance distribution	139
8	Field study	141
8.1	Introduction.....	142
8.2	Methodology.....	142
8.3	Results.....	150
8.4	Discussion.....	156
8.5	Conclusion.....	159
9	Luminance-based lighting control	161
9.1	Introduction.....	162
9.2	Method.....	163
9.3	Results.....	166
9.4	Discussion.....	171
9.5	Conclusion.....	174
10	General discussion	177
10.1	Introduction.....	178
10.2	Key findings.....	178
10.3	Strengths and weaknesses.....	183
10.4	Tips & tricks for luminance-based lighting control.....	188
10.5	Applications.....	191
10.6	Recommendations for future work.....	194
10.7	Conclusion.....	195
	References	197
	Curriculum Vitae	219
	List of Publications	221
	Acknowledgements	223
	Bouwstenen	225

Nomenclature

Abbreviations

ALDI	Ambient Light Directionality Indicator
BE	Bee-Eye
CCT	Correlated Color Temperature
CI	Confidence Interval
CIE	International Commission on Illumination
D65	CIE Standard Daylight Illuminant
DALI	Digital Addressable Lighting Interface
DFT	Discrete Fourier Transform
DGP	Daylight Glare Probability
DSLR	Digital Single Lens Reflex
DWT	Discrete Wavelet Transform
EV	Exposure Value
EXIF	Exchangeable Image File Format
FOV	Field of View
FSI	Full Spectrum Index
HDR	High Dynamic Range
IES	Illuminating Engineering Society
IF	Image Forming
JND	Just Notable Difference
KNMI	Dutch National Meteorological Institute
MAPE	Mean Absolute Percentage Error
NIF	Non-Image Forming

NMRSE Normalized Root Mean Square Error

RGB Red-Green-Blue

SPD Spectral Power Distribution

sRGB Standard Red-Green-Blue color space

SSH Secure Shell

XYZ CIE XYZ color space

Symbols

a Azimuth angle, Significance level

$\bar{y}(\lambda)$ Color matching function Y

$\Delta L_{h,m}$ Daylight variability

ΔTWE Time weighted average outside target illuminance

δ_L Relative difference in luminance

E Elevation angle

E_i Polar angle

∇L_{max} Maximum luminance gradient

Ω Solid angle

φ Relative SPD

ρ Reflectance factor, Precision component ρ_c

ρ_c Lin's Concordance Correlation Coefficient

σ Standard deviation

θ Spatial response of eye

c Focal length

$C(\lambda)$ Circadian sensitivity curve

C_b Accuracy component ρ_c

$D(n)$	Dimming level	n	Sample Size
DR	Daylight Ratio	$N_{r,g,b}$	Normalization factor for equal energy
E	Illuminance	p	P-value
$e(n)$	Control error	$p(n)$	Control input
E_{ret}	Retinal Illuminance	r	Pearson's r
f	reciprocal of the relative aperture	R^2	Coefficient of Determination
f_1^t	General $V(\lambda)$ Mismatch Index	r_i	Image radius
k	Photometric calibration factor	s_{rel}^*	Normalized Relative Spectral Responsivity of Camera
K_i	Integral gain	s_{rel}	Relative Spectral Responsivity of Camera
K_p	Controller gain	t	Shutter speed
L	Luminance	U_o	Uniformity
L_v/L_s	Vector to Scalar Ratio	$V(\lambda)$	Sensitivity curve of the human eye for photopic vision
M	Mask representing field of view	Z	Z-score
m	Margin of error		
N	Aperture		

CHAPTER 1

Introduction

This Chapter is based on:

Kruisselbrink TW, Dangol R, Rosemann ALP. Photometric measurements of lighting quality: An overview. Building and Environment. 2018 138; 42–52. <https://doi.org/10.1016/j.buildenv.2018.04.028>

1.1 Light in the office environment

As humans we spend approximately 90% of our time indoors, providing us shelter from the outside elements. For 25% of the Dutch working population a large portion of this time is spent in the office environment [1]. Consequently, it is essential that the office environment, besides shelter, provides us a healthy and comfortable environment. The thermal, indoor air, noise and lighting quality are the Indoor Environmental Quality (IEQ) aspects that are widely recognized, for instance by the WELL building standard [2], in order to achieve a healthy and comfortable indoor environment.

Lighting quality, which relates to electrical light, daylight and a combination of those, is an IEQ aspect that deserves more attention. Especially, compared to thermal and noise quality the lighting quality is too often neglected. When considered, lighting quality is often subordinate to the energy use, often driven by energy codes and standards.

Lighting is often seized as a way to limit costs associated with energy use. However, with wages (49% of operational costs [3]) representing the majority of costs associated to office buildings, enhancing the user comfort and performance by improving the lighting quality, can be considered a more efficient strategy [4, 5]. Moreover, it is a more ethical approach. Limiting the energy use can even be counter-effective as this can cause significant discomfort [6], resulting in a reduced productivity.

Lighting can actively improve the performance and comfort of the office worker when the lighting is tailored to his task and preference. In addition, lighting can also affect alertness, well-being, health and sleep quality in a positive way [7, 8]. This illustrates that lighting is not a simple and straightforward phenomenon as it affects many issues via different pathways. Moreover, light is subject to interpersonal differences [9], timing [10] and social dynamics [11]. An additional complication is that the outcomes are generally subtle, but can have detrimental effects. Due to this complexity, there is a trend towards using technology to provide applicable lighting, often referred to as ‘Human Centric Lighting’, which aims to provide high quality lighting in an energy efficient fashion.

1.2 Controlling the light

To optimize the lighting within the office environment, control systems are generally required. Lighting control systems manage and regulate devices such as lamps, luminaires and shading apparatus’, using control loops to apply and maintain the desired lit environment in an automated fashion. Automated control is generally required because the applicable lighting depends on variable aspects such as daylight, time, and occupancy. An increasing number of lighting control systems, either with an open- or closed-loop topology, have been developed to deal with this complex problem ranging from occupancy-based control systems, to daylight-linked control systems, personal-controlled systems and institutional-controlled systems [12]. These control systems have particular characteristics and levels of complexity [13]. The most commonly used control systems aim to limit the energy consumption by daylight harvesting [14], tuning the electrical light according to the daylight contribution to properly illuminate a space, or occupancy-based sensing [15], dimming or switching

1.3. Lighting quality

the electrical lighting based on the occupancy level. Such systems, merely focusing on energy reductions, might result in uncomfortable environments. In addition, control systems are available that aim to improve the visual comfort, visual performance [16], and possibly well-being and health if the non-image forming effects of light are considered as well [17]. The non-image forming effects or NIF effects are associated to the melanopsin-containing intrinsically photosensitive retinal ganglion cells (ipRGCs), having an alternative spectral sensitivity, in addition to the rods and cones [18]. However, these intricate lighting control systems are often still in their infancy. Limitations of the currently existing control systems are that they generally focus on one or two specific lighting aspects, while multiple other lighting aspects are affected as well because all luminous conditions are interrelated [6]. For instance, optimizing one single aspect can negatively influence other aspects, potentially decreasing the lighting quality, which is illustrated in Figure 1.1.

Therefore, these control systems do not necessarily provide optimal comfort and high visual performance [13]. Moreover, there are multiple examples that these systems are sabotaged by users because they are experienced as annoying [19, 20], which is often caused by faulty sensors [21]. As a result, the control system might manage and regulate the lighting based on faulty information, which is often exhibited in bad timing of, for instance, activation of the sun shading.

To successfully optimize the lighting within an office environment, a holistic approach of lighting quality is required, which should prevent counter-effective measures. The related research is part of an interdisciplinary research effort that aims to develop such a control system that is able to optimize the lit environment, called ‘OptiLight’ [22]. ‘OptiLight’ aims to develop a system that performs a mathematical optimization for ‘Human Centric Lighting’. In order to perform this mathematical optimization, comprehensive and relevant information on the lit environment is required to make an informed decision that provides human centric lighting without any hindrance. This thesis aims to quantify the lit environment in office environments, to provide holistic information for this lighting control system.

1.3 Lighting quality

Lighting quality, which is a term related to the image forming effects of light, is one of the least understood aspects in the building lighting field [23]. There is no consensus on what lighting quality exactly consists of as it is a very wide and ambiguous concept [24]. Originally, it was “a term used to describe all of the factors in a lighting installation not directly connected with the quantity of illumination” (Stein et al. cited in [25]). However, in the course of time a number of alternative definitions have been proposed, such as “good-quality lighting is lighting that allows you to see what you need to see quickly and easily and does not cause visual discomfort but raises the human spirit” [8]. These definitions explain the holistic concept of lighting quality but they do not clarify how lighting quality can be assessed or measured. In a first step, consensus should be achieved on an objective methodology to monitor lighting quality. This will also enable future studies to relate photometric measurements of lighting quality to subjective responses [26]. Subsequently, the monitored lighting quality can serve as input for lighting control system. Additionally, recommendations can be developed, based on an improved understanding of lighting quality, that can

be implemented in requirements and/or standards. Ultimately, this can culminate to lighting control systems that provide high quality lighting such as aimed for in 'OptiLight' that are accepted, and not sabotaged, by the user.

The following sections provide an overview, based on the state-of-the-art, how lighting quality can be measured objectively. This information is utilized to develop a strategy to provide holistic input on lighting quality to an automated lighting control system, such as being developed in the 'OptiLight' project. Therefore, direct and indirect objective measurements of lighting quality are explored, indicating the components the lit environment that need to be measured for a holistic approach. Direct measures use one single outcome value to describe the overall lighting quality. Indirect measurements use multiple outcome values to describe lighting quality because lighting quality can be considered a construct [23], which is an intangible entity described by (multiple) tangible components.

1.4 Direct measurement of lighting quality

Several attempts have been made to develop single indicator models to assess and quantify lighting quality [8, 23], including the Visibility Level Model, Lighting Quality Index, the Comfort, Satisfaction and Performance index, Interior Lighting Evaluation System, and the Ergonomic Lighting Indicator, as found in our structured literature review [27].

1.4.1 Visibility Level (VL) Model

The Visibility Level Model, measuring the effectiveness of the visual performance, was originally developed by Blackwell but adopted and improved by the CIE [23, 28]. In this model, visibility is “associated with the perception of objects and visual details of interest” [28]. The model considers quantity as well as quality of lighting. The author stated [28] that the visual performance approach should consist of photometric aspects, physiological aspects and mental conditions of the observer. The visibility level is described by four aspects: reference visibility level (VL_{ref}), contrast rendering factor (CRF), disability glare factor (DGF) and transient adaptation factor (TAF). However, the DGF and TAF are not easily measured outside the laboratory [23, 28].

1.4.2 Lighting Quality Index (LQI)

As an alternative for the visibility level model, Herst and Ngai suggested the Lighting Quality Index. The LQI is based on a combination of the equivalent sphere illuminance (ESI) and the visual comfort probability (VCP). The LQI is described as the percentage of the space meeting the criteria, set by the designer, for both ESI and VCP. The ESI relates to “the level of sphere illumination which would produce task visibility equivalent to that produced by a specific lighting environment”(cited in [23]) while the VCP relates to discomfort glare. However, this method was not widely accepted due to the inherent ESI system [23].

1.4.3 Comfort, Satisfaction and Performance (CSP) index

Similar to the VL and LQI, the Comfort, Satisfaction and Performance index has some limitations in applicability, considering that the maximum correlation between the CSP index and subjective response was only 0.54 [29]. Additionally, a replication of the CSP index by Perry et al. [30] found even lower correlations. The CSP is “an attempt to produce an indicator for the effectiveness of a lighting installation, as perceived by the workers who use it” [29], assuming that there are three visual quality elements that determine the effectiveness: the comfort, satisfaction, and performance level. The CSP describes comfort as a linear equation including the British glare index [31]. Satisfaction was described as the ratio between cylindrical and horizontal illuminance and performance was described as a combination of the illuminance, uniformity and color rendering. Each element was weighted similarly with a maximum score of 10 [29].

1.4.4 Interior Lighting Evaluation System (ILES)

In contrast to the previous models, the Interior Lighting Evaluation System [32] uses a multifaceted concept to assess lighting quality, directly as well as indirectly, based on measurements and surveys. In addition to photometric parameters, it also includes economic parameters and human behavior. The direct photometric component uses a cost function to calculate a quality value number, which evaluates a selection of important photometric aspects. The cost function consists of a weighing factor, indicating the importance of the parameter, and a scaling factor representing the effective value of the parameter compared to the recommended or optimal value of the parameter. The weighing factors, which are variable depending on the specific case, are based on surveys or polls [32, 33]. Additionally, ILES consists of a subjective component indirectly assessing the lighting quality. As this must be easy to administer and understand for uninformed users, a survey was designed containing 11 questions that were rated on a two or five point scale.

1.4.5 Ergonomic Lighting Indicator (ELI)

Analogous to ILES, the Ergonomic Lighting Indicator is based on a combination of objective and subjective components [34]. ELI uses five criteria important for the assessment of lighting quality: visual performance, view, visual comfort, vitality and control; all rated on a scale of 1 to 5. According to the author, this method is especially useful for communication during lighting design. ELI is based on input gathered by a questionnaire with 38 questions having an objective or subjective character. It was shown that ELI has an objectiveness level of 70%; therefore, it can be almost considered objective [35]. Nevertheless, large scale field tests are required to confirm the performance of this index [35].

1.5 Indirect measurement of lighting quality

As indicated in Section 1.4, direct measurements of lighting quality have significant limitations, preventing application in real office environments and lighting control systems. Therefore, the indirect measurement of light quality offers a suitable alternative.

1.5.1 Lighting quality aspects

A list of 11 lighting quality aspects was aggregated as displayed in Table 1.1, based on 30 studies that were found to be eligible based on a structured literature review using backward and forward citation starting from two key publications by Veitch and Newsham [23] and Gentile et al. [36]. For the full methodology we refer to the original publication [27]. The lighting quality aspects are ranked based on the relative fraction of studies that incorporate these specific aspects.

Table 1.1: Lighting quality aspects based on literature, indicating their components, their occurrence in literature (%), and their variability.

Aspect	Components	%	Variable
Quantity of light	Illuminance; Luminance	100%	Yes
Distribution of light	Uniformity; Luminance distribution	90%	Yes
Glare	Disability glare; Discomfort glare; Veiling reflections	77%	Yes
SPD ¹ of light	Appearance; Color quality	58%	Yes
Daylight	Daylight penetration; View out	45%	Yes
Luminaire characteristics	Luminous intensity distribution; Flicker	42%	No
Directionality of light	Direction; Modelling	39%	Yes
Control	Automatic control; Individual control	29%	No
Dynamics of light	Variability; Rhythm	19%	Yes
Room characteristics	Objects; Reflectances	19%	No
Economics	Energy efficiency; Investment	16%	Partly

¹ Spectral Power Distribution

Table 1.1 shows a large variation in occurrences between different lighting quality aspects. Quantity of light is considered in each study while economics were only considered in five studies, indicating a potentially lower relevance. Consequently, quantity of light, distribution of light and glare are expected to be the most relevant lighting quality aspects because they occur significantly more often than the remaining lighting quality aspects. However, this does not indicate that the remaining aspects are irrelevant.

In this thesis, the variable aspects of lighting quality, as indicated in Table 1.1, are emphasized. They represent lighting quality aspects that have a variable character throughout the day, for instance, due to daylight variability or user interaction. The variable aspects of the lit environment, in contrast to the static aspects, are relevant for lighting control applications since they can be optimized in real-time. Static lighting quality aspects, generally, cannot be optimized in real-time. As an example, it is not feasible to alternate the wall reflectance, in an automated fashion, while it can be a major contributor to the perceived lighting quality.

1.5. Indirect measurement of lighting quality

It is expected that photometric quantities of the different variable lighting quality aspects are mutually related as indicated in Figure 1.1. Figure 1.1 shows that all aspects impact or are impacted by at least one other lighting quality aspect. For instance, a change in daylight will impact the quantity of light, which subsequently might also impact the distribution of light, while there is also a direct relation between daylight and the distribution of light. Due to these mutual relations, it might not be necessary to measure each individual lighting quality aspect.

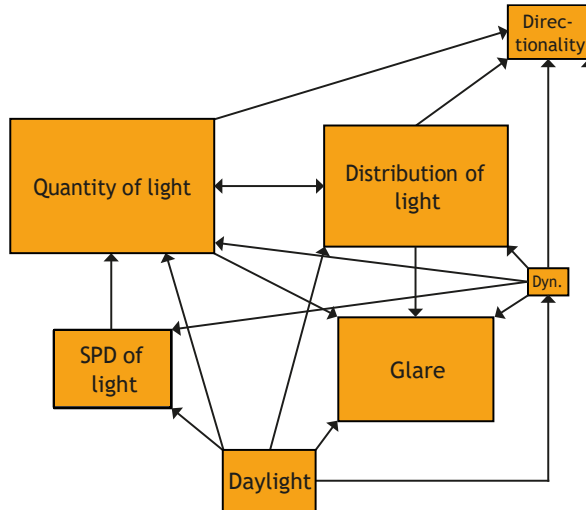


Figure 1.1: Expected relationships between photometric quantities representing variable lighting quality aspects. The block size represents the occurrence in literature as indicated in Table 1.1. The arrow direction indicates the direction of the dependency. The dynamics of light is abbreviated to Dyn.

The variable aspects of the lit environment that are to be quantified are further analysed in the following sections to explore how to measure these specific lighting aspects. A distinction is made between *ad hoc* and continuous measurements. *Ad hoc* measurements are “snapshots” of the lit environment measured with a high accuracy, typically achieved by using state-of-the-art devices and optimal measurement positions that approximate laboratory conditions. For these measurements, it is feasible to achieve a high accuracy because for one individual measurement it is usually acceptable to disturb occupants or to clear the specific space.

As opposed to *ad hoc* measurements, it is not acceptable to disturb occupants or clear a space for continuous measurements of the lit environment. Moreover, the measurement conductors cannot be present during the entire measurement period. Therefore, measurement devices are fixed, mostly at a sub-optimal position to limit interference; furthermore, as the conductors are not present state-of-the-art measurement devices cannot be used, as a safety measure. As a result, continuous measurements generally have a lower accuracy, it is not feasible to approximate laboratory conditions. Continuous measurements of lighting quality are highly relevant for lighting control systems because these systems have to respond to various dynamic behaviors. Moreover, they provide a good overview of lighting quality over time, which is essential for insight in components of the lit environment, such as

preferred luminous conditions, that are known to be variable. Consequently, continuous measurements are essential for the integration in control systems, which require continuous input on the lit environment, that aim to provide high quality lighting.

1.5.2 Quantity of light

Quantity of light is a photometric aspect that was considered in all eligible studies regarding lighting quality aspects; it indicates the amount of artificial light or daylight that falls on the surfaces of a space. The quantity of light is, to a large extent but not exclusively, responsible for the acceptability of the lighting for the visual task [37]. Generally, the satisfaction and performance increases with an increasing amount of light. As the amount of light increases, to a certain limit, the lighting becomes “more pleasant, more comfortable, clearer, more stimulating, brighter, more colorful, more natural, more friendly, more warm and more uniform. It also becomes less hazy, less oppressive, less dim and less hostile” [38]. However, for very high quantities, satisfaction decreases while the performance remains constant [36]. It is an important aspect of lighting quality because the light flux influences the satisfaction as well as the visual performance.

Photometric variables for quantity of light are the illuminance and luminance [37]. In addition to the illuminance and luminance, the daylight factor is frequently used to describe the amount of daylight (Section 1.5.6), which represents the ratio between indoor and outdoor horizontal illuminance for overcast sky conditions [39].

Illuminance

The illuminance, the areal density of the luminous flux, is measured by calibrated illuminance meters. The horizontal illuminance is only an adequate criterion for working environments where the working plane is actually horizontal [40]; especially in the current working practice with extensive use of computers, this is generally not applicable anymore. Therefore, the working plane illuminance is generally used, whether this is horizontal, vertical or tilted [8]. The working plane illuminance is the most widely used indicator for lighting quantity because it is easily measured. Moreover, recommendations and standards almost exclusively use the illuminance.

During *ad hoc* measurements, the illuminance is measured for one point at the time; therefore, a measurement grid is often established to cover the overall lighting of the space [41]. The European standard [42] provides guidelines for an appropriate grid approximating squares. Moreover, alignment of the measurement grid with the luminaire layout is to be prevented. Additionally, a zone of 0.5 m from the wall is excluded. In a simplified method, the illuminance is solely measured for relevant task positions [36].

A measurement grid, according to the previously stated guidelines, is not feasible for continuous measurements. For continuous measurements, the space should be divided into daylit zones. Daylit zones are established based on the distance from the window and the activity associated to the zone. In each zone one measurement point is placed at a location that is critical or represents the typical illuminance of that zone. In offices, each workstation should have at least one measurement point at the working plane level [43].

Luminance

The luminance is the only photometric variable that is directly related to the light flux reaching the retina and therefore most closely related to the human visual perception of brightness [44, 45]. The luminance is increasingly recognized as an important factor for visual comfort [44]. It is, therefore, advised to use the luminance to assess the amount or quantity of light. However, interpretation is complex; thus studies examining the luminance or recommendations are scarce [36, 45]. Previously, the luminance was measured by a (spot) luminance meter. However, with the current High Dynamic Range (HDR) technology [46], it is feasible to obtain luminance mapping based on images. This measurement methodology is further elaborated in Chapter 2. The luminance emphasizes the light reaching the viewer's eyes from a seating position [47]. Consequently, it is measured from the height of the viewer's eyes, and for completeness for potentially extreme situations [36]. Measuring the luminance for *ad hoc* or continuous measurements is further elaborated in Section 1.5.3.

1.5.3 Distribution of light

Twenty-eight of the eligible studies considered the distribution of the light, indicating how and to what extent the light is distributed within the space, which influences the visual comfort. The human eye can adapt to large variations of pupilar illuminance, but it cannot simultaneously manage large luminous contrasts. A poor distribution of light may result in visual stress and fatigue due to the continuous eye movements between contrasting surfaces. Alternatively, it is not desirable to have a completely uniform light distribution, which can result in dull lighting that is unpleasant and can lead to tiredness and lack of attention. It is, therefore, important to have some variations to provide a stimulating environment [44]. Generally, a poorer distribution is accepted when daylight enters from the side. Variables representing lighting distribution are the illuminance uniformity and the luminance distribution.

Uniformity

The uniformity is the ratio between the minimum and average illuminance on a surface [42], based on the illuminance measurement elaborated in Section 1.5.2. There are also examples that use the ratio between the minimum and the maximum illuminance to determine the uniformity. The uniformity is an indicator that is frequently used because it is easily determined based on illuminance measurements. Moreover, the luminance uniformity, analogous to the illuminance uniformity, can be determined [48], for instance, to indicate the uniformity of a wall.

Luminance distribution

The luminance distribution is the spatially resolved pattern of luminance in a space bounded by surfaces [47] and is often simplified to luminance ratios. The luminance distribution is measured using HDR cameras (i.e. luminance distribution measurement devices) [49], which is further elaborated in Chapter 2. Fisheye lenses are used to capture the entire luminance distribution of a room as experienced from the camera position; therefore, it is advisable to measure from the viewers' eye position. Theoretically, the luminance distribution can also be measured by a (spot) luminance meter,

but this is an imprecise and tedious process subject to major and rapid changes in the luminous conditions.

For *ad hoc* measurements, the luminance distribution is measured from the seating position at a height of 1.2 m, representing the view from the user's eye. As potential users in the room are not constantly looking at the same direction, some extreme situations need to be measured as well [36].

Continuous measurements of the luminance distribution are problematic because the respective space is occupied by the users. Two strategies can be distinguished to measure the luminance distribution while a space is occupied. For lab studies, two identical rooms located directly besides each other can be used [50, 51]. In the first room, the participant is seated; in the second room, the appropriate measurement devices are set-up according to best practice. This strategy is not feasible for field studies; consequently, the measurement devices need to be placed at a sub-optimal position during field studies, which should not cause user interference. Preferably, the monitoring device is placed at a position as close as possible to the optimal position.

1.5.4 Glare

The third lighting quality aspect is glare. Glare is defined as “the sensation produced by luminance within the visual field that is sufficiently greater than the luminance to which the eyes are adapted to cause annoyance, discomfort or loss in visual performance and visibility” [52]. Three types of glare are defined: (i) disability glare or physiological glare, (ii) discomfort glare or psychological glare, and (iii) veiling reflections [53, 54, 55]. Disability glare and discomfort glare can occur simultaneously but are distinctively different phenomena [56].

Disability glare

Disability glare, although rarely occurring in buildings [57], is stray light in the eye that disrupts vision due to intraocular light scatter [25, 55]. It immediately reduces the visual performance and even the ability to see [54]. Disability glare can be painful, although it does not necessarily induce discomfort [58].

Discomfort glare

Discomfort glare causes mental stress and annoyance due to high luminance contrasts or unsuitable luminance distributions within the visual field, without necessarily reducing visual performance or visibility [56]. Compared to disability glare, it is relatively difficult to identify as it is a visual sensation, which cannot be measured directly, with a subjective character [57]. Thereby, there is no complete theoretical understanding of discomfort glare [59, 60]. Discomfort glare does not necessarily influence the visual performance immediately, but over time negative effects such as headaches, fatigue and decreased concentration can occur [61].

A number of glare indices have been developed describing the subjective magnitude of discomfort glare [51]; nevertheless, a practical and effective discomfort glare predictor, with a high correlation to the subjective response, is still lacking [56, 62]. Generally, these indices consist of the following four quantities: luminance of the

1.5. Indirect measurement of lighting quality

glare source, solid angle of the glare source, displacement of the glare source relative to the line of sight, and the adaptation luminance [51].

Among the many glare indices, the Unified Glare Rating (UGR) [63], Daylight Glare index (DGI) [64], and Daylight Glare Probability (DGP) [56, 65] are most commonly used. The different indices cannot be simply compared to each other [59]. Glare indices that are developed for electrical lighting (e.g. UGR) are not suitable for daylight and vice versa because daylight openings have a significant larger solid angle. Moreover, users seem to accept discomfort glare from daylight to a higher extent [55]. Merits and demerits of these indices are displayed in Table 1.2.

Table 1.2: Merits and demerits of the commonly used glare indices.

Indices	Applications	Merits	Demerits
UGR	Electric	Simple. Composed based on best parts previous formulae. Established method.	Only standard light sources.
DGI	Daylight	Suitable for daylight; however, the interpretation is slightly different. Similar to UGR	Low correlation. Only suitable for uniform light sources. Based on electrical light measurements. Does not include adaptation.
DGP	Daylight	High correlation. Including observer variability. Based on daylight measurements.	Only valid for DGPs between 0.2 and 0.8.

Simulations or measurements are required to assess glare using the previous stated indices. Previously, measurements were conducted using spot luminance meters, a time consuming process which is problematic due to the dynamic character of daylight [56]. During the measurement procedure most quantities are measured, but the displacement of the glare source relative to the line of sight is consistently based on position indices as proposed by Luckiesh and Guth [66] and Iwata and Tokura [67]. A limitation is that all glare indices are based on well-defined sources. When the scene or luminaire becomes complex, it is ubiquitous which areas represent the light source and the background. Some rules to clarify this have been developed, but they lack validation [59].

In contrast to the tedious spot measurements, the required data can also be generated quickly using HDR cameras [49], similarly to the methodology described in Section 1.5.3. Wienold and Christoffersen [65] used this technology to develop the DGP under actual daylight conditions. They also developed the pre-processing tool *evalglare* for RADIANCE to estimate the DGP and the other commonly used glare metrics, based on luminance distribution measurements or simulations [65, 68].

Veiling reflections

Veiling reflections are “specular reflections that appear on the object viewed and that partially or wholly obscure the details by reducing contrast” [58]. As a result, veiling reflections reduce the visibility and may cause discomfort [69].

The contrast rendering factor (CRF), the ratio of the relative visibility under actual conditions to the relative visibility under reference conditions, is used to indicate veiling reflections. The reference condition is a completely diffuse field with an identical task background luminance. Theoretically, the CRF is measured using a visibility meter. However, even under laboratory conditions it is subject to considerable problems [69]. The CRF can also be estimated using a luminance meter [47], but this is a tedious process. Consequently, the CRF is rarely used in field measurements.

1.5.5 Spectral Power Distribution of light

The Spectral Power Distribution (SPD or $\varphi_{e,\lambda}$), a quality aspect considered by 58% of the eligible studies, represents “the radiant power emitted by a light source at each wavelength or band of wavelengths in the visible region of the electromagnetic spectrum” [70]; the light source can be daylight, a lamp, a reflecting surface or a combination of these. The SPD indicates which color components are represented within the emitted light flux; therefore, it influences the color appearance and the color quality of the light. Theoretically, the SPD can also be used to assess photometric quantities, but dedicated metrics (e.g. illuminance) and devices (e.g. illuminance meter) that do not lose any significant information are available. It should be noted that the SPD is also very important regarding the NIF effects of light [18]; however, this is outside the scope of this thesis.

The SPD of daylight is preferred as it covers the full spectrum of visible radiation [71]; hence, it displays a great variety of colors, helps to distinguish slight shades of colors and makes colors look natural [72]. The SPD is a complex multidimensional metric of which the effects are not completely understood and that is not easily communicable. Therefore, the effects of the SPD are in this chapter separated in two concepts: color appearance and color quality. Using this simplification, it is easier to describe the resulting effects of the SPD.

Color appearance

The color appearance relates to the apparent color of the emitted light, independent of the context [42], caused by available wavelengths within the visual spectrum, representing the attributes brightness, hue and colorfulness [73]. The visual effects of color appearance can be controversial, but there is some consensus that the color appearance does influence the comfort level [74, 75, 76, 77]. However, the preferred color appearance is completely dependent on the activity. Some studies concluded that the color appearance influences the room appearance [76, 78], while others did not find this effect [38]. Finally, it is suggested that the color appearance also influences the perceived brightness [38, 77, 79, 80, 81].

The color appearance of the light source is generally indicated by the correlated color temperature (CCT or T_{cp}), which is the temperature of a black body radiator having a chromaticity associated with the chromaticity of the SPD of the light source [58]. It should be noted that different SPDs with different appearances can result in identical CCTs (metamerism), due to information loss by translating the multidimensional SPD to the one dimensional CCT.

Preferably, the CCT is based on spectral measurements. It is best measured using a spectroradiometer focused at a white Lambertian reflector such as Spectralon

1.5. Indirect measurement of lighting quality

or barium sulphate (BaSO_4). The Lambertian reflector is placed horizontally, perpendicular to an electric light source, at the measurement location and is measured from a 45° angle [74]. Based on the chromaticity coordinates extracted from the SPD, the CCT can be calculated using methods developed by several scientists ranging from simple equations to complex algorithms [82, 83, 84, 85, 86]. Alternatively, devices (e.g. Chroma meters) are available that directly measure the chromaticity coordinates using three sensors sensitive to the $\bar{x}(\lambda)$, $\bar{y}(\lambda)$, and $\bar{z}(\lambda)$ color matching functions, respectively [87], originating from the CIE XYZ color space. However, the accuracy is expected to be lower as spectral response errors (f_1^t , see Chapter 3) are introduced. Finally, alternative low-accuracy methods to estimate the CCT, for instance using digital cameras [88], are available. In general, it is advised to perform the measurement of the CCT in the middle and for key positions of the considered space [89].

Light color quality

The concept of light color quality consists of different dimensions that influence the color perception of the observer in an environment. Six dimensions are identified: color fidelity, color discrimination, visual clarity (brightness), color preference, color harmony and color acceptability [90]. The color fidelity, or rendering, is the effect of the light (source) “on the color appearance of objects by conscious or subconscious comparison with their color appearance under a reference illuminant” [58]. Color discrimination is the ability to distinguish between colors [91]. Visual clarity relates to the feeling of contrast [90]. Color preference and color harmony are both aesthetic judgements for the individual objects and relationship between objects [90], respectively. Finally, the color acceptability relates to making a judgement about the whole environment [90]. Appropriate light color quality helps to improve the visual performance, comfort and well-being [42].

Table 1.3 displays a selection of commonly used color quality metrics indicating the dimensions covered by the latter. The Color Rendering Index is most widely used and the only internationally accepted metric for color quality [91]. However, except for the Color Quality Scale all metrics consider only a limited number of dimensions. It is, therefore, advised to always use a minimum of two metrics [72, 74, 92]. A metric for color acceptability is not available as the mathematical modelling of the color acceptability is unsolved [90]. For an extensive review of all metrics, we refer to the work by Houser et al. [93]. In all cases the metrics are based on the SPD; it is, therefore, recommended to measure SPD similarly as described for CCT measurements. Based on the measured SPD and data on the reference illuminants and color samples, the metrics can be calculated according to the equations provided in the references of Table 1.3.

1.5.6 Daylight

The fifth rated lighting quality aspect is daylight; two components are distinguished: daylight penetration and view out, relating to daylight entering the room and the quality of the view through the daylight openings, respectively.

Humans evolved under daylight conditions; therefore, access to daylight generally improves satisfaction, and it “is more desirable for the psychological dimensions of

Table 1.3: Commonly used light color quality indices and their references in relation to the six color quality dimensions.

	Abbreviation	Symbo	Color Fidelity	Color Discrimination	Visual Clarity	Color Preference	Color Harmony	Color Acceptability	Reference
General Color Rendering Index	CRI	R_a	X						[94]
Flattery Index	-	-				X			[95]
Color Preference Index	CPI	-				X			[96]
Color Discrimination Index	CDI	G		X					[97]
Color Rendering Capacity	CRC	-	X						[98]
Pointer's Index	PI	R_p	X						[99]
Color Quality Scale	CQS	Q_a	X	X	X	X			[91]
Feeling of Contrast Index	FCI	-			X				[100]
Memory Colour Rendering Index	MCRI	S_a	X			X			[101]
Color Harmony Rendering Index	-	R_{hr}					X		[102]

visual comfort, environmental appearance and amenity” [103]. Additionally, all previously mentioned aspects (i.e. quantity, distribution, glare and SPD) are influenced by daylight, which was already indicated in Figure 1.1, as the light within the office environment is generally composed of daylight and electrical light. Moreover, both can be controlled independently. However, as daylight is not always available, lighting quality should also be achieved without daylight. Moreover, excessive daylight can lead to discomfort. Often daylight penetration is a given, depending on the fixed window openings, weather and time. However, there are possibilities to optimize daylight penetration on the run. An increasing number of buildings are applied with dynamic sun shading (sun screens), brightness control (blinds) and/or smart glazing integrated in the façade. Sun shading and smart glazing can be used to block direct solar radiation, prevent glare and/or overheating. Often, these kinds of systems are fixed, but dynamic systems that follow the trajectory of the sun are available as well. Additionally, brightness control generally has a dynamic character as blinds are easily adjusted, manually or automatically, permitting optimizations. Hence, daylight penetration can be optimized by a control system.

Daylight Penetration

Daylight penetration is often expressed using the daylight factor or useful daylight illuminances (UDI) [104]. “The daylight factor is the ratio of internal illuminance related to the external illuminance of an overcast sky” [39]. The daylight factor is measured using a similar grid as described in Section 1.5.2, and it can be measured in situ, in scale models and using simulations. The UDI is developed to account for the limitations of the daylight factor introducing varying conditions, and it is represented as a relative fraction of the time in which daylight illuminances are within a useful range. The UDI is determined using simulations adopting the previously defined

1.5. Indirect measurement of lighting quality

measurement grid. In addition to these particular indicators, daylight can also be described with the previously mentioned aspects and their accompanying indicators (e.g. luminance).

Outside view

A high quality outside view and visual contact with the outdoor can impact the work performance and job satisfaction and can even result in improved general health [42]. Moreover, it has been mentioned that the outside view might be essential to have beneficial effects of daylight [105]. View outside is bipartite: it is influenced by the size of the window opening, and the quality of the view, which has a subjective character. A high quality view generally consists of natural aspects rather than aspects of the built environment [106]; additionally, a view with a high information content is often rated as a high quality view [107]. The quality of view is largely dependent on the given location. However, the outside view can be obstructed by the previously mentioned sun shading, brightness control and smart glazing. Hence, the quality of the view can be deteriorated drastically; therefore, it should, preferably, be considered in lighting quality control systems.

The window size is often indicated relative to the external wall area [108]. These indicators do not incorporate the different seating positions of different users; the users all experience the window size differently depending on their location. We suggest to use the solid angle assessed from the seating position, as this incorporates the view direction. Even though the quality of the outside view is largely subjective, Hellinga and Hordijk developed a method to assess the subjective view quality [109]. They developed an assessment method for quality of view, which correlated adequately with extensive quality of view surveys, but further validation is still required.

1.5.7 Directionality of light

The directionality of light is a lighting quality aspect that is accounted for in twelve of the thirty eligible studies. The directionality of a light scene can be described by the flow of light. The concept of light flow consists of two aspects: the direction of the light flow and the strength of the light flow. The strength of the light flow, also called modelling, can also be defined as the balance between diffuse and directional components of the lit environment [110].

Adequate directionality helps to distinguish details of a task, surface textures and three dimensional objects including faces [36, 110]. As a result, it influences communication, the appearance and the appreciation of an environment [111]. Moreover, the directionality of light can influence health and well-being due to a non-homogeneous distribution of the non-image forming cells in the eye, inferior-nasal retinal areas are shown to have a more effective stimulation of NIF effects [112]. The directionality of light can cause three distinct patterns on objects: the illumination pattern, the shadow pattern and the highlight pattern [111].

Direction and modelling

Theoretically, the directionality of a point within a room is determined based on an infinitesimal sphere that is met by an infinite number of luminance rays from all directions [113, 114]; consequently, these rays can be described as three dimensional bound vectors. The vectorial sum represents a vector with the illuminance as magnitude, “hence the terms vectorial illuminance or illumination vector” [114]. The magnitude of the illumination vector is described by the ratio between the “maximum difference across diameters of an infinitesimally small sphere at that point” [115]. The direction of the illumination vector is the altitude angle between the maximum and minimum luminance ray [111, 114]. The strength of the light flow is described by relating the magnitude of the illumination vector to the total amount of incident light on this infinitesimal sphere [111], also called scalar illumination [115].

Practically, it is not feasible to measure this theoretical concept, and simplifications are required to assess the directionality. Indicators for the direction of light are limited to the direction of the illumination vector. For the strength of the light flow, or modelling, several indicators are developed as listed in Table 1.4. The vector to scalar ratio is used most commonly, representing the relation between the approximated illumination vector and the approximated scalar illumination.

Table 1.4: Indicators to determine the strength of the light flow (or modelling).

Indicator	Reference
Vector to Scalar Ratio	Cuttle [111]
Cylindrical to Horizontal Illuminance Ratio	Hewitt et al. [116]
Vector to Cylindrical Illuminance Ratio	Bean [117]
Vector to Horizontal Illuminance Ratio	Love and Navvab [118]
Flow of Light Ratio	Cuttle [119]
Illuminance Contrast Energy (ICE)	Morgenstern et al. [120]
Side Forward Ratio	Veitch et al. [121]
Light Factor to Density of Light Ratio	Xia et al. [122]

Traditionally, these indicators are determined based on cubic illumination or similar technologies. Methods to measure the cubic illumination range from using a single photocell to successively measure the illuminance on the six faces of a theoretical cube to using a six-cell cubic photometer adopting a measurement grid analogous to the horizontal illuminance [119]. Subsequently, the scalar, cylindrical, horizontal and vertical illuminance are extracted by summing the relevant sensor pairs [119]. The first method is tedious and complicated while the six-cell cubic photometer is vulnerable towards calibration errors [123]. The cubic photometer is sensitive to orientation, because only six faces are available; therefore, a maximum variance of 33% can occur in the scalar illumination. For office lighting this is typically no concern [114], as most offices are designed in the three perpendicular directions.

Recently, methods have been developed to assess the directionality based on HDR imaging. Dubois et al. propose a method using a Lambertian white sphere and a HDR camera to determine the vector to scalar ratio for one selected point within a space [89]. The white sphere, divided in 24 evenly distributed sections, is monitored by two HDR cameras, each at one side of the sphere. Based on the 24 luminances or illuminances, the illumination vector and scalar are calculated according to the cubic

1.5. Indirect measurement of lighting quality

illumination method [36, 89]. Disadvantages are that two cameras are required; it is suggested to use one camera and successively measure both sides while using a grey reference surface to calibrate these measurements [89].

The method proposed by Howlett et al. [124] was able to indicate directionality, while also measuring other indices, using a single HDR camera. The authors developed the Ambient Light Directionality Indicator (ALDI), which consists of a white square-based pyramid and a reflective gnomon. The directionality is measured based on the ratio between the average luminance of two faces of the pyramid, depending on being sidelit or toplit. The gnomon provides visual evidence on the direction of the light flow and indicates whether light was coming from a diffuse source or a point source [124, 125]. A disadvantage is that the directionality is only measured in a two-dimensional plane.

All methods described, except the one proposed by Howlett et al. [124], are only used as *ad hoc* measurements, only encapsulating one single moment. The Ambient Light Directionality Indicator (ALDI) has previously been used to measure the directionality at an hourly interval, and to indicate the temporal variation of the directionality.

1.5.8 Dynamics of light

The final lighting quality aspect considered in this thesis are the dynamics of light. The dynamics of light consist of the variability of light and the rhythm of light, indicating the amount of change and the character of change, respectively, in the luminous environment over time. Dynamic lighting leads to an improved quality of visual performance, it is considered more stimulating, more pleasant, and leads to higher levels of arousal [7, 53, 126]. The dynamics of light in a lit environment are caused by daylight or by electric lighting with dynamic output. Theoretically, all previously mentioned aspects can have a dynamic character, but generally, only illuminance, luminance and the correlated color temperature are considered in dynamic lighting.

Variability and rhythm

Rockcastle and Andersen [127] developed a metric to describe the annual variation in luminance for daylight. This method derives the variability based on luminance mapping and accounts for the cumulative difference in pixels as they vary over time. Results are represented in a cumulative annual luminance variability map, similar to a luminance picture, and a temporal luminance variability map. The annual variability is the “average difference between adjacent hourly and monthly instances”. This metric is able to indicate the degree of change in luminance during a year, location of this change (annual cumulative map) and the rhythm of change (temporal map). Depending on the interest, this method could be alternated to indicate dynamics over a shorter period of time or to indicate dynamics of alternative lighting quality aspects. To indicate the dynamics of light, multiple measurements are needed. Depending on the indicator of interest, the appropriate measurements are conducted as described in the previous sections.

1.6 A monitoring device for lighting quality

Various single indicator models are available that aim to describe lighting quality directly. However, all models have significant limitations such as measurement difficulties, low correlations with the subjective responses and limited validation; as a result none of these models is widely used. Therefore, it is suggested to consider lighting quality a construct, which can be quantified based on eleven lighting quality aspects representing: quantity of light, distribution of light, glare, SPD of light, daylight, luminaire characteristics, directionality of light, control, dynamics of light, room characteristics, and economics (Table 1.1).

In this thesis, the focus lies on control applications. Consequently, static parameters such as the luminaire characteristics are avoided as they do not (significantly) vary over time. According to Section 1.5, six out of seven variable lighting quality aspects, indicated in Figure 1.2, can be measured with a luminance distribution measurement device (i.e. a luminance camera, HDR camera), daylight can also be described by the other lighting quality aspects. Moreover, the luminance distribution, representing the distribution of light, is directly related to the majority of lighting quality aspects (Figure 1.1). A luminance distribution measuring device cannot manage to measure the SPD, although algorithms exist that are able to estimate the CCT based on image data. However, more than an estimation is not possible as cameras are generally limited to three different channels representing red, green, and blue, while accurate measurements of the SPD require a multitude of channels, preferably for each individual wavelength. Moreover, the luminance distribution is not directly related to the SPD. However, this does not imply that the SPD has no significance for lighting quality. It is actually an essential component. For instance, the Kruithof rule [128] states that the CCT impacts the preferred task illuminance while the task illuminance impacts the preferred CCT. Additionally, some lighting quality aspects (directionality and dynamics) are seldom measured using the luminance distribution and are therefore not mature (yet).

Concluding, the luminance distribution can be seen as a suitable means to quantify lighting quality because the luminance distribution enables us to extract multiple relevant lighting quality aspects simultaneously and continuously providing a reasonable overview of the overall lighting quality. The expected main contributors to overall lighting quality: quantity of light, distribution of light and glare are all measured with luminance distribution measurement devices. However, it also misses out on the highly relevant SPD and the associated variables, which are, in general, rather difficult to measure. Nevertheless, alternative solutions to monitor relevant lighting quality aspects generally have an even lower applicability, as only a limited number of aspects can be extracted. For instance, an illuminance sensor is only able to extract one single illuminance value at a specific location within a room.

In addition to assessing lighting quality, multiple applications in the building realm, which can benefit from luminance distribution measurements such as lighting control and simulation can be distinguished.

Nowadays, more and more buildings are applied with smart lighting systems and automated daylight systems like automated Venetian blinds and dynamic solar shading. Relevant and actual luminance distributions can increase the performance of these systems because both the influence of the neighboring environment and the fast variations of the sky can be included in the input [129], potentially resulting in

1.7. Thesis outline

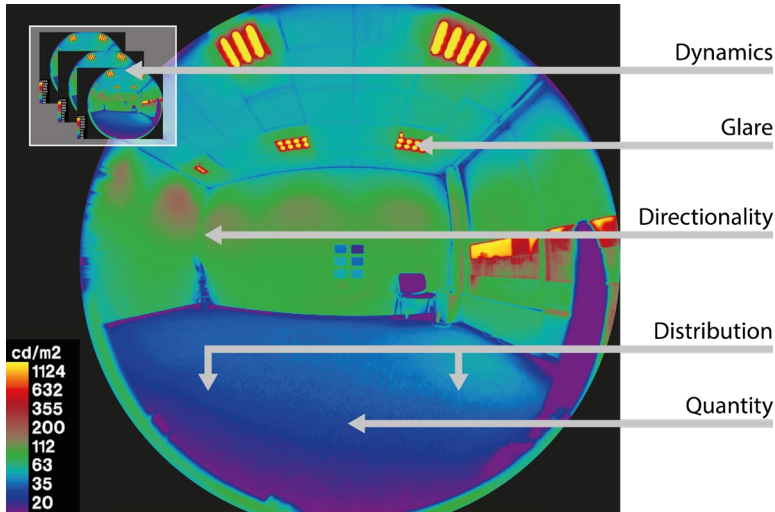


Figure 1.2: Lighting quality aspects measured with the luminance distribution, daylight is quantified based on the other lighting quality aspects.

optimized user comfort and energy performance.

Moreover, lighting simulation is an efficient way for designing comfortable and sustainable lighting conditions in the built environment. However, the reliability of the simulation depends, among others, on the quality of the a priori model data. An important aspect of daylight simulations is the sky luminance distribution. The International Commission on Illumination (CIE) developed 15 generic sky models representing sky luminance distributions for conditions varying from overcast to cloudless skies [130], which are very suitable for comparing design decisions under different sky conditions. However, these models do not represent the actual luminance distribution of the sky for any location and are not sensitive to transient luminance variations in different sections of the hemisphere [131]. Due to their generic character these models create uncertainties in the lighting simulations, which can be prevented by using actual and relevant measured luminance distributions.

1.7 Thesis outline

This chapter showed that the luminance distribution, represented as a luminance map of a room, is a suitable means to quantify and monitor lighting quality. Six out of seven relevant variable lighting quality features can be monitored using a luminance distribution measurement device. Consequently, it is hypothesized that the luminance distribution is a suitable strategy to provide relevant input for lighting control systems such as being developed in the ‘OptiLight’ project [132], which this thesis is part of.

However, implementation of the luminance distribution in lighting control systems involves numerous challenges. In a lighting control perspective, luminance distribution measurements need to be continuous, ubiquitous, and therefore, low cost;

it should also provide a reasonable accuracy and should not cause interference with office activities. However, luminance distribution measurement devices tend to be costly and their operation and calibration is complex. In addition, literature relating to continuous measurements of the luminance distribution is scarce while it introduces various practical issues relating to interference, privacy and computational costs that might obstruct further application in real office environments [133]. Therefore, the objective of this study is to validate the hypothesis that the luminance distribution is able to provide relevant input for lighting control systems in real living office environments. Resulting in the following research questions:

- **How well is lighting quality quantified in real living office environments using the luminance distribution to serve as input for lighting control applications?**
 - How is the luminance distribution measured using a camera-based system with an accuracy appropriate for lighting control applications?
 - How is the luminance distribution measured in a living office environment without causing interference, privacy issues and high computational costs?

The thesis consist of three parts as illustrated in Figure 1.3. The first part, **measuring the luminance distribution**, consisting of Chapters 2 to 4, relates to the first sub-research question. This part describes how the luminance distribution is measured autonomously and continuously using High Dynamic Range imaging using low cost components while maintaining an accuracy deemed suitable for practical applications. To further enhance the accuracy, the novel concept of spectral tuning was applied as an alternative to the conventional luminance calculation method. The aim of spectral tuning was to limit the spectral mismatch without additional hardware components

In addition, for actual implementation in lighting control systems a number of practical issues occur. Lighting control systems require continuous input on lighting quality; consequently, the luminance distribution needs to be monitored continuously, which might result in interference, privacy issues and high computational costs. Three practical aspects, which do not have sufficient scientific justification yet, were identified that relate to these issues: the spatial resolution, the temporal resolution and the measurement position of the luminance distribution measurement device. Therefore, **recommendations for continuous luminance distribution measurements**, relating to the second sub-research question, are proposed in Part II. These recommendations aim to preserve the accuracy while reducing the spatial (Chapter 5) and temporal resolution (Chapter 6) to limit privacy issues and high computational costs. In addition, an alternative measurement position (Chapter 7), for luminance distribution measurements, was proposed to prevent interference without compromising the relevancy.

Ultimately, implementation and integration in lighting control systems, such as the one being developed in 'OptiLight', was pursued to answer the main research question and assess the hypothesis. Implementation requires long-term luminance

1.7. Thesis outline

distribution measurements in living environments with a low cost and practical luminance distribution measurement device, to monitor lighting quality continuously without privacy intrusion, high computational cost and interference of office workers. Moreover, integration with existing lighting control systems should be achieved to allow the luminance distribution to provide relevant input. Implementation and integration of luminance distribution measurements was subject to Part III, **application of the luminance distribution**, which consists of Chapter 8 and 9.



Figure 1.3: Structure of Thesis: (I) Measuring the Luminance Distribution, (II) Recommendations for Continuous Luminance Distribution Measurements, and (III) Application of the Luminance Distribution.

Part I

Measuring the luminance distribution

Chapter 2 describes the development of a practical and autonomous luminance distribution measurement device based on a low cost single-board computer. The luminance distribution was determined by capturing High Dynamic Range images and translating the RGB information to the CIE XYZ color space. The High Dynamic Range technology was essential to accurately capture the data required to determine the luminance distribution as it allows to capture luminance ranges occurring in real conditions.

Chapter 3 provides an alternative method, which applies spectral tuning, to calculate the luminance based on High Dynamic Range images. This study introduces two optimization criteria incorporating the camera's spectral responsivity and the spectral power distribution of the illuminant to improve the spectral match. Both criteria are tested by means of a theoretical model and empirical data utilizing two cameras and three illuminants: LED, halogen and fluorescent light sources.

Chapter 4 applies an alternative model to derive the luminance, which was validated in Chapter 3, to six cameras with varying spectral responsivities using 205 unique spectral power distributions. Based on simulations, the measurement performance relative to the luminance and melanopic radiance is assessed



HDR



The Bee-Eye: a practical device to measure the luminance distribution

This Chapter is based on:

Kruisselbrink TW, Aries MBC, Rosemann ALP. A Practical Device for Measuring the Luminance Distribution. *International Journal of Sustainable Lighting*. 2017 19(1); 75–90. <https://doi.org/10.26607/ijsl.v19i1.76>

Kruisselbrink TW, van Duijnhoven J, Dangol R, Rosemann ALP. Improving lighting quality by practical measurements of the luminance distribution. In: *Congress of the International Ergonomics Association* vol. 827. Florence, Italy: Springer: 2019. p.190–198. https://doi.org/10.1007/978-3-319-96059-3_21

2.1 Introduction

As indicated in Chapter 1, the spatially resolved luminance distribution is a valuable measure for lighting quality. Moreover, applications such as lighting control and lighting simulation can benefit from spatially resolved luminance data as well.

Previous studies [134, 135] have shown that measurement and representation of the luminance distribution continues to be a challenge. Currently available luminance distribution measurement methods, sky scanners and cameras with proprietary software, are not suitable for broad market penetration. Sky scanners cannot handle fast variations of the sky and have a low resolution [136]. Cameras with proprietary software, on the other hand, have an extremely high price. Moreover, calibration and post-processing is tedious [49, 137].

However, along with technological advancement, it has been shown that it is possible to measure the luminance distribution with cheap commercial digital cameras using the Red-Green-Blue (RGB) information captured using High Dynamic Range (HDR) photography [49, 135, 138, 139], or using dedicated HDR vision sensors [140, 141]. Unfortunately, these methods require expertise and extensive post-processing. Moreover, its accuracy is currently not optimal.

This chapter describes a method for fast capturing the luminance distribution, indoors and outdoors, based on a low cost commercially available camera using HDR imaging. Capturing real-time luminance distributions offers possibilities to measure lighting quality, improve building automation systems, and help optimizing lighting simulations on the run.

The work described in this chapter aimed to develop a practical and autonomous camera-based luminance distribution measurement device using an inexpensive single-board computer equipped with a camera and a fisheye lens. The positive asset of this device is, in contrast to other measurement devices for the luminance distribution, that this method was to be cheap, quick, practical and completely automated. Such a practical and autonomous device can provide relevant and real time information on lighting quality when placed in the building realm. This information can, subsequently, serve as input for lighting control systems as well as lighting simulation.

2.2 Methods and results

In order to build a stand-alone device, a single-board computer, Raspberry Pi 3 model B, was deemed feasible to control the camera, carry out the computations, and communicate the results using the on-board Wi-Fi or Ethernet (Figure 2.1). The camera functionality was accounted for by the Raspberry Pi Camera Board version 2 with a CMOS sensor (Sony IMX219, 3.04 mm, f/2.0) with a maximum resolution of 3280 x 2464 pixels, comparable to cameras in smartphones. A miniature equisolid-angle fisheye lens, complementary to the Raspberry Pi Camera Board, with a measured maximum angle of view of 187° (3mm, f/0.4) was used on top of the camera sensor to provide a hemispherical image. In combination with the camera board, this lens system has a focal length of 1.13 mm and provided an equisolid-angle projection with a field of view (FOV) of 98% of the 180° hemisphere. The total costs of the components was approximately 100 Euros. The code, used to automate the measurement procedure, was composed in Python 3.

2.2. Methods and results

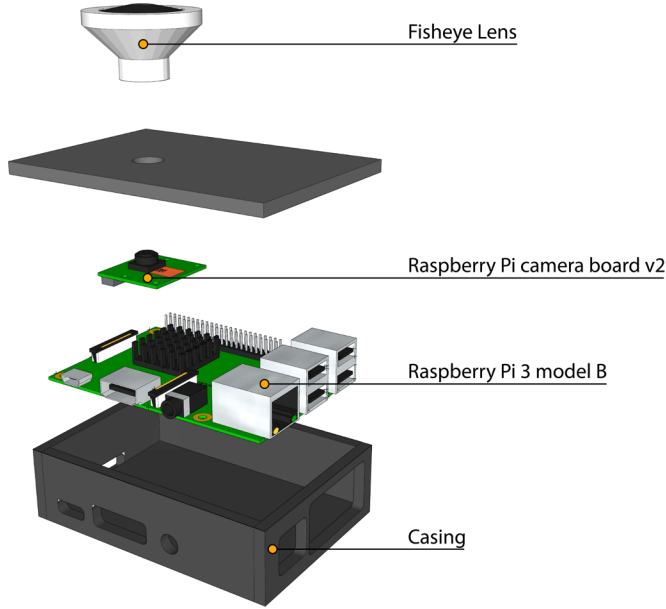


Figure 2.1: Components of the Luminance Camera, including a Raspberry Pi 3, Raspberry Pi camera board and a fisheye lens.

2.2.1 Input settings

High Dynamic Range (HDR) imaging technology is essential to determine the luminance based on digital imaging. The luminance distribution occurring in the real world can consist of luminance values in a range of 8 orders of magnitude (typically from 10^{-3} to 10^5 cd/m^2) [142] while standard 8-bit images only capture a dynamic range of 1.6 orders of magnitude [46]. The most common method to achieve a high dynamic range is the sequential exposure bracketing technique [143]. With this technique, simple digital cameras are used to take Low Dynamic Range (LDR) photographs with sequential exposure settings to cover the desired dynamic range. In order to keep the optical properties constant, it is recommended to only modify the shutter speed [143].

A measurement setup was designed, providing constant conditions, to determine which set of exposures efficiently covered the dynamic range of the real world conditions (Figure 2.2). A diffuse reflecting target (Kodak Gray Card) was illuminated with a lamp in an otherwise completely dark lab room with black interior surfaces. The lamp (Halogen, 220V, 650W) was dimmed by applying AC voltages in steps of 20V (within the range from 100V to 260V). In addition, the lamp was placed at four positions in order to achieve a range of luminance values (30 to 4500 cd/m^2) at the target, baffles were applied to prevent direct light entering the camera. The luminance of the target was measured with a Hagner Universal Photometer S2 ($\pm 5\%$) and simultaneously photographed by an OmniVision OV5647 CMOS sensor (Raspberry Pi camera module V1) with shutter speeds ranging from $17,000^{-1}$ s to 2 s ($f/2.9$, ISO-100). The influence of the monitor light was negligible since only a full-screen window with a black background (terminal) was opened during the measurements.

Based on the under/over-saturation of the digital images, empirical relations (Orange line in Figure 2.3), representing the minimum and maximum luminance, were determined, which described the luminance range of the different exposure values (EV). The EV is a logarithmic combination of the shutter speed (t) and aperture (N) as indicated in Equation 2.1. These empirical equations allowed to generate a nine-step exposure sequence to capture High Dynamic Range images. It has previously been shown that the quality of an HDR image does not significantly increase with a higher number of exposures [143].

$$EV = \log_2 \frac{N^2}{t} \tag{2.1}$$

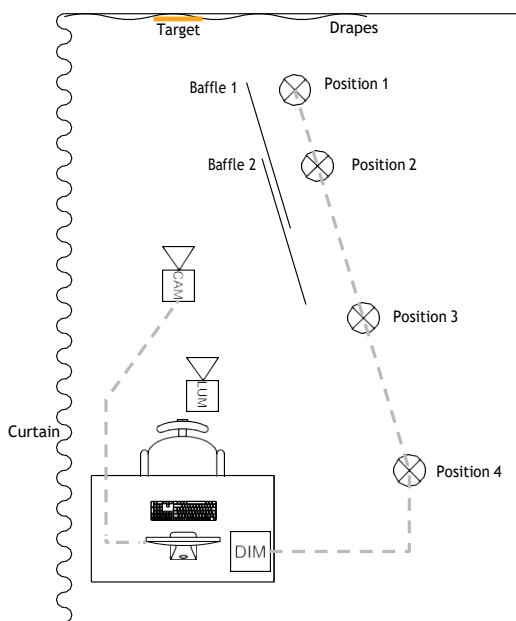


Figure 2.2: Measurement setup to relate luminance to shutter speed. Measurements were conducted in a completely black room illuminated by a single light source that was dimmed and placed at multiple positions. Baffles were applied to prevent direct light entering the camera.

Based on the relation between the EV and the luminance range, as shown in Figure 2.3, exposure values ranging from 4 to 19 EV in steps of approximately 1.8 EV were determined to be used by the camera system, as shown in Table 2.1. Additionally, the shutter speeds, translated to the properties of the Raspberry Pi camera system are displayed. The upper limit of 18.8 EV represents the fastest shutter speed of the camera. This sequence guaranteed that, except for the extreme values, each possible luminance value was captured by at least two exposures, with a theoretical maximum luminance of approximately 70,000 cd/m².

Preliminary tests with the exposure sequence showed that a number of exposures were always under- or over-saturated. For high luminance scenes, exposures 1 and 2 turned out to be always completely over-saturated, while for low luminance scenes,

2.2. Methods and results

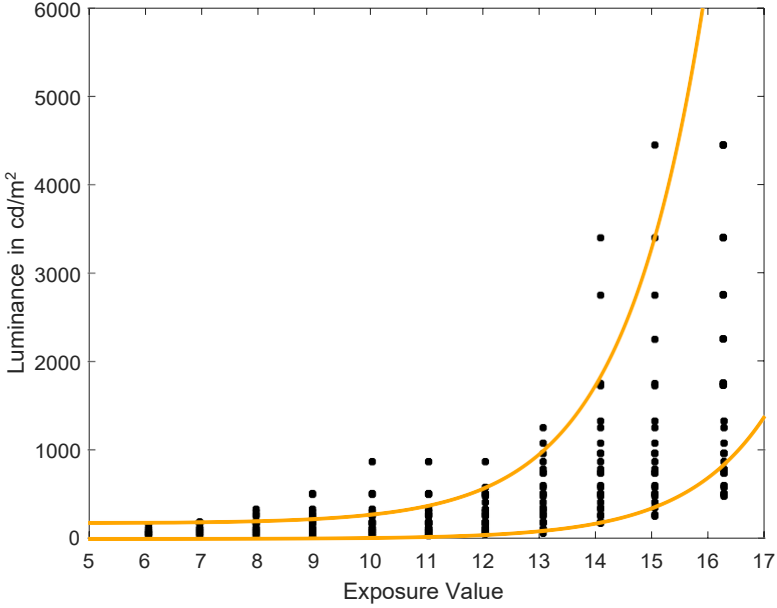


Figure 2.3: The empirical relation between luminance and Exposure Values. The luminance range of each exposure of the camera system is indicated by the orange lines representing the minimum and maximum luminance.

Table 2.1: Exposure sequence applied to the Raspberry Pi camera (v2) system to capture the dynamic range occurring in the real world. Exposures 1 and 2 might over-saturate while exposure 8 and 9 might under-saturate.

Exposure	EV	Shutter Speed [μ s]
1	4.3	200,000
2	6.2	55,556
3	8.0	16,129
4	9.8	4,608
5	11.6	1,314
6	13.4	369
7	15.2	104
8	17.1	28
9	18.8	9

exposures 8 and 9 were always completely under-saturated. Therefore, the exposure sequence was further optimized by leaving out the first or last two exposures depending on the specific conditions. This way, the quality of the HDR images increased and the influence of transient processes was limited (reduced exposure time). The most applicable sequence was determined by conducting the core of the exposure sequence (exposure 3-7) and subsequently assessing the level of saturation of the 7th exposure. When an area of exposure 7 was (almost) saturated exposure 8 and 9 were conducted instead of exposure 1 and 2 and vice versa (Figure 2.4).

Digital images captured according to the determined exposure sequence were

transformed into a single HDR image by the command-line HDR builder for the Raspberry Pi (*hdrgen*), originally developed by Ward [144]. This process uses the HDR (.hdr) format with RGBE encoding with a depth of 32 bits, providing a sufficient dynamic range (76 orders of magnitude [46]). The HDR format has a relative step size, the relative difference between adjacent values, of 1.0% [46, 145]. This format was readable using the OpenCV library (Version 3) and Imaging Processing Toolbox using Python and MATLAB, respectively. Ward's HDR builder was able to approximate the specific camera response curve using radiometric self-calibration [49, 146, 147]. The camera-specific response curve, resembling a logarithmic response, was approximated in accordance with the method described by Reinhard et al. [46], by determining the camera response curve for three scenes and averaging the results into one final response curve that was used for all subsequent luminance measurements. Measurements with another Raspberry Pi camera board showed that the differences between response curves of two similar camera boards were limited to a maximum absolute difference of 2% and a maximum relative difference, for very low exposures, of 60%, and an average relative difference of 12%. The larger differences were mainly present for exposures in the darkest 30%.

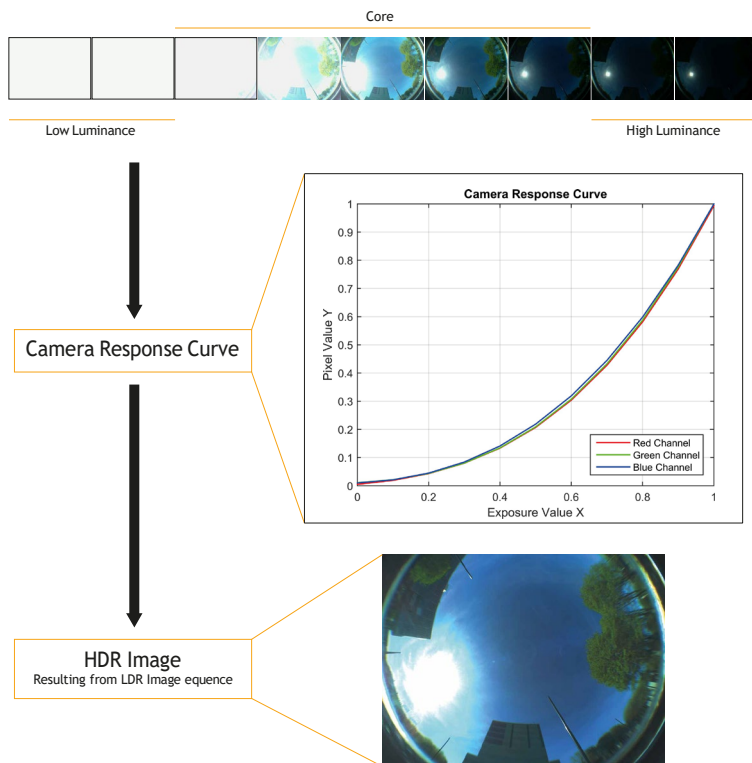


Figure 2.4: Formation of High Dynamic Range image, combination of exposure sequence, containing core exposure and high or low luminance exposures, and camera response curve into one HDR image.

2.2.2 Luminance calculation

The luminance was determined based on the floating point RGB values of an HDR image. In order to determine the luminance, the RGB color space was converted to the CIE XYZ color space. An important property of the CIE XYZ color space is that the color matching function $\bar{y}(\lambda)$ is equal to $V(\lambda)$, the sensitivity curve of the human eye for photopic vision. In other words, the Y channel indicates the incident radiation weighted by the sensitivity curve of the human eye [148], which represents the luminance. The translation of RGB values to the Y tristimulus value was performed according to the protocol described by Inanici [49]. By applying a conversion matrix depending on the primaries and the white point, the RGB tristimulus values were translated into equivalent XYZ tristimulus values. The primaries are stored in the EXIF data of the HDR image, while the white point, depending on the CCT, can be extracted from tables [46], or calculated according to three equations as described by Schanda [149].

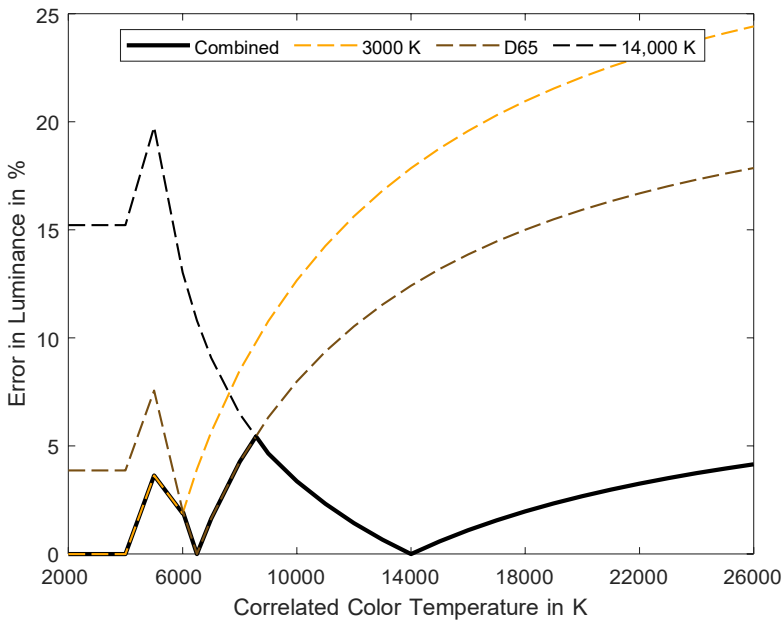


Figure 2.5: Deviation from actual luminance due to fixed CCTs, illustrating the deviation that occurs when reference CCTs of 3,000 K, D65 and 14,000 K are used including the combined reference CCTs.

All variables of the conversion matrix except the CCT are constant. The exact CCT for each condition was not determined since it is an extensive process. Most studies developing a luminance distribution measurement device assumed a constant CCT [49, 139, 148, 150], mostly 6,504 K, corresponding to standard illuminant D65, to determine the white point. Such an approach results typically in significant luminance errors, as the assumption of a constant CCT (i.e. constant white point) can cause deviations up to 17.9% in the conversion matrix for CCTs far from 6,504 K. This methodological error comes on top of uncertainties caused by noise etc. Alternatively, the luminance distribution monitoring device being developed here, is able

to conduct the calculations in accordance with three reference CCTs, each with its own conversion matrix, to limit this methodological error. Next to CIE standard illuminant D65, reference CCTs of 3,000 K and 14,000 K were proposed, reducing the maximum methodological error from 17.9% to 5.4% (Figure 2.5). This error in luminance was calculated by alternating the actual white point, relevant for the conversion matrix, based on the CCT compared to the white points associated with the three fixed CCTs. The white point was calculated based on Judd’s daylight phases [151], which is calculated differently for CCTs <4000 K and >7000 K. The CCT of 3,000 K was suitable for luminance measurements indoors (warm white), illuminant D65 for overcast skies (daylight white), and the CCT of 14,000 K for clear blue skies. The switching point, based on the daylight phases (Figure 2.5), between 3,000 K and D65 was at a CCT of 6,000 K and the switching point between D65 and 14,000 K was at a CCT of 8,600 K. When conducting measurements, the most suitable reference CCT was selected by the user (Section 2.2.4).

The primaries, originating from the HDR files’ EXIF data, and the calculated white points, led to the color space conversion matrices as displayed in Table 2.2. The luminance was calculated by extracting the CIE Y tristimulus value, leading to a simple linear equation to calculate the luminance (L), with photometric calibration factor k and primaries R , G , and B . For the three ranges of CCT used in this study the luminance is calculated according to Equations 2.2-2.4.

Table 2.2: Variables of conversion matrices to translate RGB to XYZ for reference CCTs 3,000 K, 6,504 (D65) and 14,000 K. In contrast to the primaries the white points are dependent on the CCTs, resulting in three conversion matrices.

Reference CCT	3,000 K	6,504 K(D65)	14,000 K
R Primary (x;y)		0.64; 0.33	
G Primary (x;y)		0.3; 0.6	
G Primary (x;y)		0.15; 0.06	
White Point (x;y)	0.3300; 0.3454	0.3127; 0.3291	0.2637; 0.2732
Conversion Matrix	$\begin{bmatrix} 0.4497 & 0.3536 & 0.1521 \\ 0.2319 & 0.7073 & 0.0608 \\ 0.0211 & 0.1179 & 0.8008 \end{bmatrix}$	$\begin{bmatrix} 0.4121 & 0.3577 & 0.1804 \\ 0.2125 & 0.7154 & 0.0721 \\ 0.0193 & 0.1192 & 0.9499 \end{bmatrix}$	$\begin{bmatrix} 0.3075 & 0.3615 & 0.2963 \\ 0.1585 & 0.7230 & 0.1185 \\ 0.0144 & 0.1205 & 1.5603 \end{bmatrix}$

$$L_{3,000K} = k \cdot (0.2319 \cdot R + 0.7073 \cdot G + 0.0608 \cdot B) \tag{2.2}$$

$$L_{D65} = k \cdot (0.2125 \cdot R + 0.7154 \cdot G + 0.0721 \cdot B) \tag{2.3}$$

$$L_{14,000K} = k \cdot (0.1585 \cdot R + 0.7230 \cdot G + 0.1185 \cdot B) \tag{2.4}$$

To determine the CIE Y tristimulus value accurately, all pixels require a vignetting correction. The vignetting effect of a lens refers to light fall-off at the periphery of the lens [135, 148, 152]. Especially fisheye lenses exhibit noticeable light fall-off, visible by the gradual darkening towards the corners of the image. Cauwerts et al. showed that some fisheye lenses can exhibit 73% light fall-off at the periphery of the lens [153]. The vignetting effect is a non-linear radial effect along the image radius of the lens and is often approximated by a polynomial function. It has a radial symmetric character, whereby the polynomial function can be used to determine the vignetting effect for all pixels of an image [153, 154, 155]. The applied fisheye lens, in this thesis, had a radial symmetric character as well, despite that a minor portion of hemispherical view was not captured by the sensor. Therefore, the vignetting

correction, the reciprocal of the vignetting effect, was approximated by an empirical equation along the image radius.

The vignetting effect of the miniature lens was determined in an Ulbricht's sphere (\varnothing 700 mm). According to theory, such integrating spheres create a uniform luminance distribution over its inner surface ($\pm 1\%$) [156]. The vignetting effect along the image radius was determined by dividing the luminance with the maximum luminance, which was the luminance close to the camera zenith. The vignetting correction was measured along the diameter of the image. The radial symmetry of the lens allowed to determine a function only along the image radius. This process was repeated multiple times to limit measurement uncertainties, since the vignetting effect displayed some minor differences under 'constant' conditions. In contrast to previous research [49, 153, 157], the vignetting filter was not described by a polynomial function. Curve fitting to an exponential function showed the best match. Fitting to a second-degree exponential function resulted in the function as described in Figure 2.6, with a $R^2 = 0.99$. In order to extract an applicable function outliers were neglected. The outliers at a distance of approximately 700 pixels from the image center were caused by an irregularity of the sphere. Some outliers were exhibited at a distance of 1300 pixels, the very last pixels of the hemispherical image, due to darkening caused by the image border. Figure 2.6 shows that the luminance at the lens' periphery was 47% ($1/2.1$) of the luminance in the lens' center in case no vignetting filter was applied. Application of the approximated vignetting function limited the maximum vignetting effect, which was exhibited outside the visual field of a user (at 180°), to 14% and the average vignetting to 0.02%. Consequently, the vignetting effect was not completely eliminated. Nevertheless, the reduction of the vignetting effect increased the measurement accuracy close to the periphery significantly. With this equation as derived from Figure 2.6, a post-process correction filter was defined, containing a vignetting correction factor for each individual pixel.

In a last step, a photometric calibration was required to accurately extract the luminance from the HDR image. This linear calibration factor k related the CIE Y tristimulus to the real photometric quantity luminance. The calibration factor was determined for a gray ($\rho = 0.18$) and a white ($\rho = 0.90$) sample of Kodak Gray Cards under various conditions the measurement device is to cover. The samples were placed in front of the camera and were measured with the Hagner Universal Photometer S2 ($\pm 5\%$) while the CIE Y tristimulus value was calculated with the camera system. This calibration process was repeated multiple times to avoid a calibration factor based on a single unrepresentative measurement. The final calibration factor was the average of all calibration measurements. Preferably, the device is calibrated in advance, for each measurement using the respective light source.

2.2.3 Image projection

In addition, to the vignetting effect, fisheye lenses exhibit distortions due to their extremely short focal length. The projection lines that do not pass through the center of the image are strongly bent, resulting in an angle of view up to and over 180° but with a lower resolution and large distortions at the lens' periphery [158]. Tohsing et al. suggested a straightforward method to describe the projection image of a fisheye lens by relating the elevation angle to the image radius using curve fitting [139]. This relation is described in Equation 2.5 with r_i as the image radius of the

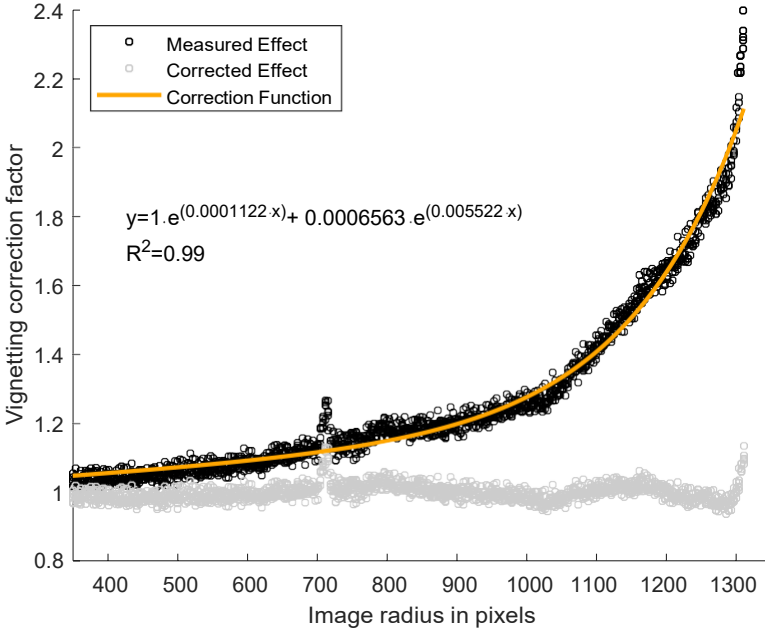


Figure 2.6: The vignetting effect and correction function (y) as approximated in the Ulbricht Sphere.

pixel, c as focal length, and E_i as the polar angle, being the opposite of the elevation angle.

$$r_i = 2c \cdot \sin(E_i/2) \tag{2.5}$$

Equation 2.5 relates every pixel to the elevation as well as to the azimuth angle. With a coefficient of determination (R^2) of 0.9994, the curve fitted equation was able to accurately determine which pixel represented what part of the photographed scene. For the maximum resolution, the camera projection as seen from sensor midpoint can be described by $2c = 1813$ pixels or $2c = 2.26$ mm.

Four identical lenses were compared to assess the variability between lenses. There was no significant difference found between the projection equations of four lenses of the same type and brand. An 180° angle was represented by a image radius of r_i of 1292, 1282, 1282 and 1282 pixels, respectively.

To provide input for automated operation it is not always necessary to get luminance information for each individual pixel due to the overly great spatial resolution and sheer amount of data. Therefore, an alternative suggestion is to use a subdivision as proposed by Tregenza [159], which is shown in Figure 2.7. Inspired by Figure 2.7 the practical luminance distribution measurement device developed in this chapter has been titled **the Bee-Eye**, this name will be used from this point onward.

Tregenza's subdivision provides the luminance distribution of a hemisphere in a limited amount of samples (145) while ensuring enough resolution to prevent major information losses for daylight applications. Only small details inbetween the samples might be missed, this was a trade-off with the complexity [159]. The single-board computer ran a script developed to map the Tregenza subdivision on the image sensor

2.2. Methods and results

using the projection equation (Equation 2.5), only very minor errors were introduced. Subsequently, the single-board computer determined the average luminance of each Tregenza sample by considering all pixels within it. The camera system was bound to an aspect ratio of 4:3 since the focal length was not customizable, resulting in a 98% field of view (FOV) (Figure 2.7).

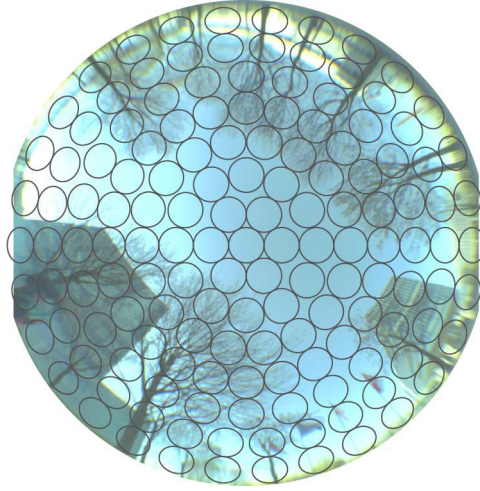


Figure 2.7: Tregenza’s subdivision in relation to a hemispherical image captured with the Bee-Eye. Due to the fixed focal length, only 98% of the hemispherical view was captured.

The applied image resolution was chosen based on the resulting file size, the processing time, and the accuracy of the Tregenza sample mapping, which led to a resolution of 901 pixels horizontally and 676 pixels vertically, instead of 3280 and 2464 pixels, respectively. With this resolution, 95% of each Tregenza sample was represented by whole pixels. Moreover, this resolution is of the same order as recommended by *evalglare* [68]. Consequently, the projection equation (Equation 2.6) was scaled to this resolution.

Depending on the application of the Bee-Eye it can be chosen to output the Tregenza subdivision. However, for some scenarios it might be beneficial to output the complete luminance distribution, or a certain luminance-based metric, such as the desktop luminance. Therefore, three separate tracks are defined on the Bee-Eye, utilizing identical image resolutions, which is further elaborated in Section 2.2.4.

$$r_i = 1813 \cdot \sin \frac{E_i}{2} \cdot \frac{901}{328} = 498.0 \cdot \sin \frac{E_i}{2} \quad (2.6)$$

2.2.4 Processing

The Bee-Eye was automated using a Python script, providing a high amount of flexibility. The program was structured as shown in Figure 2.9 and contains **three distinctive tracks**, which outputs the raw HDR image, the Tregenza subdivision or a undefined luminance metric, respectively. The program was designed as an infinite loop, which conducted a measurement every 5 minutes until interrupted by the user. Nevertheless, the measurement interval is easily adapted (minimum of 30s).

Table 2.3: Processing time, in seconds, of separate processes in the Python script, for the three alternative tracks using the Bee-Eye.

Process	HDR	Tregenza	Metric
1. Preparations	1.0	1.0	1.0
2. Capture Exposures (Dark/Bright)	9.6/9.0	9.6/9.0	9.6/9.0
3. Form HDR Image	5.3	5.3	5.3
4. Calibrate HDR Image	0.8	0.8	0.8
5. Calculate Luminance	-	0.2	0.2
6. Extract Luminance Data	-	1.9	0.1
7. Upload Data	2.2	1.39	1.0
8. Idle	281.1/280.5	279.8/279.2	281.9/281.3

To program was activated by a batch script on the personal computer. The program is structured as follows: First, the the most suitable image sequence is captured, based on the saturation level of the 7th exposure. Excessive luminance values, indicated by an over-saturated 9th exposure, will prompt the program to abort and conduct a new measurement in line with the measurement interval. If successfully, the exposure sequence is merged to a single HDR image using *hdrgen*. The HDR image is calibrated based on a predefined calibration factor determined using gray cards and a luminance meter. Moreover, the vignetting correction is applied. So far, the three tracks are identical. In case of the HDR output, the HDR is uploaded to the personal computer (or server) using Secure Shell (SSH) connection. This first track of uploading a HDR image takes approximately 20s as illustrated in Table 2.3. For the other tracks, the luminance distribution is calculated locally on the Bee-Eye. As a default, the luminance is calculated using Equation 2.3, which can be considered the conventional method [49]. However, the user is able to switch, at any time, between the alternative methods applying a CCT of 3,000 K or 14,000 K using a physical interface. In practice, this occurred seldom. Subsequently, it is chosen whether the Tregenza subdivision or an alternative luminance metric is calculated based on the luminance distribution. The output of either the Tregenza subdivision or the luminance metric is uploaded to a computer/server using SSH, also taking approximately 20s (Table 2.3). In the context of HDR imaging, a duration of 20s is neither quick or slow. For building automation applications, this duration might be too slow for some occasions.

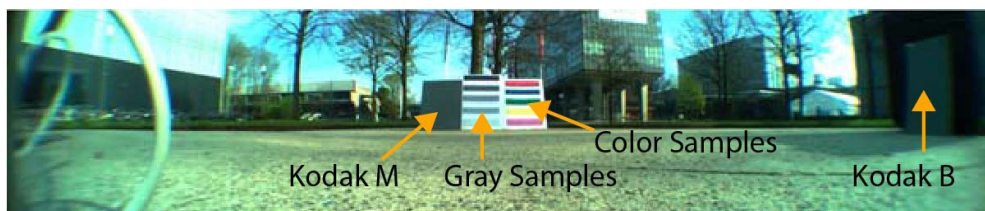


Figure 2.8: Measurement setup representing gray and colored targets to quantify the measurement accuracy. One gray target was placed at the right-hand border.

2.2. Methods and results

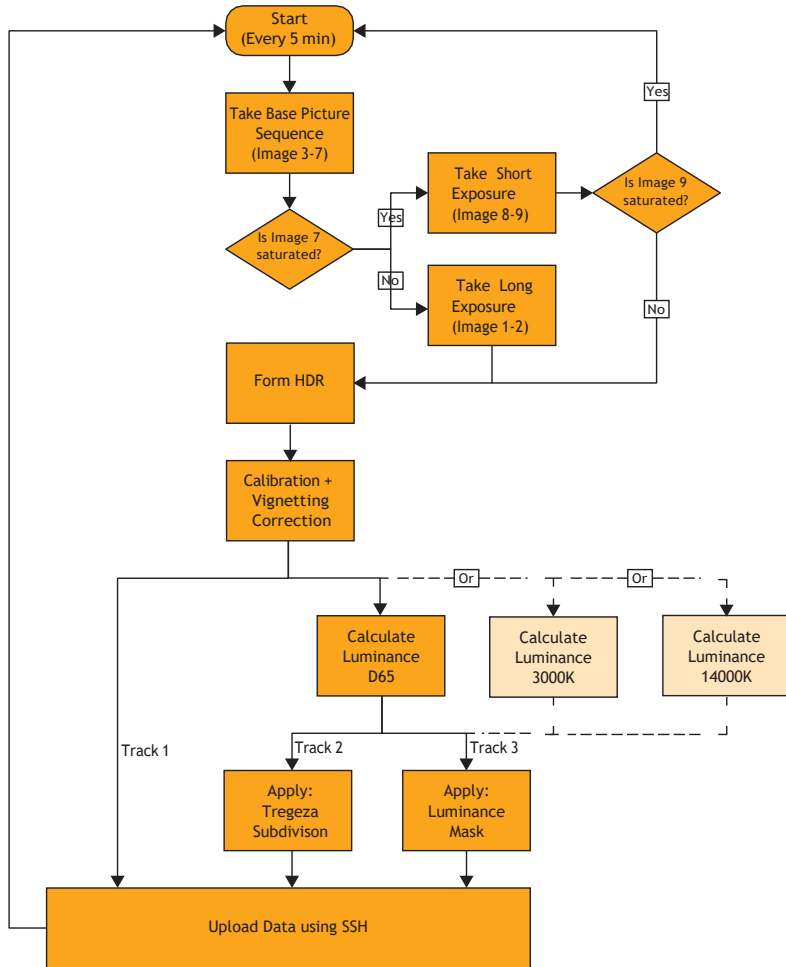


Figure 2.9: Flowchart representing the automated luminance distribution measurement using the Bee-Eye. Three measurement tracks are distinguished delivering: the raw HDR image, the Tregeza subdivision or a luminance metric.

2.2.5 Accuracy

The accuracy of the monitoring device was measured according to the method described by Inanici [49]. Two gray Kodak cards were used additional to an uncalibrated gray scale and an uncalibrated color scale. Except for one gray card, all color scales were placed in the center of the image. The remaining gray card was placed close to the periphery of the image to address the potential gradient in accuracy along the radius due to the vignetting effect (see Figure 2.8, on the far right), which was not corrected perfectly (Section 2.2.2). The luminance was measured with the Hagner Universal Photometer S2 as well as determined by the Bee-Eye. Based on a CCT measurement taken with the Konica Minolta illuminance spectrometer CL-500A, the most suitable reference CCT was determined and used. The accuracy was indicated by relating the physical measurement to the monitoring results of the Bee-Eye. This

process was repeated for multiple scenes under different indoor ($n = 2$) and outdoor ($n = 3$) conditions.

A selection of the measured data is shown in Figure 2.10 and 2.11. Other accuracy measurements showed similar results for different luminance ranges. The measurements had an average error of 10.1% for a range of 3 to 18,000 cd/m^2 . The average errors for the gray and colored targets were 8.0% and 12.5% respectively. The accuracy measurements also showed that the Bee-Eye was not suitable for very high luminance values (e.g. sun or reflections of the sun) due to saturation of the shortest exposure, which led to errors in the HDR assembly and, subsequently, to invalid results. This is a limitation of integration sensors, as opposed to logarithmic response cameras. The exact luminance that saturated the shortest exposure could not be determined but was assumed to be in the range between 18,000 and 70,000 cd/m^2 . The lower end of this range represents the highest luminance measured during the tests; the higher end of this range represents the maximum luminance associated with the applied EV derived from Figure 2.3.

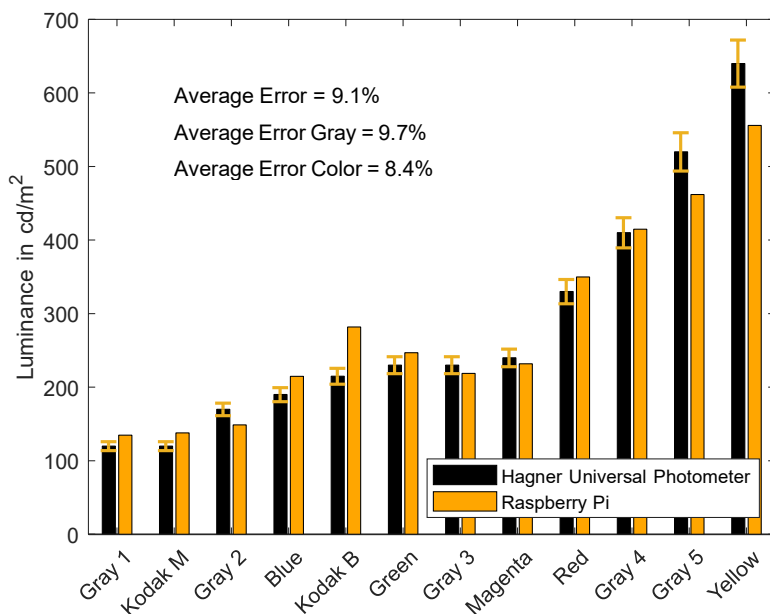


Figure 2.10: Measured accuracy for an indoor condition with a CCT of 6,370K, the error bars indicate the measurement accuracy of the Hagner Universal Photometer. Kodak M represents the grey card in the middle of the image, while Kodak B represents the grey card at the border of the image.

It was expected that close to the periphery of the sensor the measurement error would increase because the vignetting correction could not completely account for the light fall-off as indicated in Figure 2.6. The results supported this hypothesis (Figure 2.10 and 2.11), the errors close to the border (Kodak B) of the sensor were significantly higher than at the center of the image (Kodak M); it displayed an average error of 27% at the periphery compared to 8% in the center. It is assumed that this error applies to the very last pixels along the radius because in this region the impact of the

2.3. Discussion

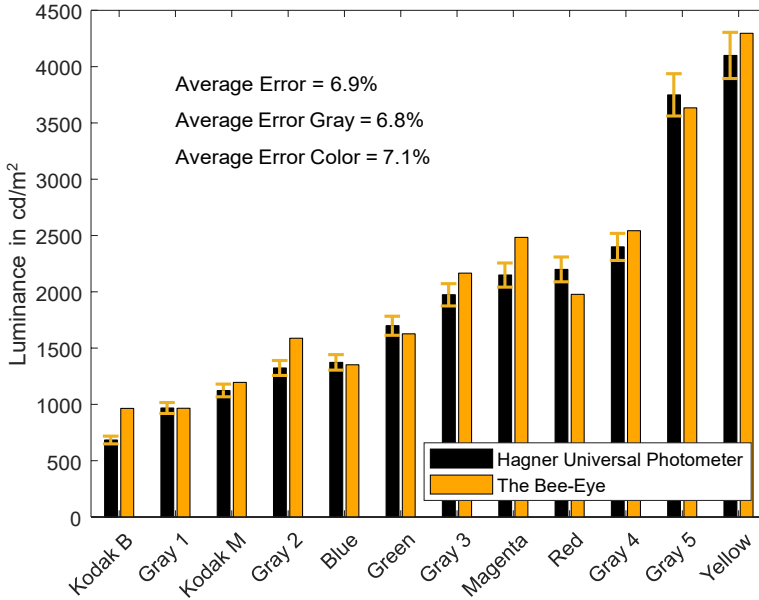


Figure 2.11: Measured accuracy for an outdoor condition with a CCT of 6,170K, the error bars indicate the measurement accuracy of the Hagner Universal Photometer. Kodak M represents the grey card in the middle of the image, while Kodak B represents the grey card at the border of the image.

vignetting effect became significant. For the other pixels, the vignetting effect was much smaller and therefore had a lower impact on the overall measurement accuracy.

2.3 Discussion

This chapter showed that it was possible to construct a continuous luminance distribution measurement device, titled the Bee-Eye, using low cost components with a practical accuracy. Most importantly, it provided applied theory and methods that can be used to build a luminance distribution measurement device.

The established exposure sequence had two variations to minimize the number of saturated exposures. It was developed in such a way that the entire range of possible luminance values was captured. The accuracy of the HDR image, and hence the accuracy of the Bee-Eye, can be improved by tuning the exposure sequence to the specific lighting situation of the measured scene. Moreover, it turned out that the shortest exposure possible was not able to capture the luminance of the sun and its direct reflections. The luminance of the sun was several orders of magnitude greater than the maximum luminance that could be captured with this exposure sequence. The accuracy was validated to $18,000 \text{ cd/m}^2$ because no higher luminance had been measured during the accuracy measurements. Although, calculations showed that the estimated maximum luminance is approximately $70,000 \text{ cd/m}^2$. With the chosen measurement setup it was not possible to reach higher luminance values on the targets (color scales). These targets were required to assure that the same luminance

was measured by the Hagner Universal Photometer and the Bee-Eye. The exposure sequence was translated into an HDR image using *hdrgen* developed by Ward [144]. The settings were assumed constant for all situations, which means that for some conditions the settings might not have been optimal.

The camera response curve was approximated with *hdrgen*, and therefore it did not represent the actual camera response curve. The maximum relative difference between the camera response curves of two cameras of the same brand and type was 60% with an average relative difference of 12%. Therefore, the applied camera response curve cannot be applied for other Raspberry Pi camera boards without consideration.

Additionally, identical camera lenses were compared. The maximum relative difference was 0.18%, therefore the lenses were found to be equal. The developed code can be used to measure the luminance distribution, with an acceptable accuracy, using another lens of the same type and brand.

The luminance calculation was based on the similarity between the tristimulus value Y and the sensitivity curve of the human eye for photopic vision ($V(\lambda)$). Therefore, the measurement device can only be applied to situations where photopic vision occurs, thus for luminance values greater than 3 cd/m^2 [160].

To calculate the luminance accurately using an RGB HDR image, the CCT, or spectral power distribution, of the light source is required. A default CCT of 6500 K (D65) is a good solution when the main light source is daylight. However, for CCTs far from 6500 K (i.e., very blue sky) this might lead to methodological errors up to 18%. In this study, three reference CCT's were suggested to limit this error to approximately 5%. A downside of this is the required user intervention, which was barely used in practice, an alternative solution is proposed in Chapter 3. This intervention will result in some uncertainties, possibly increasing the inaccuracy. However, the maximum methodological error will never exceed 18%, a range which was deemed appropriate for a practical measurement device [49, 161].

The vignetting effect was not completely accounted for, as some variance was exhibited between the different measurements. The vignetting effect extremely close to the periphery was only limited to approximately 14%. However, most of the relevant information is extracted from the center of the image, and not from its extreme boundaries. On average the vignetting effect was reduced to only 0.02%, which significantly improves the usability of the camera-lens system with had limited capabilities due to light fall-off.

The time required to a single measurement was approximately 20 s using this specific resolution. For this study, measurements were performed every 5 min. The time required to take the LDR images was the time that the device was actually vulnerable to transient conditions. This was approximately 9 s, compared to 3 min required for a sky scanner [162, 163, 164], and 1-2 min for HDR camera system measurement [136].

2.4 Conclusion

The luminance distribution measurement was conducted locally using a Raspberry Pi as a single-board computer, which was able to perform all measurements and calculations automatically, titled **the Bee-Eye**. The Bee-Eye can operate autonomously, providing either the raw HDR image, the Tregenza subdivision or another luminance-based metric. The best performance was achieved when the user selected the suitable reference CCT at the start of the measurement and changing this when the conditions had changed. The results were automatically digitized and uploaded to a server or computer. The accuracy of the device falls within an acceptable range with an average error ranging from 5.1% to 15.1% and an average error range of 3.0% to 13.0% and 7.5% to 17.5% for respectively gray and colored targets. All of this was achieved with low costs components (€ 100 Euros).

The Bee-Eye in its current form was validated within a limited performance range. Reliable results could only be guaranteed within a luminance range from 3 to 18,000 cd/m². Measurements showed that for extremely high luminance values the results became invalid due to saturation of the shortest exposure.

The device can potentially be further optimized by applying some additional improvements that are subject to further research.

In this research, two different exposure sequences were used, being the optimal exposure sequence for a limited set of conditions. To improve the quality of the HDR image it is recommended to determine the exposure sequence specifically for each condition. This prevents saturated images, meaning that all nine exposures are evenly distributed within the occurring luminance range.

The current device was limited to a maximum luminance of 18,000 cd/m². This was because high luminance values lead to saturation of the shortest exposure. The shutter speed cannot be further reduced but a neutral density filter is a feasible solution [157]. This way the current dynamic range can be shifted towards longer exposures and the shorter exposures can be used to capture higher luminance values. Disadvantages are that for darker conditions the exposure time becomes significantly higher, whereby the influence of transient processes increases. This can potentially be accounted for by adding an extra camera to the Bee-Eye and capturing exposures in parallel.

Finally, the luminance was calculated based on conversion matrices for the translation of the sRGB color space to the CIE XYZ color space, which might not always be suitable. The accuracy was already improved by differentiating between three alternative equations representing different CCT ranges. However, as an alternative, the camera's spectral RGB responsivity could be directly transformed to the $V(\lambda)$ to reduce the methodological errors introduced by the current method, which is subject to the research presented in Chapters 3 and 4.



Spectral tuning of luminance cameras

This Chapter is based on:

Kruisselbrink TW, Dangol R, Rosemann ALP, van Loenen EJ. Spectral tuning of luminance cameras: A theoretical model and validation measurements. *Lighting Research & Technology*. 2019 52(5);654–674. <https://doi.org/10.1177/1477153519880231>

3.1 Introduction

It was already indicated that the luminance distribution provides valuable information on lighting quality, which can be measured using HDR imaging devices such as the Bee-Eye (Chapter 2). To calculate the luminance, the RGB color space is generally converted to the XYZ color space using conversion matrices, resulting in r , g , and b weighting factors, dependent on the color primaries and white point. However, Chapter 2 showed that this can introduce significant methodological errors.

Generally, the sRGB color space, a device independent color space, is assumed in these conversions from RGB to XYZ because this color space is used in most applications such as internet and printing applications [46]. This assumption means that this color space is expected to provide a reasonable approximation of the camera sensor's spectral responsivity [49, 142]; however, Ramanath [165] states that "the data captured by the sensor is in the color space of the camera and has little to do with colorimetric (human) values". Moreover, Wu et al. [140] indicate that the spectral responsivity of the camera can have severe disparity with the RGB color space as manufacturers aim to achieve compelling colors. The sRGB color space is a rendered or output-referred color space designed for an output medium [46, 165], while HDR images are scene-referred images because the pixels are directly related to the radiance of the captured scene [46]. An HDR image cannot be displayed without tone-mapping, which can be considered the transformation of a scene-referred to an output-referred image [166].

HDR images are generally formed by merging multiple output-referred images. *Hdragen*, the common HDR builder, requires JPEG or TIFF files with an 8-bit depth per channel [144]. During the imaging pipeline for output-referred images, multiple corrections and transformations are applied to achieve a visually appealing image [165] but losing valuable information. To account for this information loss, radiometric calibration, based on the camera response curve, is required, which directly relates the HDR pixel values to the scene irradiances [147], while also accounting for proprietary corrections in the image pipeline. Moreover, Lenseigne et al. [167] showed that the spectral responsivity of the HDR image has large similarities, including the effect of white balancing, to the raw spectral responsivity of the camera, indicating that the color space of the HDR image is camera dependent and not necessarily similar to the spectral sRGB responsivity.

Additionally, the sRGB color space can theoretically lead to negative RGB values, as it assumes negative sensitivities for certain wavelengths in the visible spectrum to prevent information losses, while this is physically not feasible for a three-channelled camera. Summarized, the assumption of the sRGB color space seems not fitting to calculate the luminance. As a result, it is hypothesized that *the r , g , and b weighting factors based on the sRGB color space transformation, hereafter referred to as the conventional method, will result in significant spectral mismatches.*

Secondly, the conventional method is dependent on the SPD. The white point, one of the conversion matrix' parameters, is reliant on a standard illuminant, for sRGB this is standard illuminant D65. The white point is the chromaticity that corresponds to the image area that is perceived as white for a specific illuminant [58]. Chapter 2 showed that this white point is CCT reliant, and hence SPD dependent, causing significant deviations in luminance values further from the CCT of the standard illuminant (Figure 2.5).

3.2. Theoretical model

Moreover, the CIE [168] states that using a photometer with a spectral responsivity that differs from the spectral luminous efficiency function for photopic vision ($V(\lambda)$) gathers incorrect measurements. Nevertheless, the measurements can be corrected with a spectral mismatch correction factor when the relative SPD of the light source and relative spectral responsivity of the photometer are available. It is indicated that this is very important for narrow band illuminants such as LEDs, implying that the SPD can influence the spectral performance of a sensor. Furthermore, Cai [169] performed identical conventional luminance measurements, using HDR, under different types of illuminants and found significant differences in accuracy as was earlier hypothesized by Cai and Chung [143]. Therefore, the second hypothesis is that *the optimal r, g, and b weighting factors depend on the relative spectral power distribution of the illuminant*.

In the literature, a number of studies were found that optimized camera systems to capture spectral efficiencies as accurate as possible. Borisuit et al. [170, 171] suggested applying an optical filter of the sensor to match the $V(\lambda)$ and the circadian sensitivity function $C(\lambda)$, resulting in spectral mismatch errors of 8.3% and 10.4%, respectively. Similarly, Wu et al. [140] developed an optical filter to match $V(\lambda)$ by minimizing the least error in the l^2 norm space using a pool of 256 bandpass filters. Additionally, to further optimize the spectral match, the r, g, and b weighting factors were also determined using the least error in the l^2 norm space, leading to a limited spectral mismatch of only 8.9% instead of the original 52.9%. Alternatively, Geisler-Moroder and Dür [172] optimized the r, g, and b weighting factors by solving a Gramian matrix to approximate the $C(\lambda)$ based on rendered HDR images. Nevertheless, the relative errors were all greater than 5%. Similarly, Cauwerts et al. [173] optimized the color transform matrix, for photometric measurements, by minimizing the least square error in the XYZ color space using 18 color samples lit by an incandescent light source, resulting in a mean absolute percentage error of 3.4% instead of 4.4%. Also Fliegel and Havlin [174] optimized the $V(\lambda)$ match by minimizing the mean squared error of a single exposure resulting in a 10% deviation in luminance for standard illuminant A.

To assess the hypotheses, the weighting coefficients, analogous to the conversion matrices in Chapter 2, are optimized according to a theoretical model introducing the spectral responsivity of two cameras and the SPDs of three illuminants: LED, halogen and fluorescent, respectively. Moreover, the theoretical model is validated with empirical data. Based on the measurement accuracy of the theoretical model and the empirical data both hypotheses are assessed, indicating whether the luminance can be calculated in a more accurate manner compared to the conventional method described in Chapter 2.

3.2 Theoretical model

Two optimization criteria are developed for an image-based system, in addition to the conventional method, with the objective to improve the accuracy of the luminance measurement. This is achieved by improving the spectral match of the cameras relative spectral responsivity by tuning the r, g, and b weighting factors in the luminance calculation. Additionally, one performance indicator is proposed which helps to assess both optimization criteria and the conventional method, similarly and independently.

3.2.1 Conventional method

For the conventional method, the luminance (L_{conv} or L_{D65}) is calculated based on a linear combination of the RGB coefficients using fixed r, g, and b weighting factors according to Equation 2.3 (page 32), which resembles the luminous efficiency curve $V(\lambda)$. These coefficients are originating from the transformation of the sRGB to XYZ color space “based on the reference primaries, CIE standard illuminant D65, and standard CIE Colorimetric Observer with 2° field of view” [49] as elaborated in Chapter 2.

3.2.2 Optimizations

Two different optimization criteria are developed to optimize the spectral match between the relative spectral responsivity $s_{rel}(\lambda)$ of the camera and the 10 degree $V(\lambda)$ curve, as recommended by CIE committee W-1.3.1 [149], because it is more representative for the human eye compared to the 2 degree $V(\lambda)$ function. Both criteria aim to find the optimal r, g, and, b weighting factors.

Criterion 1

The first optimization criterion is based on the commonly used General $V(\lambda)$ Mismatch Index f_1^t [168], which is an indicator used to specify the spectral properties of photometers for general measurements. The f_1^t index is suitable for a general description of the photometers’ performance describing the relation between the $V(\lambda)$ and the approximated $V(\lambda)$ of the photometer. However, this index, in the current use, is only appropriate for SPDs similar to standard illuminant A. In this study, the f_1^t index is applied to luminance cameras, since one image pixel originating from the luminance distribution can be considered as a single reading from a spot luminance meter. Equations 3.1 and 3.2 describe the f_1^t index for the n th relative SPD $\varphi_n(\lambda)$ and relative spectral responsivity $s_{rel}(\lambda)$ of the camera based on the normalized spectral responsivity function s_{rel}^* . The f_1^t index is determined for the visible spectrum ranging from 380 nm to 780 nm.

$$s_{rel}^*(\lambda) = s_{rel}(\lambda) \cdot \frac{\int_{380nm}^{780nm} \varphi_n(\lambda) \cdot V(\lambda) d\lambda}{\int_{380nm}^{780nm} \varphi_n(\lambda) \cdot s_{rel}(\lambda) d\lambda} \quad (3.1)$$

$$f_1^t = \frac{\int_{380nm}^{780nm} |s_{rel}^*(\lambda) - V(\lambda)| d\lambda}{\int_{380nm}^{780nm} V(\lambda) d\lambda} \quad (3.2)$$

For cameras, the relative spectral responsivity $s_{rel}(\lambda)$ is a summation of the relative spectral responsivity for the $R(\lambda)$, $G(\lambda)$, and $B(\lambda)$ tristimuli, respectively, with weighting factors r, g, and b (Equation 3.3), analogous to the conventional method to calculate the luminance. A normalization factor $N_{r,g,b}$ is applied such that the area under $s_{rel}(\lambda)$ is equal to the area under $V(\lambda)$ (Equation 3.4). This factor does not have any physical meaning but is applied to make $s_{rel}(\lambda)$ independent of energy/area differences between different combinations of $R(\lambda)$, $G(\lambda)$, and $B(\lambda)$ such that only the effect of the improved spectral match is shown.

3.2. Theoretical model

$$s_{rel}(\lambda) = (r \cdot R(\lambda) + g \cdot G(\lambda) + b \cdot B(\lambda)) \cdot N_{r,g,b} \quad (3.3)$$

$$1 = \frac{\int_{380nm}^{780nm} V(\lambda) d\lambda}{\int_{380nm}^{780nm} s_{rel}(\lambda) d\lambda} \quad (3.4)$$

To limit the spectral mismatch of $s_{rel}(\lambda)$ relative to the $V(\lambda)$ the r , g and b weighting factors are optimized to minimize the f_1^t index according to Equation 3.5. It was chosen to limit the weighting factors to a range of zero to one with increments of 0.01 under the constraint that $r + g + b = 1$. Extension of the range, i.e. $r + g + b > 1$, has no effect since it results in similar optimizations with different normalization factors ($N_{r,g,b}$).

$$\arg \min f_1^t(r, g, b), \text{ subject to : } \begin{cases} r \in (0, 1) \\ g \in (0, 1) \\ b \in (0, 1) \\ r + g + b = 1 \end{cases} \quad (3.5)$$

Criterion 2

Criterion 2 aims to match the $V(\lambda)$ weighted SPD with the $s_{rel}(\lambda)$ weighted SPD, where criterion 1 merely aims to optimize the $V(\lambda)$ match. Therefore, the root mean square of the absolute difference between the $V(\lambda)$ weighted SPD and the $s_{rel}(\lambda)$ weighted SPD is calculated for each 1 nm increment according to Equation 3.6. The r , g , and b weighting factors are optimized such that the root mean square of this difference is minimized according to Equation 3.7. This optimization criterion can only be used relatively.

$$\Delta\varphi_{RMS} = \frac{1}{780nm - 380nm} \int_{380nm}^{780nm} |\varphi_n(\lambda) \cdot V(\lambda) - \varphi_n(\lambda) \cdot s_{rel}(\lambda) \cdot N_{r,g,b}|^2 d\lambda \quad (3.6)$$

$$\arg \min \Delta\varphi_{RMS}(r, g, b), \text{ subject to : } \begin{cases} r \in (0, 1) \\ g \in (0, 1) \\ b \in (0, 1) \\ r + g + b = 1 \end{cases} \quad (3.7)$$

3.2.3 Performance indicator

To assess criterion 1 and 2, independently, a performance indicator is introduced that defines the relative difference with the physical luminance. The relative difference in luminance $\delta_{L,n}$ is calculated based on the difference between the $V(\lambda)$ weighted SPD

(Equation 3.8) and the $s_{rel}(\lambda)$ weighted SPD (Equation 3.9, including photometric calibration factor k) according to Equation 3.10.

$$L_{V,n} = \int_{380nm}^{780nm} \varphi_n(\lambda) \cdot V(\lambda) d\lambda$$

$$L_{s_{rel},n} = k \cdot \int_{380nm}^{780nm} \varphi_n(\lambda) \cdot s_{rel}(\lambda) d\lambda \quad (3.9)$$

$$\delta_{L,n} = \frac{|L_{s_{rel},n} - L_{V,n}|}{L_{s_{rel},n}} \quad (3.10)$$

3.2.4 Input Characteristics

The input required for the optimizations are the spectral responsivity of a camera for the R, G and B channels and the SPD of the respective illuminant. In this research, optimizations were performed for two different camera sensors, Sony IMX219 (Cam 1) and OmniVision OV5647 (Cam 2), respectively, with known spectral responsivities in the range of 400 nm to 700 nm with 1 nm increments originating from Hufkens [175], including white balancing, as shown in Figure 3.1. Additionally, three different illuminants; LED (φ_1), halogen (φ_2) and fluorescent (φ_3) were used, which are also shown in Figure 3.1. The SPDs of the illuminants were measured with a Konica Minolta CL500a as elaborated in Section 3.3.1.

3.3 Methodology

To validate the previously described models, measurements were conducted with Cam 1 and Cam 2 using identical SPDs. Therefore, luminance distribution measurements were conducted with Cam 1 and Cam 2, while simultaneously point luminance measurements were conducted as a reference. The luminance, using the cameras, was calculated according to the conventional method, theoretical optimization of criterion 1, and theoretical optimization of criterion 2. Eventually, the performance of the methodologies was compared with the point luminance measurements according to Equation 3.10.

3.3.1 Measurement setup

The measurements were conducted in a dark windowless room (4.4 m x 3.6 m x 2.7 m) containing a lightbox. The lightbox (Figure 3.2), measuring 1.2 m wide, 0.8 m deep and 0.8 m high, with a diffusely reflecting white painted interior ($\rho_i = 0.85$) was placed on a table in the middle of the room. The lightbox was consecutively fitted with three illuminants, an LED (Philips Smartbalance tunable white RC484B) at 4400K, a halogen (Philips IR 250CH 250W), and a fluorescent illuminant (Freshlight Pure light 32W), respectively, with properties according to Figure 3.1 and with luminance ratios between the minimum and maximum luminance within the entire scene of approximately 1:2250, 1:1400 and 1:1000, respectively. Baffles were applied for the halogen and fluorescent illuminants to prevent direct light on the camera sensor that might cause overflow.

3.3. Methodology

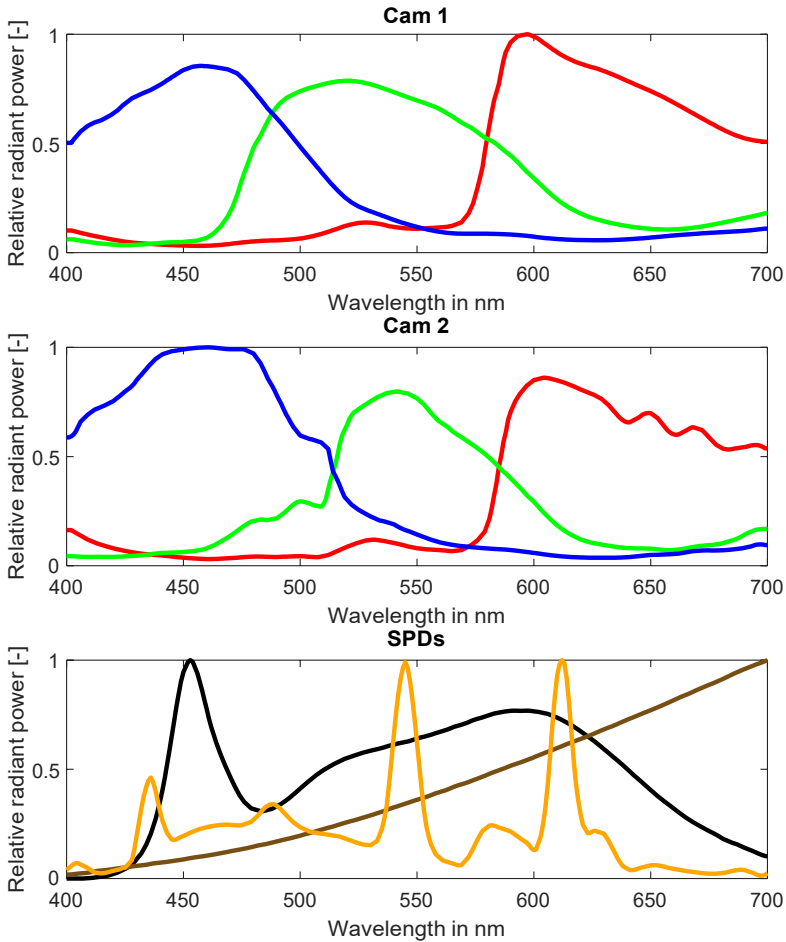


Figure 3.1: Spectral responsivities of the Red, Green and Blue channels of Cam 1 and Cam 2. Moreover, the SPDs of the LED (black), halogen (brown) and fluorescent illuminant (orange) are illustrated.

To indicate the effect of the illuminant's SPD, the luminance should be measured with a minimum of spectral disruptions to preserve the original SPD. Therefore, 10 grey samples were applied because it is impossible to measure the luminance of the illuminant directly. The targets were successively placed at the back wall in the middle of the lightbox. Grey targets have a relatively uniform spectral reflectance, by applying 10 different samples we intended to limit the effect of the imperfect uniform reflectances. The reflectances of these samples were 0.12, 0.18, 0.26, 0.28, 0.38, 0.41, 0.43, 0.74, 0.90, and 0.93, respectively.

Point luminance measurements were conducted with a Konica Minolta LS-100 luminance meter with an accuracy of $\pm 2\%$ and a general $V(\lambda)$ mismatch of 8%. Moreover, luminance distribution measurements were performed with two camera sensors, Sony IMX219 (Cam 1) and Omnivision OV5647 (Cam 2), respectively, combined with a fisheye lens (FOV 187°) and single-board computer controlled over SSH

with an average accuracy ranging from $\pm 5\%$ to $\pm 20\%$ as indicated in Chapter 2. Both devices were calibrated in advance. The camera settings were fixed and identical for both cameras as far as possible (Table 3.1). HDR images were captured using the first measurement track of the Bee-Eye as illustrated in Figure 2.9. Overflow was automatically detected, although it did not occur due to the baffles. Post-processing was done using MATLAB r2017a and consisted of luminance calculations and additional calibrations. The LS-100 ($\pm 2\%$) and the luminance cameras were placed, side by side, at 1.5 m from the respective grey sample while being focused at the centre of the grey sample. The measurement setup is further elaborated in Figure 3.2 and Figure 3.3. The SPDs of the illuminants, shown in Figure 3.1 and Figure 3.4, were measured in advance of each individual measurement in the middle of the lightbox using a Konica Minolta CL500A illuminance spectrophotometer with an accuracy of $\pm 2\%$ and a general $V(\lambda)$ mismatch of 1.5%. These SPD measurements also functioned as input for the theoretical model.

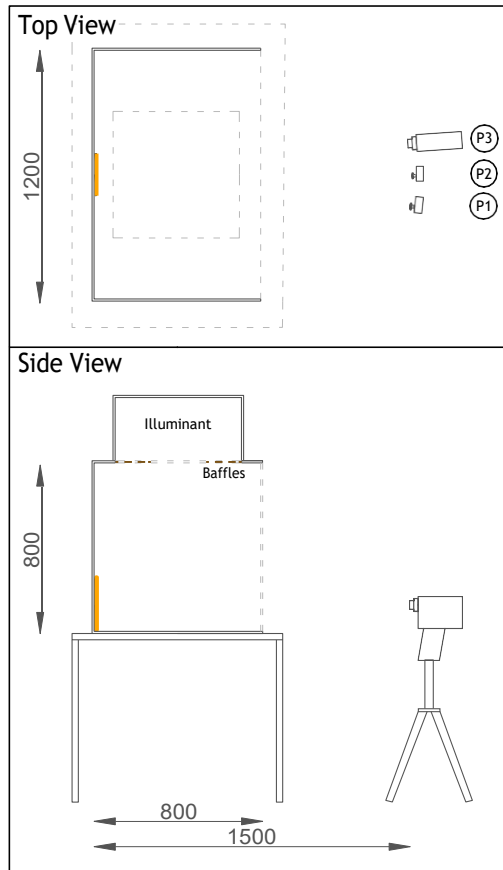


Figure 3.2: Measurement setup with the sample indicated in Orange, P1-P3 represent the measurement positions of the three devices.

3.3. Methodology

Table 3.1: Camera settings, including minimum and maximum exposure value (EV).

	Cam 1	Cam 2
Model	Sony IMX219	Omnivision OV5647
Aperture (N)	f/2	f/2.9
Resolution	901x676	901x676
ISO	100	100
White Balance	1,3,1,1,3	1,3,1,1,3
EV_{min}	4.3	5.1
EV_{max}	18.8	19.4

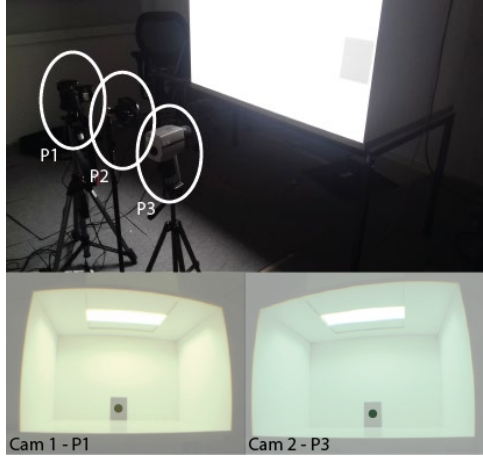


Figure 3.3: Measurement setup with the three measurement positions aligned. The bottom images represent the luminance masks corresponding to the area measured by the LS-100 luminance meter.

3.3.2 Protocol

In total, 90 measurements were simultaneously conducted for all three devices. The measurements were conducted simultaneously because some minor variations were exhibited during the measurements with the illuminance spectrophotometer for the halogen illuminant mainly. Three positions (P1 – P3) were located at 1.5 m from the sample as shown in Figure 3.2 and Figure 3.3. To account for the potential differences between measurement positions the equipment was rotated such that each device has conducted a luminance measurement for each condition (10 samples and 3 illuminants) at all three positions. Hence, each condition was measured thrice, resulting in a total of 90 measurements.

3.3.3 Analysis methods

Each luminance distribution measurement provided one single HDR image to which a luminance mask identical to the opening angle of LS-100 luminance meter (Figure 3.3) was applied. Based on the HDR image, the luminance was calculated for each illuminant, the conventional method and both optimizations, by applying the

respective r, g and, b weighting factors originating from the theoretical optimization found in Table 3.3. An individual photometric calibration (Equation 3.9, k) was applied for each camera and method (conventional, criterion 1, and criterion 2). This calibration factor was developed such that the average measured results were equal to the average expected results for the conventional method, criterion 1 and, criterion 2, respectively. Subsequently, inferential statistical methods such as one-sided and two-sided unpaired student t-tests with a confidence interval of 95% were applied. Moreover, Lin's Concordance Correlation Coefficient (ρ_c) was used to indicate the accuracy and precision (variability) relative to the reference measurement (Section 8.2.6). In contrast to Pearson's correlation coefficient, ρ_c is able to assess both precision (variability) and accuracy (bias) [176].

3.4 Results

In this section, the results of the theoretical model, or the expected results, and the measurement results both generally indicated by the performance indicator representing the relative difference in luminance (Equation 3.10) are shown. Additionally, a comparison between the results, using inferential statistics, is presented.

3.4.1 Theoretical model

Table 3.2 displays the average results of the optimizations according to the theoretical model calculated using MATLAB r2017a, with the average optimized r, g, and b weighting factors, the General $V(\lambda)$ Mismatch Index f_1^t (Equation 3.2), the root mean square of the difference between $V(\lambda)$ and $s_{rel}(\lambda)$ weighted SPDs ($\Delta\varphi_{RMS}$, Equation 3.6) and the relative difference in luminance (δ_L , Equation 3.10). The table indicates that both the f_1^t and $\Delta\varphi_{RMS}$ were improved for both optimizations. However, on average the δ_L generally did not improve, while the average standard deviation was reduced, indicating an improved precision.

Table 3.2: Average theoretical optimization results, for the conventional method, criterion 1 and criterion 2, using LED, Halogen and Fluorescent illuminants (SD between brackets) for Cam 1 and Cam 2.

		r	g	b	f_1^t	$\Delta\varphi_{RMS}$	δ_L
Cam 1	Conv.	0.2125	0.7154	0.0721	42.9% (0.2%)	9.8% (2.3%)	-7.3% (9.8%)
	Crit. 1	0.10 (0.02)	0.90 (0.02)	0.00 (0.00)	37.3% (0.2%)	8.1% (1.9%)	-7.7% (5.3%)
	Crit. 2	0.07 (0.05)	0.93 (0.05)	0.00 (0.00)	37.7% (0.6%)	8.0% (1.9%)	-9.3% (3.0%)
Cam 2	Conv.	0.2125	0.7154	0.0721	36.6% (3.2%)	8.1% (3.2%)	-4.6% (10.5%)
	Crit. 1	0.08 (0.02)	0.93 (0.02)	0.00 (0.00)	25.9% (0.1%)	6.1% (2.0%)	-3.5% (5.3%)
	Crit. 2	0.10 (0.07)	0.90 (0.07)	0.00 (0.00)	26.6% (0.06%)	5.6% (2.5%)	-5.5% (4.6%)

The theoretical optimization results are illustrated per wavelength in Figure 3.4. The dashed black line highlights the weighted SPD with a perfect $V(\lambda)$ match. As clearly seen, the conventional method, but also the optimizations, differ notably from this perfect $V(\lambda)$ match, as already indicated by the effectively large f_1^t values in Table 3.2. Moreover, the results of the optimizations, for the LED and halogen, using criteria 1 and 2 were rather similar; for the fluorescent illuminant, the differences were more distinct. In most cases, the optimizations achieved a better spectral match

3.4. Results

than the conventional method. Cam 2 achieved a better fit, mainly around 525 nm, because the spectral responsivity of Cam 2 for the green channel was more compact as illustrated in Figure 3.1.

The optimization results for the individual illuminants, cameras and methods are presented in Table 3.3 and Figure 3.4. The relative spectral sensitivities of Figure 3.4 were achieved using the r, g, and b weighting factors displayed in Table 3.3. The weighting factors differ significantly compared to the weighting factors of the conventional method. The main difference related to the conventional method is in the weighting factor of the blue sensitivity, which was zero for both optimizations and 0.0721 for the conventional method. Additionally, the weighting factors for the halogen illuminant are very different compared to the LED and fluorescent illuminant. In contrast to Table 3.2, the performance of the optimized weighting factors provided a higher accuracy indicated by a lower δ_L because the results are absolute and separated per illuminant. The expected improvements were the highest for the halogen illuminant; moreover, camera 2 showed larger improvements than camera 1.

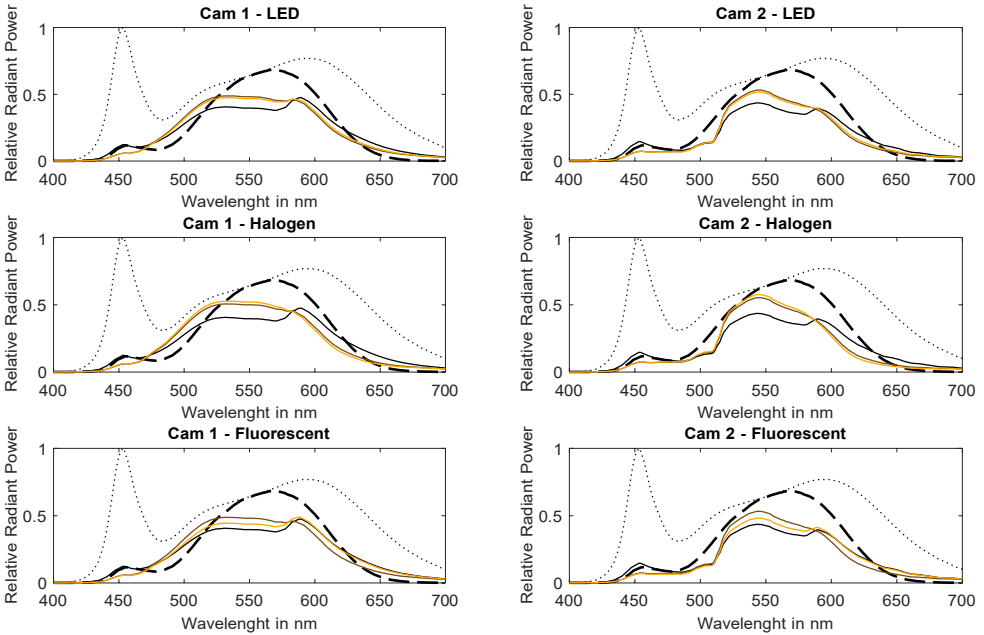


Figure 3.4: The relative spectral sensitivities weighted by the SPDs (dotted) the theoretical conventional method (black), criterion 1 (brown), criterion 2 (orange) and perfect $V(\lambda)$ match (dashed).

3.4.2 Measured Results

Based on the HDR images captured during the measurements, the luminance was determined for the conventional method and the optimizations. For the optimizations, the r, g, and b weighting factors were originating from the theoretical optimization presented in Table 3.3.

Figure 3.5 illustrates the relative difference in luminance (δ_L) for the two cameras

Table 3.3: Expected absolute results for Cam 1 and Cam 2, individually represented for the relative difference in luminance according to the conventional method ($\delta_{L,conv}$), criterion 1 (δ_{L,f_1^t}) and criterion 2 ($\delta_{L,RMS}$).

		$\delta_{L,conv}$	$r_{f_1^t}$	$g_{f_1^t}$	$b_{f_1^t}$	δ_{L,f_1^t}	r_{RMS}	g_{RMS}	b_{RMS}	$\delta_{L,RMS}$
Cam 1	LED	14.0%	0.12	0.88	0.00	12.2%	0.11	0.89	0.00	12.1%
	Halogen	7.2%	0.07	0.93	0.00	0.0%	0.00	1.00	0.00	5.0%
	Fluorescent	14.0%	0.11	0.89	0.00	10.7%	0.10	0.90	0.00	10.5%
	Average	11.6%	0.10	0.90	0.00	7.6%	0.07	0.93	0.00	9.2%
Cam 2	LED	12.1%	0.09	0.91	0.00	7.8%	0.12	0.88	0.00	8.3%
	Halogen	10.3%	0.05	0.95	0.00	4.0%	0.01	0.99	0.00	1.0%
	Fluorescent	11.9%	0.09	0.91	0.00	6.6%	0.18	0.82	0.00	9.3%
	Average	11.3%	0.08	0.92	0.00	6.1%	0.10	0.90	0.00	6.2%

compared to the point luminance measurements conducted with the Konica Minolta LS-100. Additionally, the absolute luminances measured with the Konica Minolta LS-100 are displayed. Figure 3.5 shows that the relative difference in performance between the three different methods was relatively constant for the 10 samples. Only camera 2 exhibited substantial differences in performance between samples under the fluorescent illuminant. Moreover, the relative differences found between illuminants and cameras were substantially different. Both luminance cameras exhibited the lowest performance for the halogen illuminant; furthermore, the optimizations even

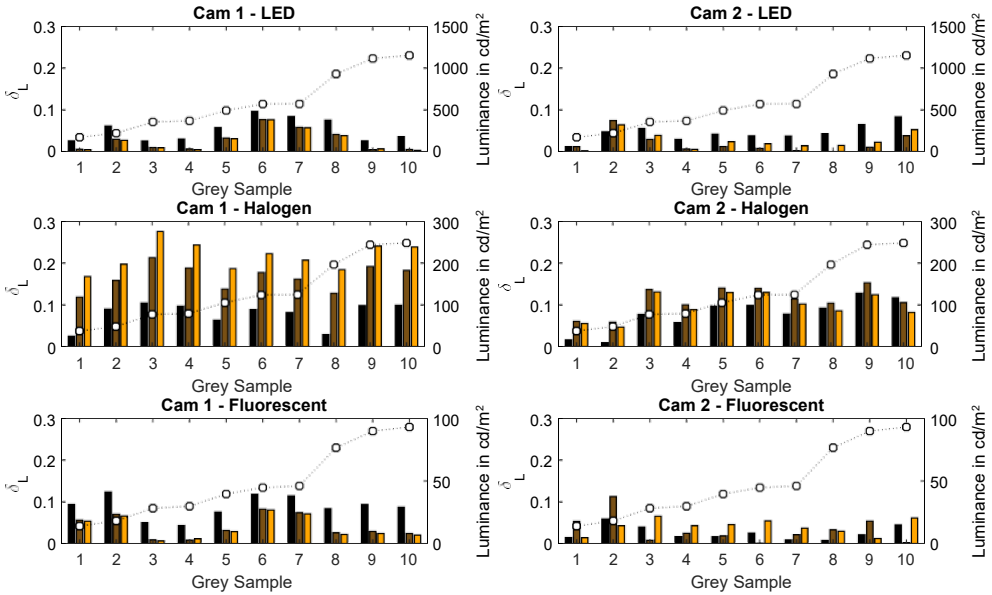


Figure 3.5: The relative difference in luminance from camera-based luminance measurements compared to point luminance measurements for the conventional method (black), criterion 1 (brown) and criterion 2 (orange). Results are averaged based on the three different measurement orientations and ranked according to the spectral reflectance (low to high).

3.4. Results

had a negative effect on the relative difference in luminance for the halogen illuminant compared to the conventional method. The other illuminants, except the fluorescent illuminant for camera 2, show an improved performance.

The average performance of the optimizations for the respective illuminants and cameras, with error bars representing the standard deviation, is shown in Figure 3.6. It shows that the results for the LED and fluorescent illuminants, for both cameras, were rather similar. A small improvement of δ_L was achieved for both optimizations relative to the conventional method. However, for the halogen illuminant, the difference was higher and in the opposite direction. As a result, the average results for camera 1 and 2 did not show an improvement because the improvement of the LED and fluorescent illuminant was compensated by the deterioration under the halogen illuminant. The results between camera 1 and camera 2 were relatively analogous with the exception that for camera 1 the optimization according to criterion 1 was generally having a more pronounced effect, where for camera 2 the optimization according to criterion 2 was more pronounced.

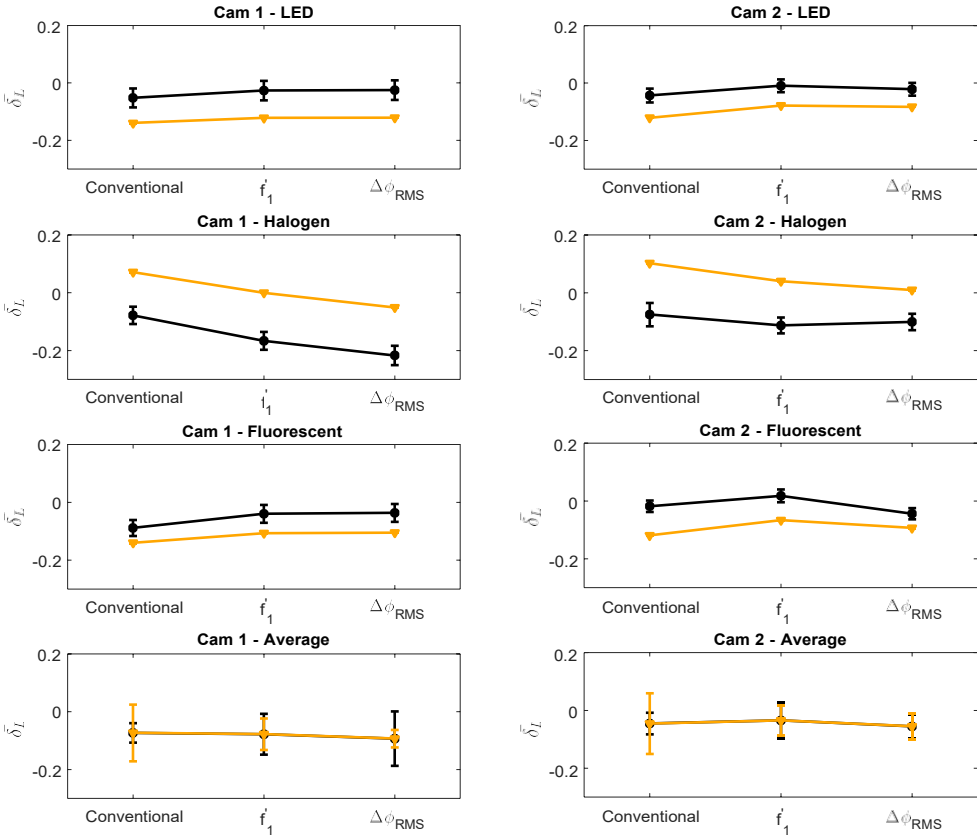


Figure 3.6: Error bar plots of the average δ_L separated by illuminant and camera. The error bars represent the standard deviation. The black error bars represent the measured results and the orange error bars represent the expected results

3.4.3 Comparison

Based on the theoretical method introduced in Section 3.2 we were able to formulate expectations of our measurement results. However, the expected results, as indicated in Figure 3.6, did not exactly match the measured results. Based on a t-test, it was also found that the measured δ_L for all samples (illuminants, cameras and methods) were significantly different ($p < 0.001$) compared to the expectations. Nevertheless, the trend between the measured and the expected values were very much alike, almost as if a shift in relative differences was enforced. To elaborate on these trends, the relative differences between the conventional method and the two optimization criteria were further illustrated in Figure 3.7. Figure 3.7 maintains the hypothesis that the trend between the expected and measured performance was much alike. However, for Cam 2 some larger differences were found for the halogen and fluorescent illuminants. The majority of the measured relative differences were visually similar to the expected relative differences (Figure 3.7). However, a t-test showed that all measured differences were significantly different ($p < 0.001$) from the expectations.

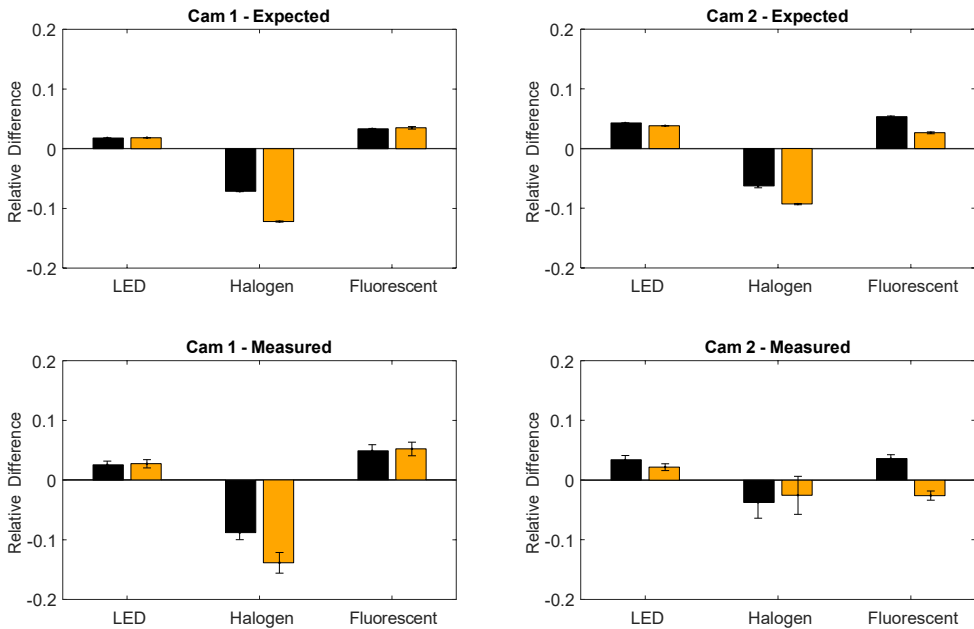


Figure 3.7: The relative difference in luminance between the conventional method and optimizations, criterion 1 (black) and 2 (orange), respectively, according to the theoretical model and measurements. The error bars represent the standard deviation.

Additionally, Table 3.3 showed that the optimizations according to criterion 1 and criterion 2 were expected to have an improved performance compared to the conventional method, as indicated by a lower δ_L . Therefore, a t-test was applied to evaluate whether criterion 1 and 2 had a significant lower measured δ_L for the three illuminants and two cameras compared to the conventional method. The p-values in Table 3.4 show that both optimizations for the LED illuminant performed significantly better than the conventional method. Similarly, the improvements thanks to the optimizations for the fluorescent illuminant were significant for Cam 1.

3.4. Results

Table 3.4: P-values of a one-sided t-test ($X - Y < 0$) with X as the conventional method and Y as criterion n as measured in the lightbox with a confidence interval of 95%.

		LED	Halogen	Fluorescent
Cam 1	Criterion 1	< 0.001	1.00	< 0.001
	Criterion 2	< 0.001	1.00	< 0.001
Cam 2	Criterion 1	< 0.001	1.00	0.49
	Criterion 1	< 0.001	1.00	1.00

Using an alternative approach, the differences between optimization methods and the conventional method were analyzed using Lin's Concordance Correlation Coefficient and the result is presented in Figure 3.8. Nearly all combinations had an almost perfect (< 0.99) agreement with the reference measurement. However, only a substantial ($< 0.95 - 0.99$) agreement was achieved for all conventional methods for camera 1 and all measurements with the halogen illuminant. A t-test was implemented to test whether the correlation (ρ_c) was significantly higher for the optimizations according to criterion 1 and 2 than for the conventional method. To conduct this test, normally distributed data (truncated to 0.1) was generated with ρ_c as mean and the standard deviation based on the confidence interval. Based on the p-values in Table 3.5 it can be concluded, for Cam 1, that both criteria 1 and 2 for the LED and fluorescent illuminants performed better than the conventional method, similar as found in Table 3.4. Again, this was not the case for the halogen illuminant. Contrary to Cam 1, the results in Table 3.5 for Cam 2 were not identical to the results found in Table 3.4. The correlation of criterion 1 under the fluorescent illuminant and of criterion 2 under the halogen illuminant were significant better than the conventional method, whilst Table 3.4 did not find a significant difference.

Table 3.5: P-values of a one-sided t-test ($X - Y > 0$) with X as ρ_c originating from the conventional method and Y as ρ_c originating from criteria n with a confidence interval of 95%.

		LED	Halogen	Fluorescent
Cam 1	Criterion 1	< 0.001	1.00	< 0.001
	Criterion 2	< 0.001	1.00	< 0.001
Cam 2	Criterion 1	< 0.001	0.999	< 0.001
	Criterion 1	< 0.001	0.035	1.00

For a majority of cases, the two optimization criteria provided similar results indicating that one of the two might be redundant. However, a t-test (Table 3.6) showed that δ_L of criterion 1 and criterion 2 were significantly different except for the samples measured under the LED illuminant.

Similar differences were found for the Concordance Correlation Coefficients between criteria 1 and 2 using a t-test as shown in Table 3.7. However, in contrast to Table 3.6, the difference for camera 2 under the LED illuminant was also significant.

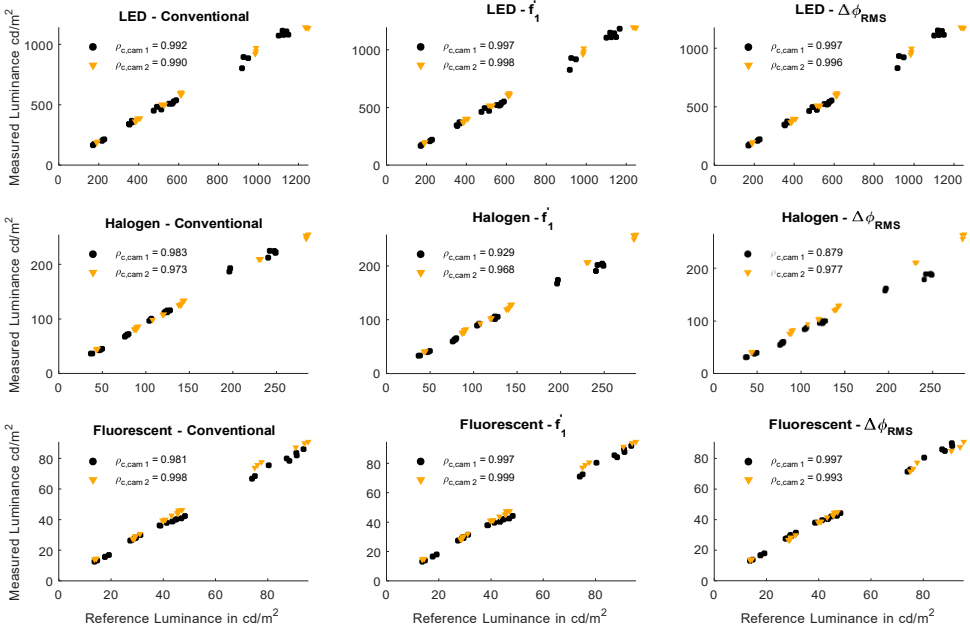


Figure 3.8: Lin’s concordance correlation coefficient of cameras 1 and 2 relative to the three illuminants and the conventional method, criterion 1 and criterion 2.

Table 3.6: P-values of a two-sided t-test ($X - Y \neq 0$) with X as δ_L for criteria 1 and Y as δ_L for criteria 2 with a confidence interval of 95%.

	LED	Halogen	Fluorescent
Cam 1	0.104	< 0.001	< 0.001
Cam 1	0.073	< 0.001	0.005

Table 3.7: P-values of a two-sided t-test ($X - Y \neq 0$) with X as ρ_c originating from criteria 1 and Y as ρ_c originating from criteria 2 with a confidence interval of 95%.

	LED	Halogen	Fluorescent
Cam 1	0.391	< 0.001	0.033
Cam 1	< 0.001	< 0.001	< 0.001

3.5 Discussion

This chapter showed that image-based luminance distribution measurements can be improved by optimizing the r, g, and b weighting coefficients based on the camera’s spectral responsivity and the SPD of the respective illuminant. It was hypothesized that both these aspects could improve the accuracy of the luminance distribution relative to the conventional method. This was tested using a theoretical model and validated with empirical data originating from the measurements.

The results of the theoretical model showed that the conventional method introduces significant spectral mismatches up to approximately 40% (Table 3.2), as was

3.5. Discussion

also indicated by Wu et al.[140]. The DIN 5032 Part 7 [177] distinguishes four performance categories, classes L, A, B, and C, for the General Spectral $V(\lambda)$ Mismatch. The maximum f_1^+ index for each class is 1.0%, 1.5%, 3.0%, and 5.0%, respectively, emphasizing the significance of a mismatch of 40%. As a result, the relative difference in luminance, found for the conventional method, can also be considered significant. However, on average, the optimizations did not always improve the relative difference in luminance, as indicated in Table 3.2, but a small increase in the spectral match was achieved. This is because these optimizations were bound to the fixed spectral responsivities $R(\lambda)$, $G(\lambda)$ and $B(\lambda)$, which sets limitations to the optimizations.

However, the results, per illuminant shown in Table 3.3, showed that the optimized r, g, and b weighting factors based on the SPD improved the accuracy as was hypothesized. In correspondence with Geisler-Moroder and Dür [172] the relative error, for the theoretical model, was generally higher than 5%. Table 3.3 also shows that for these specific cameras the B channel was not required because especially the G channels show large similarities to the $V(\lambda)$. Nevertheless, this match is far from perfect, therefore, it is corrected by the R channel as the peak of the G channels are below 555 nm. Additionally, energy in the blue area, which has relatively little relevance for $V(\lambda)$, is still captured due to the large overlaps between the spectral responsivities of the G and B channels. Thus, making the correction even suitable for a high blue content illuminants such as daylight. Moreover, substantial differences were found between the different optimization criteria, depending on the camera and illuminant. Nevertheless, both criteria perform better than the conventional method. It was found that criterion 1 is a robust optimization as indicated by less variation in r, g, and b weighting factors, while criterion 2 generated less spread in the relative difference in luminance.

The measurement results also showed differences between the two cameras. For instance, Cam 2 had lower relative differences in luminance compared to Cam 1, for the conventional method. This indicated that the spectral mismatch of Cam 2 was lower than Cam 1, as shown by the results of the theoretical model (37% to 43%, Table 3.2). Apparently, the spectral responsivity of Cam 2 was more similar to sRGB responsivity than Cam 1; nevertheless, the errors that were introduced are still substantial. During the optimizations, incorporating the spectral responsivity of the camera, lower spectral mismatches were achieved, always resulting in improved accuracies. The lowest spectral mismatch corresponds to the highest performance (Table 3.2). Hence, there is strong evidence that the conventional method introduces spectral mismatches at the expense of the measurement accuracy.

The measurement results showed that the performance of Cam 1 and Cam 2 under the LED and fluorescent illuminant were significantly improved for both illuminants (Table 3.4), except for Cam 2 under the fluorescent illuminant using optimization criterion 2, likely due to measurement noise amplified by the narrow bandwidth of the fluorescent SPD. Moreover, Table 3.4 also indicates that the optimizations could not improve the performance of both cameras under the halogen illuminant, it even resulted in a decreased performance. However, for the halogen illuminant this can be explained by methodological issues, described later in this section. In contrast to the theoretical model, there is only limited evidence to acknowledge that the SPD has an effect on the optimal r, g and b weighting factors.

Also, the measurement results, shown in Figure 3.5, showed some differences between criterion 1 and 2, albeit smaller than in the theoretical model. Nevertheless,

the differences were generally significant (Table 3.6). These relative differences are in correspondence to Fliegel and Havlin (10%) [174], but significantly higher than found by Cauwerts et al.[173] who used DSLRs and an extensive calibration process. For Cam 1, criterion 1 seems to perform slightly better, aside from the halogen illuminant, while for Cam 2 criterion 2 seems to perform better.

Both the theoretical model and the empirical data provided some evidence that both hypotheses can be accepted. However, the relative differences in luminance for these two approaches differed significantly (Table 3.4), against expectation. Visually (Figure 3.6), the trends of improvement look rather similar for the theoretical and practical method, indicating that the relative difference in luminance was shifted, for instance, due to the calibration factors applied to the empirical data. However, inferential statistics showed that the trend was significantly different as well (Figure 3.7). There are a number of potential explanations for the differences between the two methodologies, both at the theoretical side as well as at the practical side.

The model on which the expected results were based is a simplified model that does not account for the image pipeline. During this image pipeline, multiple corrections are introduced such as demosaicing, gamma correction, and color transformation to achieve a visually pleasing image. During the HDR building process, these corrections are partly corrected by the camera response curve. However, the camera response curve was in this case, and also typically, approximated using the algorithm by Mitsunaga and Nayar [147] using *hdrgen*. Approximation errors in this function can lead to both a decrease or increase relative to the expected results. Moreover, the cameras exhibited noise that might have compromised the accuracy which was not accounted for in the theoretical model. For the theoretical model, the spectral responsivities of Cam 1 and Cam 2 (Figure 3.1) were taken from the specifications sheets [175]. The spectral responsivities of Cam 1 [178] and Cam 2 [146] were also measured, by third parties, using monochromators. Some differences can be found, mainly around 700 nm the responsivities from the specifications sheets are much higher. This might be caused by inconsistencies between cameras of the same manufacturing and model. For this exact reason, in best practice, the camera response curve is determined for each individual sensor [49]. However, this might also be caused by a potentially applied infrared filter, which seems not present in the specification sheets. This can explain why large differences were found between the theoretical model and empirical data, especially for the halogen illuminant that had a lot of energy in this area. Due to the assumed high spectral responsivity in the red area, low weighting factors were applied for the R channel. In the case of an infrared filter, this leads to an underestimation of the red light, which is, in fact, exhibited for the underestimated halogen in Figure 6. Therefore, we can conclude that the contradicting results for the halogen illuminant are caused by the inconsistent input instead of an inadequate optimization algorithm. After all, the theoretical model (Table 3.3) showed improvements for all illuminants. Consequently, when possible, it is advised to measure the spectral responsivity of the camera instead of using the specification sheets.

Moreover, due to practical reasons, the measurements could not exactly replicate the theoretical model. Instead of direct measurements of the illuminant, indirect measurements, using 10 different grey samples, were applied, introducing a spectral responsivity that was not always perfectly uniform. These indirect measurements were chosen because direct measurements of the illuminant led to luminance values

3.5. Discussion

that were too high to capture using luminance cameras. Additionally, light sources are not completely uniform. As a result, it was not possible to compare the absolute luminance values of the theoretical model with the measured luminance; nevertheless, the relative difference in luminance could be compared. Grey targets were used to disrupt the SPD of the illuminant as little as possible. For instance, using colored targets would add an additional level of complexity, as this would also introduce the spectral reflectance, which is also variable over the space, next to the spectral responsivity and the SPD of the illuminant. Moreover, the reference luminance measurements using the Konica Minolta LS-100 had an uncertainty of $\pm 2\%$, according to the specifications, which might have caused these differences.

Additionally, a photometric calibration factor was applied to the empirical data to limit the inaccuracies introduced in the hardware. It was found that the calibration factor, besides the average luminance, also influenced the standard deviation of the relative luminance. Therefore, it can be concluded that this calibration factor had a large effect on the measurement results. The calibration factor can be determined in multiple ways. In this research, it was chosen to calibrate the luminance cameras, for all methods, such that the average relative difference in luminance was similar to the expected relative difference in luminance. This allowed us to examine the relative differences in luminance and its trends for each individual illuminant.

Even though this study aimed to answer the fundamental questions whether the spectral responsivity and the SPD of the illuminant should be integrated in the luminance distribution measurement, the practical aspects should not be neglected. It can be argued that instead of optimizing the r, g, and b weighting factor, the easy solution would be to apply a calibration factor to each individual camera, similar to the work performed by Jung and Inanici [179], and/or the illuminant, especially for *ad hoc* measurements. However, this requires an additional measurement device to take the calibration measurements when the conditions change. This is a consideration for the end user, related to the desired accuracy. The optimizations stated in this research could be implemented and automated on the luminance camera, the only requirement is that the spectral responsivity of the camera is measured once, or extracted from databases [180], and that information is acquired about the SPD. We envision that such a system can be used during long-term measurements such as conducted in Chapter 8 and/or in lighting control systems as illustrated in Chapter 9. This means that the luminance camera has a fixed position, which would generally mean that there is one fixed SPD, the luminaires, with the addition of a variable daylight SPD. To account for these SPDs, some measurements are required, but these are not more extensive than general commissioning. Also, a number of studies have already proven that it is possible to estimate the illuminant based on camera readings [181, 182, 183]. Alternatively, one could choose to only implement the spectral responsivity of the camera, which is proven to improve the accuracy [173]. Moreover, these optimizations have a physical basis where a photometric calibration only corrects faulty measurements. Ultimately, a combination of both would achieve the highest accuracy because the optimizations are also not able to achieve a perfect spectral match. Another possibility is to improve the spectral match by applying an optical filter, which has proven that low spectral mismatches can be achieved [140, 170], which are not feasible with the digital corrections presented in this study.

3.6 Conclusion

The theoretical model and the empirical data showed that the spectral responsivity of a camera had an impact on the accuracy of the luminance measurement. Therefore, it can be concluded that the r, g and b weighting factors originating from the sRGB color space can lead to significant mismatches; however, these mismatches can be of different scale depending on the camera and its spectral responsivity.

Moreover, we found substantial evidence that the SPD had an influence on the accuracy of the luminance distribution. Generally, the r, g, and b weighting factors originating from an optimization including the SPD led to an improved performance. Only the measurements under the halogen illuminant resulted in a decreased performance; however, this was caused by inaccuracies in the applied spectral responsivities of the camera close to 700 nm, which did not contain an infrared filter. Nevertheless, the optimization algorithms in this study seem to work. After all, the theoretical model showed improvements for all illuminants.

Two optimization criteria were developed that performed significantly different, incorporating the spectral responsivity and the SPD, however, criterion 1 performed better on average. Nevertheless, it could not be concluded which criterion was most suitable for what situation.

For further assessment, it is recommended to generalize these conclusions by performing similar measurements with and without daylight (high blue content) using different cameras that have a significantly different spectral responsivity (Chapter 4), allowing different scales of potential improvement. Also, a different approach should be developed to improve the theoretical model such that cameras can be analysed quickly and on a large scale.

Implementation of these optimizations can be complex, especially implementing the effect of the illuminant can be complicated. For long-term measurements it is relevant to implement the spectral responsivity of the camera and/or the SPD of the illuminant because these conditions do not allow to perform a photometric calibration for each individual measurement. Ultimately, the end user needs to make the consideration what method to use. However, for *ad hoc* measurements it might be more practical to use the conventional method with an additional photometric calibration.

HDR for luminance and melanopic radiance: cameras and SPDs

This Chapter is based on:

Kruisselbrink TW, Dangel R, van Loenen EJ. HDR IMAGING FOR LUMI-NANCE AND MELANOPIIC RADIANCE: CAMERAS AND SPECTRAL POWER DISTRIBUTIONS. In: Proceedings of the 5th CIE Symposium on Colour and Visual Appearance. CIE; 2020.

4.1 Introduction

The luminance distribution, relevant for high quality lighting (Chapter 1), can be measured using camera-based systems as indicated in Chapter 2. Nevertheless, the accuracy and applicability of these camera systems can still be improved. Chapter 3 showed that fixed r , g , and b weighting factors to calculate the luminance, according to the conventional method, can have a negative impact on the measurement accuracy as they can introduce significant spectral mismatches due to its underlying assumptions. As a result, different cameras, with different spectral responsivities, might perform differently in terms of luminance distribution measurements.

Moreover, the applicability of luminance cameras can be extended by measuring other spectral sensitivities such as α -opic radiances that are found to be relevant for the Non-Image Forming (NIF) effects of light [184]. Especially, the melanopic radiance, impacting the melanopsin containing intrinsically photosensitive retinal ganglion cells (ipRGCs) can be considered important as this results in biological and behavioural effects of light [18]. However, the integration process of the different α -opic radiances is not understood completely yet. Therefore, it is recommended to provide all α -opic quantities ($n = 5$). This system is currently also adopted by the CIE [184].

The objective of this chapter is to model the performance of six different cameras in relation to luminance measurements using HDR imaging. Moreover, we explore to what extent the accuracy of each camera can be improved by using an alternative luminance model, incorporating the spectral responsivity and the SPD as introduced in Chapter 3. To improve the applicability of these camera-based systems, for human centric lighting applications, the alternative model was also applied to explore the feasibility of measuring α -opic radiances using HDR imaging. In this study, only the melanopic radiance was assessed using the six different cameras as a proof of principle.

4.2 Methodology

Six commercially available cameras were selected, ranging from high-end Digital Single Lens Reflex-cameras (DSLRs) to simple smartphone cameras with, visually, significantly different spectral responsivities. Their spectral responsivities were selected from 400 nm to 700 nm with steps of 10 nm. The green and blue channels of the cameras are illustrated in Figure 4.1. Cameras 1, 2, 3, and 6 represent DSLRs, Cam 4 represents a mobile phone camera and Cam 5 represents a point and shoot camera. The spectral responsivities originate from a database by Jiang et al. [180] and were measured with a PR-655 spectrometer (± 1 nm, 2%) in combination with an integrating sphere and monochromator. The spectral responsivities of HDR images were considered identical to the cameras' raw spectral responsivity [167]. Additionally, 205 SPDs, as illustrated in Figure 4.2, of light sources that are commercially available were collected, containing LEDs (117), fluorescents (35), incandescent (17), halogens (31), metal halides (4) and sodium pressure lamps (1) from 300 nm to 900 nm with steps of 0.5 nm originating from the Lamp Spectral Power Distribution Database (LSPDD) by Roby and Aubé [185].

The luminance, considering one single pixel, was calculated based on simulations,

4.2. Methodology

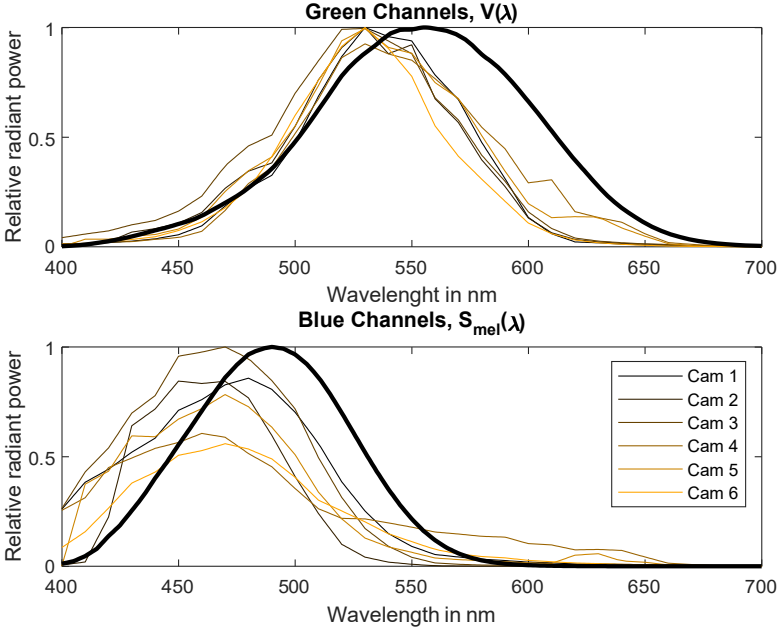


Figure 4.1: The spectral responsivities of the green and blue channels of the 6 cameras. Additionally, the photopic action spectrum $V(\lambda)$ and the melanopic action spectrum $S_{mel}(\lambda)$ are illustrated in black.

using MATLAB r2017a, for all 205 SPDs using the spectral responsivities of the six cameras and two distinct luminance models that were proposed in Chapter 3. These models were used to determine the weighting factors of the R, G, and B tristimuli according to the conventional (Section 3.2.1) and a spectral mismatch indicator (f_1^t) optimization (Section 3.2.2). The latter method is a camera and SPD dependent optimization incorporating the effect of the camera’s spectral responsivity as well as the SPD of the light source.

In the conventional method, the luminance (L) was calculated using a linear combination of the R, G, and B coefficients using fixed weighting factors in order to approximate the photopic luminous efficiency curve $V(\lambda)$ according to Equation 2.3. The linear combination was based on the transformation of the sRGB color space to the XYZ color space applying “reference primaries, CIE standard illuminant D65, and standard CIE Colorimetric Observer with 2° field of view” [49].

The alternative luminance model, applied in this chapter, was based on the General $V(\lambda)$ Mismatch Index f_1^t [168], generally used to indicate the spectral properties for general photometric measurements. The metric was applied because a single pixel of a luminance camera can be considered a photometer. The inputs for this metric were the $V(\lambda)$ and the spectral responsivities as illustrated in Figure 4.1. Moreover, instead of Standard Illuminant D65, the 205 SPDs served as input to determine the most suitable weighting factors for the R, G and B Channels for each individual SPD according to Equations 3.1 to 3.5. Subsequently, the weighting factors that were found were applied analogous to the conventional method.

The optimizations resulted in weighting factors for the R, G, and B channel for

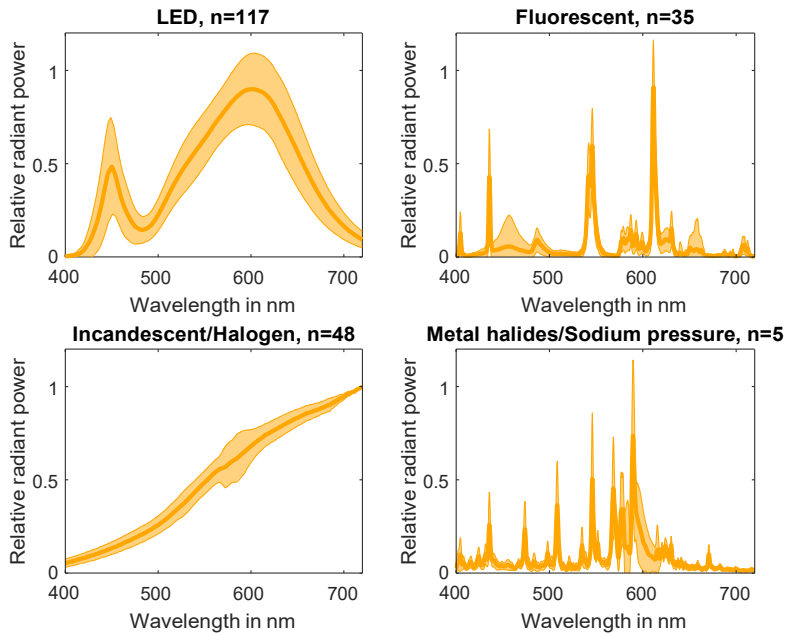


Figure 4.2: Average SPDs originating from Lamp Spectral Power Distribution Database [185]. The shaded area represents the standard deviation.

each individual camera and SPD. The measurement error (δ_L) between the approximated luminance using the simulated cameras and the actual luminance (perfect $V(\lambda)$ match), similar to Equation 3.10, was assessed based on the Correlated Color Temperature (CCT) and the Full Spectrum Index (FSI), which are both one-dimensional indicators of the SPD that were expected to have an effect on the luminance calculation performance.

The CCT, the temperature of a Planckian radiator associated with the chromaticity of the SPD, was calculated according to the method by Hohm and Krochmann [186]. For 7 SPDs, the CCT could not be calculated because the distance to the Plackian locus was disproportionate, therefore, these SPDs were not considered for the respective analyses. The FSI [187] is a metric that indicates how much an SPD differs from an equal energy spectrum, which was deemed relevant to indicate the continuity of the SPD. The FSI was calculated based on the sum of squared deviations between the cumulative SPD and cumulative equal energy spectrum. An FSI of 0 represents an equal energy spectrum, bigger FSI values are associated with non-continuous, or peaky, SPDs.

4.3 Results

In this section, the simulation results according to the conventional model and the alternative, spectral mismatch based, model for luminance and for melanopic radiance measurements are displayed.

4.3.1 Conventional method

The conventional model to calculate the luminance using cameras introduced large deviations as is illustrated in Table 4.1. Spectral mismatches up to 46% were found, which can be considered very large as the lowest DIN classification for luminance meters is below 5% [177]. Moreover, large differences were found for the measurement error (δ_L); both the mean as the standard deviation exhibit large differences. High spectral mismatches align with high average (and standard deviation) measurement errors. Based on the results, it is likely that the spectral responsivity of camera 4 has the most similarities with the sRGB responsivity as it performs relatively well. The expensive DSLRs had the lowest performance.

Table 4.1: Average spectral mismatch and average, non-absolute, luminance measurement error for camera 1 to 6 according to the conventional model. The standard deviations are illustrated between brackets.

	f_1^c	δ_L
Cam 1	40.8% (4.1%)	-12.7% (8.0%)
Cam 2	39.8% (2.8%)	-13.0% (11.1%)
Cam 3	46.5% (3.2%)	-16.8% (11.1%)
Cam 4	17.0% (1.2%)	-3.6% (4.0%)
Cam 5	26.9% (1.1%)	-7.5% (6.6%)
Cam 6	42.2% (4.8%)	-13.7% (8.4%)

Figure 4.3 illustrates the absolute measurement error, as indicated in Table 4.1, relative to the CCT. In general, all cameras show a similar trend where high inaccuracies were introduced for low CCTs. The error decreases towards a CCT of 6500 K. This effect was mainly visible for cameras with high spectral mismatches, for cameras with relatively low spectral mismatches the dependency on the CCT, or SPD, was limited. The error decreased towards a CCT of 6500 K because this is the CCT of the standard illuminant applied in the conventional method. It is expected that for CCTs higher than 6500 K the errors will increase again. This indicates a dependency on the SPD when the conventional method is applied to calculate the luminance.

A similar analysis was conducted using the FSI as an indicator for the SPD (Figure 4.4). Again, a clear trend was found, showing a dependency on the SPD. Figure 4.4 illustrates that using the conventional method to calculate the luminance was more accurate for SPDs that have a full spectrum, such as an incandescent. On the other hand, it illustrates that it has more difficulties to measure SPDs that contain peaks such as fluorescent light sources. In contrast to Figure 4.3, this effect was also clearly visible for the cameras with a relatively low spectral mismatch, in these cases only the magnitude of the errors was lower compared to the others.

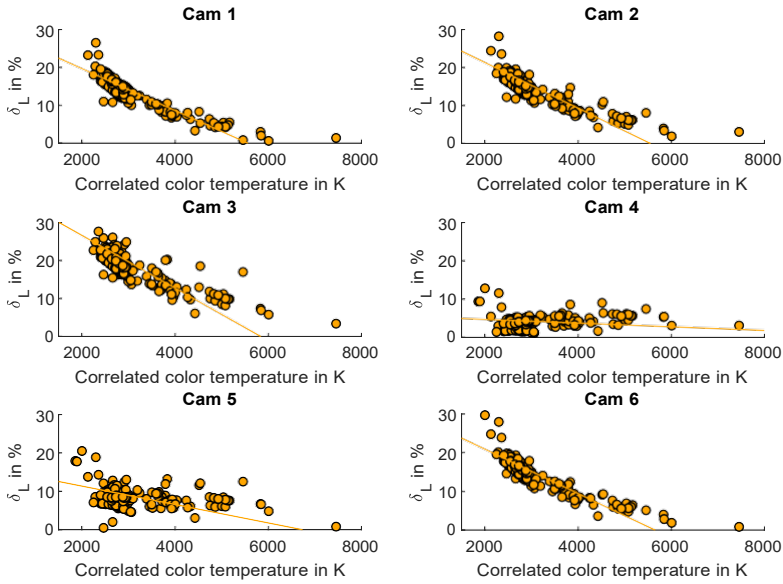


Figure 4.3: Relation between the correlated color temperature (CCT) and the absolute measurement error (δL) of the six luminance cameras according to the conventional method. A linear trend-line is indicated in orange.

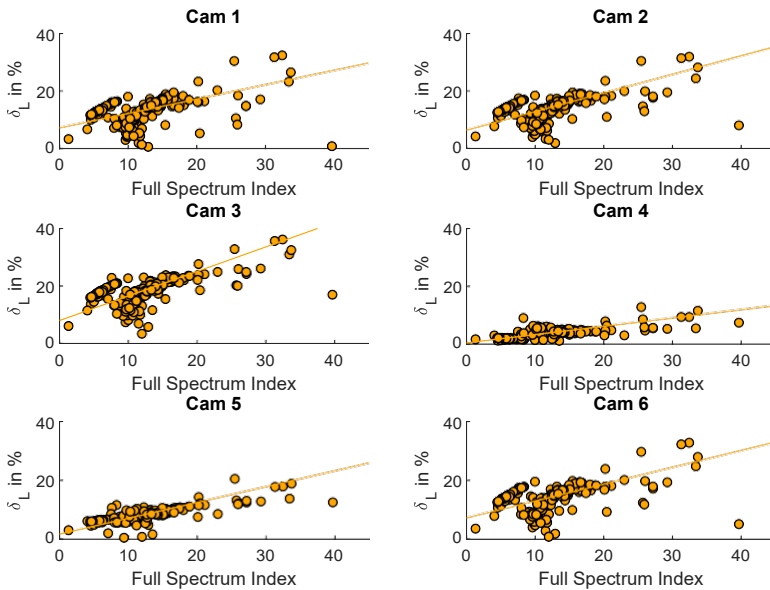


Figure 4.4: Relation between the full spectrum index (FSI) and the absolute measurement error (δL) of the luminance cameras according to the conventional method. A linear trend-line is indicated in orange.

4.3.2 Spectral mismatch optimization

Based on the optimized luminance calculation, according to the alternative model proposed in Chapter 3, the spectral mismatches and measurement errors have been reduced drastically, as is shown in Table 4.2. The maximum spectral mismatch has been reduced to approximately 20% compared to a spectral mismatch of 46% for the conventional method. Consequently, the average measurement error has been decreased to a maximum of approximately 6%. Especially, for camera 6 the optimization was fruitful. On the other hand, the performance for camera 4 did not show a significant improvement. Moreover, for this camera, the weighting factors for R, G, and B channels were relatively similar to the conventional method. For the other cameras, the weighting factors were largely different to the conventional method. First, the blue channel was generally not required as the information of the blue part of the spectrum was captured using the green channel. Moreover, a larger part of the camera's red channel was required because the maximum responsivity of the green channel was generally below 550 nm, which requires the red channel to compensate.

Table 4.2: Average r,g,b weighting factors, spectral mismatches and, non-absolute, luminance measurement errors for camera 1 to 6 according to alternative model. The standard deviations are illustrated between brackets.

	r	g	b	f_1^c	δ_L
Cam 1	0.52 (0.02)	0.48 (0.02)	0.00 (0.00)	17.7% (1.0%)	-1.8% (2.9%)
Cam 2	0.42 (0.02)	0.58 (0.02)	0.00 (0.00)	19.8% (0.8%)	-4.5% (3.7%)
Cam 3	0.46 (0.02)	0.54 (0.02)	0.00 (0.00)	20.8% (1.2%)	-5.6% (4.2%)
Cam 4	0.21 (0.01)	0.76 (0.04)	0.02 (0.00)	16.0% (0.3%)	-2.3% (1.8%)
Cam 5	0.28 (0.01)	0.72 (0.01)	0.00 (0.00)	20.9% (0.3%)	-2.8% (1.1%)
Cam 6	0.51 (0.01)	0.49 (0.01)	0.00 (0.00)	11.0% (0.8%)	-1.6% (2.3%)

Due to the optimization for each individual SPD, the dependency on the CCT was almost non-existing. Figure 4.5 illustrates that no clear pattern was occurring between the CCT and the measurement error. In contrast to the conventional method, the maximum absolute error was generally reduced to approximately 10% compared to a maximum error of >30% for the conventional method.

Figure 4.6 shows that, in contrast to the CCT, the optimization remained dependent on the FSI. The performance for full spectrum SPDs was still higher than for SPDs with peaks. Apparently, continuous SPDs were easier to match using only three channels of the cameras' responsivity. For peaky SPDs, the specific wavelengths might not be present in the cameras' spectral responsivity. Again, for high performing cameras, the dependency on the FSI decreases. A hypothetical camera with a perfect spectral match will show no dependency to the FSI or any performance indicator.

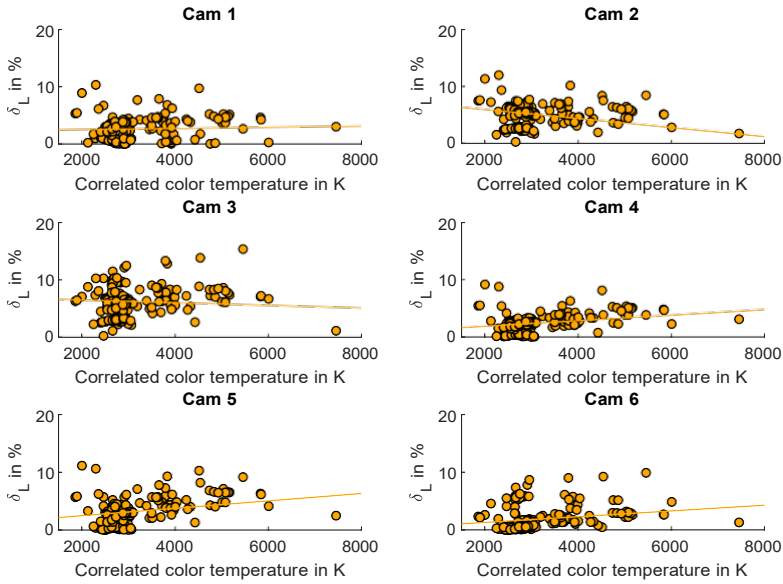


Figure 4.5: Relation between the correlated color temperature (CCT) and the absolute measurement error (δL) of the luminance cameras according to the alternative model. A linear trend-line is indicated in orange.

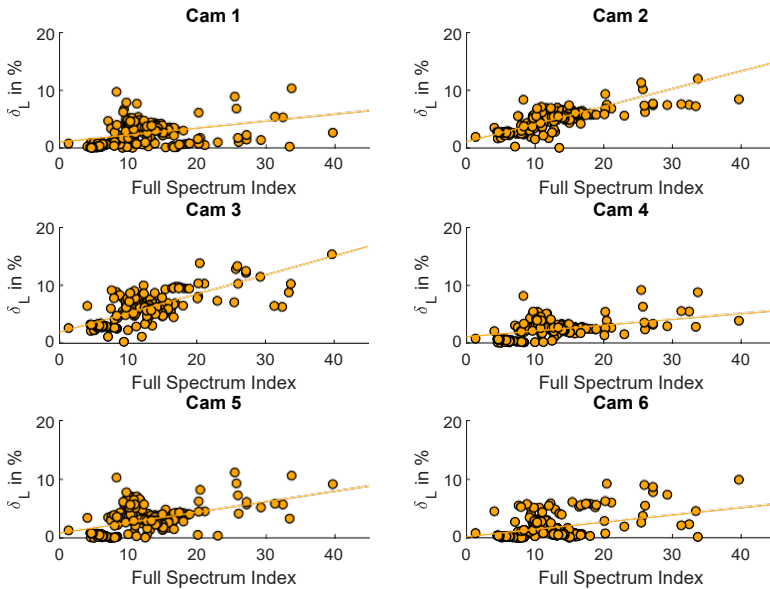


Figure 4.6: Relation between the full spectrum index (FSI) and the absolute measurement error (δL) of the luminance cameras according to the alternative model. A linear trend-line is indicated in orange.

4.3.3 Melanopic radiance

In the analysis, for the melanopic radiance, one single SPD was discarded as it contained one single peak at 650 nm, which was outside the melanopic sensitivity. As expected, the accuracy of the optimized luminance (Section 4.3.2) was not achieved. Table 4.3 gives an indication of the measurement capabilities of the cameras for the melanopic radiance. Cameras are, after all, developed for measurements that match our visual experience. Nevertheless, for some cameras the performance was better than for the conventional luminance measurements, although the variance between cameras was quite high. It shows that the capabilities were largely dependent on the spectral responsivity of the camera, for instance, camera 4 performed well for the conventional luminance measurement, but was not able to accurately measure the melanopic radiance. The DSLRs seem to be performing better. Similar to the optimized luminance, the melanopic radiance was generally measured with only two channels, in this case the red channel was not required. The blue channel was highly normative as this aligns relatively well with the melanopic sensitivity (Figure 4.1).

Table 4.3: Average r, g, and b weighting factors, spectral mismatches and, non-absolute, measurement errors for camera 1 to 6 for melanopic radiance measurements (δ_s). The standard deviations are illustrated between brackets.

	r	g	b	f_1^c	δ_s
Cam 1	0.00 (0.00)	0.12 (0.02)	0.88 (0.02)	33.6% (0.8%)	-3.1% (2.7%)
Cam 2	0.00 (0.00)	0.29 (0.03)	0.71 (0.03)	39.5% (1.0%)	11.1% (5.7%)
Cam 3	0.00 (0.00)	0.28 (0.03)	0.72 (0.03)	37.1% (1.0%)	1.9% (3.7%)
Cam 4	0.00 (0.00)	0.06 (0.03)	0.94 (0.03)	62.4% (2.0%)	20.0% (26.9%)
Cam 5	0.00 (0.00)	0.16 (0.03)	0.84 (0.03)	44.4% (1.0%)	4.2% (4.2%)
Cam 6	0.00 (0.00)	0.11 (0.03)	0.89 (0.03)	37.0% (1.7%)	6.4% (7.1%)

Figure 4.7 illustrates that for cameras that have large measurement errors (δ_s), there was some dependency on the CCT. Difficulties arise when the melanopic radiance was measured for SPDs with a low CCT. This error was introduced by the misalignment between the high amount of energy for longer wavelengths and the melanopic sensitivity for the lower wavelengths. The resulting measurement errors can be very high (>100% for camera 4, cropped out of Figure 4.7 for readability) but for others it was reasonable.

Again, Figure 4.8 illustrates an almost linear dependency on the FSI, which is much clearer for the low performing cameras. The melanopic radiance is more accurately measured for full spectra, similar to the finding in Section 4.3.2.

4.4 Discussion

The objective of this study was to assess the capabilities of six cameras to measure the luminance and melanopic radiance, based on simulations. Besides the conventional model to calculate the luminance, an alternative model, which was based on the General $V(\lambda)$ Mismatch Index, was used to assign the most suitable weighting factors for the R, G and B channels for luminance and melanopic radiance measurements.

The conventional model, to calculate the luminance, introduced significant av-

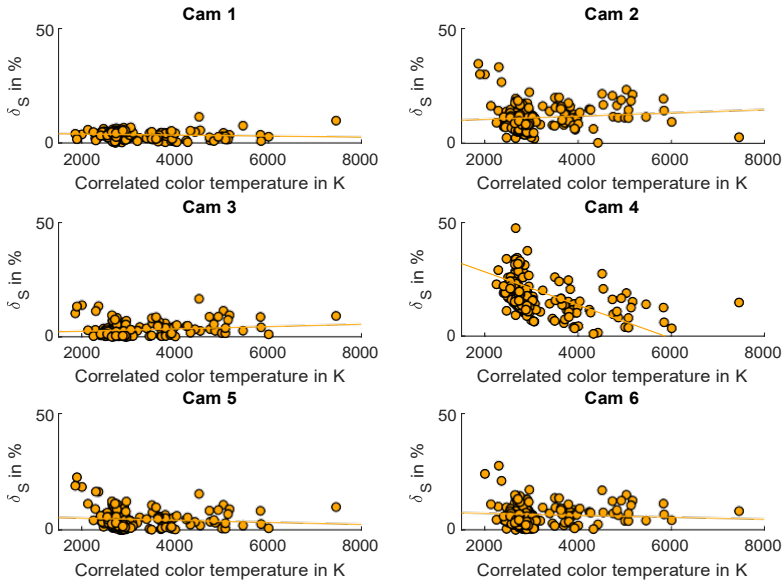


Figure 4.7: Relation between the correlated color temperature (CCT) and the absolute measurement error (δ_S) of the melanopic radiance measurement according to the alternative model. A linear trend-line is indicated in orange.

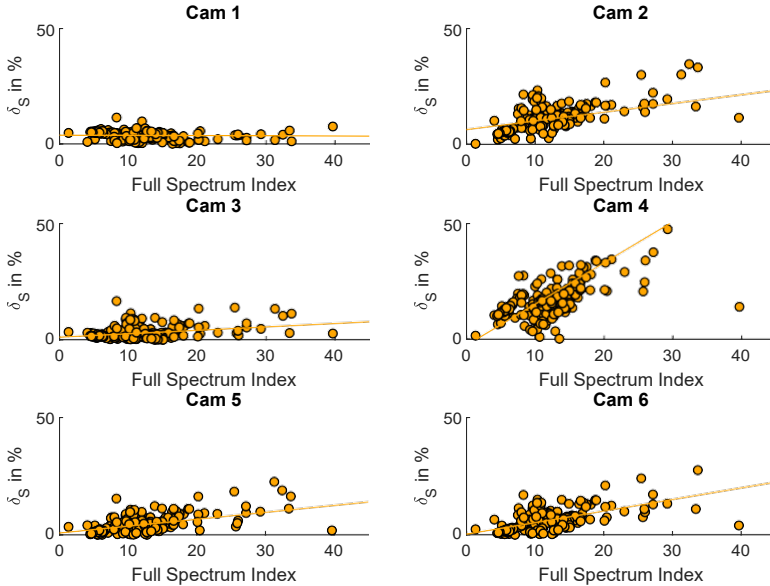


Figure 4.8: Relation between the full spectrum index (FSI) and the absolute measurement error (δ_S) of the melanopic radiance measurement according to the alternative model. A linear trend-line is indicated in orange. For readability, an outlier (>100%) was cropped out, for cam 4.

4.4. Discussion

average luminance measurement errors ranging from approximately 4% to 17%. In all cases, the alternative model was able to reduce the average measurement errors, ranging from approximately 2% to 6%, to a large extent. Additionally, some cameras were able to measure the melanopic radiance relatively accurately with average measurement errors below 5%. However, large differences were found between cameras, for instance, camera 4 was not able to provide accurate measurements (>20%).

This study indicated that luminance and melanopic radiance measurements are sensitive to the SPD of the light source because the CCT and the FSI were proven to influence the performance of the camera systems. The CCT, roughly indicating which wavelengths contained the most energy, affected the performance for measurements with the conventional model and the melanopic radiance measurement. For the conventional method, SPDs very different to standard illuminant D65 had a lower performance because the R, G, and B channels of the camera were combined such that a more bluish (6500 K) light source was measured accurately. For this reason, the blue channel determined approximately 7% of the luminance. This effect disappeared for the alternative model, because the weighting factors were specifically determined for each individual illuminant, resulting in almost no importance of the blue channel. Nevertheless, the standard deviation for the improved weighting factors was low, indicating that it is fairly safe to use the mean weighting factors instead of SPD dependent weightings (Table 4.2 and Table 4.3). For the melanopic radiance, low CCT light sources performed worse as they mainly contained energy in the reddish part of the SPD, while the melanopic sensitivity is sensitive to the blue part. As only three channels, in practice only two, were applied, the blue component could not be extracted exclusively. Consequently, also energy outside the melanopic range was captured, which reduced the performance.

As expected, the FSI showed that continuous SPDs were generally measured more accurately. Especially, very peaky SPDs did not perform well as the sensitivity of the cameras can be very low for these specific wavelengths. For continuous SPDs, the wavelengths with low sensitivity are easily accounted for by the wavelengths with high sensitivity.

Large differences were found between cameras, as their spectral responsivities differ. Consequently, their capabilities to capture the luminous or melanopic sensitivities vary. The differences for the optimized luminance measurements were limited as most cameras aim to achieve a visually pleasing image which results in high sensitivity, and overlap between the channels, for the range of the luminous sensitivity ($V(\lambda)$). Using the optimization, the most suitable combination between channels can be found, which differed significantly for the different cameras. The melanopic radiance showed the biggest differences between cameras as their spectral responsivity was generally low for the relevant wavelengths. Moreover, the blue channels were not aligned as well with the melanopic sensitivity as the green channels were aligned with the luminous sensitivity. On average, the expensive DSLRs seem to be able to achieve slightly higher accuracies when the spectral match is optimized.

When a low spectral mismatch is achieved, the dependency on the SPD is low. However, when the spectral mismatch is significant, which is often the case for these camera systems, then the SPD is relevant. For instance, the CCT and FSI of a SPD have a larger influence on low performing cameras as wavelengths outside the region of interest are captured as well.

4.5 Conclusion

Analogous to Chapter 3, this chapter showed that the conventional method to calculate the luminance can introduce significant errors depending on the spectral responsivity of the camera. It is therefore advised, to either pick a suitable camera, with a suitable spectral responsivity, and/or optimize the weighting factors for the R, G and B channels. However, the Blue channel seems to have no or limited relevance for luminance measurements. Consequently, the spectral mismatches can be reduced drastically, especially for continuous SPDs, reducing the sensitivity to variable conditions.

Moreover, it was shown that the melanopic radiance can be approximated by such camera systems. However, the applied camera has even higher importance, as some cameras are not able to achieve an acceptable spectral mismatch and differences between weighting factors for different SPDs were limited.

It is recommended to perform physical measurements to validate the results found. In this study, only simulations were conducted, which might not always be a correct impression of reality. For instance, the spectral responsivity of the cameras might be different in practice, which was exhibited in Chapter 3. Moreover, the imaging pipeline is more complex as illustrated in the applied models. Finally, 205 SPDs were applied that are commercially available. However, in practice the light source will have a mixed character containing daylight as well as an artificial light source.

Part II

Recommendations for continuous measurements of the luminance distribution

Chapter 5 provides insight into the spatial resolution required for accurate luminance distribution measurement. A reduced spatial resolution minimizes the privacy content because clear details cannot be distinguished anymore when the spatial resolution is sufficiently low. Moreover, a lower spatial resolution drastically reduces the computational costs associated with luminance distribution measurements.

Chapter 6 aims to recommend a suitable temporal resolution using Discrete Fourier Transform. Analogous to Chapter 5, the temporal resolution, or measurement interval, relates to privacy and computational costs as well. A high temporal resolution might allow undesirable tracking of people, while it also can cause a sheer amount of data. However, a low temporal resolution might miss out on relevant high frequency daylight variations, which cannot be reconstructed.

Chapter 7 proposes an alternative, ceiling-based, measurement position that limits interference with the office workers. In best practice, the luminance distribution is measured from eye level, which is unworkable for long term measurements. Moreover, eye level measurements, or measurements in the vicinity of the office worker, will cause interference and might capture privacy sensitive data.



HDR



The spatial resolution

This Chapter is based on:

Kruisselbrink TW, Dangol R, van Loenen EJ. Recommendations for long-term luminance distribution measurements: The spatial resolution. *Building and Environment*. 2020 169;106538. <https://doi.org/10.1016/j.buildenv.2019.106538>

5.1 Introduction

Luminance distribution measurement devices such as the Bee-Eye (Chapter 2) allow integration in lighting control systems that aim to provide high visual comfort and limit the energy use. In addition these devices can be used for long term field studies. However, this introduces additional practical issues, which argue for a lower spatial resolution of the luminance distribution, representing the horizontal and vertical width in pixels. Firstly, continuous high resolution HDR imaging can enable one to monitor individuals, hampering the application of such systems due to privacy concerns [188, 189]. Secondly, continuous high resolution HDR imaging requires significant computational resources, as the system has to transfer and analyze bulky pixel data, while low resolution HDR images might be sufficient to measure the luminance with an acceptable accuracy as discussed by Inanici [188].

As previously indicated, the spatial resolution of the HDR images has an increased significance for long term measurements of the luminance distribution, such as conducted in [190, 191, 192]. Nonetheless, the applied spatial resolution is often not specified in literature. Studies that specified the spatial resolution [146, 155, 161, 193, 194] generally use the maximum spatial resolution supported by the applied imaging sensor, even for long term measurements [193, 194]. In Chapter 2, a spatial resolution of 901 x 676 pixels was applied with an imaging sensor that supports resolutions up to 3280 x 2464 pixels, which was an consideration between file size and Tregenza's subdivision. Summarized, spatial resolutions found in the literature ranged from 320 x 240 [141] to 6000 x 4000 pixels [194] for measurement periods ranging from 2 weeks to a year.

A sufficiently low spatial resolution prevents face recognition and limits the ability to track persons and monitor their behavior. In this thesis, facial recognition is applied as an indicator for privacy sensitive data captured by luminance distribution measurement devices. Multiple studies have researched [195, 196, 197, 198] the threshold spatial resolution for automated face recognition, which ranged between face resolutions of 21 x 16 and 64 x 48 pixels. Below this threshold resolution, the ability to recognize faces decreases rapidly [199]. This threshold was determined from multiple algorithms such as principal component analysis (PCA), linear discriminant analysis (LDA) and elastic bunch graph matching (EBGM), while subjects faced the camera. Based on these studies [195, 196, 197, 198], Wang et al. [199] proposed to use 32 x 24 pixels, with an eye-to-eye distance of 10 pixels, as a threshold face resolution. It is expected that this threshold resolution is an overestimation, relative to the context researched in this thesis, because in real applications subjects are moving, not directly facing the camera, and image quality can be poor. Furthermore, HDR imaging for luminance distribution measurements often makes use of fisheye lenses to achieve extremely wide angles of view, adding additional distortions. However, to date, no further studies have been found in the literature that researched privacy sensitive information in HDR images.

Moreover, a low spatial resolution also limits the computational costs. Long term and continuous luminance distribution mapping can only be conducted autonomously as it is not feasible to perform each measurement manually. Both, in long term field studies and in lighting control systems, these measurements have to be managed by some, depending on the complexity (related to e.g. calculation method, luminance metric), intelligence. Preferably these kind of systems are integrated into a standalone

5.2. Methodology

system using a single-board computer [138], micro-controller [200], or microprocessor [201], often with limited computational resources. Therefore, it is desired to limit computational costs, such as the processing time and CPU usage. Especially in the case of bulky data such as high resolution luminance distributions it can be beneficial to reduce the spatial resolution.

The objective of this chapter is to limit the spatial resolution of HDR images for long term luminance distribution measurements without compromising the accuracy while minimizing the computational costs and the ability to recognize faces. High resolution luminance distribution measurements were conducted in a mock-up office using three Bee-Eyes (Chapter 2). Based on these measurements, scaled data sets were constructed with decreasing spatial resolutions. Subsequently, the performance of the scaled spatial resolutions was compared with the initial high resolution measurements. To be able to further generalize the findings, this process is repeated in a real living office environment collectively having large similarities with the majority of existing office environments. Finally, the performance of the HDR images with reduced resolutions were related to the face recognition threshold resolution and the processing time, to develop spatial resolution recommendations for long term, continuous, luminance distribution measurements in office environments.

5.2 Methodology

5.2.1 Measurement device

In this study, all measurements were conducted with three identical Bee-Eyes, having a Cortex-A53 (1.4 GHz, quad-core) processor, as developed in Chapter 2. The first measurement track as illustrated in Figure 2.9 was utilized. Due to the fixed aspect ratio (4:3) and the fisheye lens two strips of approximately 350 pixels, left and right, were ineffective in the original spatial resolution of 3280 x 2464 pixels. The luminance was calculated according the conventional method where the R, G and B floating point values of the HDR images are translated to CIE XYZ color space according to Equation 2.3, which resulted in an approximated spectral $V(\lambda)$ mismatch f_1^t of 43% (Chapter 3). Due to this significant spectral mismatch, the photometric calibration factor k was determined in advance using reference spot measurements with a Konica Minolta LS 100 of a grey ($\rho = 0.18$) and white ($\rho = 0.90$) card for LED lighting only, to reduce the aforementioned measurement error [166].

5.2.2 Lab study

High resolution luminance distribution measurements were conducted in a mock-up office environment at the Building Physics and Services laboratory at Eindhoven University of Technology, between 12-11-2018 and 25-12-2018. The mock-up office measuring 5 m x 5.5 m was oriented west and consisted of four workplaces, containing a desk and a monitor (turned off), as illustrated in Figure 5.1. Measurements were performed during morning periods (8:30 – 12:00) and afternoon periods (13:00 – 16:30) at an interval of ten minutes for two days with clear sky conditions, two days with intermediate sky conditions, and two days with overcast sky conditions. For each weather type one day was measured with and without the electric lighting

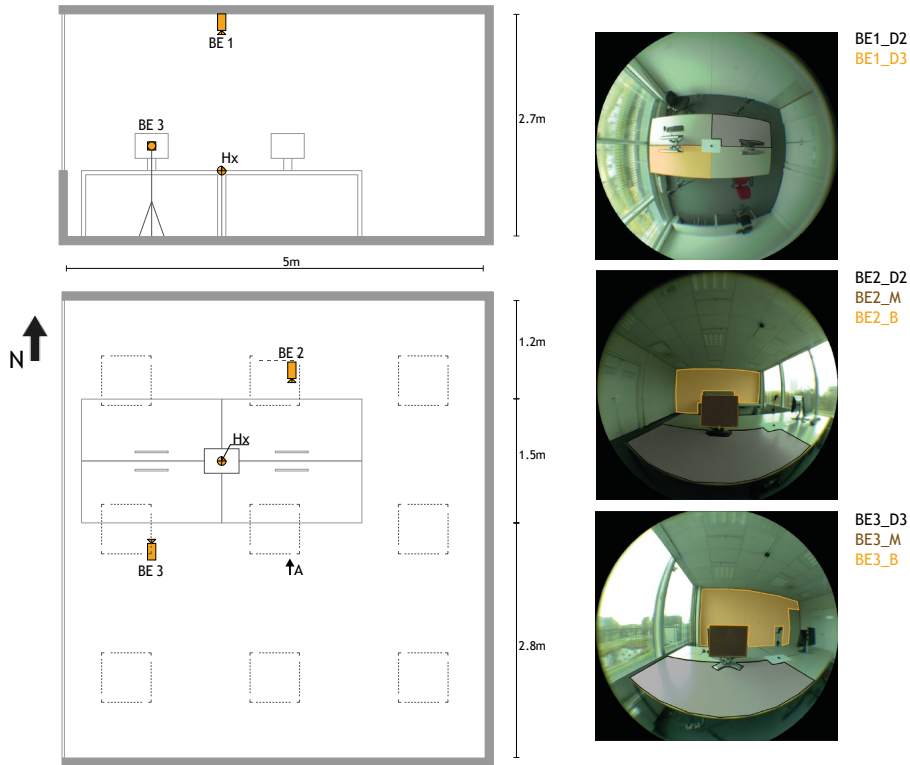


Figure 5.1: Mock-up office environment. Bee-Eye 1 (BE) was attached to the ceiling, while Bee-Eye 2 (BE2) and Bee-Eye 3 (BE3) were placed on tripods facing south and north, respectively. The luminance was extracted for six unique surfaces (**D**esktop, **M**onitor and **B**ackground areas) of which the desktop areas (D2 and D3) are measured both with horizontal and vertical orientations. Position A is elaborated in Section 5.2.6.

(9x PHILIPS RC461B G2 PSD W60L60 1xLED34 S/840) switched on, providing an additional uniform 750 lx on the horizontal work plane. The luminance distribution was monitored by a single horizontally oriented Bee-Eye (BE1) attached to the ceiling measuring two desktop surfaces (Figure 5.1, BE1 D2 and BE1 D3) and two vertically oriented Bee-Eyes (BE2 and BE3) attached to tripods at 20 cm distance from the desks at a height of 1.2m. Two opposing, north and south oriented, desks were monitored with varying distance (1.2m – 2.8m) to the background area measuring the luminance of the desktop (D), monitor (M) and background (B) area (Figure 5.1). The initial spatial resolution of the Bee-Eyes was determined with the constraint that a single measurement had a duration of less than one minute, resulting in a spatial resolution of 2130 x 1600 pixels instead of the maximum supported resolution in order to limit the processing time of the measurements as well as to reduce the time required for post processing.

5.2.3 Field study

Additionally, a field study was conducted for three consecutive weeks (14-01-2019 to 03-02-2019) in a Dutch office landscape (51°35'N 4°47'E). During this three week period, the sky conditions were mainly overcast with some days of clear and intermediate sky conditions. The office was located on the first floor and consisted of twelve desks divided into three groups, as is displayed in Figure 5.2. For each group of desks, a calibrated Bee-Eye was attached to the ceiling (three in total), analogous to the lab study. The floor area, the area where the occupants move, was masked such that a limited amount of privacy-sensitive content was captured (Figure 5.2). Measurements were conducted daily from 08.30 to 17.30 with an interval of 10 min in a spatial resolution of 901 x 676 pixels (Chapter 2).

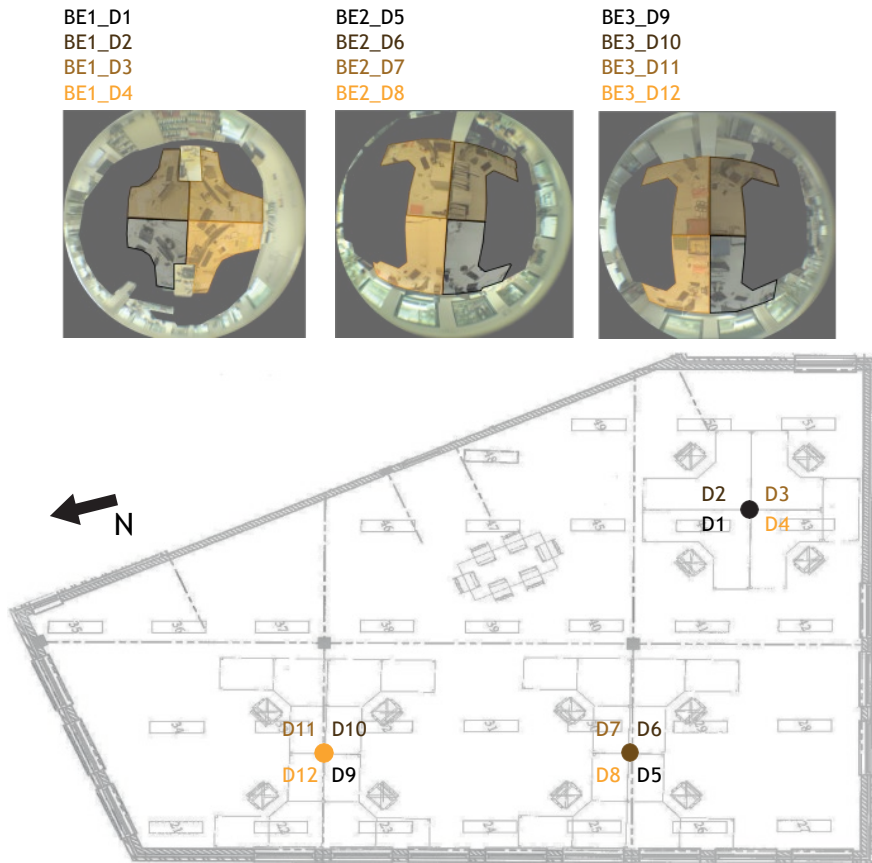


Figure 5.2: Living office landscape environment, including FOV and measurement surfaces of the three Bee-Eyes. Bee-Eye 1 (BE1) is associated to desks 1 (D1) to 4 (D4), Bee-Eye 2 (BE2) is associated to desks 5 (D5) to 8 (D8) and Bee-Eye 3 (BE3) is associated to desks 9 (D9) to 12 (D12).

5.2.4 Interpolation

During the measurements, elaborated in Sections 5.2.2 and 5.2.3, one single HDR image was captured every ten minutes with each Bee-Eye. These initial HDR images were digitally scaled by steps of 10% to achieve identical HDR images with ranging spatial resolutions. An additional lab study was conducted to verify whether digital scaling of the HDR image was appropriate to scale HDR images to a lower spatial resolution and to determine the most suitable interpolation method. Therefore, two series of HDR images were captured in a windowless room at the Building Physics and Services laboratory at Eindhoven University of Technology, preventing fluctuations due to the dynamic nature of daylight. The windowless room measured 4.4 m x 3.0 m and was illuminated with fluorescents and LEDs. To achieve steady conditions between different HDR images, the electrical lighting was turned on approximately half an hour in advance to ensure a stable lumen output. Each series consisted of five HDR images with resolutions of respectively, 901 x 676, 451 x 338, 300 x 225, 226 x 169 and 901 x 676 pixels. The latter was used to indicate the error margin due to temporal noise. The first HDR image of the series was scaled by 50% (451 x 338), 33% (300 x 225) and 25% (226 x 169) using nearest-neighbor, bilinear, and bicubic interpolation, respectively, matching the spatial resolution of the other original HDR images. The luminance for the scaled and original HDR images was calculated according to Equation 2.3, L_{sca} and L_{org} , respectively. Due to the constant conditions, the scaled HDR images should yield the same luminance as the respective original HDR images. The mean and median luminance values were calculated for the full HDR image and the background area only. The average relative differences ($\Delta L = |L_{org} - L_{sca} / L_{org}$) of the scaled copies with the original HDR images are presented in Table 5.1.

Table 5.1: The average differences ($\overline{\Delta L}$) of the mean and median luminance of the digitally scaled HDR images, using nearest-neighbor, bilinear, and bicubic interpolation.

	Mean			Median		
	Nearest	Bilinear	Bicubic	Nearest	Bilinear	Bicubic
50% scale	0.83%	0.83%	0.83%	0.41%	0.44%	0.37%
33% scale	1.51%	1.52%	1.52%	1.10%	1.30%	1.20%
25% scale	2.34%	2.41%	2.41%	0.87%	0.71%	0.76%
Noise	0.58%	0.58%	0.58%	0.52%	0.52%	0.52%

Table 5.1 shows that until 50% scaling the deviations were rather limited, the median luminance was even within the tolerance of temporal noise. For smaller scaling factors the relative differences seemed to be increasing. This was mainly due to the scaling of very bright spots, also indicated by the differences found between the mean and median luminance as outliers have a smaller effect on the median luminance. For areas without very bright spots the differences in mean luminance between the original and resized image were negligible (0.2%–0.7%). Moreover, the results show only minor differences between the interpolation methods. Therefore, it was assumed that the different interpolation methods provide a sufficiently accurate re-scaling of the original HDR images. Nevertheless, the bilinear interpolation “the output pixel value is a weighted average of pixels in the nearest 2-by-2 neighborhood” [202]. The bicubic interpolation has similar deviations, however, this method can result in pixel values outside the original range, which is not representative for this situation.

5.2.5 Analysis

All initial HDR images were gathered from the measurements described in Section 5.2.2 and 5.2.3 and replicates were made for each individual HDR image with varying spatial resolutions between 90% and 10% of the initial resolution. The initial images were resized by bilinear interpolation using MATLAB R2017a, resulting in nine different linearly scaled copies of the initial HDR images. In other words, series of ten identical linear scaled HDR images were available for the analysis with relative spatial resolutions of 100% to 10% with step sizes of 10% as indicated in Figure 5.3.

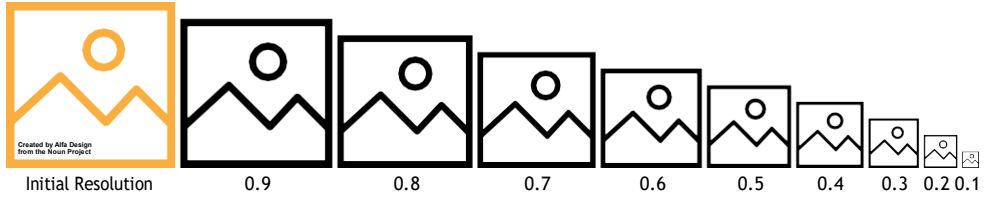


Figure 5.3: A single series of resized HDR images as scaled by MATLAB with the initial resolution indicated in orange.

Subsequently, these series of HDR images were converted into luminance maps according to Equation 2.3. Based on these luminance maps, the visual comfort indicators mean and maximum luminance of the respective surfaces (Figure 5.1 and Figure 5.2) were extracted, representing the light flux and glare sensation, respectively. Additionally, the illuminance on the Bee-Eye sensor was calculated using Equation 5.1 with elevation angle E and azimuth angle a . To allow inter-comparisons between different measurements, independent of the absolute luminance, the mean and maximum luminances extracted from the scaled luminance maps were normalized (L_n) relative to the initial luminance map. Moreover, the illuminance measurements were normalized (E_n) in a similar manner.

$$E = \int_0^{2\pi} \int_0^{\frac{\pi}{2}} L \cdot \cos E \cdot \sin a \cdot dE da \quad (5.1)$$

In 1760 Bouguer [203] found, using two candles illuminating a screen, that the just notable difference (JND) in luminance described by the ratio $\delta L/L$ was constant and independent to the absolute luminance. A constant ratio of approximately 0.016 was considered just notable [204], which was also confirmed using modern methods [205]. This means that a luminance increase of 1.6%, achieved by alternating the distance of one candle, will result in a just notable difference in luminance. In this study, the objective was to measure the luminance accurately, relative to the end user, with a low spatial resolution for a longer period of time. Therefore, this study allowed a spread of $\pm 1.6\%$ with a confidence interval (CI) of 95% ($\sigma = 0.0082$) relative to the initial luminance map as this will not affect the experience of the end user.

Inferential statistics were used to determine whether the normalized indicators (mean luminance, maximum luminance, and illuminance) of the resized HDR images (Y) were statistically different from a standard normal distribution with $\mu = 1$ and $\sigma = 0.0082$ (X), representing the initial HDR image and its tolerated JND spread. Based on the One-sample Kolmogorov-Smirnov test it was concluded that $X - Y$

was not normally distributed ($p < 0.001$). Therefore, the non-parametric Wilcoxon signed rank test was applied to verify whether X and Y were different ($\alpha = 5\%$, CI 95%). Also, for large data sets ($n > 300$) the p-value tends to approach zero quickly, therefore the results, solely focusing on the p-value, may not have a practical significance [206]. Thus, it is advised to focus on the effect size, which gets more precise for an increasing sample size. Therefore, for this study, which resulted in an extensive amount of data, effect sizes were calculated according to $r = Z/\sqrt{n}$ (r is Pearson's r , Z is Z-score and n is sample size) [207]. Effect sizes of 0.1, 0.3 and 0.5 were considered small, medium and large effects, respectively. The resized images were considered similar to the initial HDR image when the effect size was medium (≤ 0.3), indicating a difference with only limited practical significance. Large effect sizes were tolerated when they were followed by small or medium effect sizes for lower spatial resolutions, to account for the zigzagging effect, which is an observed artifact of the digital scaling (Section 5.4.2).

It was hypothesized that large luminance gradients have a negative impact on the performance of the resized luminance maps. Figure 5.4 illustrates a large luminance gradient in the background area, due to the shadow of the window frame, compared to the small gradient of the bright surfaces. However, these details might vanish when the resolution is lowered. As a result, it was expected that the luminance gradient, representing the scene complexity, might give reasoning behind the effects found for reduced spatial resolutions. Therefore, the gradient of each individual pixel was determined for the initial luminance map according to Equation 5.2. Subsequently, the maximum gradient ($\sqrt{L_{max}}$, Equation 5.3) was extracted as an one-dimensional indicator for the gradient within the luminance map.

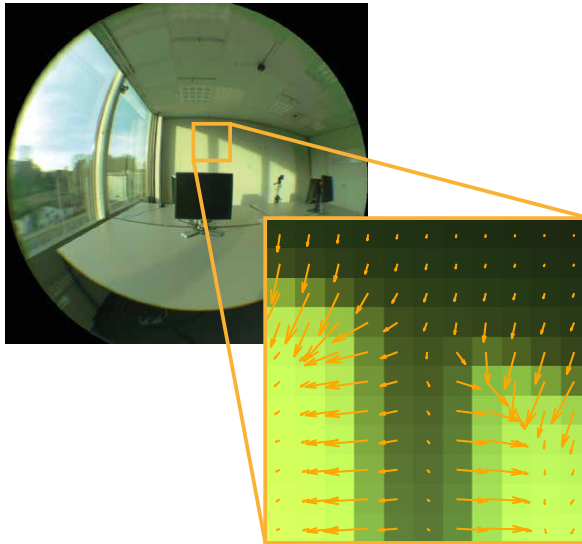


Figure 5.4: Snapshot of an obvious luminance gradient ($\approx 140 \text{ cd/m}^2$) as indicated by the arrow size, HDR image originating from Bee-Eye 3 during the lab study. The arrows indicate the magnitude of the gradient caused by the shadow of the window frame.

5.2. Methodology

$$\frac{\partial L_n}{\partial xy} = \frac{\partial L_n}{\partial}^2 + \frac{\partial L_n}{\partial y}^2 \quad (5.2)$$

$$\nabla L_{max} = \max \frac{\partial L_n}{\partial xy} \quad (5.3)$$

The maximum luminance gradient (∇L_{max}) was related to the performance of a scaled luminance map, which was quantified by the difference in maximum luminance between the normalized initial luminance map and the luminance maps with a linear resolution scale of 0.1, according to Equation 5.4. The $\Delta L_{n,max}$ relative to a scaling factor of 0.1 was used because this exhibits large differences and hence potentially more distinct effects.

$$\Delta L_{n,max} = |\max L_{n,1} - \max L_{n,0.1}| \quad (5.4)$$

5.2.6 Facial recognition

For lower resolutions, facial recognition becomes less easy; below the threshold facial resolution of 32 x 24 pixels and an eye-to-eye distance of 10 pixels [199] (Figure 5.5), the capabilities to automatically recognize faces decreases drastically. However, it does not guarantee that face recognition becomes impossible. For long term measurements, it is preferable that automated facial recognition is prevented. A laboratory study was conducted using the measurement setup described in Section 5.2.2 to determine the facial and eye-to-eye resolution in a standard office environment relative to the spatial resolution. Six horizontal (using BE1) and six vertical (using BE2) oriented HDR images with a maximum spatial resolution of 3240 x 2462 pixels were captured while a participant was seated at location A (Figure 5.1) focusing at Bee-Eye 1, Bee-Eye 2 and a monitor, consecutively. Using bilinear interpolation 20 scaled images were created for each of the twelve initial HDR images with diminution steps of 5%. For each reduced spatial resolution, the face height, face width, and eye-to-eye distance were measured, in pixels, to indicate the potential facial recognition capabilities.

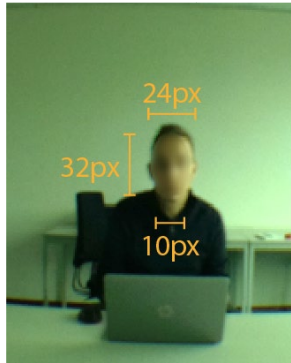


Figure 5.5: Cropped HDR image used to determine facial and eye-to-eye resolution taken with Bee-Eye 2 with the participant facing Bee-Eye 2.

5.2.7 Computational Costs

The spatial resolution of the HDR images is directly linked to the computational costs. In this chapter, the computational costs were indicated by the processing time required for a single luminance measurement. The processing time, but also the computational costs in general, are increasingly important for long term measurements as this determines the dimensioning of the automated system to a large extent. The processing time was determined for a luminance measurement according to track one of the Bee-Eye (Figure 2.9). The CPU usage did not show significant differences for varying resolutions and was, therefore, not considered. The processing time was calculated, in an office environment, for 20 different spatial resolutions, with an initial spatial resolution of 3240 x 2462 pixels, with diminution steps of 5% similar to Section 5.2.6 This was repeated thrice to include potential variability in processing time.

5.3 Results

5.3.1 Lab study

This section describes the effect of reduced resolutions, under varying conditions, as found in the lab study. 92% of the measurements in the mock-up office environment were successful resulting in a total of 728 initial HDR images, the remaining 8% of the measurements failed mainly due to excessive luminance values exceeding the dynamic range of the Bee-Eyes. In the majority of these cases, direct sunlight hit the image sensor saturating the shortest exposure (9 μ s) feasible with this hardware, returning inappropriate luminance values. Consequently, these saturated HDRs were not considered. Table 5.2 shows the effect sizes, introduced in Section 5.2.5, representing the magnitude of the differences for the mean luminance between initial HDR images and HDR replicates for the eight predetermined surfaces of the mock-up office environment as indicated in Figure 5.1. Effect sizes exceeding the threshold (> 0.3) are annotated in bold. It shows that the effect of a decreased resolution was generally limited for the mean luminance. With exception to the monitors, acceptable effect sizes were exhibited up to a resolution scaling factor of 0.2, representing a spatial resolution of 426 x 320 pixels. No clear differences in performance were found between desktop and background surfaces and between desktop surfaces measured with a horizontally oriented Bee-Eye (B1) and vertically oriented Bee-Eye (BE2_D2 and BE3_D3). The monitors performed differently, especially BE2_M (monitor facing north) performed much worse even though both monitors were turned off, this might be due to their low luminances being sensitive to minor absolute changes in luminance having a disproportional large effect on the relative difference. As a result, the monitors require a higher resolution for an accurate assessment. Figure 5.6 illustrates that the effect of a decreased resolution, for Bee-Eye 3, was indeed small as the average (normalized) mean luminance is practically horizontal ($L_n \approx 1$). For the desktop and background surfaces, only minor deviations were visible from $L_n \approx 1$ for scaling factors of approximately 0.2 – 0.1, which corresponded to the effect sizes found in Table 5.2. Bee-Eye 1 and Bee-Eye 2 exhibited similar results as Bee-Eye 3.

5.3. Results

Table 5.2: Effect sizes of the mean luminance extracted from the relevant surfaces with an initial resolution of 2130 x 1600 pixels as measured in the mock-up office environment. S.F. represents the scaling factors. Effect sizes that violated the threshold conditions are indicated in bold.

S.F.	BE1_D2	BE1_D3	BE2_D2	BE2_M	BE2_B	BE3_D3	BE3_M	BE3_B
0.9	0.03	0.01	0.02	0.21*	0.01	0.01	0.01	0.02
0.8	0.01	0.02	0.02	0.26*	0.04	0.01	0.01	0.02
0.7	0.01	0.00	0.03	0.21*	0.05	0.01	0.02	0.00
0.6	0.02	0.03	0.02	0.23*	0.03	0.02	0.01	0.02
0.5	0.11*	0.20*	0.05	0.25*	0.15*	0.01	0.09	0.11*
0.4	0.05	0.06	0.01	0.63**	0.05	0.01	0.12*	0.05
0.3	0.13*	0.01	0.01	0.64**	0.09	0.02	0.12*	0.07
0.2	0.30*	0.07	0.01	0.82**	0.22*	0.07	0.45**	0.17*
0.1	0.75**	0.22*	0.12*	0.86**	0.01	0.31**	0.81**	0.53**

* Medium effect size, ** Large effect size

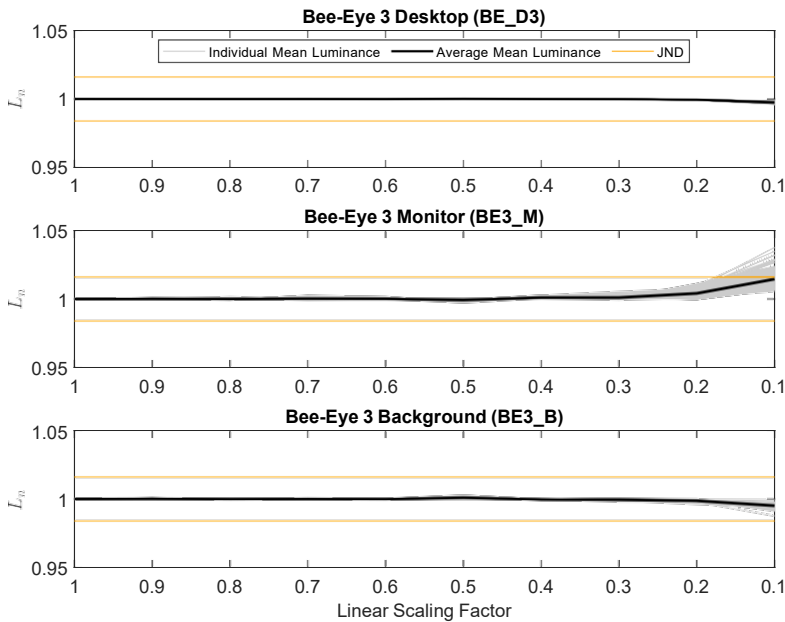


Figure 5.6: Normalized mean luminance of scaled HDR images relative to an initial resolution of 2130 x 1600 pixels measured in the mock-up office environment with BE3.

In contrast to the mean luminance, the maximum luminance generally exhibited a large effect due to a reduced spatial resolution as indicated in Table 5.3. Also, Figure 5.7 illustrates that for every reduction in resolution the maximum luminance of the surface also decreased significantly. Even a scaling factor of 0.9 led to a maximum luminance outside the JND threshold. This same effect was exhibited for Bee-Eye 1 and 2. This indicates that, for instance, glare caused by specular reflections of excessively high luminances, representing a low number of pixels, can go undetected for low spatial resolutions resulting in a potentially underestimated discomfort glare assessment, which is an important drawback of a reduced spatial resolution.

Table 5.3: Effect sizes of the maximum luminance extracted from the relevant surfaces with an initial resolution of 2130 x 1600 pixels as measured in the mock-up office environment. S.F. represents the scaling factors. Effect sizes that violated the threshold conditions are indicated in bold.

S.F.	BE1_D2	BE1_D3	BE2_D2	BE2_M	BE2_B	BE3_D3	BE3_M	BE3_B
0.9	0.86**	0.86**	0.85**	0.60**	0.86**	0.61**	0.34**	0.87**
0.8	0.74**	0.86**	0.86**	0.59**	0.87**	0.84**	0.85**	0.86**
0.7	0.86**	0.87**	0.87**	0.32**	0.87**	0.77**	0.70**	0.83**
0.6	0.87**	0.86**	0.87**	0.63**	0.87**	0.86**	0.87**	0.84**
0.5	0.87**	0.87**	0.87**	0.85**	0.87**	0.87**	0.87**	0.87**
0.4	0.87**	0.87**	0.87**	0.85**	0.87**	0.87**	0.54**	0.87**
0.3	0.87**	0.86**	0.87**	0.86**	0.87**	0.87**	0.85**	0.87**
0.2	0.87**	0.87**	0.87**	0.74**	0.87**	0.87**	0.85**	0.87**
0.1	0.87**	0.87**	0.87**	0.86**	0.87**	0.87**	0.42**	0.87**

* Medium effect size, ** Large effect size

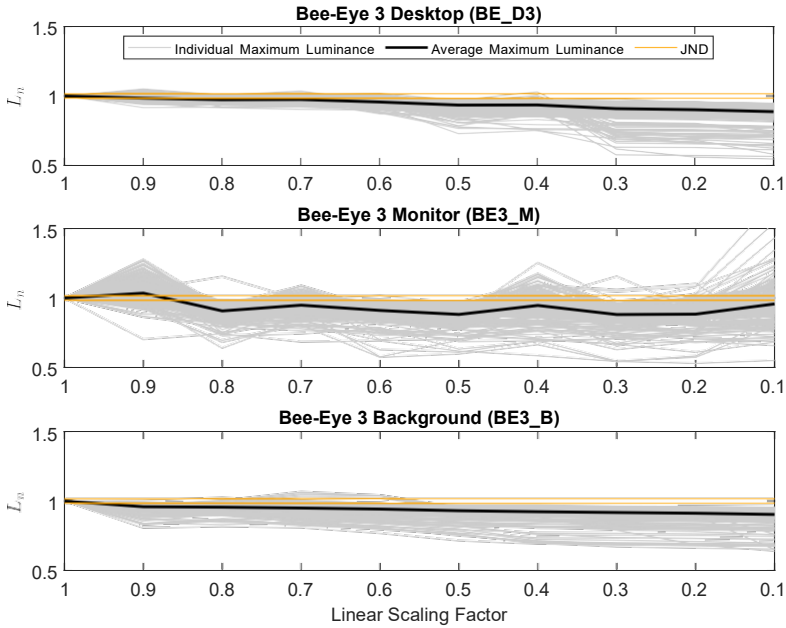


Figure 5.7: Normalized maximum luminance of scaled HDR images relative to an initial resolution of 2130 x 1600 pixels measured in the mock-up office environment with Bee-Eye 3.

The results indicated that the maximum luminance can only be measured with a resolution of at least 2130 x 1600 pixels. Therefore, we aimed to approximate the required spatial resolution for maximum luminance measurements. The average normalized maximum luminance values (L_n) of all surfaces (black line in Figure 5.7) for the scaling region between 0.9 and 0.2, except the monitors, showed distinct linear relations (adj- R^2 0.77-0.99). Scaling factors 1 and 0.1 were not considered in this case because these were, respectively, forced to L_n of 1 (wrong assumption to be the ground truth) or showed extreme deviations. Extrapolating these linear

5.3. Results

relations resulted in approximated scaling factors ranging between 0.95 and 1.43 for an accurate representation of the maximum luminance. A scaling factor of 1.43 relative to a resolution of 2130 x 1600 pixels resulted in a resolution of 3046 x 2280 pixels. When rounding off, a spatial resolution of 3000 x 2250 pixels seems to be an appropriate approximation of the spatial resolution needed for accurate maximum luminance measurements. However, more importantly, it indicates that a high spatial resolution is required for accurate maximum luminance measurements.

It was hypothesized, that the maximum luminance gradient of a surface has a large effect on the performance of lower spatial resolutions. Figure 5.8 shows the relation between the maximum luminance gradient (∇L_{max}) and the relative performance of the lowest resolution ($\Delta L_{n,max}$). It shows that these aspects were rather strongly related, with correlation factors varying between 0.20 and 0.80. Generally, a higher gradient resulted in a lower relative performance, as was expected, although the spread is substantial. This shows that large luminance gradients had generally a negative effect on the performance of the reduced resolutions as was hypothesized.

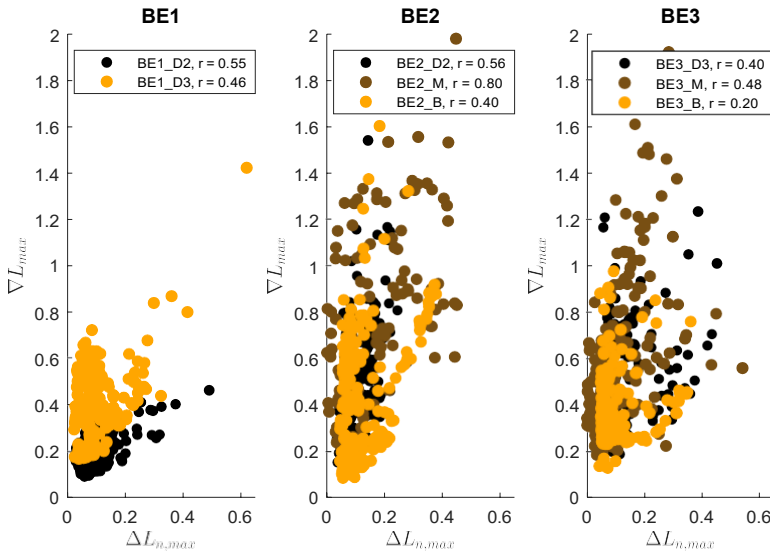


Figure 5.8: Correlation plot of the maximum gradient (∇L_{max}) relative to the performance of the luminance map with scaling factor 0.1 ($\Delta L_{n,max}$) measured in the mock-up office environment. The figure illustrates that a reduced performance, indicated by a high $\Delta L_{n,max}$, is highly correlated to increased gradient.

Similar analyses have been conducted for the illuminance on the sensor, which was derived from the luminance distributions according to Equation 5.1. In contrast to the mean luminance, a clear difference was found between horizontally and vertically applied Bee-Eyes representing significant different FOVs. The two vertically oriented Bee-Eyes (BE2 and BE3) captured a more complex scene including a large portion of the outside environment, which required a spatial resolution of at least 640 x 480 pixels (scaling factor of 0.3). BE3 (North oriented) performed slightly better, indicated by lower effect sizes, than BE2 (South oriented). For the horizontally oriented device, with a much simpler scene, a spatial resolution of 213 x 160 sufficed. Nevertheless, for all orientations, a significant reduction in resolution could

be achieved. Figure 5.9 also illustrates that until a scaling factor of 0.3, almost no deviations occurred from the horizontal line. Additionally, it shows smaller effects for the horizontally applied Bee-Eye (BE1).

Table 5.4: Effect sizes of the illuminance extracted from the relevant surfaces with an initial resolution of 2130 x 1600 pixels as measured in the mock-up office environment. Effect sizes that violated the threshold conditions are indicated in bold.

Scaling Factor	BE1	BE2	BE3
0.9	0.06	0.11*	0.01
0.8	0.06	0.11*	0.05
0.7	0.05	0.10	0.04
0.6	0.06	0.16*	0.14*
0.5	0.06	0.12*	0.09
0.4	0.06	0.19*	0.19*
0.3	0.07	0.22*	0.16*
0.2	0.10	0.35**	0.35**
0.1	0.12*	0.54**	0.43**

* Medium effect size, ** Large effect size

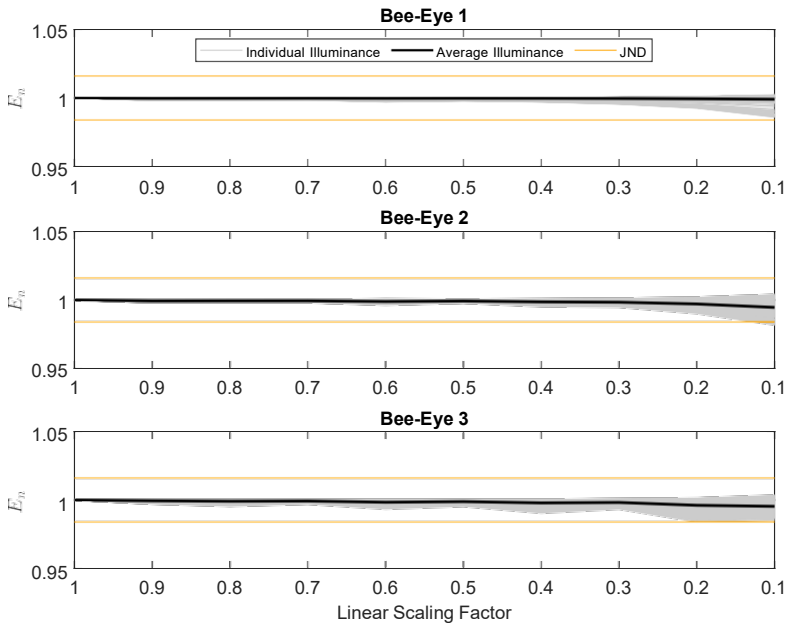


Figure 5.9: Normalized illuminance of scaled HDR images relative to an initial resolution of 2130 x 1600 pixels measured in the mock-up office environment.

5.3.2 Field study

This section illustrates the effect of a reduced resolution on the measurement accuracy as found in the field study. During the field study, 98% of the measurements

5.3. Results

succeeded, resulting in 3,380 unique HDR images.

Table 5.5 shows the effect sizes of the scaled resolutions for the normalized mean desktop luminance starting with an initial resolution of 901 x 676 pixels measured in the real office environment. When all surfaces were included, a spatial resolution of 450 x 338 pixels, corresponding to a scaling factor of 0.5, was required for an accurate representation of the mean luminance in this office environment, which shows large similarities to the spatial resolution of 426 x 320 pixels found, excluding the monitors, in the lab study. However, a large spread was exhibited between the different desktops, for instance, for desk 4 (BE1 D4) a resolution of 180 x 135 pixels would have been sufficient. This large spread was not exhibited during the field study, which is likely caused by the living environment. On the other hand, during the lab study, the lower number of surfaces and larger absolute step sizes in resolution might have faded the spread. The findings of Table 5.5 correspond to Figure 5.10. There exist almost no deviations until a scaling factor of 0.5 (zigzagging effect excluded, Section 5.4.2). Beyond a scaling factor of 0.5, a reduction in performance was always observed, either very earlier but in a smooth manner (BE3 D10) or very late but in an abrupt manner (BE3 D12).

Table 5.5: Effect sizes of the mean luminance extracted from the relevant surfaces with an initial resolution of 901 x 676 pixels as measured in the living office landscape. Effect sizes that violated the threshold conditions are indicated in bold.

S.F.	0.9	0.8	0.7	0.6	0.5	0.4	0.3	0.2	0.1
BE1 D1	0.18*	0.03	0.29*	0.21*	0.44**	0.15*	0.18*	0.77**	0.84**
BE1 D2	0.01	0.08	0.13*	0.13*	0.14*	0.25*	0.03	0.59**	0.86**
BE1 D3	0.13*	0.20*	0.16*	0.03	0.14*	0.17*	0.49**	0.40**	0.40**
BE1 D4	0.15*	0.10	0.06	0.04	0.20*	0.07	0.07	0.25*	0.85**
BE2 D5	0.18*	0.18*	0.03	0.16*	0.13*	0.32**	0.53**	0.60**	0.82**
BE2 D6	0.11*	0.12*	0.12*	0.07	0.19*	0.42**	0.74**	0.74**	0.86**
BE2 D7	0.05	0.09	0.00	0.10	0.22*	0.13*	0.22*	0.42**	0.85**
BE2 D8	0.16*	0.18*	0.01	0.28*	0.14*	0.11*	0.46**	0.55**	0.87**
BE3 D9	0.19*	0.22*	0.00	0.21*	0.29*	0.28*	0.68**	0.57**	0.86**
BE3 D10	0.10	0.01	0.12*	0.01	0.14*	0.61**	0.56**	0.85**	0.87**
BE3 D11	0.13*	0.19*	0.07	0.21*	0.35**	0.09	0.29	0.34**	0.86**
BE3 D12	0.36*	0.29*	0.04	0.30**	0.23*	0.12*	0.46**	0.23*	0.87**

* Medium effect size, ** Large effect size

The lab study showed that for maximum luminance measurements a spatial resolution of approximately 3000 x 2250 pixels was required both for photometric monitoring at eye level and from the ceiling. In correspondence to this, the field study, measuring from the ceiling, showed that all scaling factors had a large effect on the accuracy, indicating a spatial resolution higher than 901 x 676 was required. In contrast to the lab study, no additional extrapolation was conducted because this is questionable for resolutions so far from its initial range. Therefore, it was assumed that for the field study also a spatial resolution of approximately 3000 x 2250 pixels was required.

Analogous to Figure 5.8, Figure 5.11 illustrates the relationship between the luminance gradient (∇L_{max}) and the relative performance of the luminance map with a linear scaled resolution of 0.1 ($\Delta L_{n,max}$). Again, the results showed large similarities with the lab study with correlation factors ranging between 0.34 and 0.75.

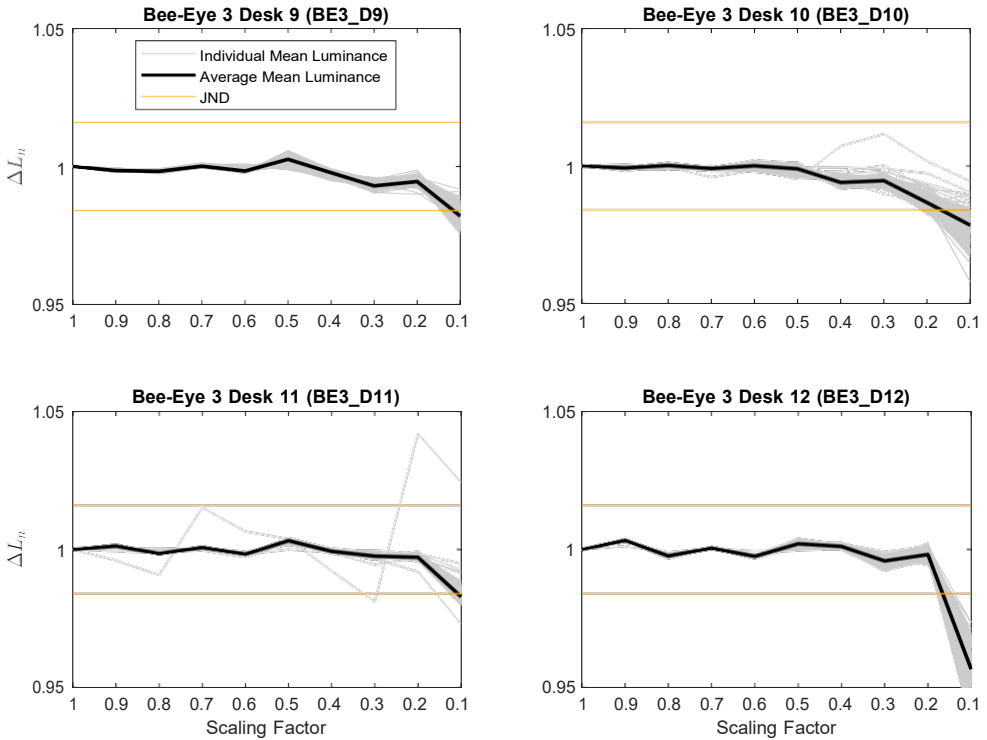


Figure 5.10: Normalized mean luminance relative to an initial resolution of 901 x 676 pixels measured in the living office landscape with Bee-Eye 3.

Figure 5.11 shows that this relation was exponential. Nevertheless, the implication remains that the measuring performance for lower spatial resolution decreases when large luminance gradients are present. Hence, complex scenes with large luminance gradients might require higher spatial resolutions.

The lab study showed that a resolution of 640 x 480 pixels was suitable for illuminance measurements. However, for the ceiling-based measurements, even a scaling factor of 0.1 sufficed. The ceiling-based measurements, during the field study, required a spatial resolution of 720 x 540 pixels according to Table 5.6. This is a spatial resolution which is higher than found during the lab study, especially compared to the ceiling-based (BE1) measurements. This is explained by the larger luminance gradients found on the desktops during the field study (Figure 5.11) caused by it being a living environment where multiple objects were placed on the desktops. Similar to the mean desktop luminance (Table 5.6) a relatively large amount of spread was exhibited between suitable spatial resolutions for illuminance measurements by the three devices. However, it also shows that generally a higher spatial resolution was required for illuminance measurements than the mean luminance.

5.3. Results

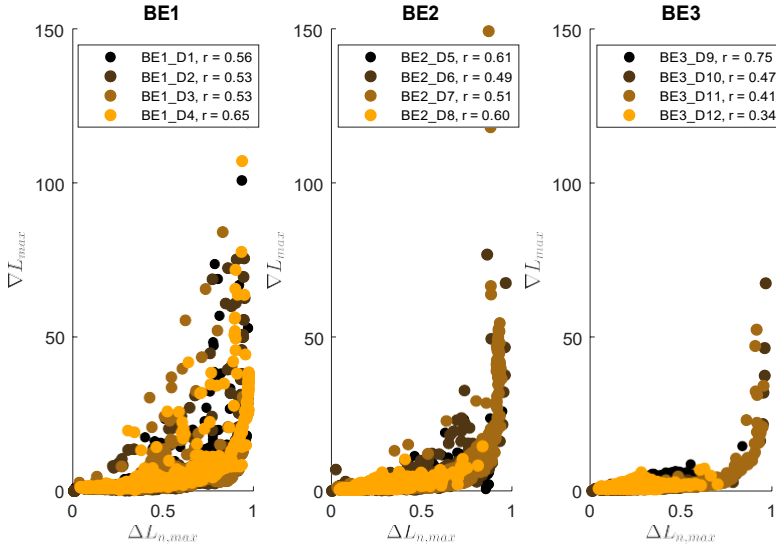


Figure 5.11: Correlation plot of the maximum gradient (∇L_{max}) relative to the performance of the luminance map with scaling factor 0.1 ($\Delta L_{n,max}$) measured in the living office landscape. The figure illustrates that a reduced performance, indicated by a high $\Delta L_{n,max}$, is highly correlated to increased gradient.

Table 5.6: Effect size table of the illuminance extracted from the Bee-Eyes with an initial resolution of 2130 x 1600 pixels measured in the living office environment.

Scaling Factor	BE1	BE2	BE3
0.9	0.16*	0.12*	0.32**
0.8	0.15*	0.11*	0.30*
0.7	0.23*	0.12*	0.34**
0.6	0.39**	0.19*	0.57**
0.5	0.33**	0.17*	0.45**
0.4	0.39**	0.20*	0.51**
0.3	0.51**	0.29*	0.69**
0.2	0.59**	0.42**	0.75**
0.1	0.69**	0.63**	0.80**

* Medium effect size, ** Large effect size

5.3.3 Facial Recognition

The relation between the spatial resolution of the Bee-Eyes and the facial resolution is displayed in Figure 5.12. It shows that the eye-to-eye resolution threshold was a much stricter criterion than the horizontal and vertical face resolution. The eye-to-eye resolution threshold was met for scaling factors lower than 0.33, representing a spatial resolution of 1082 x 813 pixels, while the horizontal and vertical face resolution thresholds were met for scaling factors of 0.46 (1490 x 1133) and 0.44 (1426 x 1083), respectively. It shows that the initial spatial resolution in the lab study (2130 x 1600

pixels) allowed facial recognition while the spatial resolution applied in the field study (901 x 676 pixels) did not allow this. The eye-to-eye distance seems to be the most suitable and robust indicator as it exhibited relative little spread, as compared to, mainly, the vertical face resolution. Nevertheless, one should take into account the distance between the face and camera, which was in this context approximately 1.7m to 2m. This is easily accounted for by a linear scaling factor.

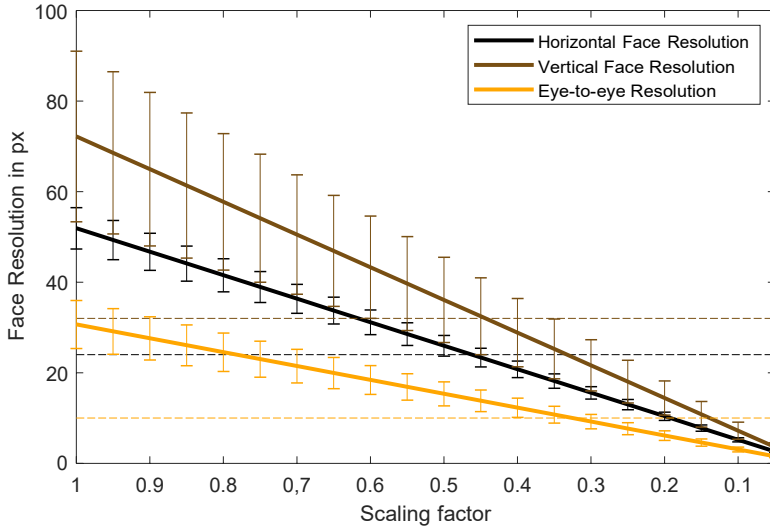


Figure 5.12: Face resolutions and thresholds relative to scaling factors of a spatial resolution of 3280 x 2464 pixels, the dashed lines indicate the respective thresholds for automated face recognition.

5.3.4 Computational Costs

Figure 5.13 shows the average processing time, used to indicate the computational costs, in relation to the spatial resolution. The processing time was approximated by an exponential function. According to these measurements a scaling factor of 0.74, resulting in a spatial resolution of 2437 x 1830 pixels, limits the processing time to exactly sixty seconds. As an example, measurements with a resolution of 450 x 338 pixels, which was sufficient for mean luminance measurements, had an estimated processing time of approximately 12s, which can be considered very minor for a luminance camera. Alternatively, the processing time can be minimized by using a stronger processor or optimized software. This allows for small interval (< 1 min) measurements that might be needed to capture the fast variations of daylight [129]. Nevertheless, processing times much lower than 10 s are not expected to be feasible. Additionally, one can assume that other computational costs such as data storage behave familiar and can also be reduced significantly.

5.4. Discussion

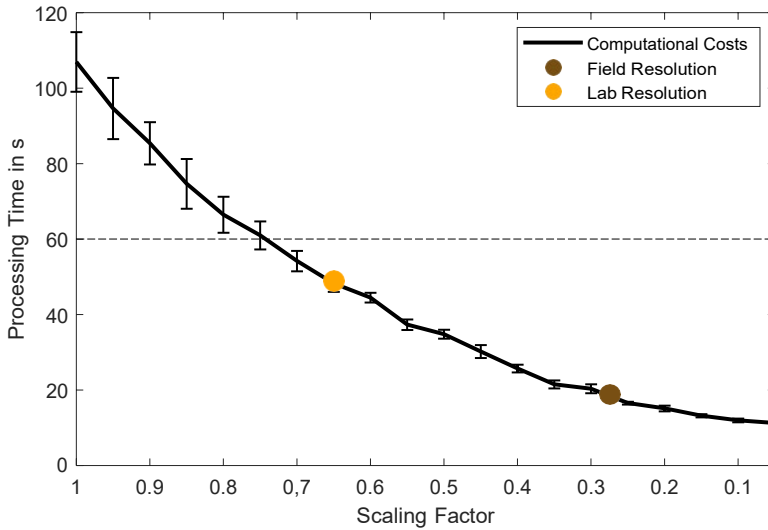


Figure 5.13: The processing time for a single measurement relative to the spatial resolution of 3280 x 2562 pixels, the dashed line represents the 1 minute threshold.

5.4 Discussion

5.4.1 Mean luminance

The objective of this research was to validate whether the luminance can be measured with relatively low spatial resolutions making it suitable for long term measurements, but for lighting control systems that aim to provide high visual comfort as well. Both the lab and field study confirmed that there is no need to apply the maximum spatial resolution of a camera when measuring the mean luminance. The lab and field study found almost identical resolutions of 426 x 320 and 450 x 338, respectively, which was rounded off to 440 x 330 pixels. This was only validated for the experimental conditions applied in this research.

For instance, a higher ceiling might result in a higher minimum required spatial resolution. Nevertheless, the experimental conditions resemble the conditions for numerous office environments. The overall complexity of the field study, resulting in larger luminance gradients, was much higher because it contained numerous objects on the desk surfaces in contrast to the empty desks in the lab study. However, the influence of the larger luminance gradient was limited for the mean luminance.

The results of the lab study (Table 5.2) showed that the monitors, especially BE2.M, exhibited a lower measurement performance for the mean luminance compared to the desk and background surfaces. Zooming in on this monitor, it turned out that this was mainly caused by the monitor frame which contained a number of chrome like buttons with a maximum diameter of only 14 pixels in the initial resolution, which was not present for monitor BE3.M. The pixels representing the buttons had a luminance several orders of magnitude larger than the average luminance of the computer screen (Figure 5.14); hence, having a large effect on both the maximum and mean luminance of the monitor while only being a small detail. This effect also

appears in Figure 5.8 were a high correlation ($r = 0.8$) was found between the maximum gradient (transition button to black monitor) and the performance of the lower resolution for BE2.M. This shows that down-sampling, relative to mean luminance, differs from simply averaging the luminance even though there are large similarities, which was also clearly indicated in Figure 5.10. Due to the alignment of pixels (Section 5.4.2), the effect of luminance masks and the effect of bilinear interpolation small differences arise. The effect size analysis was repeated for the monitor screen only, leaving out the monitor frame. This resulted in a low sensitivity (small effect size up to a scaling factor of 0.2) relative to the spatial resolution because the screen itself was very uniform as indicated by the large spread of the pixel locations representing the maximum luminance values (Figure 5.14). Additionally, in Figure 5.6 the monitor of Bee-Eye 3 also showed larger deviations for the three smallest scaling factors compared to the other two surfaces. This was caused by the low luminance values of the black computer screen. As a result, a small change in luminance, due to the image resizing, resulted in a big relative change. Moreover, the monitor surface was somewhat smaller than the other surfaces that were considered in this study, making it also more sensitive to small changes.

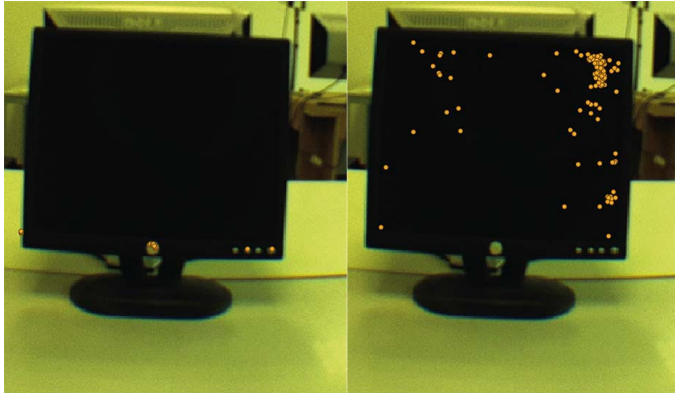


Figure 5.14: Left monitor displays the pixels of the maximum luminance when considering the entire monitor while the right monitor displays the pixels of the maximum luminance for the screen only.

5.4.2 Maximum luminance

The maximum luminance is an important indicator as it is a major contributor to discomfort and disability glare as the glare source luminance (often, but not exclusively, the maximum luminance) is one of the four quantities reoccurring in all established glare indices [51]. Hence, the maximum luminance is essential for visual comfort. Therefore, it is important to be able to measure this luminance value accurately; however, it is also desirable to do this with a relatively low spatial resolution to limit, for instance, the computational costs. The maximum luminance was largely affected by the spatial resolution of the luminance camera because the it is generally represented by a low number of pixels. In those cases, for lower spatial resolutions, the high luminance pixels are averaged with lower luminance pixels in the vicinity. The

5.4. Discussion

measurements in the lab and in the field indicate that the spatial resolution used in the lab study was not sufficient to measure the maximum luminance. This is contradicting the recommended spatial resolution of 1000 x 1000 pixels for discomfort glare measurements as stated in the RADIANCE *evalglare* manual [68]. In the lab study, this recommended spatial resolution would have led to an underestimation of the maximum luminance.

In practice, this effect might be even more distinct as the luminance gradient between the sun and the sky hemisphere can be enormous. In this study, only the maximum luminance values of the respective surfaces were considered, already resulting in high spatial resolution requirements even though the luminance gradient was comparatively low. An additional validation, in the field, directly relating glare to the spatial resolution would be beneficial to assess the magnitude of this effect. On the other hand, the maximum luminance might be caused by noisy pixels. This might have occurred for a number of luminance maps; however, due to the large amount of tested luminance maps this could only have had minor effect on the final spatial resolution.

Based on extrapolation of the average maximum luminance it was approximated that a spatial resolution of 3000 x 2250 pixels might have been appropriate for accurate maximum luminance measurements. This spatial resolution is much higher than the recommended resolution of *evalglare* and also, as already indicated, much higher than the resolution required for mean luminance measurements. It was assumed that for the field study, a similar spatial resolution was required for the maximum luminance. Indicated by the large similarities found between the spatial resolution for the mean luminance of the lab and field study. Consequently, one could argue that the maximum luminance, and also glare, is less straightforward to monitor during long term measurements than the mean luminance.

A zigzagging effect was exhibited, especially for BE_{3M} in Figure 5.7. However, similar effects, but less distinct, were found throughout the results. This effect was caused by interpolating in small consecutive steps. Pixels with a large influence (very high or very low luminance) can be more effectively divided among the available pixels for a certain scaling factor. For instance, a certain luminance pattern might be effectively covered by a scaling factor of 0.8, meaning that the majority of pixels is covered entirely by the luminance pattern. While on the other hand for a scaling factor of 0.7 a large number of pixels is covered only partly by the luminance pattern. This effect is dependent on the specific luminance pattern, therefore this effect was not exhibited in all cases. Additionally, it is also difficult to predict. This phenomenon was also found in Table 5.1 for the median luminance scaled by 33%.

5.4.3 Illuminance

The illuminance at the sensor was calculated by integrating the luminance distribution according to Equation 5.1. The lab study found that a resolution of 639 x 480 pixels was appropriate for illuminance measurements while the field study suggested a slightly higher spatial resolution of 720 x 540 pixels. However, for the ceiling based measurement (BE₁) in the mock-up office, a spatial resolution of 213 x 160 sufficed. It should be clearly noted that this ceiling-based measurement (BE₁) is generally not necessarily relevant, in contrast to the vertical illuminances measured by BE₂ and BE₃, which are very relevant especially related to the non-image forming effects

of light [112]. However, it is applied to indicate the effect of the luminance gradient on the spatial resolution that can be used, which showed that for scenes with low complexity, as captured by BE1, accurate measurements can be conducted with very low spatial resolutions but for more complex conditions (larger gradients) higher spatial resolutions are required. The vertically oriented measurements of the same scene required higher resolutions because the complex daylight openings represented a much larger part of the field of view while the empty desks represented a smaller area. Also, for ceiling-based measurements of a more complex scene, such as measured in the field study, higher spatial resolutions were required. This was considered a complex scenario because it contained a lot of small details such as objects on the desk surfaces. This complexity impacted the measured illuminance because small but important details might get omitted in low resolutions. Therefore, a higher complexity, and hence a larger luminance gradient, has a negative effect on the accuracy of illuminance measurements in lower spatial resolutions as was already indicated in Figure 5.8 and Figure 5.11.

5.4.4 Practical Aspects

Besides the measurement accuracy, two practical aspects were identified that are relevant for the spatial distribution: facial recognition and processing time. Both these aspects argue for a lower spatial resolution while for the accuracy of the luminance measurements higher resolutions are preferred. To limit the facial recognition a maximum resolution of 1082 x 813 pixels was identified for the experimental conditions tested. Therefore, limiting the ability to automatically recognize faces can be combined with mean luminance and illuminance measurements; however, this was not feasible for maximum luminance measurements. Therefore, the mean luminance and illuminance are more suitable for long term measurements because there is no direct risk of automated facial recognition.

Different face recognition thresholds were found depending on the gaze direction and the facial resolution indicator. However, the eye-to-eye distance performed most robustly because it was rather easy to extract independent of the gaze direction. The horizontal and vertical face resolutions were difficult to extract when the gaze direction differed because of the roundish shape of the human head. Moreover, the eye-to-eye threshold formed a stricter requirement.

Because daylight can exhibit variations within a few minutes and even seconds [129] a low processing time is preferred to measure these daylight variations. Similar to the facial recognition it was not feasible to combine a low processing time with accurate maximum luminance measurements. On the other hand, for mean luminance and illuminance measurements, the processing time could be reduced drastically, to approximately twelve seconds for illuminance measurements and even lower for mean luminance measurements. However, the actual processing time on other devices might differ as it also depends on the processor and the software that is applied. Nevertheless, this research indicates that the processing time and henceforth the computational costs behave exponentially, whereby reducing the resolution by a factor 2 reduces the processing times by a factor of approximately 2.7. Therefore, it is valuable to consider reducing the resolution to limit computational costs significantly, especially for measurements at a high interval.

5.4.5 Validity

This study included two case studies to recommend suitable spatial resolutions for luminance distribution measurement devices. Naturally, only two case studies have a limited validity. Nevertheless, the study indicates that the luminance can be reduced for certain occasions. A systematic analysis of the spatial spectrum in the frequency domain using Fourier Transforms might be able to improve the validity. Reducing the spatial resolution will eliminate the high frequency part of the spectrum, which might correlate to the luminance gradient and the measurement error of the metrics applied in this study. By including this approach in future research, more insight is expected in the underlying principles as the two methods will be complementary. Moreover, the validity can be improved by performing additional case studies.

5.5 Conclusion

Since technology has enabled us to measure luminance distributions continuously for a longer period of time, new issues have presented themselves. For instance, the spatial resolution of a luminance map can be considered a very important aspect as this impacts the measurement accuracy, but also the ability to prevent automated facial recognition and the processing time. This study tried to recommend a spatial resolution that satisfies these three relevant requirements (accuracy, face recognition, and processing time) for long term visual comfort measurements such that luminance cameras, like the Bee-Eye, can be implemented in lighting control systems to achieve high visual comfort.

It was shown, that for a typical office environment, both for mean luminance and illuminance measurements, all three requirements can be satisfied. The mean luminance can be accurately measured with a spatial resolution of 440 x 330 pixels under any weather condition in the experimental conditions applied in this study. This resolution is lower than the face recognition threshold and it limits the processing time to approximately twelve seconds, which reduces computational costs by a factor of nine relative to the maximum spatial resolution of this specific imaging sensor. For illuminance measurements, a slightly higher spatial resolution of 720 x 540 pixels is required because it is, in contrast to the mean luminance, more sensitive to luminance gradients. However for very simple scenes, with limited luminance gradients, the spatial resolution can be decreased even further. The spatial resolution is dependent on the luminance gradient of the measured surface: a very large luminance gradient, or complex scene, will generally require a higher spatial resolution, although this effect is more pronounced for illuminance and maximum luminance measurements.

In contrast to the mean luminance and the illuminance, the three requirements cannot be met simultaneously for maximum luminance measurements. For accurate measurements of the maximum luminance, spatial resolutions were required that exceeded the spatial resolutions applied during this study. It was (roughly) estimated that a spatial resolution of approximately 3000 x 2250 pixels might have been suitable for an accurate representation of the maximum luminance under these conditions. This also indicates that for discomfort glare a very high spatial resolution, higher than suggested in the *RADIANCE evalglare* manual [68], might be required as the maximum luminance is a major contributor to discomfort glare. This effect might even be more extreme when daylight and direct sunlight are considered.

However, more research, which directly relates the DGP to the spatial resolution, is required to verify these findings. Consequently, this would have allowed facial recognition and would have resulted in significant computational costs. Nevertheless, it is recommended that similar measurements are conducted with higher initial spatial resolutions to find a suitable resolution for maximum luminance measurements in a more accurate manner. In general, the validity of these recommendations can be improved by additional case studies and alternative analysis of the spatial spectrum in the frequency domain using Fourier Transforms.

This research has shown that spatial resolution does influence the accuracy of the luminance distribution. Therefore, the spatial resolution should be chosen wisely depending on the required accuracy, office dimensions, presence of human subjects and the available time and resources, especially for long term measurements. Therefore, a toolbox has been developed based on the findings to assist others to select a relevant spatial resolution for their luminance camera for office conditions similar to the experimental conditions applied in this study. This MATLAB based toolbox, *Spatial Resolution Luminance Camera Toolbox*, can be installed as a MATLAB application or as a standalone application, which can be downloaded from the MathWorks file exchange [208].

The temporal resolution

6.1 Introduction

In addition to the spatial resolution, studied in Chapter 5, the temporal resolution is relevant for long term monitoring as well. The temporal resolution, or measurement interval, representing the number of measurements per time interval and relates to the relevancy, privacy and the computational costs of the luminance distribution measurements. A very high temporal resolution, using a luminance camera, can cause a sheer amount of data, which requires significant computational resources with possible little relevancy, while a low temporal resolution might omit relevant daylight variations [129]. Moreover, a very high temporal resolution might allow undesirable tracking of people, which should be prevented as this might hamper the application of luminance cameras due to privacy concerns.

Luminance distribution measurements have been conducted, previously, for longer periods of time. A distinction was made between studies that conducted a monitoring campaign related to evaluation and studies related to implementation in lighting control systems.

Konis and Lee [193] used a 5 minute interval, to quantify the variation in scene luminance, to evaluate the performance of a louver system, for approximately 1 year. Painter et al. [190], to evaluate occupants' experience with a novel facade technology, also conducted luminance distribution measurements for an entire year, and chose to apply a data sampling interval, for the luminance distribution measurements, of 30 min, which was deemed appropriate for monitoring human behaviour. Occupant interaction, such as changing the lighting scenes, occurs relatively infrequently, thus measurement intervals between 15 minutes and 1 hour were expected to be appropriate for yearly measurements, as errors were likely to be cancelled out [209]. An alternative scanning interval of 20 minutes was applied to assess occupant interaction for a measurement period up to 60 days [191]. In addition, these evaluation studies tend to measure a wide range of (lighting) metrics such as the illuminance, most of them at a much higher temporal resolution ($\approx 30s$) because HDR imaging is less straightforward and requires more computational resources.

Studies that implemented luminance-based control generally employed a higher sampling rate, as these systems have to respond quickly to changing conditions. Newsham and Arsenault [188] applied a temporal resolution of 1 minute for a proof-of-concept light and shading controller, which was the shortest interval possible with the applied imaging device. However, also measurement intervals of 5 minutes have been found in the literature related to luminance-based shading control [194].

To determine a suitable temporal resolution for continuous luminance distribution measurements, daylight variations were analyzed using a discrete Fourier transform (DFT) [210]. Due to the HDR technology, measurements cannot be performed at very high intervals as multiple images have to be captured and merged (Chapter 2), using the current spatial resolution (901 x 676 pixels) this takes approximately 20 seconds using the Bee-Eye. Moreover, luminance cameras produce a huge amount of data that all needs to be processed and analyzed, which argues for lower temporal resolutions. Down-sampling the temporal resolution eliminates the high frequency part of the spectrum, which cannot be reconstructed since the information is lost. Therefore, a Fourier-transform was utilized to investigate the frequency domain of daylight variations to propose a temporal resolution that is deemed suitable for luminance distribution measurements being implemented in lighting control systems.

6.2 Methodology

A DFT was applied to three alternative daylight data sets elaborated in Table 6.1. The outdoor horizontal illuminance was measured at the SolarBEAT [211] facility located on the roof of the Building Physics and Services laboratory at Eindhoven University of Technology (51°26'46.2"N 5°29'06.0"E). The desktop illuminance and the luminance distributions were measured in a mock-up office room located in said laboratory analogous to the lab setup in Chapter 5 (Figure 5.1, Page 80). The illuminance was measured at position Hx while the three Bee-Eyes were applied at positions BE1, BE2, and BE3, respectively (Figure 5.1), to illustrate locational effects on the daylight variability. Only days without missing data were considered.

Table 6.1: Summary of the data sets applied in the discrete Fourier transforms. The sample size indicates the actual days, without missing data, used by the DFT.

Indicator	Unit		Measuring period	Interval	Sample size	Device
Horizontal illuminance	lx	Outdoor	01-01-2016 to 31-12-2016	1 m	286 days	-
Desktop illuminance	lx	Indoor	14-11-2018 to 07-01-2019	30 s	50 days	Hagner E4-x
Luminance distribution	cd/m ²	Indoor	23-11-2018 to 04-01-2019	1 m	5 days	Bee-Eyes

The luminance distribution was measured during 5 morning and 5 afternoon periods at an interval of 1 min in a spatial resolution of 901 x 676 pixels. Morning period measurements were conducted from 8:30 to 12:00 while afternoon period measurements were conducted from 13:00 to 16:30.

The multidimensional output of the Bee-Eyes was translated to one-dimensional luminance-based metrics, suitable for DFT in the time domain, such as the mean Desktop Luminance, mean Background Luminance and the Desktop/Background Luminance ratio. For the ceiling-based device only two independent desktop luminances were extracted as is displayed in Table 6.2.

Table 6.2: Luminance-based metrics and characteristics relative to the Bee-Eyes, for data set 3, as used in the discrete Fourier transforms. Further illustration is found in Figure 5.1.

Device	Position	Orientation	Distance to window	Indicators
Bee-Eye 1	Ceiling	-	1.90 m	Desktop D2, Desktop D3
Bee-Eye 2	Eye level	South	2.75 m	Desktop D2, Background, Ratio
Bee-Eye 3	Eye level	North	1.05	Desktop D3, Background, Ratio

The DFT was performed using the Fast Fourier Transform algorithm (*fft*) of MATLAB R2017a. The Fourier transform requires a stationary signal as input, which can be interpreted as a signal with a constant mean and variance over time [212], as the *fft* function aims to extract infinite (co)sines from a finite time series. In the case of daylighting, the assumption of stationarity is violated [212]. The Discrete Wavelet Transform (DWT) seems more appropriate because it does not require a stationary signal as it is able to extract finite quasi-harmonic components from a

signal. However, Houtveen and Molenaar [213] showed that the DFT and the more complex DWT yielded similar results with only marginal differences, based on a signal representing heart rate variability, where the DWT was the theoretically valid method. Non-stationary signals can cause discontinuities at the end of each sampling period when using DFT. This is called leakage and can cause a bias in amplitude and frequency of the harmonic estimate [214]. To limit leakage associated with finite signals, window functions can be applied over each sampling period that reduce the discontinuity at the boundary of the sampling period. A window can be seen as a multiplicative weighting that brings the data smoothly to zero at the sampling period boundaries for many orders of derivatives. Based on a comparative study, Harris recommended the 4-sample Blackman-Harris or the 4-sample Kaiser-Bessel window for most applications [214]. For this study, it was chosen to apply a window function to the non-stationary daylight signals instead of using the more complex DWTs.

6.2.1 Input

According to the Nyquist rate, only frequencies larger than twice the sampling rate can be extracted from a signal. This implies that the maximum frequencies that can be extracted are 2 minutes, 1 minute and 2 minutes, respectively, for data sets 1 to 3. However, the objective was to extract frequencies starting from 1 minute, analogous to [188]. Therefore, for data set 1 and 3, nearest neighbor interpolation was applied, as an imputation, to transform the sampling rate to 30s.

Data sets 1 and 2, representing complete days of data, suggest a natural window as each individual day was considered as one sampling period. Hence, it can be seen as an infinite signal because there are no discontinuities at the boundaries of the sampling period (darkness at beginning and end). After the Fourier transform, the outputs of the 286 and 50 individual DFTs were averaged to one DFT for the outdoor horizontal illuminance and one DFT for the desktop illuminance.

For data set 3, with sampling periods of 3.5 hours, a 4-sample Blackman-Harris window was applied which brings the data at the boundary smoothly to zero in a cosine-like manner. An example is given in Figure 6.1 where the raw signal (black), which has very large discontinuities, is translated to a signal (orange) without discontinuities.

6.2.2 Output

The *fft* function computed the DFT for decreasing frequency bins, starting from 1/60 Hz, 1/59 Hz and so on. For readability, the frequency was translated to the time domain. However, the bin size was very narrow for short durations and the bin size for the long durations was very large. Therefore, discretization was applied such that the single side amplitude spectrum was described by one minute bins, which was considered more intuitive in the context of this research. The amplitude of a one minute bin was represented by the sum of all amplitudes in that respective minute. Additionally, the amplitude of each bin was scaled by the average total power of the entire data set.

The single side amplitude spectra were extracted for a range of conditions, such as the sky type, according to each condition shown in Table 6.3. For the desktop

6.2. Methodology

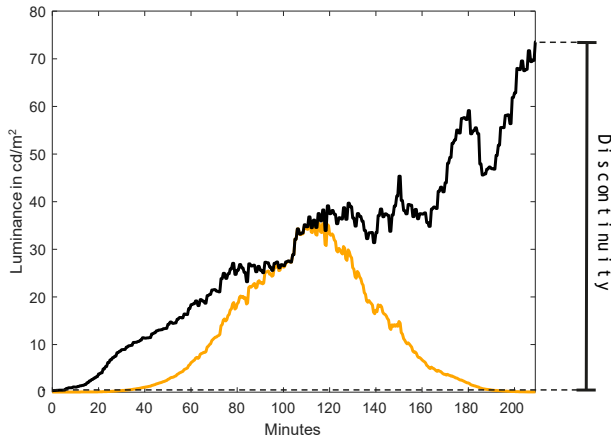


Figure 6.1: Example of 4-sample Blackman-Harris windowing function, which translates a signal, originating from the luminance data set, with a large discontinuity (black) to a signal without any leaking (orange).

illuminance and the luminance distribution, a distinction has been made between conditions with the artificial lighting switched off and switched on. Subsequently, to determine a suitable temporal resolution, the single side amplitude spectra were transformed to the normalized cumulative power weighted by the normalized total power. These normalized cumulative power functions describe the remaining power relative to a decreasing temporal resolution. In the context of this study, a relative power threshold of 85% was used to define a suitable temporal resolution, which is somewhat arbitrary. However, this threshold is a compromise between the objective to reduce the amount of data and the objective to maintain the power of the measured signal. Moreover, it is expected that the sensor signal might contain some high frequency noise. The sensitivity of the threshold was considered by reviewing the respective temporal resolutions for a threshold of 90% and 80% as well.

Table 6.3: The different conditions analyzed using discrete Fourier transforms relative to the Horizontal illuminance, Desktop illuminance, Luminance distribution and Desktop luminance.

Data	Aspect	Condition
Horizontal illuminance	Weather	Clear sky; Intermediate sky; Overcast sky
Horizontal illuminance	Season	Winter; Spring; Summer; Autumn
Desktop illuminance	Weather	Clear sky; Intermediate sky; Overcast sky
Luminance distribution	Indicator	Desktop luminance; Background luminance; Luminance ratio
Desktop luminance	Position	Ceiling-based; Eye level

The sky conditions were based on the daily average cloud cover, on a scale of 1 to 8, as determined by the Royal Netherlands Meteorological Institute (KNMI), measured at the weather station in the vicinity (≈ 7 km). In this study, a clear sky

was defined as a cloud cover ranging from 1 to 4, the cloud cover of an intermediate sky was ranging from 5 to 7 and the cloud cover of an overcast sky was 8.

6.3 Results

6.3.1 Horizontal illuminance

Figure 6.2 illustrates the average single side amplitude spectra of the outdoor illuminance for clear ($n = 93$), intermediate ($n = 177$) and overcast skies ($n = 96$), respectively. It shows that the variability was rather similar for clear and intermediate skies. However, the power of the one minute frequency was larger for intermediate sky conditions, due to moving clouds in front of the sun. As expected, for overcast sky conditions, the variability of daylight was significantly lower. Also, the individual differences between amplitudes was much smaller for overcast skies, due to relatively constant conditions during these days.

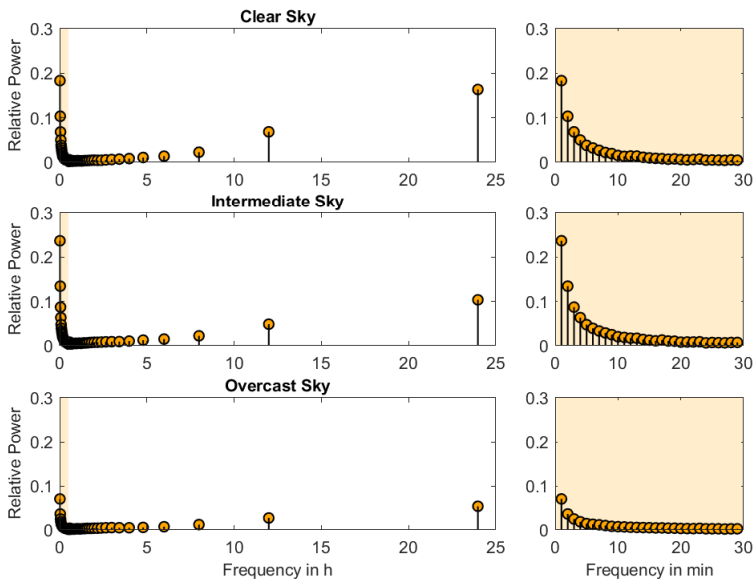


Figure 6.2: Average single side amplitude spectrum per sky condition measured between 01-01-2016 and 31-12-2016.

In order to define a suitable temporal resolution, the cumulative normalized power is shown in Figure 6.3 relative to a clear sky, intermediate sky and overcast sky. This figure indicates how much of the total power of the original signal is present relative to a certain temporal resolution. For instance, a temporal resolution of 18 minutes is only able to deduct 50% of the power of the original signal for clear sky conditions, indicating that this might not be a suitable measurement interval. Similar to Figure 6.2, it indicates that the variability for overcast sky conditions was significantly lower than the others. Figure 6.3, compared to Figure 6.2, also clarifies the differences between intermediate and clear skies. Especially, for intermediate sky conditions the

6.3. Results

temporal resolution has a large influence on the total power of a signal. In general, the total power of a signal was very sensitive for small interval changes at high temporal resolutions. For very low temporal resolutions the effect on the total power of a signal was negligible, as the cumulative trend is close to horizontal. Similar analyses have been conducted for the different seasons as indicated in Table 6.4. During spring and summer high temporal resolutions were required because, in the Dutch climate, this are relatively long days with often intermediate sky conditions. For instance, during the winter, a low temporal resolution suffices due to the short days with mainly overcast skies and/or clear skies. Overall, independent of the conditions, a 2 minute interval was required to capture 85% of the power of the total signal. This aligns with the temporal resolution of the highly variable conditions such as intermediate sky conditions, indicating that highly variable conditions have a very large effect on the average power of the signal.

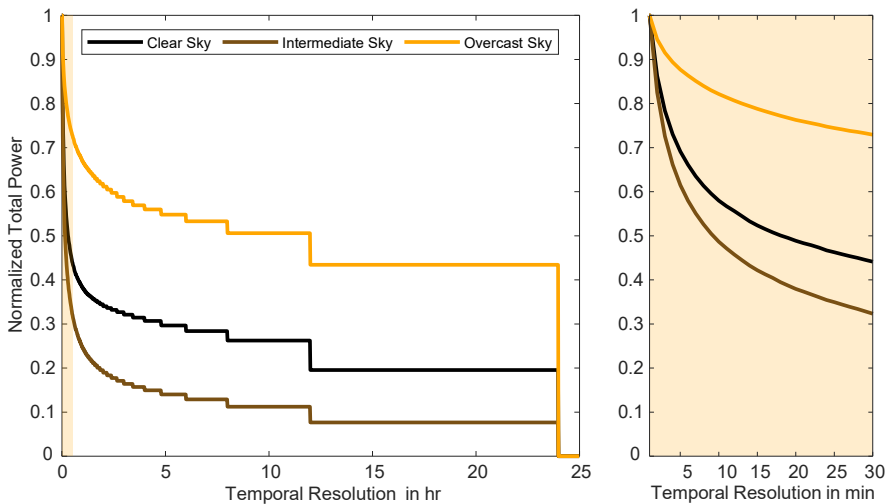


Figure 6.3: Normalized total power of the daylight signal relative to the temporal resolution per sky condition measured between 01-01-2016 and 31-12-2016.

Table 6.4: Temporal resolution according to the normalized total power threshold for conditions measured between 01-01-2016 and 31-12-2016. In grey, the temporal resolutions for the alternative thresholds are illustrated.

Aspect	Conditions	90% threshold	85% threshold	80% threshold
Total	All	2 min	2 min	2 min
Weather	Clear	2 min	2 min	3 min
	Intermediate	2 min	2 min	2 min
	Overcast	4 min	7 min	13 min
Season	Winter	6 min	15 min	39 min
	Spring	2 min	2 min	3 min
	Summer	2 min	2 min	2 min
	Autumn	2 min	4 min	6 min

6.3.2 Desktop illuminance

Identical analyses were conducted for the desktop illuminance measured in the mock-up office, although the single side amplitude spectra are not illustrated. Compared to the outdoor illuminance, the amplitudes of the lower frequencies were stronger, while the peak towards the 1 minute interval was more leveled off. Nevertheless, the variability of daylight under overcast sky conditions remains very low.

Figure 6.4 shows the cumulative normalized power of the desktop illuminance relative to the sky conditions with the electrical lighting switched off ($n = 5$, $n = 15$, $n = 14$, respectively). Again, the overcast sky conditions were much more robust to the temporal resolution than the clear and intermediate sky conditions similar to Section 6.3.1.

Remarkably, for the desktop illuminance, the clear sky condition was in some cases more sensitive to the temporal resolution than the intermediate sky conditions as found in Figure 6.4, mainly for the intermediate and low temporal resolutions. For high temporal resolutions, Table 6.5 illustrates that the variability was slightly lower, 3 minutes compared to 2 minutes, compared to the outdoor illuminance mainly due to shading by the building construction (daylight opening at one side). Additionally, the artificial lighting largely impacted the required temporal resolution as well (Table 6.6). Due to the constant fixed artificial lighting, the required temporal resolution, for 85% of the power, decreased to 8 minutes. Moreover, even lower resolutions were required for intermediate and overcast sky conditions.

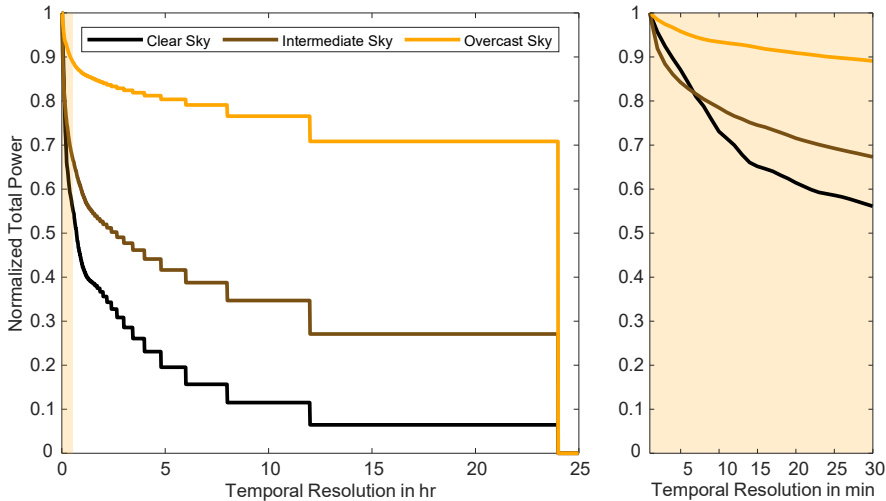


Figure 6.4: Normalized total power of the desktop illuminance signal relative to the temporal resolution per sky conditions with the lighting turned off.

6.3. Results

Table 6.5: Temporal resolution for the desktop illuminance according to the normalized total power threshold with the lights off. In grey, the temporal resolutions for the alternative thresholds are illustrated.

Aspect	Conditions	90% threshold	85% threshold	80% threshold
Total	All	2 min	3 min	4 min
Weather	Clear	4 min	6 min	7 min
	Intermediate	3 min	5 min	7 min
	Overcast	24 min	1 h 35 min	6 h

Table 6.6: Temporal resolution for the desktop illuminance according to the normalized total power threshold with the lights on. In grey, the temporal resolutions for the alternative thresholds are illustrated.

Aspect	Conditions	90% threshold	85% threshold	80% threshold
Total	All	4 min	8 min	14 min
Weather	Clear	-	-	-
	Intermediate	11 min	23 min	46 min
	Overcast	33 min	1 h 35 min	4 h 47 min

6.3.3 Luminance Distribution

In this section the results of the DFT based on the luminance distribution measurements are displayed, which were mainly measured during overcast and intermediate sky conditions and mainly with the electrical light switched off (70%). Therefore, no analyses have been conducted relative to the sky conditions. The single side amplitude spectra all showed large amplitudes at 3.5 hours due to the Blackman-Harris window that was applied, which will not be the case in practice. The desktop and background luminance performed rather similar according to the single side amplitude spectra. Consequently, the sensitivity to the temporal resolution for the Desktop/Background ratio, a combination of the desktop and background luminance, was two orders of magnitude lower.

Figure 6.5 shows the cumulative normalized total power relative to the desktop and background luminance and its ratio when the artificial lighting was turned off. It shows that the sensitivity of the desktop luminance to the temporal resolution was actually quite high compared to the background luminance. Moreover, in contrast to the findings in Section 6.3.2, the background luminance showed a higher variability when the artificial lighting was turned on (Table 6.7 and 6.8), most likely caused by different weather conditions in combination with the small sample size. The Desktop/Background ratio was extremely robust to the temporal resolution, almost no power is lost for lower temporal resolutions when only daylight variations are considered. Naturally, this is not the case when the artificial lighting and/or sun shading are also variable. The data shows that a ceiling-based measurement position was slightly more sensitive to daylight variations than measurements at eye level, for desktop luminance measurements, mainly when the artificial lighting was turned on. It is hypothesized that this is due to the lower amount of pixels, representing the desktop surface, of the ceiling-based measurement.

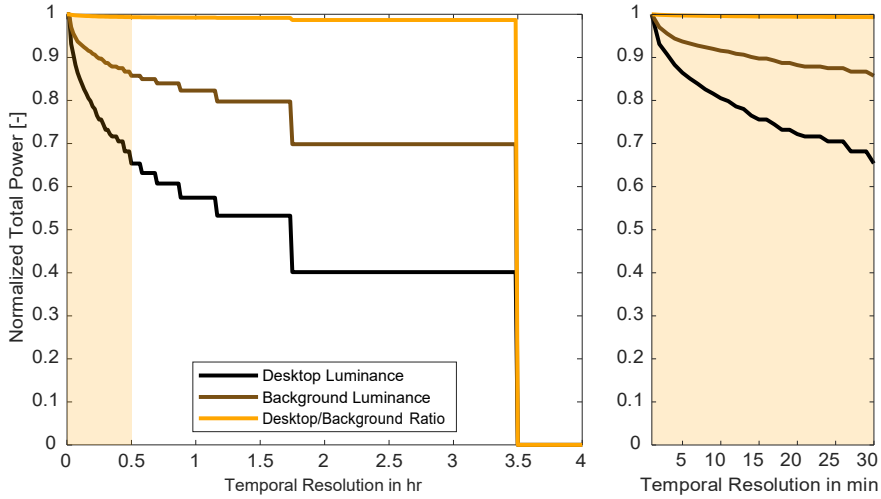


Figure 6.5: Normalized total power of the luminance signal relative to the temporal resolution per luminance metric with the lighting turned off.

Table 6.7: Temporal resolution for the luminance distribution according to the normalized total power threshold with the lights off. In grey, the temporal resolutions for the alternative thresholds are illustrated.

Aspect	Conditions	90% threshold	85% threshold	80% threshold
Indicator	Desktop luminance	3 min	5 min	9 min
	Background luminance	27 min	1 h 9 min	1 h 44 min
	Desktop/background	3 h 29 min	3 h 29 min	3 h 29 min
Position	Ceiling	3 min	6 min	11 min
	Eye	3 min	6 min	10 min

It was hypothesized that the desktop luminance has a strong correlation with the desktop illuminance indicated in Section 6.3.2. With the artificial lighting turned off, temporal resolutions of 3 and 5 minutes were required for the illuminance and luminance measurements, respectively, to maintain a power of 85%. When the artificial lighting was turned on, a temporal resolution of 8 and 9 minutes was required, respectively. Hence, only minor differences were exhibited between the desktop illuminance a desktop luminance due to variable weather conditions but also due to the larger measurement area of the luminance, making it slightly more sensitive. This places the results found for the illuminance in Section 6.3.2 and the luminance in Section 6.3.3 on approximately the same level.

6.3.4 Sensitivity

As indicated in Section 6.2, a threshold of 85% was assigned, which was arbitrary to a certain extent. Therefore, the resulting temporal resolutions were also calculated for a threshold of 90% and 80% to indicate the sensitivity of this assumption.

The results show (Tables 6.4 to 6.8) that the sensitivity of this assumption was high for conditions that required relatively low temporal resolutions. On the other

6.4. Discussion

Table 6.8: Temporal resolution for the luminance distribution according to the normalized total power threshold with the lights on. In grey, the temporal resolutions for the alternative thresholds are illustrated.

Aspect	Conditions	90% threshold	85% threshold	80% threshold
Indicator	Desktop luminance	4 min	9 min	17 min
	Background luminance	4 min	13 min	29 min
	Desktop/background	3 h 29 min	3 h 29 min	3 h 29 min
Position	Ceiling	3 min	7 min	14 min
	Eye	11 min	24 min	35 min

hand, conditions that required a high temporal resolution such as the outdoor illuminance measurements, shown in Table 6.4, were not sensitive to the threshold that was assumed. This indicates that for very high temporal resolutions the assumption of 85% is acceptable. However, in the context of this thesis, the emphasis lies on indoor measurements, generally with the artificial lighting switched on. This implies that the temporal resolution is, to a certain extent, dependent on the set threshold. For instance, desktop luminance measurements resulted in temporal resolutions of 4 minutes, 9 minutes and 17 minutes for a 90%, 85% and 80% threshold, respectively, representing a significant range. Therefore, the temporal resolution should be chosen carefully.

In general, the sensitivity is rather low when the slope of the cumulative total power is steep but it increases when the slope becomes more flat. However, the area where the slope is steep, is generally decisive.

6.4 Discussion

In this chapter the DFT was applied to three data sets, with varying characteristics, with the objective to determine a suitable temporal resolution for long term luminance distribution measurements.

Generally, the results indicated that the highest temporal resolution was required for intermediate sky conditions with the electrical lighting switched off. All three data sets required a temporal resolution, utilizing a 85% power threshold, below or equal to 5 minutes. In some cases, the clear sky conditions were considered equal or even more variable compared to intermediate sky conditions. Sky conditions were rated as clear when the cloud cover was below 4. Hence, it does not guarantee a perfect clear sky. This classification was applied to provide more homogeneous data sets, as perfect clear skies occur infrequently in the Dutch climate.

Also, the variability of overcast skies was relatively high according to the DFT, for instance, Figure 6.2 shows a minor but distinct peak for the 1 min interval where one expects almost no dependency on higher frequencies. Firstly, perfect overcast sky conditions do not exist, still some minor variations can be exhibited. Secondly, the sensor outputs are expected to contain some noise for the higher frequencies. These artefacts might have caused the relatively high variability for the higher frequencies. However, the effects of these artefacts are limited, as the 85% threshold accounts for some noise and other sky conditions are decisive.

When the electrical lighting was turned on, the required temporal resolution

decreased to 8 and 9 minutes, for desktop illuminance and desktop luminance, respectively. However, the respective data sets, with the electrical lighting on, were relatively small. Therefore, the effect of the variable weather conditions, compared to when electrical lighting was switched off, is difficult to seize. Moreover, the sensitivity of the assumption that 85% of the total power of a signal is a suitable threshold was relatively high for these conditions. Therefore, it seems appropriate to be at the higher side of these temporal resolution. It would be beneficial, although, if a threshold could be applied with a more fundamental basis.

For the luminance distribution, the desktop luminance was most sensitive to the variability of daylight most likely due to a higher component of direct light. The background surface, especially measured with Bee-Eye 2, contained relatively large surfaces that did not capture direct light, which was not the case for the desktop surface. Ratios turned out to be almost insensitive to daylight variations as both components are subject to almost identical daylight variations.

Finally, the DFT applied to the luminance distribution should be considered carefully. Discrete Wavelets Transforms (DWT) were actually the valid method for this non-stationary signal. However, Houtveen and Molenaar [213] showed that windowing is able to prevent bias in amplitude and frequency, which was only validated based on heart rate data. However, the luminance data had different characteristics with very large discontinuities, as indicated in Figure 6.1.

The appropriate temporal resolution is based on the most extreme conditions, for instance desktop luminance measurements under intermediate sky conditions. They exhibit the largest variation and are, therefore, normative for the temporal resolution. Nevertheless, luminance measurements, in the context of this thesis, are conducted within the office environment with the electrical lighting generally turned on. Consequently, a temporal resolution of 5 to 6 minutes is deemed appropriate. With this temporal resolution, the 85% thresholds for indoor measurements including electrical light were well satisfied. Moreover, the temporal resolution is almost in the range of indoor measurements without electrical lighting because this could occur occasionally as well. Finally, a temporal resolution of 5 or 6 minutes can be equally divided within an hour, which is not the case for 7 or 8 minute intervals. A temporal resolution of 5 to 6 minutes is much higher than applied by the evaluation studies [190, 191, 193] and corresponds to the temporal resolution applied in the luminance-based control system developed by Goovaerts et al. [194]. On the other hand, it is significant lower than applied by Newsham and Arsenault [188], which was also the highest temporal resolution that was possible for their camera system.

An alternative approach could be to assign a dynamic interval, which is a temporal resolution that is dependent on the current environmental conditions. A basic algorithm to achieve this conducts measurements at the highest interval but does not process the latest captured HDR image if there is no, or limited, difference to the previous measurements. A disadvantage is that due to the added complexity it requires even more computational resources. Moreover, it becomes difficult to deploy alternative applications such as occupancy sensing to the camera system [188]. However, it does reduce the amount of data. Alternatively, a basic photo sensor might be utilized to detect changing conditions.

6.5 Conclusion

Besides the spatial resolution, the temporal resolution is an aspect that has to be carefully considered when performing long term luminance distribution measurements. The temporal resolution representing the number of measurements per time interval is a consideration between relevancy, computational resources and privacy, of which the latter two argue for lower temporal resolutions. Based on the Discrete Fourier Transform (DFT) of three alternative data sets representing in- and outdoor illuminance and luminance measurements, a temporal resolution of approximately 5 to 6 minutes has been proposed for luminance distribution measurements in office environments.

Utilizing the DFT to specify suitable temporal resolutions seems a useful method. However, it is complicated to assign an appropriate threshold that has sufficient fundamental basis. Moreover, especially the data sets containing the desktop illuminance and the luminance distribution were relatively small. It is therefore, advised to conduct long term measurements, for a year, at high intervals to create a data set that allows accurate extraction of the discrete Fourier transforms.

Ceiling-based luminance distribution measurements

This Chapter is based on:

Kruisselbrink TW, Dangol R, van Loenen EJ. Feasibility of ceiling-based luminance distribution measurements. *Building and Environment*. 2020 172;106699. <https://doi.org/10.1016/j.buildenv.2020.106699>

Kruisselbrink TW, Dangol R, van Loenen EJ. CEILING-BASED LUMINANCE MEASUREMENTS: A FEASIBLE SOLUTION? In: *Proceedings of the 29th Quadrennial Session of the CIE, Washington D.C., USA; International Commission on Illumination*; 2019. pp. 1166–1174. <https://doi.org/10.25039/x46.2019.P0077>.

7.1 Introduction

As illustrated earlier, a number of practical issues occur when luminance distribution measurement devices, such as the Bee-Eye, are implemented in real-life office environments (e.g. lighting control systems) for longer periods of time. For instance, the spatial (Chapter 5) and temporal resolution (Chapter 6) might need to be reduced to prevent privacy concerns and limit the computational costs. Preferably, to indicate visual comfort or visual performance, luminance distributions are required that correspond to the FOV of the user. This is not feasible for long term measurements because this, most likely, interferes with the daily activities within the office environment. Therefore, an alternative position should be applied such that it does not interfere and still approximates the FOV of the respective user. Furthermore, such a position should be easy to apply, preferably without complex commissioning.

Three distinct strategies, from low to high obtrusiveness, that aim to measure the luminance distribution from an alternative position have been identified based on the available literature. These strategies aim to capture relevant information without interfering with the users and their activities.

The first strategy, or the *ceiling-based strategy*, performs top-down measurements of the luminance distribution facing the work plane from the ceiling [141, 215, 216]. Hence, a luminance distribution with a different FOV is measured from a different angle of view compared to the actual FOV of the user. The objective of this *ceiling-based strategy* is to minimize interference with the office activities [216] while measuring the quantity of light on the desktop surface. A pilot study (Section 7.2) indicated that, for practical applications, ceiling-based luminance measurements seem a feasible solution.

The second strategy, the *partition- or monitor-mounted strategy*, intends to measure the luminance distribution with a similar angle of view relative to the user by placing the luminance camera on top of a monitor or partition in line with the users primary viewing direction [45, 217, 218]. In this configuration, the obtrusion for the user is limited. However, due to the translational displacement, the luminance camera omits the direct task area. Additionally, it might be experienced as very obtrusive for the office worker at the opposite workplace.

Motamed et al. [218] studied the effect of a luminance camera on top of a monitor relative to the user's FOV on the Daylight Glare Probability (DGP) by introducing a translational change of 100 cm. Measurements in a small office space with the desktop parallel to the window resulted in a relative difference in DGP with a root mean square (RMS) value of 11%.

In the third strategy, the *vicinity strategy*, the luminance camera is placed somewhere in the direct vicinity of the user, this can be either by small translational [188, 190, 191, 218] and/or angular [188, 218, 219] displacements relative to the user. Compared to the previous strategies this might cause some obtrusion (i.e. limited elbow room, privacy intrusion), but the relevant FOV, including the direct task area, is captured.

Motamed et al. [218] also measured the effect of translational (± 30 cm) and angular ($\pm 30^\circ$) displacements relative to the user's FOV on the Daylight Glare Probability (DGP). It turned out that the DGP is more sensitive to angular changes than to translational changes of the FOV with a maximum relative difference in DGP of 32%. Additionally, Fan et al. [219] applied either translational (23 to 118 cm)

7.2. Pilot

or angular displacements (15° to 45°) relative to the user's FOV under overcast sky conditions in a one-window office. The relative difference in luminance was determined based on six luminance patches in the FOV of the user. The average relative differences were rather similar between translational and angular displacements with relative errors generally below 25%. For this research [219], it was proposed to place luminance cameras at 30° from the user's FOV at a distance of 30 to 50 cm behind the user.

Finally, some alternative measurement positions have been introduced in the literature, which cannot be categorized. Goovaerts et al. [194] placed the luminance camera such that it provided an overview of the entire office environment while measuring glare, independent of a certain user, to control the automated blinds. Kim et al. [220], also to control the blinds, placed the luminance camera directly on the window surface such that the luminous conditions of the exterior environment were monitored. For such systems, one single measurement device would suffice for a single space. However, disadvantages of such systems are that they cannot be related to a user, as the lit environment experienced is largely dependent on the viewing direction. For instance, illuminance differences up to a factor of 20 can be exhibited in an office environment [221].

Open-plan offices are currently the most applied office typology, they are cost-effective and are intended to boost collaboration [222]. Especially in Europe, these offices either lack partitions or the partitions are very low. Therefore, the strategy to place the luminance camera on a partition is not feasible. Similarly, the strategy to place the luminance camera in the vicinity of the user is not very suitable for practical application in open-plan offices due to its obtrusiveness. Ceiling-based luminance cameras seem to be the most suitable position in this context, they do not cause any obtrusion and, moreover, they allow measurements for multiple users at once.

Therefore, the objective of this study was to identify the most suitable position for ceiling-based luminance distribution measurements in an open office environment and to assess its performance under real office conditions. The research presented in this chapter consists of two phases preceded by a pilot study. The pilot study was employed to assess the feasibility of ceiling-based luminance distribution measurements. Subsequently, in the first phase, the most suitable ceiling-based measurement position was identified for four independent indicators representing the visual performance (2x), visual comfort and the NIF effects. In the second phase, the performance of this most suitable position, found in phase one, was assessed under real office conditions.

7.2 Pilot

The objective of this pilot study was to validate whether ceiling-based luminance distribution measurements are able to approximate luminous conditions as experienced by the user within a typical office environment. This will indicate whether it is feasible to perform ceiling-based measurements instead of luminance distribution measurements at eye level with the objective to prevent interference with office activities.

7.2.1 Methodology

Luminance distribution measurements, using three Bee-Eyes, were conducted in the mock-up office illustrated in Figure 5.1 (Page 80). Measurements were conducted for two days with clear sky conditions, two days with intermediate sky conditions and two days with overcast sky conditions during November and December 2018. Each day was described by a morning (8.30 - 12h) and afternoon (13 - 16.30h) period. For each weather condition and day period measurements were conducted with and without the electrical lighting (9x PHILIPS RC461B G2 PSD W60L60 1xLED34 S/840) turned on, providing an equally distributed 750 lx, resulting in a total of 6 measuring days.

Two Bee-Eyes were placed at eye level, using tripods, representing the FOV of a seated virtual office user facing south (virtual user 1, BE2) and north (virtual user 2, BE3), respectively, as displayed in Figure 5.1. To compare these with the proposed ceiling-based solution, one Bee-Eye (BE1) was attached to the ceiling.

For each individual luminance distribution, the average luminance on the desktop area directly in front of the two virtual users was extracted from Bee-Eye 2 and Bee-Eye 3. Additionally, the luminance from the identical desktop areas was extracted from Bee-Eye 1, representing an identical desktop area, with different distortions, from a different angle of view as displayed in Figure 7.1.

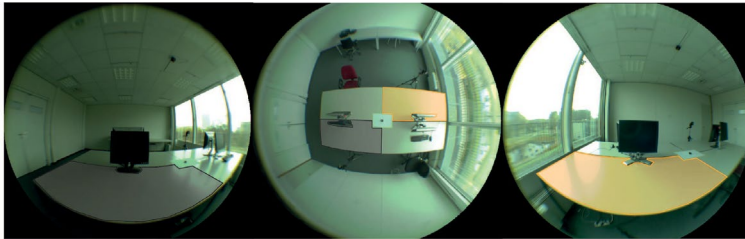


Figure 7.1: Luminance mask applied in the pilot study, BE2, BE1 and BE3, respectively. The black mask relates to virtual user 1 while the orange mask relates to virtual users 2.

The Normalized Root Mean Square Error (NRMSE) was used to indicate the differences between the approximated (ceiling-based) desktop luminance and the actual desktop luminance (eye level) experienced by the virtual user. Comparisons were conducted for all day periods, 12 in total, containing a wide range of conditions. A unique calibration factor (k) was applied to the luminance measured by the ceiling-based camera ($L_{ceiling}$), according to Equation 7.1, for each individual day period, to approximate the experienced luminance (L_{eye}). Additionally, all measurements were compared, using the NRMSE, with only one single fixed calibration factor, relative to each device, that matched the average desktop luminance of all ceiling-based measurements to the average desktop luminance measured at eye level.

$$\bar{L}_{eye} = k \cdot \bar{L}_{ceiling} \quad (7.1)$$

7.2.2 Results

In this section, the comparison between the average desktop luminance measured from the ceiling relative to the measurements at eye level, conducted during the pilot study,

7.2. Pilot

is displayed. Figure 7.2 displays the average desktop luminance values measured for overcast sky conditions in the afternoon with the electrical lighting off and on. It shows large correspondence between the approximated luminance, originating from the ceiling measurements, and the actual luminance measured from eye level when a unique calibration factor was applied for each day period, although the predictions were statistically different ($p = 0.0176$ and $p = 0.0016$) for both virtual user 1 and virtual user 2. Almost all peaks and dips were observed in both the approximated and the actual measured luminance, only small variations were found relative to the order of magnitude. Similar effects were exhibited during mornings and other weather types. Also, the approximations with a fixed calibration factor (Figure 7.2, Orange with transparent marker) showed reasonable resemblance to the eye level measurements.

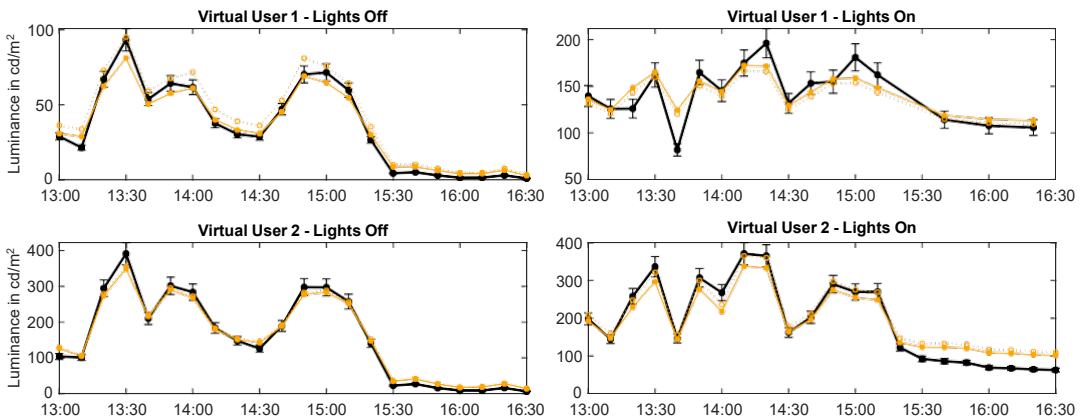


Figure 7.2: Luminance of the ceiling-based measurement (Orange) relative to the actual luminance measured at eye level (Black) with errorbars representing the average deviation for grey surfaces (Chapter 2). Filled markers represent approximations with a unique calibration factor while transparent markers represent a fixed calibration.

Table 7.1: Difference between approximated and actual desktop luminance, including calibration factor k . The fixed NRMSE applied the mean k ($k = 0.96$). The standard deviation is indicated between brackets.

		k	NRMSE	NRMSE (fixed k)
Total		0.96 (0.11)	10.3% (4.8%)	14.6% (9.4%)
Lighting	Lights On	1.00 (0.07)	9.5% (5.1%)	10.6% (4.0%)
	Lights Off	0.91 (0.11)	11.0% (5.1%)	18.6% (11.9%)
Period	Morning	0.94 (0.12)	9.8% (4.5%)	16.8% (11.9%)
	Afternoon	0.97 (0.08)	10.7% (5.1%)	12.4% (5.0%)
Sky	Clear	1.00 (0.09)	7.8% (5.0%)	12.6% (7.0%)
	Intermediate	0.98 (0.07)	12.1% (5.2%)	12.4% (4.0%)
	Overcast	0.89 (0.12)	10.9% (2.7%)	18.9% (13.2%)
Virtual user	1	0.98 (0.13)	10.2% (5.2%)	16.6% (12.0%)
	2	0.93 (0.07)	10.3% (10.3%)	12.6% (4.9%)

Table 7.1 shows that, on average, the NRMSE between the approximation and the actual luminance was 10.3% with a standard deviation of 4.8% when a unique calibration factor was applied for each day period. It also shows that this calibration factor k was very close to 1, also it exhibited only little variance. The NRMSE generally was high for highly variable conditions. For instance, the largest difference was found during intermediate sky conditions. The largest variation was found for the prediction of the desktop luminance in front of virtual user 1, which was oriented south.

On average, the prediction using a fixed calibration factor had an NRMSE that was 4.3% higher. However, the average variability of the NRMSE, indicated by the standard deviation, was more than doubled. For the individual conditions, the fixed calibration always resulted, for the NRMSE, in an increase ranging from 0.3% to 8.0%. Remarkably, the variability of the NRMSE showed generally either a large decrease or a large increase for a fixed calibration factor relative to a unique calibration factor.

Moreover, the approximations showed a large agreement with the actual values, indicated by Pearson's correlations of 0.994 and 0.995, respectively. An average bias of 17.0% relative to virtual user 1 and 11.3% relative to virtual user 2 was found. This shows some similarities to the NRMSE (16.6% to 12.6%) found in Table 7.1.

7.2.3 Conclusion

This pilot showed that the experienced desktop luminance can be approximated, to a certain extent, using a ceiling-based luminance camera, although the approximations were statistically different compared to the actual luminance values. For a practical application, assuming a fixed calibration factor, the ceiling-based camera introduced an NRMSE of 14.6% and a mean bias of 14.2%, which for practical applications such as lighting control systems can be considered sufficient. Consequently, the feasibility of ceiling-based luminance distribution measurements is further elaborated in the remainder of this chapter.

7.3 Experimental setup

Additional luminance distribution measurements, using the Bee-Eyes, were conducted, with the objective to further assess the feasibility of ceiling-based luminance distribution measurements, in a mock-up office room (5 m x 5.5 m) with west-facing façade and a window opening of 5.5 m x 1.35 m, at the Building Physics and Services laboratory at the Eindhoven University of Technology. The façade was designed such that it corresponds to an 'average' office façade with an average simulated (Relux 2019.3.3.0) daylight factor of 6.2% (min = 2.1%, max = 16.5%). Four alternative ceiling-based positions were identified, as shown in Figure 7.3, which were expected to be able to approximate the luminous conditions to a certain extent, relative to the FOV of six virtual users (E1-E6). The actual luminous conditions for the virtual users were also measured, at a height of 1.2 m and at a horizontal distance of 20 cm from the desktop edge, corresponding to the eye position of a seated user. The lighting (9x PHILIPS RC461B G2 PSD W60L60 1xLED34 S/840) was turned on and provided a uniformly distributed 500 lx with a CCT of 4000 K on the desktop. Each desk contained an identical monitor (DELL 1708FPt, 300 cd/m^2) with an identical

7.3. Experimental setup

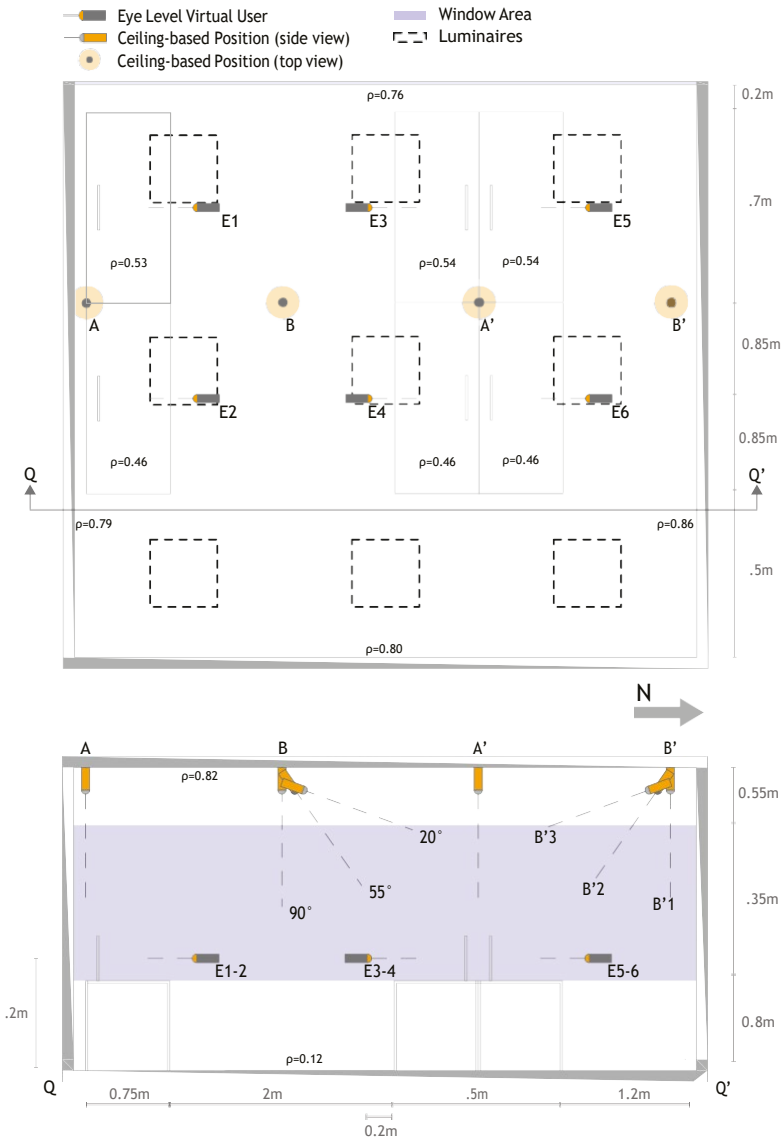


Figure 7.3: Floorplan and section of the mock-up office environment, the measurement positions are indicated by the grey-orange icons, it also indicates the wall, ceiling, floor and desktop reflectances of the surfaces (ρ).

monitor test screen [223] at full brightness.

For this research, four distinct locations were identified in the ceiling: one directly above the desks (A and A'), analogous to the pilot study, and three directly above the aisle (B and B') with three distinct orientations: at 90°(1), 55°(2) and 20°(3) relative to the ceiling, such that the projection center focused at the floor underneath, center of the adjacent tables (B'2 to E5-6), and the center of the distant tables (B'3 to E1-2), respectively. The non-perpendicular orientations (2) and (3) were lowered 10

cm relative to the ceiling to capture some direct sight of the ceiling. As an example, positions A and A' were grouped as one (A) because the measurement position relative to the virtual users was identical, only the absolute location was different.

Bee-Eye luminance distribution measurement devices, using the first measurement track (Section 2.2.4), were applied to measure four luminance based metrics, representing visual performance (2x), visual comfort and NIF effects, as described in Sections 7.3.1, 7.3.2 and 7.3.3. A photometric calibration factor was applied locally at the Bee-Eye, further post-processing was done using MATLAB R2019a. The Bee-Eyes were simultaneously calibrated (photometric calibration), in the mock-up office environment with electrical lighting only (500 lx, 4000 K), using a Konica Minolta LS-100 luminance meter ($\pm 2\%$, $f_1 = 8\%$) and a white ($\rho = 0.90$) and grey ($\rho = 0.18$) standard reflector.

7.3.1 Visual performance

The visual performance was indicated by the average **Desktop Luminance**, similar to the pilot study in Section 7.2, because of its analogy to the often used desktop illuminance, and by the average **Monitor Luminance**. The average Desktop Luminance was extracted by masking the respective desktop area for each measurement position, as illustrated in Figure 7.4. Similarly, the average Monitor Luminance was extracted by masking the respective monitor screen. For position A, no Monitor Luminance mask was applied because ceiling-based position A does not provide any view of the monitor screens.

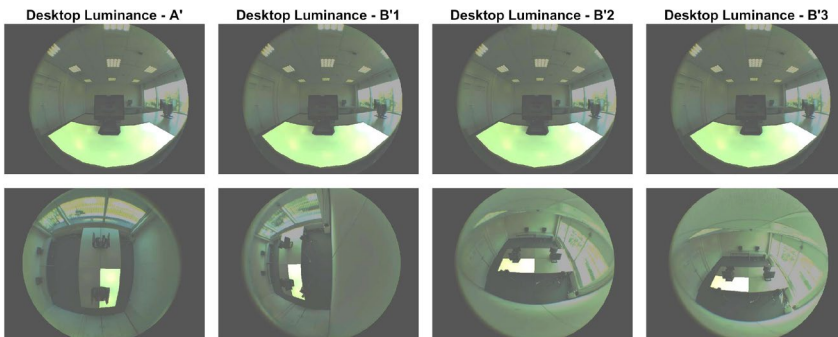


Figure 7.4: Desktop luminance masks for virtual user 6 and their respective ceiling-based alternatives.

7.3.2 Visual comfort

Besides visual performance, visual comfort is essential for achieving high-quality lighting (Chapter 1), which is “lighting that allows you to see what you need to see quickly and easily and does not cause visual discomfort, but raises the human spirit” [8]. In this study, visual comfort was indicated by the average luminance in the 40° **luminance band (B40)**. The B40 Luminance was first introduced by Loe et al. [224] as an indicator for visual comfort as it encompasses the main viewing area of a person

7.3. Experimental setup

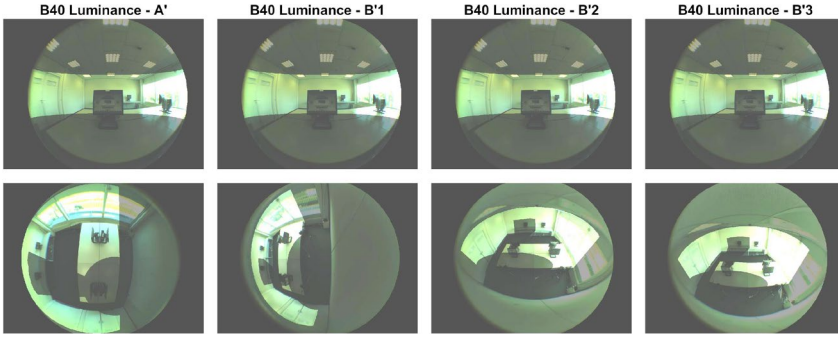


Figure 7.5: B40 luminance masks for virtual user 6 and their respective ceiling-based alternatives.

looking around in space. Later on, Van Den Wymelenberg and Inanici [225] showed that the B40 Luminance was one of the highest-ranked metrics for subjective visual preferences. Additionally, it was indicated that this metric is scene independent when applied at eye level, and hence does not require any commissioning.

However, this scene independence becomes a disadvantage for a ceiling-based position because the 40° FOV of the user needs to be translated to the alternative ceiling-based position. The translation was performed manually by masking the surfaces that were represented by the reference B40 Luminance mask. Due to the different orientation and location of the ceiling-based positions certain surfaces might be omitted while others were enlarged or compressed, as is indicated in Figure 7.5. This translation could be automated for a more accurate conversion if space and camera (projection equation) are well defined, but this does require complex geometric models to translate image coordinates of the reference camera to the image coordinates of the ceiling-based camera.

7.3.3 NIF effects

The most relevant measurable photometric quantity for the non-image forming (NIF) effects based on the luminance distribution is the **Retinal Illuminance**, which represents the total flux on the retina under the assumption that the sensitive cells are relatively equally distributed [226]. The total flux on the retina is largely influenced by the cutoff shading due to the human facial structure and the spatial response function of the eye [227]. The cutoff shading represented by the human FOV was based on Van Derlofske et al. [227] and Khademagha et al. [228] and is shown in Figure 7.6.A. A distinction can be made between monocular vision and binocular vision, representing the areas that are covered by a single eye and both eyes, respectively. Additionally, the spatial response, due to the anatomy (not from the distribution of cells [229]), of the retina differs from the standard cosine function. Based on ray-tracing of a healthy 45 years old eye Van Derlofske et al. found a spatial response of the retina as illustrated in black in Figure 7.6.B.

To extract the Retinal Illuminance from luminance maps, three distinct components were identified: masking of the FOV, application of the retina's spatial respon-

sivity and the application of the pixels' solid angle. Using the equisolid-angle fisheye projection equation [158], Equation 2.6, the FOV of the left and right eye were translated to an image resolution of 901 x 676 pixels as shown in Figure 7.6.A. Additionally, Figure 7.6.B shows the translated spatial response using the projection equation for an image radius of 901 x 676 pixels. The solid angle (Ω) of this projection type is constant (equisolid) for each pixel, which was $1.22 \cdot 10^{-6}$ sr. By combining the FOV ($M_{i,j}$), the spatial response ($\theta_{i,j}$) and the solid angle ($\Omega_{i,j}$) of each pixel with the original luminance map ($L_{i,j}$), the illuminance on the retina (E_{ret}) for a single eye can be determined as indicated in Equation 7.2. The Retinal Illuminance, as experienced by the user, was assumed to be the average Retinal Illuminance for both eyes.

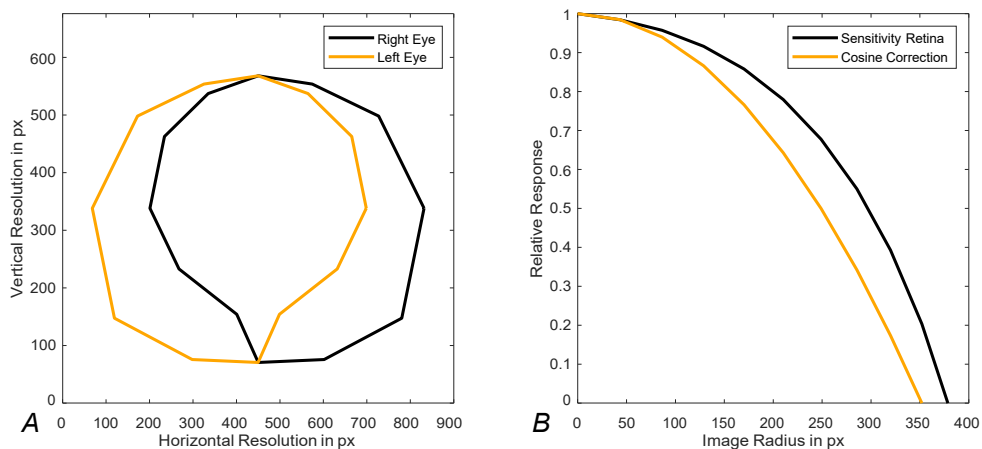


Figure 7.6: FOV (A) representing the FOV of the right and left eye. Sensitivity of the human eye (B) relative to the standard cosine function.

$$E_{ret} = \sum_{i=1}^{901} \sum_{j=1}^{676} L_{i,j} \cdot M_{i,j} \cdot \theta_{i,j} \cdot \Omega_{i,j} \quad (7.2)$$

To extract the Retinal Illuminance experienced by the user, while measuring from a ceiling-based position, the FOV and the spatial response were manually translated, the solid angle remained equal. The FOV was translated similar to the B40 Luminance mask in Section 7.3.2. Again, some differences were introduced for the different surfaces. The retina's spatial response was translated by extrapolating the focal point (sensitivity of 100%) of the reference measurement at eye level to the ceiling-based FOV. Subsequently, the reference spatial response, divided into quartiles, was scaled such that the midpoint was allocated to the extrapolated focal point for the ceiling-based position, introducing distortions in the X and Y direction. Moreover, the total sensitivity of the ceiling-based masks was aligned with the total sensitivity of the reference masks. The Retinal Illuminance masks for the left eye are illustrated in Figure 7.7.

7.4. Phase 1

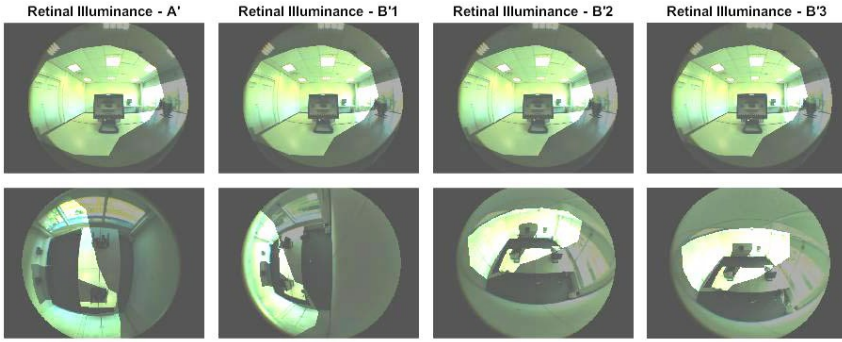


Figure 7.7: Left eye Retinal Illuminance masks for virtual user 6 and their respective ceiling-based alternatives.

7.4 Phase 1

7.4.1 Methodology

In the first phase of this study, luminance distribution measurements were performed aiming to find the most suitable ceiling-based position in the mock-up office described in Section 7.3. Three calibrated Bee-Eye luminance distribution measurement devices (BE1-BE3) were used to measure the four alternative ceiling-based positions consecutively in combination with two reference measurements at eye level (E1-E6). Starting from Position A relative to E1 and E2, all positions and appropriate combinations, according to Table 7.2, were measured. All positions and combinations were measured with and without daylight. The measurements were performed on 29-07-2019 under clear sky conditions without direct sunlight (during morning), with an average global irradiance of 596 ± 120 W/m² and an average cloud cover of 35.38% measured at the nearest weather station. Direct sunlight was prevented such that the measurements could be conducted consecutively, without abrupt variations in daylight. Therefore, there was no need to conduct all seven dependent measurements simultaneously.

Table 7.2: Measurement sequence during Phase 1. This sequence was measured with and without daylight.

BE1	A	A'	A'	B1	B1	B2	B3	B'1	B'2	B'2	B'3	B'3
BE2	E1	E3	E5	E1	E3	E3	E3	E5	E1	E5	E1	E5
BE3	E2	E4	E6	E2	E4	E4	E4	E6	E2	E6	E2	E6

Two sets, with and without daylight, of 36 luminance maps were captured; 24 luminance maps from the six virtual user positions (E1-E6) and 12 from ceiling-based positions A, B1, B2, and B3. The luminance range, without daylight, for the virtual users and ceiling-based positions was approximately 1:1750 and 1:700, respectively. During post-processing, the relevant luminance-based metrics representing the visual performance, visual comfort and the NIF effects, described in Sections 7.3.1, 7.3.2, and 7.3.3, were extracted from the luminance maps relative to virtual users 1 to 6.

The four alternative positions were assessed using the Coefficient of Determination (R^2), which is a measure of how well observed data (at eye level) is predicted by a model (ceiling-based), relative to each luminance-based metric. High coefficients indicate a high ability to approximate the luminous conditions as experienced by the virtual users.

Additionally, a linear model was developed for each luminance-based metric and each position, which relates the predicted luminance for the ceiling-based position to the actual measured luminance at eye level. This model, for the most suitable position, will be verified during the second phase.

7.4.2 Results

The results of the first phase are summarized in Figure 7.8 and Table 7.3. Figure 7.8 shows that all ceiling-based positions were able to accurately predict the Desktop Luminance as experienced by the virtual user, for all cases more than 98% ($= R^2$) of the variance was explained by the ceiling-based positions. Position A had a slightly lower performance than the variants of position B. However, for the B40 Luminance, position A outperformed the variants of position B (Table 7.3). On average, considering visual performance, visual comfort and NIF effects, the performance of position A and position B3 were very similar. However, position B could measure the Monitor Luminance, which was not possible for position A. The performance of positions B1 and B2 were comparatively low (Table 7.3). Therefore, based on these measurements, position B3, an aggregate of B3 and B'3, was found to be the most suitable ceiling-based position, this position also had the largest similarities with the FOV and the angle of view of the eye-level measurements.

The coefficients (Table 7.3) of the linear model ($Actual = a.Predicted + b$) were generally smaller (closer to 1.0) for the Desktop and Monitor Luminance, due to their simplicity; it is rather straightforward to extract these luminance metrics because they were strictly defined by a surface. For the B40 Luminance and Retinal Illuminance, the corrections were more distinct because of the high complexity. However, this only had a limited effect on the coefficient of determination, which was subject to the variance which cannot be accounted for by the correction model.

Table 7.3: Model parameters relative to the four alternative ceiling-based positions

Position		Desktop Lum.	Monitor Lum.	B40 Lum.	Retinal Illum.	Average
A	R^2	0.978	x	0.730	0.955	0.888
	a	1.46	x	3.19	1.42	
	b	32	x	48	-51	
B1	R^2	0.997	0.778	0.603	0.697	0.769
	a	1.25	0.84	4.54	3.98	
	b	15	-4	94	231	
B2	R^2	0.994	0.813	0.638	0.899	0.836
	a	1.29	0.57	4.10	2.20	
	b	19	-14	95	106	
B3	R^2	0.996	0.898	0.701	9.69	0.891
	a	1.27	0.66	4.61	2.79	
	b	12	-9	80	135	

7.4. Phase 1

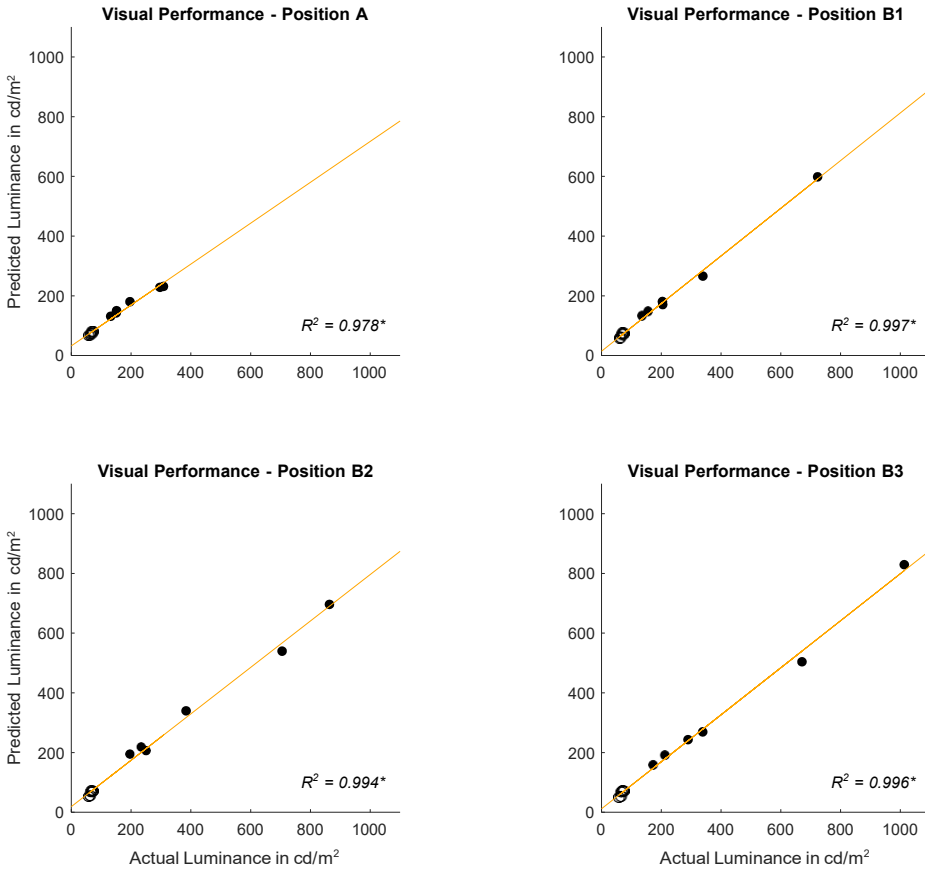


Figure 7.8: Correlation plots for the Desktop Luminance relative to the four alternative ceiling-based positions, the measurements with daylight are illustrated with a solid marker face.

Model A

The conditions measured each virtual user (E1 to E6) were rather different. Therefore, linear models ($y = ax + b$, with x originating from the ceiling-based measurement) for each individual virtual user, based on two measurements (with and without daylight) for position B'3, were developed as shown in Table 7.4 (only E1, E5, and E6 are shown). From here on these specific models, relating the ceiling-based measurements to the eye level measurements, are referred to as *Model A*. *Model A* shows that the coefficients for different virtual users were profoundly different, especially for the B40 Luminance and Retinal Illuminance indicating that each desk requires individual commissioning when a ceiling-based system is applied. In practice, this would mean that the commissioning is relatively simple and straightforward because only two measurements are required per desk. However, the model might not be suitable for the wide range of conditions that can be exhibited during the day and even during the year.

Table 7.4: Model parameters (*Model A*) for relevant virtual users for alternative ceiling-based position B'3.

Virtual User		Desktop Lum.	Monitor Lum.	B40 Lum.	Retinal Illum.
E1	<i>a</i>	1.26	0.74	3.08	1.70
	<i>b</i>	-2.00	0.00	-90.9	-154.8
E5	<i>a</i>	1.34	0.61	4.48	2.87
	<i>b</i>	-14.8	9.4	-186.1	-443.4
E6	<i>a</i>	1.27	1.03	2.04	2.45
	<i>b</i>	-20.6	-4.8	-51.3	23.0

7.5 Phase 2

7.5.1 Methodology

During the second phase, four Bee-Eyes were installed in the mock-up office environment (Figure 7.3) to assess the performance under varying conditions for the most suitable position, position B3, as found in Phase 1. One Bee-Eye was attached to the ceiling at position B'3, which was one of the two locations of position B3. Three Bee-Eyes functioned as reference measurement at eye level for three virtual users, virtual user one (E1), virtual user five (E5), and virtual user six (E6), respectively (Figure 7.3). Continuous measurements were conducted simultaneously from 05:30 to 22:00 on 03-08-2019, which exhibited variable weather conditions (average global irradiance of 157 \pm 27 W/m² and cloud coverage of 97.7 %) and a peak luminance ratio of 1:5200. A temporal resolution of 10 minutes, resulting in exactly 100 measurements per device, was applied. Again, the Desktop Luminance, Monitor Luminance, B40 Luminance, and the Retinal Illuminance were extracted during the post-processing phase, using MATLAB R2019a, using luminance masks analogous to Phase 1 (e.g. Figure 7.4). The measurement performance was assessed using the Mean Absolute Percentage Error (MAPE), which is an intuitive measure of prediction accuracy.

To achieve acceptable MAPEs, models such as *Model A* were required to enhance the relation between ceiling-based measurements and eye level measurements. Three models, *Model A* (Table 7.4), *Model B*, and the *Simplified Model B* were implemented in the analysis.

Model B

As *Model A* was only based on two measurements, it was expected that this model might not be suitable for all relevant conditions. Therefore, a more elaborate model was developed based on additional measurements in the mock-up office environment to 'train' a new model. Identical measurements were performed from 05:30 to 22:00 on 04-08-2019 with again an interval of 10 minutes. For each virtual user and luminance-based metric 100 data points, originating from the additional measurements, were used to fit new models to $y = ax + b$, as shown in Table 7.5, independent of the test data (measured on 03-08-2019). Outliers, which were values more than three scaled Median Absolute Deviations (MAD) from the median, as illustrated in Figure 7.9, were removed from this data set because they largely (negatively) affected the model.

From here on this elaborated model is referred to as *Model B*. In contrast to *Model A* originating from Phase 1, this model requires more extensive commissioning as reference measurements have to be performed for an entire day; however, this model is suitable for a much wider range of conditions than *Model A*.

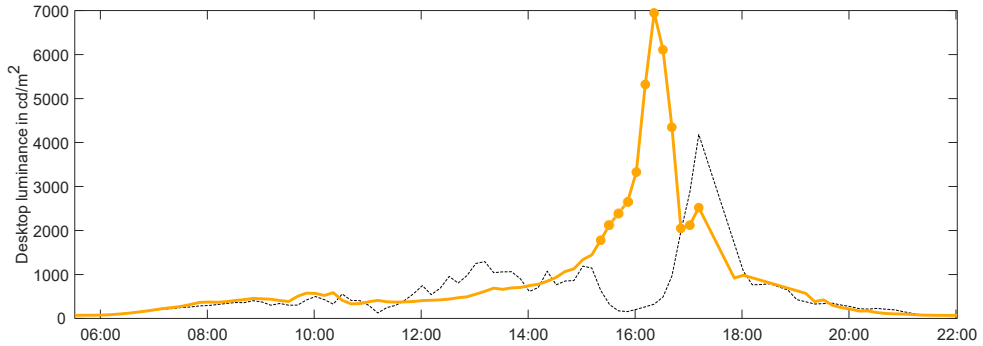


Figure 7.9: Training data (orange, 04-08-2019) for *Model B* with outliers emphasized by a marker and test data (black, 03-08-2019) of the Desktop Luminance. The outliers are removed from the data set

Table 7.5: Model parameters for *Model B* based on 100 independent samples measured from position B'3.

Virtual User		Desktop Lum.	Monitor Lum.	B40 Lum.	Retinal Illum.
E1	R^2	0.996	0.988	0.933	0.955
	a	1.30	0.55	2.38	1.22
	b	-7	8	-26	-5
E5	R^2	0.994	0.947	0.895	0.939
	a	1.27	0.60	6.19	3.02
	b	-3	14	-208	-48
E5	R^2	0.999	0.992	0.916	0.976
	a	1.35	1.00	2.32	1.10
	b	-25	-5	-9	100

Simplified Model B

Additionally, a *Simplified Model B* has been developed, it only differs from *Model B* for the B40 Luminance and the Retinal Illuminance representing visual comfort and NIF effects, respectively. Previously, the luminance masks for these luminance based metrics were translated to the ceiling-based position as accurately as possible, described in Sections 7.3.2 and 7.3.3, being complex and time-consuming. Therefore, in the *Simplified Model B*, semi-independent alternative masks (Figure 7.10) were applied for the B40 Luminance and the Retinal Illuminance, which were not complicated to apply; however, this might go at the expense of the accuracy. The simplified ceiling-based B40 Luminance mask consists of two parallel lines that have

an opening angle of approximately 40° . In contrast to the original B40 Luminance mask, the alternative mask does not diverge towards the periphery. The alternative Retinal Illuminance mask was only compressed vertically to avert irrelevant floor and ceiling surfaces, while the horizontal FOV was unchanged. As identical masks were applied for each virtual user, only the model was able to account for the differences between the virtual users. Therefore, the procedure described for *Model B* was replicated to develop new models for the B40 Luminance and the Retinal Illuminance, the individual models of the *Simplified Model B* are shown in Table 7.6.

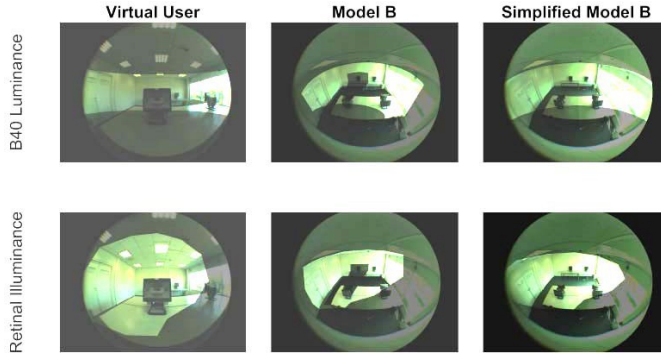


Figure 7.10: Simplified alternative luminance mask for the B40 Luminance and the Retinal Illuminance compared to the original luminance mask applied in *Model B*.

Table 7.6: Model parameters for *Simplified Model B* based on 100 independent samples measured from position B'3. The values in grey are identical to *Model B*.

Virtual User		Desktop Lum.	Monitor Lum.	B40 Lum.	Retinal Illum.
E1	R^2	0.996	0.988	0.907	0.969
	a	1.30	0.55	1.53	7.82
	b	-7	8	42	110
E5	R^2	0.994	0.947	0.915	0.954
	a	1.27	0.60	5.59	41.50
	b	-3	14	-116	-264
E5	R^2	0.999	0.992	0.916	0.974
	a	1.35	1.00	2.65	9.63
	b	-25	-5	-4	134

Uncertainty

In addition to the MAPE an uncertainty analysis has been conducted, which helps to translate ceiling-based measurements (L_{ceil}) to eye level measurements (L_{eye}) for practical applications. In a first step, the relative uncertainty was calculated according to $\delta L = |L_{ceil} - L_{eye}| / L_{eye}$ for each luminance based metric independent to the virtual users, again extreme outliers were removed. As this value (δL) is an average relative uncertainty it does not illustrate the potential error. Therefore, the

margin of error (m), based on the 95% Confidence Interval (CI), was also calculated according to $m = 1.96 \cdot \sigma_L$ (σ = standard deviation), as normality was assumed according to the Central Limit Theorem. Finally, the uncertainty of a ceiling-based measurement was indicated by $L = \delta L \pm m$.

7.5.2 Results

The overall results are displayed in Figure 7.11, each bar represents the MAPE for the different luminance-based metrics. It is clear that the Desktop and Monitor Luminance (average MAPE of 3.8% and 4.3%, respectively) were performing significantly better than the more complicated B40 Luminance and Retinal Illuminance, which had average MAPEs of 22.5% and 25.5%, respectively.

Especially, for Model A these differences were even more distinct. Both the Desktop and Monitor Luminance, using *Model A*, achieved an acceptable MAPE of 3.7% and 6.2%, respectively, while for the Retinal Illuminance an unacceptable MAPE of 52.1% was found. Also for the B40 Luminance, this error was rather high, indicating that the elementary *Model A* was not suitable for complex luminance masks. However, when the respective surfaces are strictly defined (e.g. desktop) this model could be applied. Overall, *Model B* performed significantly better (average error of 9.9% relative to 21.3%), as it captured a wide range of conditions while *Model A* was only a snapshot of, in this case, two conditions. These gains, relative to *Model A*, were mainly exhibited for the Monitor Luminance and the Retinal Illuminance. The Desktop Luminance showed a very similar performance while for the B40 Luminance the gains were marginal. Nevertheless, with this model, even the complex Retinal Illuminance can be measured with an acceptable MAPE for practical applications. However, this requires extensive commissioning to apply the luminance masks and develop the model. Therefore, a *Simplified Model B* was applied relative to the B40 Luminance and Retinal Illuminance to reduce the effort required for commissioning. The effect of this simplification was limited, the B40 Luminance showed a minor decrease in performance while the Retinal Illuminance showed even a minor increase in performance, indicating that this simplification was acceptable compared to the original *Model B*.

Besides differences between luminance-based metrics and models, also differences were exhibited between the three virtual users that were monitored as illustrated in Figure 7.12 for *Model B*. Overall, these results indicate that large ratios of daylight openings (Desk E5) resulted in a lower performance because the luminance for daylight openings is several orders of magnitude higher and can exhibit large variations. Only for the B40 Luminance, this effect was not found for this model. It performed especially poorly for the desk further away from the window (Desk E6), which also contained a large portion of the outside view. This was mainly caused by the applied model and not the luminance mask, as this effect was not found for *Model A*. Additionally, alternative models in the analysis phase did not show this effect. Moreover, also for the *Simplified Model B*, this effect was less pronounced. Therefore, it is likely that the conditions during the training of *Model B* were significantly different compared to the test data for virtual user E6, indicating the importance of relevant calibration conditions.

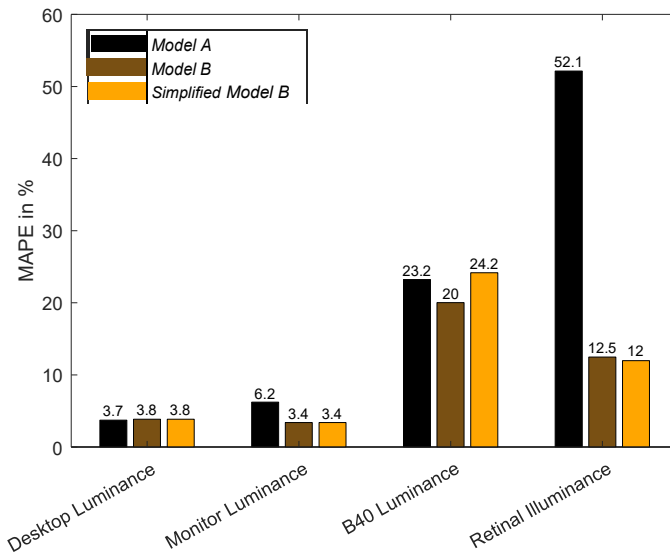


Figure 7.11: Mean Absolute Percentage Error (MAPE) for *Model A*, *Model B* and the *simplified Model B* relative to the Desktop Luminance, Monitor Luminance, B40 Luminance, and the Retinal Illuminance.

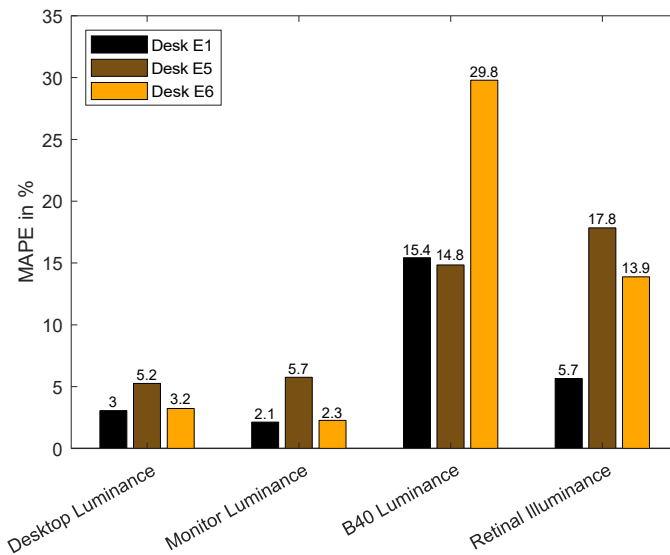


Figure 7.12: Mean Absolute Percentage Error (MAPE) for Desk E1, Desk E5 and Desk E6 B relative to the Desktop Luminance, Monitor Luminance, B40 Luminance and the Retinal Illuminance for *Model B*.

Table 7.7 shows the average measurement uncertainty of the ceiling-based position. Similar to Figure 7.11, *Model B* was outperforming *Model A* as the margin of errors and uncertainties are lower. For instance, the Retinal illuminance, for *Model A*, has a margin of error over 100% meaning that illuminances twice as big as reality can be measured. Theoretically, according to these results, negative values could also be measured; however, in practice, these values will be truncated to zero, as it is not practically possible. In contrast to the MAPE, the margin of error of the B40 Luminance was lower for the *Simplified Model B* compared to the original *Model B*, albeit negligible. Nevertheless, this luminance-based metric will be very difficult to measure in practice due to a margin of error of approximately 50% for *Model B*.

Table 7.7: Uncertainty of ceiling-based measurement relative to the luminance-based metrics and models.

	<i>Model A</i>	<i>Model B</i>	<i>Model B Simplified</i>
Desktop Luminance	$-3.9\% \pm 15\%$	$-0.5\% \pm 13\%$	$-0.5\% \pm 13\%$
Monitor Luminance	$1.7\% \pm 15\%$	$2.8\% \pm 7\%$	$2.8\% \pm 7\%$
B40 Luminance	$-15\% \pm 60\%$	$-1\% \pm 51\%$	$-2\% \pm 48\%$
Retinal Illuminance	$5.7\% \pm 109\%$	$0.2\% \pm 32\%$	$0.2\% \pm 32\%$

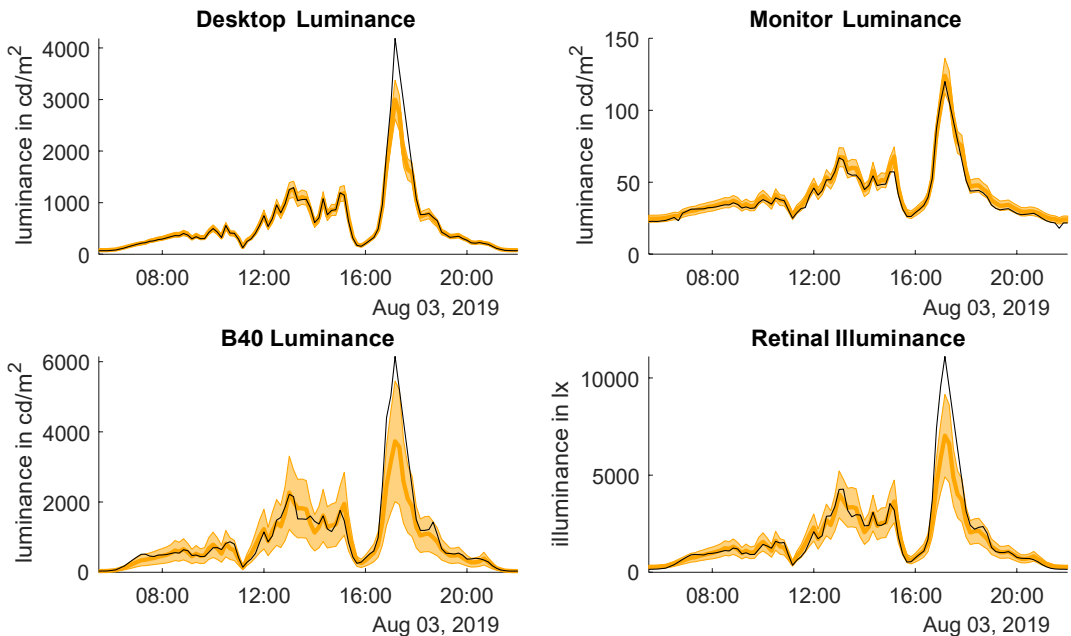


Figure 7.13: Absolute luminance measured for virtual user 5 (E5) at eye level (black) and approximated from position B'3 (orange) using *Model B*. The light orange area represents the margin of error.

Figure 7.13 gives more insight in the measurement uncertainty of the ceiling-based position relative to virtual user 5 (E5) when applying *Model B*. Consistently, the B40 Luminance and the Retinal Illuminance exhibit larger uncertainties indicated by the

large spread. Nonetheless, the actual Desktop Luminance also occasionally exceeds the expected error margin under extreme conditions. In this specific scenario, only one of the 100 measurements falls out of range, which can occur due to the 95% CI that was used to determine the error margin. Nevertheless, this is not necessarily problematic as this occurs only for extreme conditions, which will still be extreme with large measurement inaccuracies.

When looking into the uncertainties of each individual virtual user, as shown in Figure 7.14, it becomes clear that lower luminance values are generally overestimated while higher luminance values are generally underestimated (see also Figure 7.13). The over-estimations are generally limited in magnitude but numerous, while the underestimations can be very large but occur less often. As a result, the average uncertainties were low, even for the B40 Luminance and Retinal Illuminance as indicated in Table 7.7. Nevertheless, the margin of error can be very large, making it complicated to apply in practice. Even for the well-performing Desktop Luminance virtual user E5 is expected to have an error margin of almost 15%. However, most of the time this is within 5%.

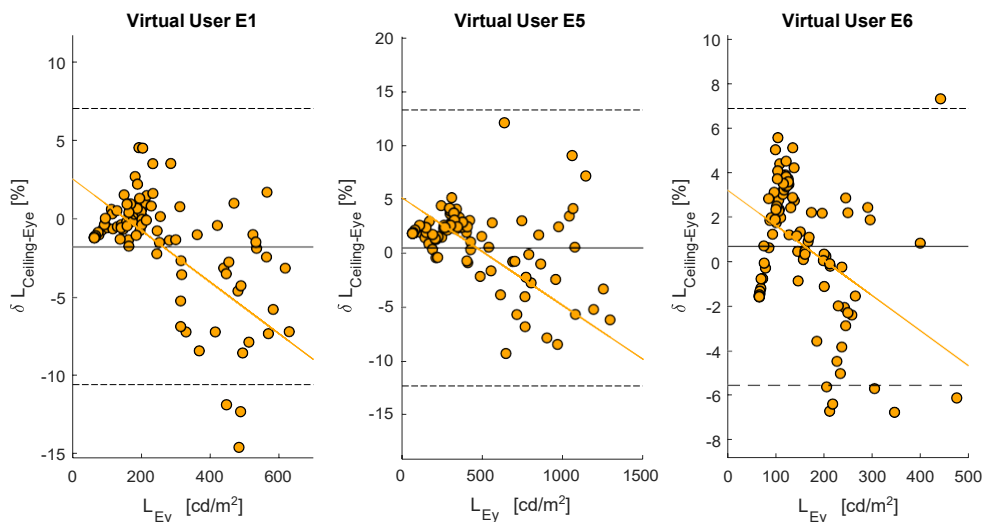


Figure 7.14: Bland and Altman plot for Desktop Luminance measured using *Model B*, each dot represents δL for an individual measurement, with a trend line in orange. The average bias or uncertainty is indicated by the black line, the dotted lines indicate the 95% CI.

7.6 Discussion

This study aimed to assess the feasibility of ceiling-based luminance distribution measurements as an alternative measurement position for open office environments. Measuring the luminance distribution from a ceiling-based position allows measurements over a longer period of time as it does not cause interference with daily activities, making it suitable for implementation in lighting control systems. However, it was expected that this goes at the expense of the accuracy.

7.6. Discussion

The study showed that the Desktop and Monitor Luminance were sufficiently accurately measured using a ceiling-based position above the aisle with a 20-degree angle relative to the ceiling (B3), only minor errors were introduced. Only for extreme conditions, relatively high inaccuracies were present. Nevertheless, to our knowledge, this ceiling-based position is scarcely referred to before in the literature. The B40 Luminance and the Retinal Illuminance were more complex to measure accurately using this ceiling-based position. Even with the elaborate *Model B* relatively high inaccuracies were found. Moreover, the masking procedure was rather complex and will, therefore, result in high commissioning costs. However, the simplified masking procedure did not have a significantly lower performance.

In comparison with the *partition- or monitor-mounted* and the *vicinity strategy* the *ceiling-based strategy*, originally expected to have the lowest performance, does not perform significantly worse. Direct comparisons with each strategy could not be made due to a difference in methodologies making it impossible to rank the different strategies. For the *partition- or monitor-mounted strategy*, a normalized root mean square error (NRMSE) of 11% was found for DGP [218], indicating that this partition- or monitor-mounted position also provides reasonable approximations. For the *vicinity strategy* [219], relative errors were generally below 25% which was always the case for the Desktop and Monitor Luminance (Table 7.7). The Retinal Illuminance performed only slightly worse (0.2%±30%), but did require a complex model to achieve this.

The luminance masks that were strictly defined by a surface, the Desktop and Monitor Luminance, performed well. The translation for these luminance masks from eye level to ceiling-based is straightforward, especially when the view is unobstructed. Only minor distortions occur due to the fisheye projection, closer to the periphery these distortions increase. Nevertheless, the effect is limited, as the luminance for virtual user 1 (E1), the reference measurement with the largest distortions, was measured rather accurately. The angle of view has an effect, however, the specular reflections in the mock-up office, and most likely in other offices, were limited (specular reflection desktop_≈3%). This indicates that similar high accuracies can be expected for other strictly defined non-transparent, predominantly diffuse surfaces, such as the background wall. This does not hold for the window area as the angle of view has a large influence due to the directionality of sunlight.

The B40 Luminance and Retinal Illuminance were not easily translated as they do not contain strictly defined surfaces. Their scene independence, at eye level, turns into a disadvantage for ceiling-based positions. Moreover, they contain a large area of the outside view, which is sensitive to the angle of view. Figure 7.12 indicates, for the Retinal Illuminance, that without a large portion of outside view (E1) relatively high accuracies can be achieved. Also, a complex but accurate translation of the FOV is not necessarily required, simplified semi-independent luminance masks performed practically identical to the more accurate but complex luminance masks, making it easier to implement in practice.

The differences in the MAPE between *Model A* and *Model B* for the Desktop and B40 Luminance were negligible, the Monitor and Retinal Illuminance did show significant increases for *Model B*. For the Desktop Luminance a high performance was achieved for *Model A*, indicating a good fit. For the B40 Luminance, both models had a low performance, indicating that a good fit was not possible, which was already shown by the low R^2 in Section 7.4.2. Therefore, for visual comfort, it is

advised to use another luminance-based metric because the performance of the B40 Luminance was very low for ceiling-based measurements, preferably one based on strictly defined surfaces such as luminance ratios between task and background area [230], even though the uncertainty increases for a ratio. As an example, the ratio between the Desktop Luminance and Monitor Luminance was estimated to have an uncertainty of 30% (15% + 15%) and 20% for *Model A* and *Model B*, respectively, which is still much lower than for the B40 Luminance.

The most suitable ceiling-based position and its performance were based on measurements in August in a Dutch climate. The most suitable position was determined based on two measurements of which one with daylight, without direct sunlight. Of course, this does not represent all relevant conditions. Nevertheless, we do not expect very different findings for a wider range of conditions. For instance, continuous Desktop Luminance measurements using position A resulted in higher inaccuracies, NRMSE of 14%, as was shown in the Pilot study (Section 7.2), for varying conditions compared to position B3 (NRMSE of 5%). Moreover, the performance of position B3 was assessed only for a single day, sunrise to sunset, with varying daylight conditions. Naturally, this does not cover all conditions during the year. However, it does cover high luminance values, low sun elevations, and variable weather conditions and is, therefore, a reasonable approximation for a wide range of conditions. Nevertheless, some minor deviations, without practical significance, might be expected to the MAPE and error margin for different conditions during the year.

It is advised to limit the number of monitored users by a single luminance camera to a maximum of four, as was conducted during this research (virtual users E1, E2, E5, and E6, were virtual user E2 was not actively measured during the second phase). Additionally, measurements were only conducted in one single office environment, which was designed to approximate the ‘average’ open office condition. Three virtual reference users were applied to indicate the difference within the office environment, indicating some variability between environmental conditions such as the distances to the window, luminance camera, and the background. The effect of daylight coming through the window was found to be normative to the performance of the ceiling-based measurement. Therefore, it is expected that for office environments with similar daylight conditions the error margins will be of a similar magnitude. However, for a glazed façade at multiple orientations, for instance, it will be highly recommended to perform additional measurements, as the daylight conditions are simply too different.

Figure 7.13 illustrates that the extreme conditions, high luminance values, were not accurately measured, even for the well-performing Desktop Luminance. The luminance and directionality were excessive for these conditions, resulting in severe inaccuracies. However, these extreme conditions are far outside the comfort range, with and without the severe inaccuracies introduced by ceiling-based measurements. As an example, both measurements (eye level – ceiling-based) will adjust the blinds in case of a luminance-based automated blind system. For this specific reasoning, outliers were removed for *Model B* and the uncertainty analysis.

The findings of Figure 7.14, overestimation for lower luminance values and underestimation for higher luminance values, might indicate that a model based on a third-degree polynomial could have been used to limit the uncertainty. However, initial tests with such a model did not lead to significant improvements that justified the added complexity. Therefore, these models were not deemed appropriate for practical implementation and were, therefore, discarded.

7.7. Conclusion

The findings of this study imply that relevant luminance distributions can be measured using sub-optimal ceiling-based positions in open office environments. This strategy prevents interference with daily activities and allows measurements for multiple users at once. Henceforth, luminance cameras can be integrated with lighting control algorithms, which is expected to improve the overall lighting quality in office environments. Luminance-based metrics that consist of strictly defined surfaces that are non-transparent and predominantly diffuse are relatively easy to approximate. The commissioning, to capture the required models, during installation is rather limited as only two reference measurements (*Model A*) are required per user position. When the office environment has undergone significant changes, for instance due to reorganization, this commissioning should be repeated otherwise irrelevant measurements might be conducted. Slightly higher accuracies can be achieved by extensive commissioning (*Model B*), incorporating a wider range of conditions, but this gain is limited and, therefore, not advised for luminance-based metrics that consist of a strictly defined surface. Moreover, the performance of *Model B* could be improved further by a longer training period, incorporating an even wider range of conditions, such as seasonal effects. This gain is expected to be smaller than the measurement accuracy (5%-15%, Chapter 2) of luminance distribution measurement devices and has, therefore, limited practical significance.

For more complex luminance based metrics, such as the Retinal Illuminance, extensive commissioning (*Model B*) is required to develop a correction model and to capture relevant outcomes. Such a model is more important than the luminance mask as it can account for minor mishaps in the mask. Nevertheless, even with extensive commissioning useful approximations are not guaranteed, which was exhibited for the B40 Luminance. Therefore, it is advised to use surface-bound luminance based metrics instead of complex luminance based metrics when available, otherwise extensive commissioning is vital.

7.7 Conclusion

The objective of this research was to assess the feasibility of ceiling-based luminance distribution measurements in open office environments. A ceiling position above the aisle with a 20-degree angle relative to the ceiling was found to be the most suitable position because its FOV has large similarities with the FOV and angle of view of the user. This position was assessed using four luminance based metrics: Desktop Luminance, Monitor Luminance, B40 Luminance, and Retinal Illuminance, representing visual performance (2x), visual comfort and NIF effects, respectively. The Desktop and Monitor Luminance achieved an acceptable accuracy, MAPEs of 3.7% and 6.1%, for the elementary *Model A*. The Retinal illuminance was able to achieve reasonable accuracy (MAPE of 12%) when the elaborate *Model B* was applied. For the B40 Luminance, inaccuracies > 20% were found for *Model A* and *Model B*. Therefore, it is advised to use surface-bound luminance based metrics, similar to the Desktop and Monitor Luminance, to replace complex luminance masks such as the B40 Luminance. The findings show that ceiling-based measurements are feasible when accounting for the uncertainty; however, a linear correction model is required to capture relevant data, which requires some effort during the commissioning.

For future research, it is advised to translate the conducted measurements to mul-

tiple different real office environments under different weather conditions such that the introduced uncertainties have more foundation for different office environments and different weather and climate conditions. Additionally, only four of the numerous luminance-based metrics were assessed, it is depending on the application whether these are the most relevant metrics. Finally, an alternative approach would be to apply neural networks to train a ceiling-based luminance camera to extract relevant information on multiple lighting quality aspects relative to the user.

Part III

Application of the luminance distribution

In the previous two parts of this thesis, the first, but essential, steps towards practical and continuous luminance distribution measurements for lighting quality are made. The next step is to apply and implement this knowledge in real office scenarios.

Chapter 8 aims to implement the methodology developed in Part I and the recommendations of Part II while monitoring a living office environment. The objective was to validate the methodology and recommendations from Part I and II. Therefore, two identical mock-up offices are used, representing a lab condition and a field condition. In the lab condition state-of-the-art measurements are conducted as a benchmark. In the field condition, all recommendations are applied while the mock-up office is being used by a office worker. Based on relevant lighting quality aspects, the field condition measurements are related to the benchmark.

Chapter 9 focuses on the implementation of a luminance camera such as the Bee-Eye in a lighting control system. Two basic luminance-based lighting control systems are applied in two identical mock-up office environments to verify whether luminance-based control using a versatile sensor such as the Bee-Eye is feasible. Both the ability to provide visual comfort and the energy reduction are assessed.





CHAPTER 8

Field study

8.1 Introduction

The objective of this thesis was to conduct practical and continuous luminance distribution measurements for lighting quality, which serves as input for a lighting control system developed in the 'OptiLight' project. Lighting quality, in this thesis, is indicated by 7 variable lighting quality aspects of which 6 are measurable by a single luminance camera (Chapter 1). Consequently, a luminance camera, the Bee-Eye, was developed that is autonomous and practical in use (Chapter 2). Moreover, an alternative method was developed to derive the luminance using floating point RGB values that was expected to improve the spectral match of such camera systems, and ergo the accuracy (Chapters 3 and 4).

However, some complications [36, 231] are expected when measuring the luminance distribution continuously in an office environment among others related to privacy, interference and computational costs. To deal with these issues, relevant aspects including the spatial resolution, the temporal resolution and the measurement position were investigated individually, in Chapters 5 to 7. Nevertheless, their impact and validity as a whole remains unknown when applied to a real office scenario. Most importantly, the effect of human behavior on these recommendations was not assessed yet. Office workers might not tolerate such a camera-based system in their office environment due to privacy concerns. Consequently, human behavior might hinder the measurements knowingly (sabotage [20]) or unknowingly (obstruct part of camera FOV [21]). Therefore, the objective of this chapter is to validate whether the luminance distribution is able to yield relevant input for lighting control systems, providing high quality lighting, while being implemented in a real office scenario. Consequently, the recommendations proposed earlier in this thesis are applied to prevent hindrance.

To show the relevancy of these recommendations, a living office environment needs to be monitored continuously. A plain field study, however, cannot provide, or approach, the ground truth, which is required to test the validity of the recommendations. Often, subjective responses obtained in surveys, are used as a means to evaluate field measurements [192]. Nevertheless, an alternative approach was issued, analogous to [50, 51]. These studies utilized two identical and adjacent spaces to assess visual comfort. One space was occupied by a participant while the other space was used to conduct high quality measurements. Using this methodology, the ground truth can be measured, providing a benchmark, without bothering the participant. These types of studies are generally only feasible in a lab setting as identical spaces are not commonly available. Consequently, the spaces need to be set up as a simulated work environment [48] to mimic a real living office environment in the lab.

8.2 Methodology

8.2.1 Experimental setup

Measurements were conducted in two identical adjacent mock-up office rooms (5 m x 2.75 m) with west facing façades at the Building Physics and Services laboratory at the Eindhoven University of Technology as shown in Figures 8.1 and 8.2. Measurements were conducted for 5 consecutive days, from 09:00 to 17:00, starting from

8.2. Methodology

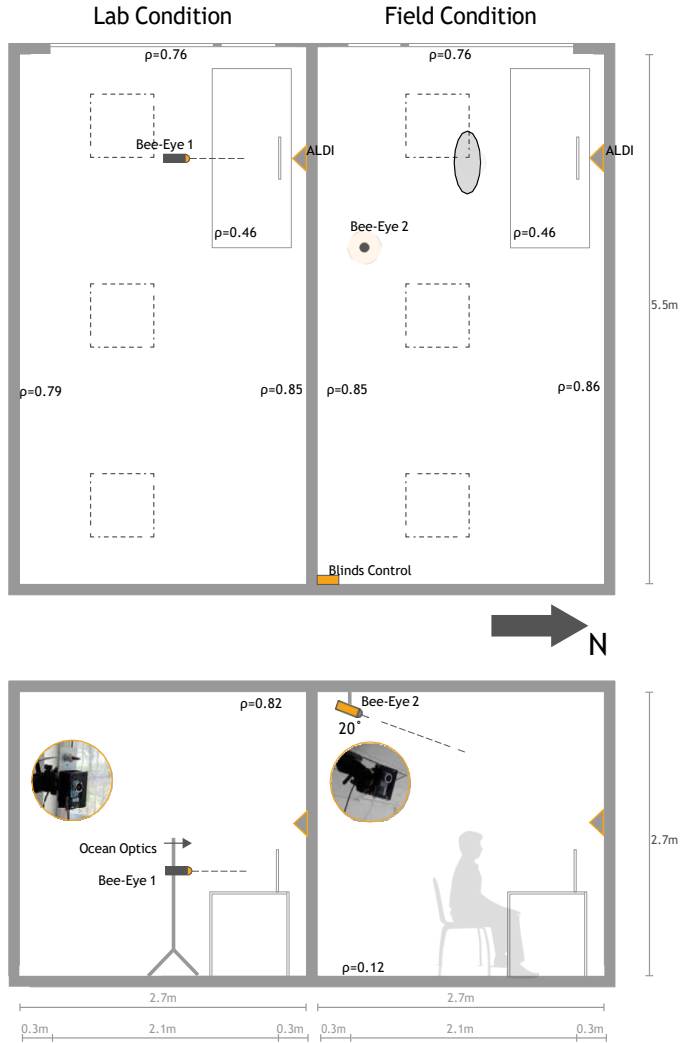


Figure 8.1: Measurement setup for the lab and field condition. The mock-up offices were designed to be identical. In the lab condition, highly accurate measurements were conducted. In the field condition, a real office environment was mimicked. (ρ = reflectance and ALDI = Ambient Light Directonality Indictor)

23-03-2020. This week exhibited clear sky conditions (average cloud cover $\bar{7}$ 19%) with a an average global irradiance of $420 \pm 164 \text{ W/m}^2$. The normalized irradiance is illustrated in Figure 8.3 for the 23rd of March. The mock-up office rooms represent one lab condition (Section 8.2.3) and one field condition (Section 8.2.4). Both mock-up offices were identically furnished as a private office environment, with a north oriented desktop positioned close to the window (Figure 8.2), only minor differences were exhibited. The lighting (2x3 PHILIPS RC461B G2 PSD W60L60 1xLED34 S/840), with a CCT of 4100 K, provided an illuminance of approximately 400 lx on the desktop in both office environments, without any daylight dependent

dimming. The non-transparent blinds ($\rho = 0.76$) were controlled, simultaneously for both offices, by the participant in the field condition using wall-mounted buttons. Two identical monitors (DELL 1907FPt, 300 cd/m^2) were installed in each mock-up office. Both offices were equipped with a Bee-Eye luminance camera as developed in Chapter 2 utilizing the first measurement track (Section 2.2.4) to measure the relevant lighting quality aspects continuously. The luminance-based metrics, defined in Section 8.2.2, were calculated during the post-processing phase using MATLAB R2019a, although they also could have been determined on the run.



Figure 8.2: Impression of the similarity between the Lab and Field condition indication only minor difference between the office environments.

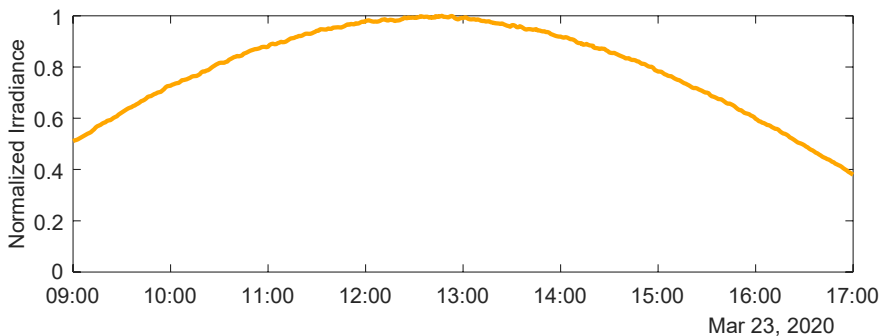


Figure 8.3: Normalized horizontal irradiance, indicating clear sky conditions, measured by the SolarBEAT [211] facility on top of the Building Physics and Services laboratory measured on the 23rd of March.

8.2.2 Lighting Quality Aspects

Chapter 1 showed that the luminance distribution is a suitable tool to extract different lighting quality aspects simultaneously. Information on the quantity, distribution, glare, daylight, directionality and the dynamics of light can be extracted. In this chapter, a distinction has been made between lighting quality aspects relevant for visual performance and visual comfort. The luminance-based metrics used in this chapter to quantify these aspects are indicated in Table 8.1.

Table 8.1: Lighting quality aspects and respective luminance-based metrics as applied in field study.

Category	Aspect	Metric	Reference
Visual Performance	Quantity	Task Luminance	[42]
	Distribution	Desktop Uniformity	[42]
Visual Comfort	Distribution	Task/Adjacent/Background Ratio	[232]
	Glare	DGP	[51]
	Daylight	Daylight Ratio (Task Area)	[233]
	Directionality	Vector to Scalar Ratio (ALDI)	[111, 124]
	Dynamics	Daylight Variability (Task Area)	[127]

The Task Luminance (L_{task}) was extracted by masking the desktop and monitor surface of the luminance map [234], which are the areas that mainly encompass the task area. The Luminance Uniformity (U_0) was extracted for the desktop area only, using the luminance instead of the more often used illuminance. In this study, these luminance-based metrics represent the visual performance.

Relative to the visual comfort, the distribution of the light is measured using the Task/Adjacent/Background Ratio, which is further elaborated in Figure 8.4. In practice, this metric is described by two ratios, the Task/Adjacent Ratio and the Task/Background Ratio. Glare was indicated by the Daylight Glare Probability (DGP) as discomfort glare originating from daylight was expected to be decisive compared to the discomfort glare occurring from the fixed electrical lighting. The DGP represents the probability that a person is disturbed by daylight glare [51]. The DGP was determined using the *evalglare v2.06* software [51, 68] using the default 2000 cd/m² luminance threshold. To achieve representative results, the HDR images were cropped, and when required the spatial resolution was reduced, using bilinear interpolation, to the recommended 800 x 800 pixels.

As daylight is generally preferred over electrical light [235], the Daylight Ratio was determined as well. The Daylight Ratio (DR) was indicated by the ratio between the total task area luminance (L_{task}) and the task area luminance originating from daylight ($L_{task} - L_{task,e}$), according to Equation 8.1, on a scale from 0 to 1. The luminance originating from electrical light ($L_{task,e}$) was determined at night and represented a luminance of 43 cd/m².

$$DR = 1 - \frac{L_{task} - (L_{task} - L_{task,e})}{L_{task}} \quad (8.1)$$

The directionality of the light was indicated by the Vector to Scalar Ratio (L_v/L_s) indicated by Equation 8.2 [89, 114]. A high L_v/L_s indicates a strong directionality [111]. The Vector to Scalar Ratio was originally measured using cubic illumination

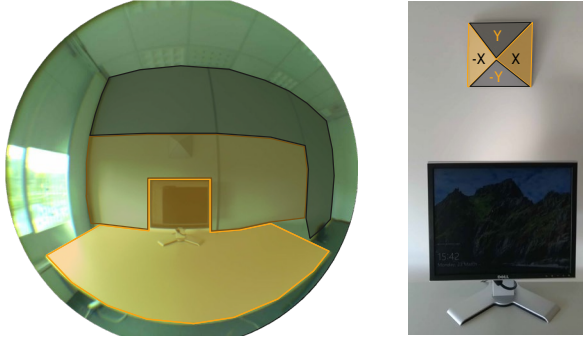


Figure 8.4: *Left* : The task (orange), adjacent (brown) and background (black) areas as measured in the lab condition. It gives also a impression of the blinds ($\pm 50\%$ closed). *Right* : The Ambient Light Directionality Indicator (ALDI) attached just above the monitor.

[119]. However, alternative methods have been proposed by [36] and [124]. In this study, an Ambient Light Directonality Indictor (ALDI, [124]) was attached to the wall just above the monitor. An ALDI is a pyramid shaped ornament, with a base of 20 cm by 20 cm, from which the surface luminance for each surface was extracted (L_x , L_{-x} , L_y , L_{-y}), as illustrated in Figure 8.4, in order to determine the Vector to Scalar Ratio (Equation 8.2).

$$L_v/L_s = \frac{\max(|L_x - L_{-x}|, |L_y - L_{-y}|)}{\frac{1}{4} \cdot L_x + L_{-x} + L_y + L_{-y}} \quad (8.2)$$

Finally, the Daylight Variability ($\Delta L_{h,m}$) was calculated based on the Task Luminance (L_{task}), using Equation 8.3, adopted from [127]. The average task luminance at a point in time ($L_{h,m}$) was related to the luminance measured one hour ago ($L_{h-1,m}$), five minutes ago ($L_{h,m-1}$), five minutes into the future ($L_{h+1,m}$), and one hour into the future ($L_{h+1,m}$). Hence, measurements were effectively conducted from 08:00 to 18:00 to derive $\Delta L_{h,m}$ for 09:00 to 17:00. This metric was calculated in the post-processing phase; however, for real-time measurements either the future measurements are disregarded or are predicted using forecasting algorithms [236].

$$\Delta L_{h,m} = \frac{1}{4} \cdot \left(\frac{|L_{h,m} - L_{h+1,m}|}{L_{h,m}} + \frac{|L_{h,m} - L_{h-1,m}|}{L_{h,m}} + \frac{|L_{h,m} - L_{h,m+1}|}{L_{h,m}} + \frac{|L_{h,m} - L_{h,m-1}|}{L_{h,m}} \right) \quad (8.3)$$

8.2.3 Lab Condition

In the lab condition, which was unoccupied during the entire study, high accuracy luminance distribution measurements were conducted as a reference. These measurements were considered the benchmark. Luminance distributions were captured using a Bee-Eye luminance camera, with a spatial resolution of 2130 x 1600 pixels and a temporal resolution of 1 minute, from eye level (1.2 m) of a virtual user (Figure 8.1).

8.2. Methodology

The luminance was calculated based on the conventional method using Equation 2.3 (page 32), including a single photometric calibration (Section 8.2.5) and a conditional calibration for each specific measurement (K_{SPD}). The conditional calibration was based on an additional spectral measurement using an Ocean Optics USB400 Fiber Optic Spectrometer, with an opening angle of 1.8° , focused on the wall directly above the monitor. The 1.8° wall projection was monitored by the Bee-Eye as well to calculate the respective K_{SPD} calibration factor for each individual measurement. The monitor was activated and displayed a duplicated version of the monitor in the field condition.

8.2.4 Field Condition

In the field condition, the mock-up office was in use by a single participant during the entire measurement period. Consequently, an alternative measurement method had to be applied to measure the luminance distribution. The participant was instructed to use the mock-up office as his own private office to conduct his own work to limit experimental biases such as the observer effect. The electrical lighting was fixed, but the participant was free to alter blinds depending on his preference using wall mounted buttons. A single Bee-Eye luminance camera was attached to the ceiling above the aisle with 20° orientation relative to the ceiling, corresponding to the most suitable ceiling-based position found in Chapter 7. The measurements were conducted with a low spatial resolution of 440×330 pixels, as was recommended in Chapter 5. Consequently, this spatial resolution does not satisfy the required spatial resolution for the maximum luminance measurement, which is relevant for the DGP. A temporal resolution of 5 minutes was selected according to Chapter 6.

An alternative method to derive the luminance using the floating point RGB values was applied according to the spectral mismatch optimization, Equation 3.5 (page 47), proposed in Chapter 3. Therefore, in advance, the SPD of the office lighting was measured once with the blinds fully closed, half closed and fully retracted using the Ocean Optics spectrometer (180° FOV) as shown in Figure 8.5. Additionally, the spectral responsivity of the Bee-Eye, as illustrated in Figure 3.1 (page 49), was used as input leading to average recommended weighting factors for the RGB floating point values as shown in Table 8.2. Moreover, a single photometric calibration was applied using the alternative weighting factors (Section 8.2.5).

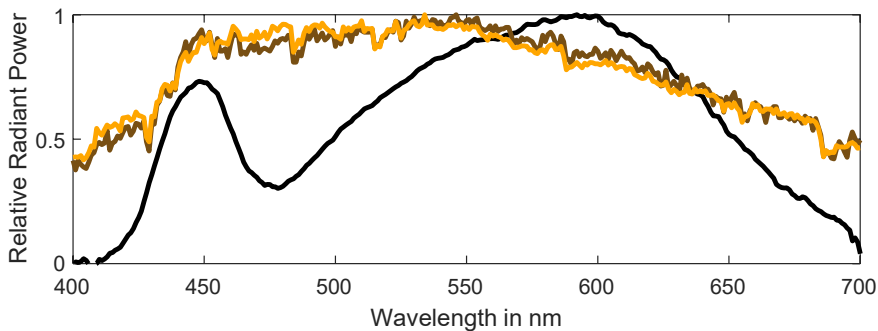


Figure 8.5: Normalized reference SPDs, representing the office lighting with the blinds fully closed (black), half closed (brown), and retracted (orange).

Table 8.2: r, g and b weighting factors for luminance calculation in field condition. The average r, g, and b weighting factors are applied to Bee-Eye 2.

	r	g	b	f_1^r	δL
Blinds fully closed	0.12	0.88	0.00	37.3%	2.66%
Blinds half closed	0.10	0.90	0.00	37.3%	12.68%
Blinds retracted	0.10	0.90	0.00	37.4%	13.79%
Average	0.1067	0.8933	0.0000	37.3%	9.71%

Model

Analogous to Chapter 7, models were used to relate the ceiling-based measurements to the eye level measurements conducted in the lab condition. In contrast to Chapter 7, fitting to a second degree polynomial showed distinctively better results for a number of luminance metrics. 25 randomly selected data points from the original data set (Chapter 8) were used to develop models according to $Actual = a \cdot Predicted^2 + b \cdot Predicted + c$ for each relevant surface. Both the Daylight Ratio (Equation 8.1) and the Daylight Variability (Equation 8.3) did not require a specific model because these were directly based on the Task Luminance (L_{task}) with its own specific model. The respective models are indicated in Table 8.3.

Table 8.3: Model parameters based on 25 samples to relate the ceiling based measurements to the benchmark.

	R^2	a	b	c
Task Luminance (L_{task})	0.82	-8.8E-4	2.25	-17.35
Uniformity (U_0)	0.21	-8.6E0	1.77	0.05
Adjacent Luminance (L_{adj})	0.72	3.1E-4	0.84	16.06
Background Luminance (L_{back})	0.86	-1.3E-3	1.49	-11.50
DGP	0.01	1.3E2	-34.06	2.38
Area -X Luminance (L_{-x})	0.31	-1.9E-7	0.00	0.17
Area X Luminance (L_x)	0.68	-2.8E-6	0.00	0.50
Area -Y Luminance (L_{-y})	0.29	-2.0E-3	1.92	-35.35
Area Y Luminance (L_y)	0.61	-4.1E-4	0.64	33.74

8.2.5 Photometric Calibration

A photometric calibration was applied to both Bee-Eyes in advance. Within the mock-up office the luminance of a standard grey ($\rho = 0.18$) and standard white card ($\rho = 0.90$) was extracted simultaneously for Bee-Eye 1, Bee-Eye 2 and a Konica Minolta LS-100 luminance meter ($\pm 2\%$, $f_1^r = 8\%$). This procedure was conducted thrice with the blinds fully closed, half closed and fully retracted. The average calibration factor, of both Bee-Eyes, was calculated based on these six luminance measurements. For Bee-Eye 2, applied in the field condition, the photometric calibration was determined relative to the alternative luminance calculation introduced in Section 8.2.4.

8.2.6 Analysis

The analysis was twofold. First, the lit environment in the single-office environment was evaluated, using the seven lighting quality aspects, according to the benchmark measured in the lab condition. Moreover, the correlation between the different luminance-based metrics were explored analogous to Veitch and Newsham [9], which is considered very relevant for future field studies [231]. Secondly, it was assessed whether the alternative measurements, in the field condition, were able to replicate/approximate the findings of the benchmark measurements. The visualizations that are provided refer to one single day, while the remaining analysis was based on the complete data set of five consecutive days.

In contrast to Chapter 7, the Mean Absolute Percentage Error (MAPE) was not used as the primary assessment criterion. It was expected that for a number of luminance-based metrics the output would be rather close to zero (such as the Uniformity and the Daylight Variability) and for values close to zero the MAPE will be very high and hence compromise the informativity of the MAPE [237].

As a first alternative, statistics were applied to assess whether the output from the field condition originated from the same distribution as the output from the lab condition. Normality of the data (*Lab-Field*) was assessed using the One-sample Kolmogorov-Smirnov test, which yielded $p < 0.001$ for all metrics. Consequently, the non-parametric Wilcoxon signed rank test was applied ($\alpha = 5\%$, $CI\ 95\%$) to assess the difference between the lab and field condition. Analogous to Chapter 5, the focus was on the effect size indicating the practical significance, as the p-value tends to go to zero quickly for large data sets [206]. The effect size was calculated according to Equation 8.4 with r as Pearson's r , Z as the Z-score and n as the sample size [207]. Generally, effect sizes of 0.1, 0.3 and 0.5 are considered small, medium and large effects, respectively.

$$r = Z / \sqrt{n} \quad (8.4)$$

Secondly, analogous to Chapter 3, Lin's Concordance Correlation Coefficient (ρ_c) was utilized to assess both the accuracy (C_b) and precision (ρ) of the alternative method relative to the benchmark [176]. Accuracy, or 'trueness', is considered a description of systematic errors (bias), while precision is considered a description of random errors (variability) [176, 238]. There is no clear cut agreement on the interpretation of ρ_c as indicated in Table 8.4.

Table 8.4: Alternative classifications of strength of agreement for Lin's Concordance Correlation Coefficient (ρ_c).

Agreement	McBride [239]	Landis & Koch [240]
Almost perfect	> 0.99	> 0.80
Substantial	0.95 – 0.99	0.60 0.80
Moderate	0.90 – 0.95	0.40 0.60
Poor	< 0.90	< 0.40

8.3 Results

8.3.1 Lighting Quality in the lab condition

In this section, lighting quality as measured in the lab condition is evaluated. The black line in Figures 8.6 to 8.8 indicate the respective luminance-based metrics measured in the lab conditions. The daylight contribution is illustrated in Figure 8.3.

Figure 8.6 evaluates the visual performance, which was defined by the Task Luminance and Uniformity. Both the Task Luminance ($\approx 180 \text{ cd/m}^2$) and Uniformity (≈ 0.15) were rather constant in the morning, as no direct sun light was entering the office environment. Assuming a Lambertian surface the task illuminance was estimated to be approximately 1200 lx, which is well above the requirements (500 lx, [42]). The Uniformity was well below the requirements (for illuminance 0.6, [42]). However, people tend to accept lower uniformities caused by daylight openings [241]. The afternoon, allowing direct sun light, represented more variable conditions. The Task Luminance increased drastically while the Uniformity decreased drastically. Mainly due to the increased Task Luminance the blinds (impression in Figure 8.4) were, according to user feedback, utilized twice, at 13:15 ($\pm 30\%$ closed) and 15:15 ($\pm 80\%$ closed), which is clearly visible in both subplots. The blinds were only retracted at the start of the next day. Lowering the blinds increased the Uniformity as the luminance gradient on the desktop surface was reduced.

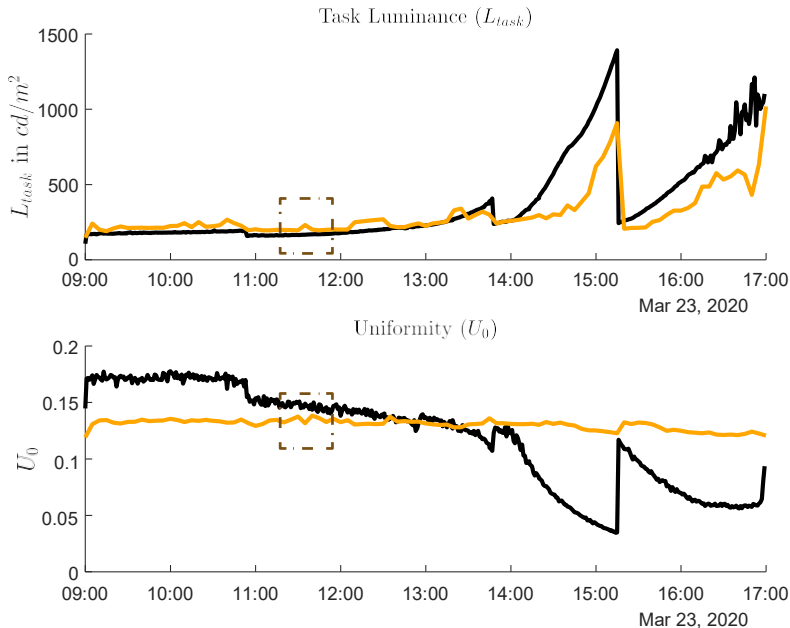


Figure 8.6: Task luminance (L_{task}) and Uniformity (U_0) representing the visual performance. The black line indicates the benchmark (lab condition), the orange line represents the alternative method (field condition), and the brown box marks an example of noise caused by human behavior.

8.3. Results

Figure 8.7 relates to the Task/Adjacent/Background Ratio, the first metric for visual comfort. The Task/Adjacent/Background Ratio was separated into two distinct ratios to allow visualization. A trend analogous to the Task Luminance was found, with increasing ratios towards the end of the day. Again, the use of the blinds was clearly visible. The Illuminating Engineering Society (IES) suggests a Task/Adjacent/Background Ratio of 1:3:10 [232], which was almost within reach in the late afternoon (1:2:3.5). However, in the early morning, the homogeneity within the room was close to 1:1:1. So, the lighting was more homogeneous than recommended, due to large daylight openings and similar surface finishes. Nevertheless, there are some studies [9, 234] that propose lower ratios, within order of magnitude as found in this study, compared to the IES as it is largely dependent on the environmental context. For instance, De Bakker et al. found a preference for "task \approx adjacent \approx background" [234].

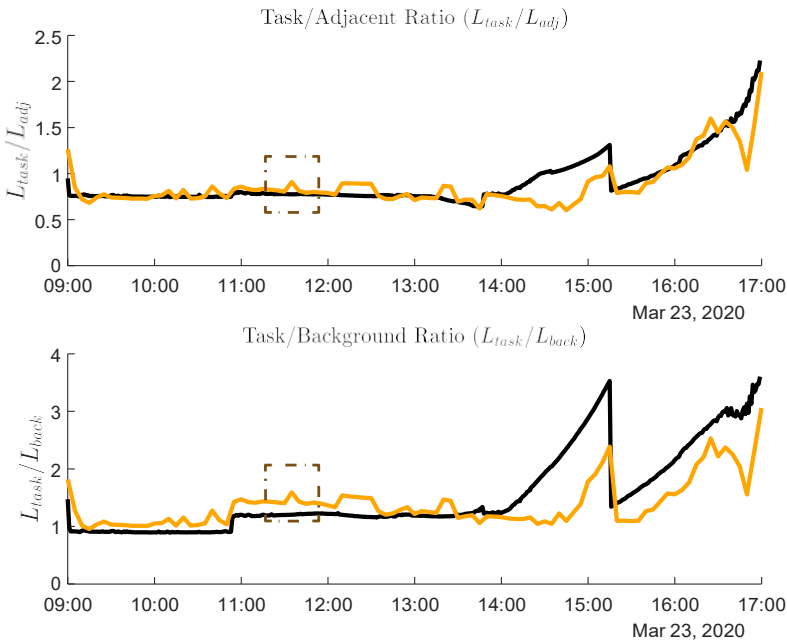


Figure 8.7: Task/Adjacent (L_{task}/L_{adj}) and Task/Background (L_{task}/L_{back}) ratios, metrics relevant for visual comfort. The black line indicates the benchmark (lab condition), the orange line represents the alternative method (field condition), and the brown box marks an example of noise caused by human behavior.

The remaining lighting quality aspects, representing glare, daylight, directionality and dynamics of light, are illustrated in Figure 8.8. The DGP, representing glare, also largely resembled the pattern of the Task Luminance. Although, the peak at 13:15 was more distinct for glare, while the increase towards 17:00 was almost non-existing. It should be noted that the DGP is only valid between 0.2 and 0.8 [51], which was not exceeded during this study. It is not likely that the use of blinds was initiated by daylight glare as a DGP between 0.33 and 0.38 is only categorized as perceptible [65]. In conclusion, the hypothesis that blinds were activated based on the Task Luminance maintains valid.

As the office contained large daylight openings the Daylight Ratio was high during the entire study, ranging between 70% and 100%. Again, large correspondence was found with the Task Luminance, on which this metric was partly based. The Daylight Ratio does not have a specific requirement. However, one can assume that generally daylight is appreciated over artificial light [235].

The Vector to Scalar ratio mainly exhibited changes when the blinds were used. The increase of daylight, for instance during the beginning of the afternoon, had a limited effect. Only in the late afternoon, when direct sunlight was exhibited within the office space a clear increase was found. According to literature, a Vector to Scalar ratio between 1.2 and 1.8 is preferred for daylight quality in office environments [242], which was only achieved occasionally, close to 17:00. Again, due to similar surface finishes with high spectral reflectances the lighting distribution had a large diffuse component.

Finally, the Daylight Variability behaved distinctively different than the previous lighting quality aspects. Although, the moment of closing the blinds is clearly visibly by a large increase in ΔL_{task} . Due to the weather conditions, a clear sky, the variability throughout the week was rather low; so, the blinds were the main agent that impacted the Daylight Variability. Especially during the morning the variability was very low, indicating a very constant lit environment, which was already indicated by the Task Luminance.

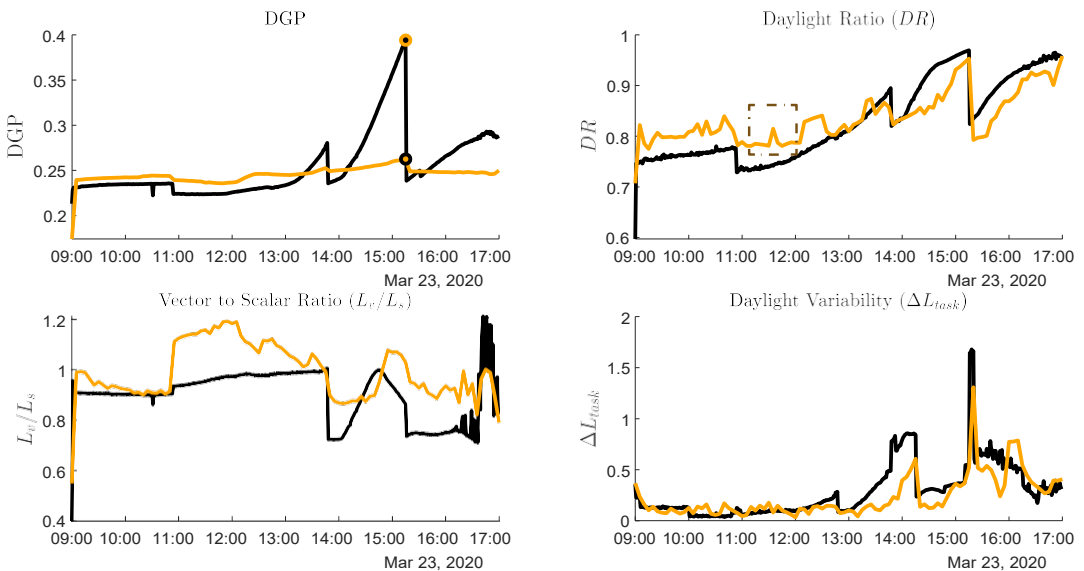


Figure 8.8: DGP, Daylight Ratio (DR), Vector/Scalar Ratio (L_v/L_s) and the dynamics of light (ΔL_{task}) ratios, metrics relevant for visual comfort. The black line indicates the benchmark (lab condition), while the orange line represents the alternative method (field condition), the DGP markers relate to Figure 8.10, and the brown box marks an example of noise caused by human behavior.

In general, relatively little noise was exhibited despite the high temporal resolution. The minor differences between two consecutive measurements, analogous to Chapter 6, indicate that a temporal resolution of 1 minute is not necessarily required

8.3. Results

for indoor luminance distribution measurements. Moreover, multiple luminance-based metrics showed similar patterns throughout the day, indicating that some metrics might be redundant. Table 8.5 shows the correlations between the different metrics. First, it shows that the Vector to Scalar Ratio (L_v/L_s) and the Daylight Variability (ΔL_{task}) performed very different compared to the other metrics. Remarkably, the Uniformity (U_o) and DGP often had a moderate (negative) correlation with the remaining metrics. The remaining metrics were, to a certain extent, based on the Task Luminance and consequently showed substantial correlations.

Table 8.5: Correlation, using Pearson's r , between the different luminance based metrics as measured in the lab condition.

	L_{task}	U	L_{task}/L_{adj}	L_{task}/L_{back}	DGP	DR	L_v/L_s	ΔL_{task}
L_{task}	1.00							
U_o	-0.69	1.00						
L_{task}/L_{adj}	0.65	-0.70	1.00					
L_{task}/L_{back}	0.76	-0.89	0.90	1.00				
DGP	0.74	-0.54	0.33	0.51	1.00			
DR	0.70	-0.85	0.57	0.73	0.67	1.00		
L_v/L_s	0.04	0.04	-0.26	-0.10	0.24	0.17	1.00	
ΔL_{task}	0.01	-0.08	0.11	0.10	-0.09	-0.26	-0.36	1.00

8.3.2 Agreement of alternative method in the field condition

The following section aims to relate the alternative measurements in the field condition to the findings described in Section 8.3.1, corresponding to the orange lines in Figures 8.6 to 8.8. First, it was assessed whether the distribution of the output yielded by the alternative method in the field condition was different than the output of the benchmark measured in the lab condition. Table 8.6 shows the results of the Wilcoxon signed ranked test. Both the Task Luminance and the Daylight Ratio did not have a significantly different median when applying the alternative method. Also, the effect size for these two metrics was considered small. This indicates that on average the Task Luminance and the Daylight Ratio were not different from the alternative method. Medium effect sizes were exhibited for the Task/Adjacent Ratio, Task/Background Ratio and the Daylight Variability, indicating that, with careful consideration, the average performance of these metrics might be estimated using alternative field measurements. Very large effect sizes were exhibited for the Uniformity, DGP and Vector to Scalar Ratio. This indicates that these aspects are not accurately estimated using this specific methodology, which was already evident from Figures 8.6 and 8.8.

The accuracy and precision were relatively high for the Task Luminance as is indicated in Table 8.7, which corresponds to the findings in Figure 8.6. The accuracy (C_b) is higher than the precision (ρ) mainly due to noise, which adds a certain amount of variability. It is hypothesized that the noise was caused by the participant regularly

Table 8.6: p-value and effect size, representing the statistical and practical significance, of the difference between the alternative (field) and benchmarked (lab) method, assessed with the Wilcoxon signed rank test.

Metric	p-value	Effect size
Task Luminance	0.919	0.005
Uniformity	< 0.001	0.861
Ratio Task/Adj	0.002	0.153
Ratio Task/Back	< 0.001	-0.495
DGP	< 0.001	0.865
Daylight Ratio	0.398	-0.038
Vector to Scalar ratio	< 0.001	-0.547
Daylight Variability	< 0.001	-0.448

blocking a certain part of the task area as seen from the Bee-Eye, a clear example is illustrated in Figure 8.9. The snapshot in the middle corresponds to the Task Luminance peak accentuated in Figure 8.6 but also in Figures 8.7 and 8.8. The luminance increased due to absence of the participant. The 11:40 instance also shows that due to movement during the capturing of the HDR image, ghosting might occur [46], which results in an intermediate case of obstruction. This indicates the numerous different levels of variability due to the user. Combined, a ρ_c of 0.75 was found for L_{task} , according to McBride this is rated as a poor agreement. However, in the context of this work, this requirement seems rather strict as control algorithms always have to deal with noisy data. According to Landis and Koch, a substantial agreement was achieved, which seems more appropriate when reviewing Figure 8.6.



Figure 8.9: Origin of noise due to human movement, the task area is indicated in orange.

The Uniformity, on the other hand, had a low accuracy and a low precision resulting in a negligible agreement (Table 8.7). This is also illustrated in Figure 8.6, the Uniformity measured in the field condition has no similarities relative to the benchmark. The Uniformity is very sensitive because it is dependent on the minimum luminance of the desktop area, which can be represented by a single pixel. Due to either the participant or objects on the desktop, the minimum luminance value is easily manipulated. For instance, a black notebook reduces the minimum luminance significantly.

The luminance distribution, related to visual comfort, was divided in two related metrics: the Task/Adjacent Ratio and the Task/Background Ratio. They were assessed separately as they performed differently. The Task/Adjacent Ratio had a very high accuracy but a low precision, resulting in a poor concordance. This does not

8.3. Results

Table 8.7: Accuracy, precision, and concordance of the alternative method relative to the benchmark.

Metric	Accuracy (C_b)	Precision (ρ)	Concordance (ρ_c)
Task Luminance	0.97	0.77	0.75
Uniformity	0.29	0.35	0.10
Ratio Task/Adj	0.94	0.37	0.35
Ratio Task/Back	0.88	0.62	0.54
DGP	0.21	0.72	0.15
Daylight Ratio	1.00	0.82	0.82
Vector to Scalar ratio	0.78	0.36	0.28
Daylight Variability	0.87	0.57	0.49

directly relate to Figure 8.7 where a good match for accuracy and precision seems to be found. However, some differences were exhibited in between the five consecutive days. Again, variability is likely caused by the participant obstructing the task area as the adjacent area was mainly unobstructed.

The Task/Background Ratio had a lower accuracy compared to the Task/Adjacent Ratio but the precision was much higher leading to a moderate concordance with the benchmark. The precision was improved relative to the Task/Adjacent Ratio because the background luminance was rather robust. It was a large area that was mainly unobstructed, which might clarify the small improvement in performance relative to the Task/Adjacent Ratio.

Glare is an important lighting quality aspect. However, using this methodology it was not possible to estimate when glare was occurring as is clearly visible in Figure 8.8. Still, the precision was rated as substantial (Table 8.7). However, this was mainly caused by the fact that glare was only occurring occasionally. When there was no glare, the measurements in the field were able to accurately measure the quantity of no glare. It was not possible to estimate the DGP when glare was actually occurring, resulting in a low accuracy and low concordance. The cause is twofold: Figure 8.10 shows that the actual glare source is much larger (more pixels) for the benchmarked method. Moreover, the spatial resolution for the alternative method was much lower, potentially averaging out high luminance values, which was already comprehensively discussed in Chapter 5.



Figure 8.10: Glare source areas, indicated in orange, measured at 15:15 on Mar 23 for the benchmark and alternative model.

In contrast to the DGP, the Daylight ratio was estimated accurately and precisely with a concordance of 0.82, which according to Landis and Koch can be considered an almost perfect agreement. The Daylight Ratio is the metric with the best performance during this study. It even outperformed the Task Luminance on which it is based, although the difference was minor. The slight increase might be attributed to the translation to a range of 0 to 1, instead of the 'infinite' range of the Task Luminance. The variability that was present was likely caused by the participant, indicated by the severe increase in daylight attributed to the absent participant at 11:35 in Figure 8.9

The Vector to Scalar ratio measured in the field condition shows a distinctly different pattern than the L_v/L_s measured in the lab condition as illustrated in Figure 8.8. Moreover, the precision was estimated to be very low whereby the high amount of variability makes the pattern unrecognizable while the accuracy was still substantial. Nevertheless a very low concordance of 0.28 was achieved. It was expected that this was caused by the low spatial resolution. The ALDI, with a width of 20 cm by 20 cm, compromised only a few pixels (11±1 pixels) in the respective luminance map, making it very sensitive to measurement errors. Another issue that might have played a role is the skewed alignment with the Bee-Eye. However, this was not expected to be decisive.

Finally, the Daylight Variability achieved a moderate agreement with the benchmark. The accuracy was good, but a large increase in variability was found resulting in a relatively low precision. The participant is, again, expected to be the main cause of this increased variability. By moving in front of the camera, the participant changed the Task Luminance on which this metric was based. However, as indicated in Equation 8.3, five instances of Task Luminance were used, which were all susceptible to noise caused by the participant, making it much more susceptible to noise than for instance the Task Luminance. This effect is discernible in Figure 8.8, where the luminance peak of 11:35 is dispersed over multiple consecutive peaks. Consequently, this results in a lower performance.

8.4 Discussion

This study aimed to assess whether a wide range of luminance-based metrics, representing lighting quality, can be measured sufficiently accurate in the field study. Field measurements, which have a high ecological validity [3], have a high relevancy as this can overcome multiple limitations of lab studies and can also serve as input for lighting control systems, but are subject to multiple practical issues. This thesis already introduced a number of recommendations for field measurements. However, their interaction and the effect of the user was still lacking. Therefore, measurements were conducted in two identical offices representing a lab and field condition, where the field condition was actively used during the measurement period.

The measurements in the lab condition were able to accurately quantify the different lighting quality aspects (Figures 8.6 to 8.8). Consequently, it served as a benchmark for the alternative measurements in the field condition. These benchmark measurements showed that a number of luminance-based metrics had a substantial to almost perfect correlation as indicated in Table 8.5. This might indicate that there is no need to measure all these metrics to quantify the lit environment. As an example,

8.4. Discussion

the Task Luminance and Task/Background Ratio were found to have a substantial agreement. Therefore, the Task/Background Ratio could have been estimated using only the Task Luminance. However, it is not advised to dismiss the Task/Background Ratio completely as the requirements to achieve a comfortable indoor environment can be completely different for these correlated metrics. For instance, in this study, the requirements were amply met for the Task Luminance, while the requirements for the Task/Background Ratio, according to the IES, were not met.

The measurement results of the alternative method showed that it is rather complex to measure overall lighting quality in a real office environment that is actively being used. The Task Luminance and Daylight ratio were measured with the highest accuracy, there was no practically significant difference between the alternative method and the benchmark (Table 8.6). Both metrics were measured with a reasonable accuracy. Nevertheless, the precision for the Task Luminance was far from perfect (Table 8.7). Similarly to the Task Luminance, Chapter 7 measured the Desktop Luminance and Monitor Luminance (together the Task Luminance) from a ceiling-based position and found significantly lower MAPEs (3.6% and 6.2%) compared to a MAPE of 25% for the Task Luminance in this study. The performance of the other metrics was even lower, the Task/Adjacent/Background Ratio and the Daylight Variability were measured with a moderate accuracy. Hence, caution is required for these metrics when measuring in the field (using this methodology). The Uniformity, DGP and Vector to Scalar Ratio did not provide relevant data. Therefore, it is advised not to use these metrics without further accommodations.

Two explanations can be distinguished for this reduced performance. Firstly, a number of concessions have to be made when conducting a field study. State-of-the-art measurements are often not feasible. For luminance distribution measurements the luminance camera often cannot be calibrated continuously, the spatial and temporal resolution might need to be reduced, and the measurement position is most likely sub-optimal, which were all subject to individual research in Chapter 3, 5, 6, and 7, respectively. These aspects were all expected to have some negative effect on the measurements. Moreover, there might also be an interaction effect between these aspects, indicated by the increased MAPE relative to Chapter 7. The effect of the temporal resolution is likely very limited as the benchmark measurements showed almost no variability in the 1 to 5 minute region; be it that the weather conditions were relatively constant. The sub-optimal measurement position, in this case located at the ceiling, was expected to have the largest influence. These issues mainly relate to the systematical errors (bias) indicated by C_b in Table 8.7.

Secondly, the participant is expected to have, unknowingly, largely influenced the measurements. Only by being present at the desktop the luminance distribution as seen from the Bee-Eye is affected, which was illustrated in Figure 8.9. Moreover, the participant moves and (re)places items within the office, adding a highly variable and irregular unknown component. Evaluating the Task Luminance in Figure 8.6 illustrates the variability, even though a good agreement was maintained relative to the benchmark, while the measurements in the lab conditions showed almost no variability. It was expected that this variability was caused by the participant moving in and around the office as indicated by the accentuated area in Figure 8.6. Moreover, the ceiling-based position proposed in Chapter 7 might be more sensitive to movements of the participant than, for instance, a luminance camera directly above the task area. The effect of the participant was mainly quantified by the precision, relating

to random errors, indicated in Table 8.7. Consequently, in field studies, humans are a significant source of noise, which should be accounted for.

A solution to the, in some cases, poor measurement performance in the field condition might be found in the high correlations between the different luminance based metrics (Table 8.5). As an alternative approach, a luminance-based metric, such as the Task Luminance, that is sufficiently accurate measured in the field condition might be used to approximate other relevant luminance-based metrics based on the correlation instead of a physical measurement. Nevertheless, not all metrics that were not accurately measured, such as the Vector to Scalar Ratio, have reliable correlations. Nonetheless, such an alternative approach might help to reduce the number of luminance-based metrics that have to be monitored (continuously).

The two mock-up offices were designed to be identical with due diligence. Nevertheless, some minor differences were exhibited between the lab and field condition. Most noticeable are the window stiles that were not identically aligned (Figure 8.2). The effect was expected to be limited, as it is only a relatively small detail, and did not cast a direct shadow on the region of interest during the measurement period. Moreover, minor differences were found between the surface finishes. However, reflectance measurements showed only negligible differences in the spectral properties (Figure 8.1). These minor differences, and the reduced spatial resolution, are also partly corrected by the models that relate the ceiling-based measurements to eye level. Quadratic models were utilized because this improved the agreement for a number of luminance-based metrics, such as the Task Luminance, significantly, compared to linear models. However, for some luminance-based metrics (e.g. Uniformity) this still resulted in a very poor agreement (Table 8.3). The conditions were distinctively different such that the model could not account for this.

It is a complex task to apply an assessment criterion that is appropriate for a wide range of metrics with varying scales, to relate alternative measurements to a benchmark. Section 8.2.6 already indicated that the MAPE was not suitable for the majority of metrics applied in this study. To deal with this issue, two distinct methods were used to achieve a robust assessment. First, the average performance was assessed based on the effect size (Table 8.6). However, the effect size does not have strict thresholds, and they are open for interpretation. This study used the widely applied Pearson's r classification. Secondly, Lin's Concordance Coefficient was utilized to get more insight in the accuracy and precision of the alternative method (Table 8.7). Again, the assessment of the ρ_c is not straightforward. McBride [239] and Landis and Koch [240] proposed extremely different thresholds. An almost perfect agreement according Landis and Koch can be considered a poor agreement according to McBride (Table 8.4). The classification by McBride was developed in the context of national health, while Landis and Koch's classification was developed in the context of observer data, which consequently takes into account some noise. The classification by Landis and Koch seems most applicable in context of this research because minor measurement errors have no detrimental effect and lighting control systems can be equipped to handle noisy or inconsistent data [243, 244]. Using both assessment criteria we aimed to achieve a robust assessment.

This study implemented methods and recommendations from different chapters in this thesis, such as the alternative method to derive the luminance with the objective to limit the spectral match, as proposed in Chapter 3, to the most suitable ceiling-based position proposed in Chapter 7. Consequently, it was rather difficult to extract

8.5. Conclusion

the main cause of the reduced performance of the alternative method applied in the field condition. Nevertheless, one of the objectives was also to show the applicability of the previous chapters. Using this methodology, a full coverage without missing data was achieved.

Finally, the participant was a major noise source, which could be limited by adding additional intelligence to the Bee-Eye. Recognition software could be applied based on the camera images to discern obstructions of the relevant surfaces caused by the users. For instance, this will massively improve Uniformity measurements as only the minimum luminance of the relevant surface is extracted. On the other hand, when obstructions are really big, little relevant surface might be available for the measurement, making it again susceptible to measurement errors analogous to the Vector to Scalar Ratio in this study. Another solution might be to discard the areas that are expected to be obstructed by the user in advance.

Measuring the lit environment, and more specifically lighting quality, in the field is not straightforward. It is not feasible to exactly mimic a laboratory study, concessions are required to, for instance, prevent interference with the users, which might reduce the relevancy of the measurements. Measures to deal with these practical issues do reduce the accuracy, there might also be an interaction effect between these measures. Most importantly, the presence of users is the largest complexity as they unknowingly, and potentially knowingly, affect the measurements. Consequently, users can be considered a major source of noise, which might require some additional intelligence to deal with it.

8.5 Conclusion

The luminance distribution was shown to be an excellent tool to quantify lighting quality (Chapter 1), which can, subsequently, serve as input for lighting control systems. However, application in highly relevant real office scenarios is not straightforward. This chapter aimed to assess whether continuous measurements, using a luminance camera, in a simulated office environment, while dealing with field measurement related limitations (e.g. sub-optimal measurement position), were able to yield relevant output. State-of-the-art measurements were conducted in an identical office environment as a benchmark.

The results showed that it is rather complex to conduct relevant measurements based on the luminance distribution in a real office scenario. Nevertheless, The Task Luminance and Daylight Ratio were measured with a substantial agreement ($\rho_c > 0.75$), also the impact of field measurement related limitations in the real office scenario were small ($r < 0.05$). However, the Task/Adjacent/Background Ratio and the Daylight Variability achieved only a moderate agreement ($\rho_{\pm} 0.5$), and exhibited a medium effect due to the limitations ($r < 0.50$). The remaining luminance-based metrics, Uniformity, DGP and Vector to Scalar Ratio, were unfortunately not able to achieve an acceptable agreement ($\rho_c < 0.30$).

The agreement of the measurements was subject to systematical and random errors. The systematical errors were mainly caused by field related limitations, that were required to allow measurements in real office scenarios, such as a sub-optimal measurement position. The random errors were mainly caused by the participant. A user might obstruct the relevant FOV of the luminance camera, which is highly

variable and irregular due to movements of the user. Consequently, users can be considered a massive source of noise, which might be limited by reducing the area obstructed by the participant.

Concluding, measurements in real office scenarios need to be conducted carefully, otherwise some luminance-based metrics such as the Uniformity, DGP and Vector to Scalar Ratio, might provide irrelevant output. For a number of luminance-based metrics (Task/Adjacent/ Background Ratio and Daylight Variability) additional accommodations are required to achieve reliable results. However, multiple metrics such as the Task Luminance and Daylight Ratio have high correlations, indicating that not all metrics need to be measured physically. Additionally, some added intelligence might be able to limit the noise by filtering out the user, using recognition software.

Luminance-based lighting control

This Chapter is based on:

Kruisselbrink TW, Dangol R, van Loenen EJ. A comparative study between two algorithms for luminance-based lighting control (Accepted for publication in Energy and Buildings).

9.1 Introduction

Lighting is an essential component related to the comfort of the indoor environment as was indicated in Chapter 1. Moreover, 15% of the global electricity use is dedicated to lighting [245]. Therefore, it can be beneficial to implement lighting control systems to improve visual performance, visual comfort and/or limit the energy use. However, various problems are exhibited using these systems, mainly related to the calibration and commissioning of the photo-sensor [246]. These photo-sensors are sensitive to their position, their spectral responsivity does not align with the luminous efficiency curve ($V(\lambda)$), and there is no established commissioning procedure [216, 247]. Moreover, an extensive monitoring campaign showed that 25% of the users switched off the automatic control of the blind system [19] indicating users' dissatisfaction. Therefore, it is suggested to use an image sensor, such as the Bee-Eye, that provides spatially resolved luminance data to improve these control systems [138, 188], which, due to technological advances and low costs, has a low economic risk for implementation.

Firstly, the luminance distribution is directly related to the experienced brightness [50], in contrast to the more often used illuminance. Additionally, the luminance distribution, measured with such a sensor, also contains valuable data on multiple relevant lighting quality aspects as indicated in Chapters 1 and 8. Potentially, also data relevant to the Non-Image Forming (NIF) effects of light could be extracted (Chapter 4). Finally, such an image sensor could also be used for building control and safety applications [188]. Hence, an image sensor measuring the luminance distribution can be considered a valuable and versatile addition to not only daylight-linked control systems, but also other lighting and building control systems. Nevertheless, the application and implementation of these sensors is currently still limited as these systems are expensive, relatively slow, require detailed commissioning, and might cause privacy concerns [138, 188, 216]. Especially, for advanced lighting control systems the complexity of commissioning is problematic [21].

Individual luminaires are often controlled using the Digital Addressable Lighting Interface (DALI), which is an industry standard open protocol, specified in International Electrotechnical Commission (IEC) 62386, developed for digital, bi-directional, communication between all components of a lighting control system [138]. DALI allows a controller to send 16-bit commands, one byte for the address (up to 64) and one byte for the data. Consequently, lighting levels are specified by an 8-bit value. A maximum of sixteen scenes can be programmed. Alternatives to DALI are, among others, KNX [248], LiFi [249], DMX [250].

The objective of this chapter was to illustrate the feasibility of luminance-based lighting control using highly versatile luminance cameras. Therefore, two alternative lighting control algorithms that utilize DALI in combination with a luminance camera were assessed, on their visual and energy performance, as a proof of principle. The visual performance was assessed based on the desktop illuminance and desktop uniformity while the energy performance was assessed based on the energy consumption during the measurement period.

9.2 Method

Two alternative algorithms (Section 9.2.2 and 9.2.3), with varying complexity and commissioning procedures, were simultaneously applied, in two identical rooms (Section 9.2.1). The algorithms aimed to control the electrical lighting, using a DALI controller, based on the average desktop illuminance measured by the Bee-Eye with the objective to apply daylight harvesting, which is required by many building energy codes [21]. Both algorithms aimed to provide a desktop illuminance in the range of 750 to 1000 lx, under varying conditions, such that both visual and non-visual support was provided [251]. Moreover, this range prevented immediate saturation due to daylight because sunshading was not accounted for, in this study, to limit the degrees of freedom.

9.2.1 Test bed

The algorithms were implemented in a test bed located in the Building Physics and Services laboratory at Eindhoven University of Technology illustrated in Figure 9.1. The test bed consisted of two identical, West facing, rooms each equipped with two Philips PowerBalance Tunable White (RC464B LED80S/TWH PSD W30L120 PCV PIP) luminaires with a power draw of 73 W. The correlated color temperature (CCT) of the luminaires was fixed at 4300 K. The luminaires were controlled using DALI ballasts.

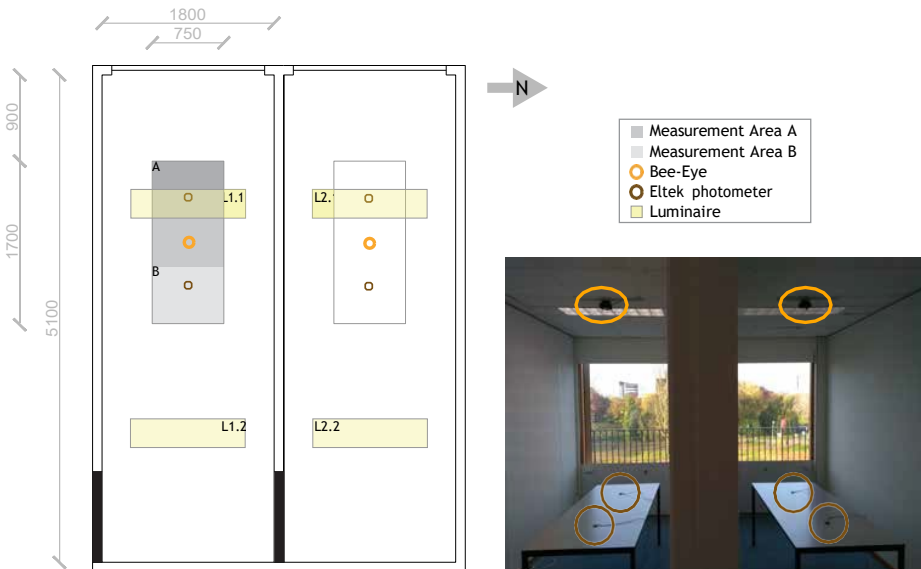


Figure 9.1: Floor plan and photograph of the two identical rooms with windows of 1500mm x 1800mm. The illuminance sensors were located at 400mm of the desktop edge.

In each room a calibrated Bee-Eye luminance camera, originating from Chapter 2, was mounted on the ceiling directly above the desktop to monitor the desktop luminance according to the third measurement track (Section 2.2.4), providing relevant

data unobtrusively (Chapter 7). Subsequently, the average desktop illuminance was derived from the spatially resolved luminance, under the assumption that the desktop was perfectly diffuse ($\rho = 0.57$). However, a small specular component of approximately $\rho = 0.03$ was measured. Prior validation measurements were conducted using a Konica Minolta CL-200A Chroma meter, which showed an acceptable validity for this specific use case.

The process was automated on the Bee-Eye luminance camera using Python. A control chain was established with the control module (PC) as the central node. The Bee-Eye was connected to the control module by means of a wireless secure shell (SSH) connection, while the DALI controller was connected by means of a DALInet converter.

In order to monitor the performance of the lighting control algorithms (Section 9.2.2 and 9.2.3), two Eltek LS50 photometers were attached to each desktop, on the central axis, at a distance of 400mm from the desktop edges as illustrated in Figure 9.1. The photometers were calibrated in an Ulbricht sphere using a Hagner E4-x.

Measurements were conducted from 10:00 on 11-11-2019 to 18:00 on 13-11-2019. The sunshine duration, as was measured by the KNMI (Dutch National Meteorological Institute), was 2.0h, 3.8h and 1.1h, while the cloud cover was 100%, 75%, and 100% for the 11th, 12th and 13th of November, respectively. The cloudcover was based on eight discrete sections of the sky hemisphere.

9.2.2 Algorithm 1

The first algorithm, applied in the room on the left-side, aimed to apply proportional control to determine the dimming levels for each luminaire in order to achieve the target average desktop illuminance of 875 lx (E_t), with an allowed 15% spread, based on the daylight contribution. The commissioning to apply this system was relatively elementary. During the commissioning phase only the output of the luminaires was related to the DALI input (using DaliConfig [252]) using steps of 10%. The output, in lux, was measured in the middle of the desktop surface using a Konica Minolta CL-200A Chroma meter. The relation between in- and output was linear and described by Equation 9.1.

$$Out = In \cdot 18.92 + 5.9 \quad (9.1)$$

Algorithm 1 defines dimming level $D(n)$, at instance n , of the individual luminaires according to Equations 9.2 and 9.3. Equation 9.2 determines control input $p(n)$, according to the proportional control law, relative to control error $e(n)$ and controller gain K_p [253]. The control error represents the difference between measured illuminance $E_m(n)$ and target illuminance E_t . Because there is no exact knowledge about the characteristics of the system (daylight), too high gains can lead to an unstable system, and too low gains can lead to long settling times [253], the controller gain was set to 1.0.

Based on the calculated control input, the dimming level is calculated using Equation 9.3, which employed the linear relation found in Equation 9.1. Relative to luminaire 1 and 2, illuminance $E_m(n)$ was measured for area A (close to window) and area B (away from window) (Figure 9.1), respectively. These areas were defined such that both luminaires were controlled semi-independently to actively enhance

9.2. Method

the uniformity. Each minute, the new dimming levels were calculated locally by the Bee-Eye luminance camera. A batch script on the control module requested each new reading of the new dimming levels and administered the dimming levels to the DALI controller.

$$p(n) = K_p \cdot e(n) = K_p \cdot (E_m(n) - E_i) \quad (9.2)$$

$$D(n) = D(n-1) \frac{p(n) - 5.9}{18.92} \quad (9.3)$$

9.2.3 Algorithm 2

The second algorithm, applied in the room on the right-side, aimed to assign the most suitable, predefined, scene to achieve a targeted desktop illuminance between the 750 and 1000 lx. Based on extensive commissioning, thirteen scenes were developed, in advance, as illustrated in Table 9.1, that aimed to achieve the target illuminance relative to the daylight contribution. Twelve (1-12) scenes were selected using discrete steps of 75 lx covering the relevant illuminance range, while one scene (0) was assigned for conditions exceeding the desired illuminance range. During the commissioning, scene 1 was established at first, in a dark room, using the Konica Minolta CL-200A Chroma meter. Based on the dimming curve, analogous to Equation 9.1, the remaining scenes were defined as well. Subsequently, the scenes were tuned accordingly, under daylight conditions, using the Chroma meter to achieve the desired illuminance values provided by the electrical lighting. As an example, scene 3 was applied when a daylight contribution of 180 lx was measured. The daylight contribution (E_d) was calculated, according to Equation 9.4, utilizing the measured illuminance (E_m) and the average desktop illuminance of the electrical light (E_e) associated with the previous scene ($S(n-1)$). Every 30s, the most suitable scene was determined, locally, by the Bee-Eye. A batch script on the control module requested and administered the appropriate predefined scene to the DALI controller.

$$E_d(n) = E_m(n) - \bar{E}_e(S(n-1)) \quad (9.4)$$

9.2.4 Analyses

First, the relative duration with an average desktop illuminance, average of two Eltek photo-meters, outside the target range was determined for the entire period and during office hours only (09:00 to 17:00). Subsequently, the performance of the two algorithms was assessed using the time-weighted average illuminance outside the targeted illuminance (ΔTWE) calculated according to Equation 9.5. The ΔTWE was also calculated for only the under- (ΔTWE_-) and over-estimations (ΔTWE_+), respectively. Due to the spatially resolved measurement of the illuminance the uniformity on the desktop surface could be monitored by the Bee-Eyes as well. Additionally, both systems were designed with the aim to limit low uniformities. Therefore, the uniformity was also derived from the two Eltek photometers. The illuminance uniformity achieved by the control systems was related to the the illuminance uniformity measured with daylight only, which was monitored from 15-11-2019 to 17-11-2019 in

Table 9.1: Dimming levels for Luminaire 1 ($D_{L2.1}$) and luminaire 2 ($D_{L2.2}$) of the pre-defined scenes of algorithm 2, the scenes were selected based on the calculated daylight contribution (E_d). Scene 1 also represents the reference static system.

Scene	$D_{L2.1}$ in %	$D_{L2.2}$ in %	E_d in lx
0	0	0	>900
1	40	57	0-75
2	36	57	75-150
3	32	53	150-225
4	28	49	225-300
5	24	45	300-375
6	20	41	375-450
7	16	37	450-525
8	12	33	525-600
9	8	29	600-675
10	2	25	675-750
11	0	21	750-825
12	0	17	825-900

the same office environments. The KNMI measured sunshine duration of 1.3h, 4.2h, and 5.1h and a cloud cover of 100%, 100%, and 87%, respectively.

$$\Delta TWE = \frac{|E_t - E_m(n)|}{\Delta t} \quad (9.5)$$

Additionally to the performance, the energy consumption was calculated for each algorithm. Based on the maximum power (73 W) of the luminaires, assuming a linear relation between power and dimming level, the energy consumption was calculated for the measurement period (Q) based on the logged dimming levels. Additionally, the energy consumption was extrapolated to a year (Q_{year}), not taking into account change in weather and season, and was calculated for office hours only ($Q_{off.h}$) while assuming 260 working days per year. The energy consumption of a static system, meaning a fixed lumen output, with a target illuminance of 875 lx was calculated as a reference (Algorithm 2, scene 1, Table 9.1).

9.3 Results

9.3.1 Performance

In this section the performance of both algorithms is assessed. Figure 9.2 shows the average illuminance, measured with the Eltek photometers, during the measuring period. Additionally, it represents the daylight contribution measured with the SolarBEAT facility [211] on the roof of the Building Physics and Services lab. A clear distinction can be made between the day and night periods. Due to the variability of daylight, large variations were exhibited during the day. The variability of the three different days corresponds to the sunshine duration as measured by the KNMI (Dutch National Meteorological Institute) of 2.0h, 3.8h and 1.1h, respectively for the 11th, 12th and 13th of November. During the 12th of November excessive illuminances

9.3. Results

were measured due to, mainly, the daylight conditions. The high sunshine duration yielded illuminances above 1000 lx and most likely also caused glare. The excessive illuminances, on the 12th of November, were not due to the control system as the trends between algorithm 1 and 2 are very similar and because the luminaires were turned off for the majority of the afternoon. However, differences and deficiencies were found between the control systems, which are elaborated based on the 13th of November.

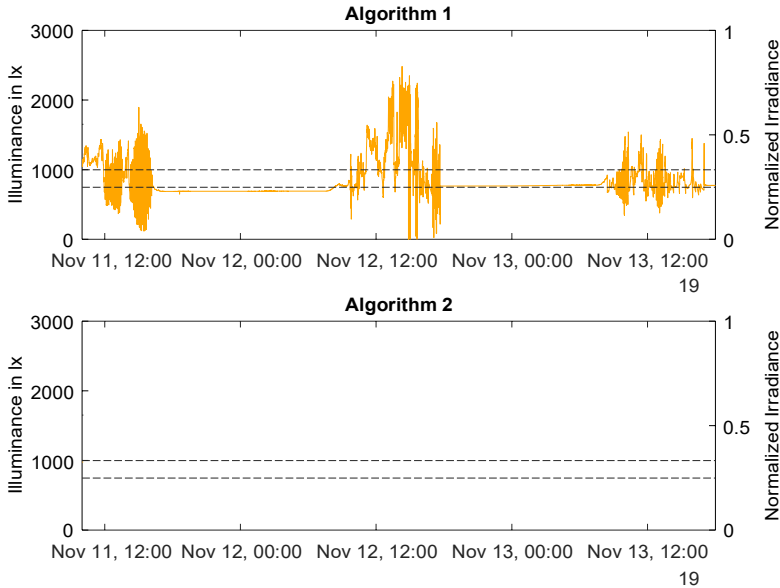


Figure 9.2: Average illuminance measured for algorithm 1 and algorithm 2. The dashed black lines represent the target illuminance. The daylight contribution is indicated by the black dashed line representing the normalized horizontal irradiance.

Figure 9.3 focuses on the 13th of November, as details are hard to distinguish in Figure 9.2. Distinct differences were exhibited between algorithm 1 and algorithm 2. Algorithm 2 seemed better able to maintain the target illuminance. Nevertheless, some instabilities were monitored, for instance, both the minimum and maximum illuminance were violated at a certain point during the day, albeit very briefly. The systems were often able to correct the violations within a short sampling period. Especially, algorithm 1 exhibits some oscillations (combinations of over- and under-shoots) around 10:00 and 13:00, often when daylight increases. Algorithm 2 exhibits a similar effect, but less distinct, when daylight decreases. These oscillations are also clearly visible, especially for algorithm 1, in Figure 9.4, which represents the corresponding dimming levels of both luminaires and both algorithms during the 13th of November. As expected, luminaire 2 always had a higher output compared to luminaire 1 because the daylight contribution in the back of the room was lower. Remarkably, for algorithm 1, luminaire 2 had often a higher output during the day than during the night. This occurs because the algorithm was actively trying to enhance the uniformity on the desktop. Because more daylight was available close to the window (especially in the afternoon), more compensation was required in the back of the

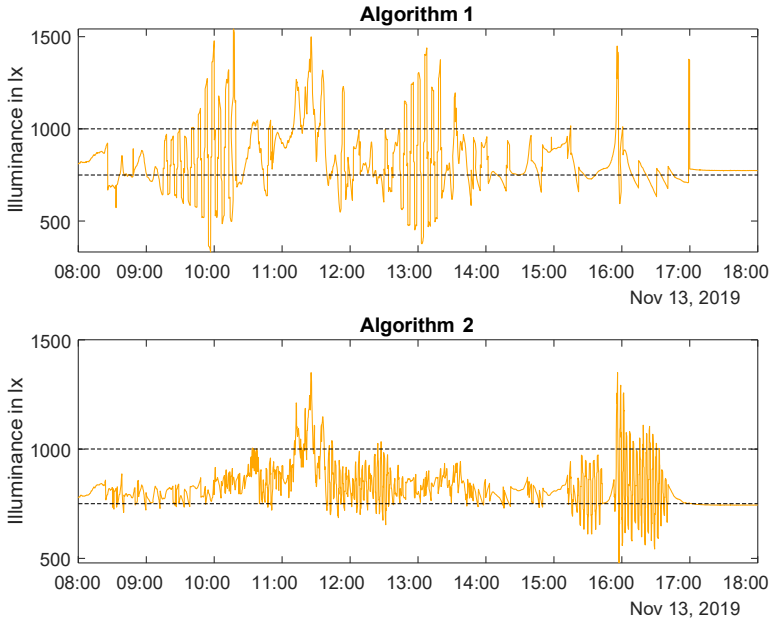


Figure 9.3: Average illuminance measured on 13th of November for algorithm 1 and algorithm 2, respectively. The dotted black lines represent the target illuminance.

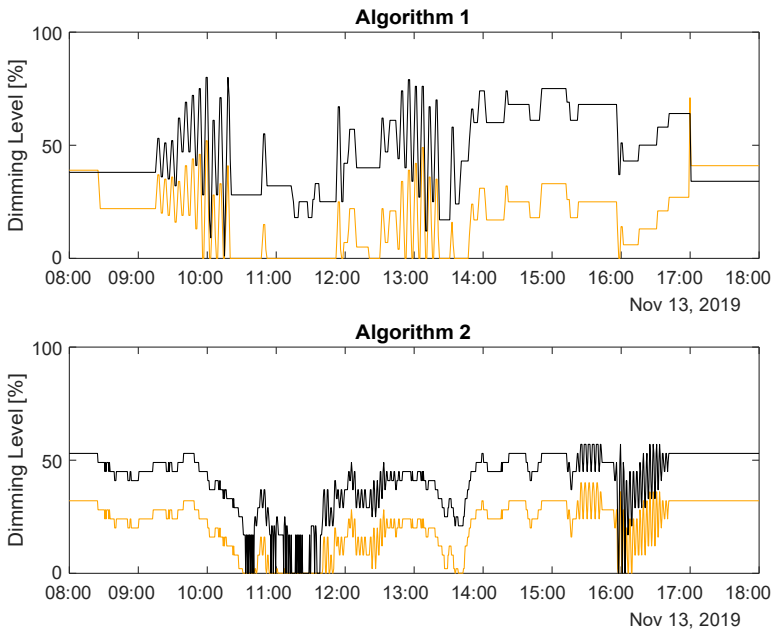


Figure 9.4: Dimming levels of luminaire 1 (orange, close to window) and luminaire 2 (black, back of the room) for algorithm 1 and algorithm 2, respectively.

9.3. Results

Table 9.2: Relative duration (%) outside the targeted illuminance (Δt) for algorithm 1 and algorithm 2. Δt_- and Δt_+ represent duration below and above target.

	Total period			Office hours		
	Δt	Δt_-	Δt_+	Δt	Δt_-	Δt_+
Algorithm 1	55.3	39.3	16.0	26.4	10.9	15.4
Algorithm 2	45.8	34.4	11.4	16.7	5.3	11.4

room. This is an effect that was not exhibited for algorithm 2, as the uniformity was passively implemented in the predefined scenes. Nevertheless, the dimming levels of luminaire 1 for both algorithms exhibited large similarities.

The findings in Table 9.2 correspond to the findings in Figures 9.2, 9.3 and 9.4. Again, algorithm 2 performed better indicated, according to Table 9.2, by a lower duration outside the target illuminance. Considering the total period, the average illuminance was insufficient for a long duration, which should have been prevented because more light could always be added. These incidents mainly happened at night, both algorithms had one night with an illuminance just below the target as illustrated in Figure 9.2, which was most likely caused by measurement inaccuracies of the luminance camera and/or due to specular reflections of the electrical lighting. When only considering office hours, low illuminance occurrences were drastically reduced. During office hours, illuminances above the target were occurring significantly more often than below target. However, these occurrences could not always be prevented when a surplus of daylight was available. For instance, both algorithms monitored an illuminance peak around 11:00 (Figure 9.3), when the luminaires close to the window were completely dimmed (Figure 9.4). For algorithm 2, even luminaire 2 was almost completely dimmed.

The time-weighted illuminance outside the targeted illuminance, illustrated in Table 9.3, shows again that algorithm 2 was outperforming algorithm 1. The ΔTWE , in most cases, was at least twice as high for algorithm 1 compared to algorithm 2. Together with Table 9.2, this indicates that algorithm 1 exceeds the target illuminance more often and more definite than algorithm 2. Table 9.3 also indicates that, in general, the low illuminance occurrences are minor compared to the high illuminance occurrences, especially those outside office hours, which were caused by small measurement inaccuracies of the luminance camera.

Table 9.3: Time-weighted illuminance outside the targeted illuminance (ΔTWE) for algorithm 1 and algorithm 2 in illuminance per hour (Eh^{-1}). ΔTWE_- and ΔTWE_+ represent time-weighted illuminance below and above target.

	Total period			Office hours		
	ΔTWE	ΔTWE_-	ΔTWE_+	ΔTWE	ΔTWE_-	ΔTWE_+
Algorithm 1	4,976	1,867	3,109	3,823	817	3,005
Algorithm 2	2,470	526	1,944	2,371	426	1,944

The uniformity on the desktop (U_0) is illustrated in Figure 9.5 representing the ratio of the minimum illuminance to the average illuminance. Overall, the uniformity on the desktops was relatively high. In practically all cases, the uniformity was above 0.6 as is required according to NEN 12464-1 [42]. The lower uniformities were

mainly exhibited when there was a surplus of daylight resulting in no or limited luminous output of the luminaires. When the electrical lighting was decisive, the uniformity was generally above 0.8. Again, algorithm 2 outperformed algorithm 1, albeit limited. Assessing the complete measuring period, Table 9.4 shows that also with daylight only, the uniformity was very high. The difference with algorithm 1 was non-existent due to measurements at night which have uniformities of almost one. However, when looking at office hours only, so only including day conditions, large differences were found. Even though the average uniformity was significantly lower during day conditions, the uniformity, with daylight only, was still above the NEN 12464-1 requirement. However, it is worth to mention that the desktop surface was rather small, very close to the window and only two measurement points were used for determining the uniformity.

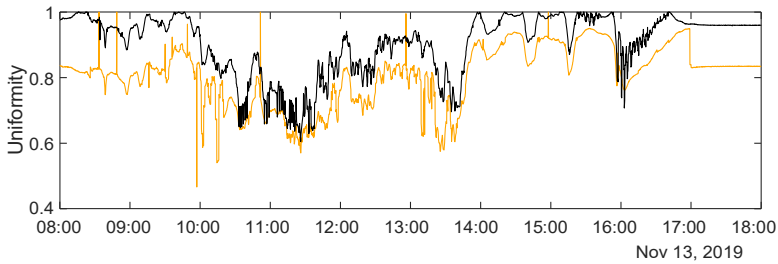


Figure 9.5: Desktop uniformity (U_0) measured on 13th of November for algorithm 1 (Orange) and algorithm 2 (black).

Table 9.4: Uniformity (U_0) of algorithm 1, algorithm 2 and daylight condition.

	U_0	$U_{0,off.h}$
Algorithm 1	0.82 ± 0.09	0.76 ± 0.12
Algorithm 2	0.92 ± 0.10	0.85 ± 0.12
Daylight	0.80 ± 0.13	0.63 ± 0.07

9.3.2 Energy

Besides the performance of the algorithms also the energy use was measured as indicated in Table 9.5. Both algorithms use significant less energy compared to steady lighting. For office hours, a reduction of 50% and 70% was achieved for algorithms 1 and 2, respectively, compared to lighting with a fixed output of 875 lx. The gains were very high because the monitored desktops were very close to very large windows. Therefore, daylight dimming was very effective because the daylight contribution was significant at all times during the measurement period. Consequently, there was no need to continuously provide 875 lx using the electrical lighting.

9.4. Discussion

Table 9.5: Energy consumption of algorithm 1, algorithm 2 and the static condition, respectively. The energy consumption is indicated in kWh for the respective measurement period (Q) and for the entire year (Q_{year}). Additionally, the energy consumption is calculated for office hours only ($Q_{off.h}$ and $Q_{off.h,year}$).

	Q	$Q_{off.h}$	Q_{year}	$Q_{off.h,year}$
Algorithm 1	2.65	0.81	414	73.7
Algorithm 2	2.86	0.48	448	43.7
Static	3.97	1.62	620	147.3

9.4 Discussion

In this study, two alternative luminance-based daylight-linked controllers were implemented in a mock-up office environment, referred to as algorithm 1 and algorithm 2. Algorithm 2 seemed to be working more accurate on all aspects considered in this study. However, both algorithms were able to reduce the energy consumption compared to static lighting.

Especially algorithm 1 exhibited some artefacts in the form of oscillations that resulted in a reduced performance. It exceeded the target illuminance more often and more distinct than algorithm 2, also the uniformity was generally lower. Nevertheless, the energy savings were significant, but comparatively lower than algorithm 2. The oscillations in the morning of November 13th, illustrated in Figure 9.4, required 1.3% more energy compared to no oscillatory behaviour of the same system at the same time (50.1 W to 49.4 W). The lower energy performance is mainly attributed to the system actively enhancing the uniformity.

One cause of the large oscillations for algorithm 1 could be the distribution of area A and area B. Especially, area B, intended to control luminaire 2, was mainly affected by luminaire 1. Consequently, a change in luminaire 1 also had a very large impact on area B, prompting luminaire 2 to change accordingly. A characteristic of this artefact is that the oscillations, of luminaire 1 and 2, are not in phase, as they are responding to each other. However, the results show that this was not the case, indicating that the oscillations were caused by something else.

The oscillations seem to be an artefact of the proportional control as literature states that ringing (oscillation around the set point) can occur due to improper control settings [254]. Under certain conditions, the controller gain (K_p) overshoots the set point as is illustrated in the example of Figure 9.6 for $K_p = 2.0$, which can result in instability in the form of oscillations. If K_p is reduced, the overshoot is reduced, and the oscillations are limited. However, due to the reduced gain the settling time increases, more time steps are generally required to achieve the set-point, such as for $K_p = 0.5$. The most suitable gain is dependent on the specific system and is often actively tuned in order to achieve accurate control, which requires some practical experience. 50% of the controller gain that causes oscillations is often used as a guideline for an appropriate K_p . For the example, this guideline would result in a controller gain for Figure 9.6 and for algorithm 1 of approximately $K_p = 1.0$ and $K_p = 0.5$, respectively.

As an improvement to Proportional control an Integral and Derivative term are often added to such systems, commonly known as PI or PID controllers [255]. For instance, the integral part aims to eliminate the steady-state error by accounting for

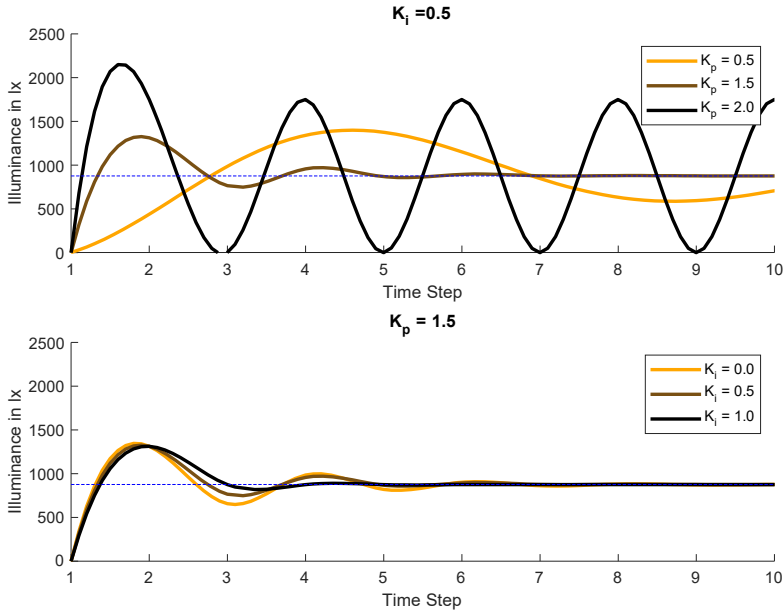


Figure 9.6: Examples of controller K_p and integral gain K_i , relative to target illuminance of 875 lx indicated in blue.

the historic cumulative control error using a constant integral gain K_i . However, this may slow down the response of the controller. An example of integral control is illustrated in Figure 9.6. A high K_i reduces the steady-state error, but slows the response. Nevertheless, the effects are rather minor compared to the effect of the proportional term. The same is valid for the derivative term, which applies damping by controlling the rate of change in error. So the integral and derivative terms account mainly for fine-tuning of the system at the expense of added complexity and slightly longer settling times.

In theory, algorithm 1 should be able to assign appropriate dimming levels. However, practice shows that due to the relative complexity (100x100 solutions), this is often not the case. Algorithm 2 was in theory less accurate due to its low complexity (13 solutions). However, this study showed that this algorithm was, in fact, more accurate while it required less complexity.

Both algorithms showed that a significant reduction in energy could be achieved compared to a steady-state system. For office hours an energy reduction of 50% and 70% was achieved. According to the literature review conducted by Williams et al. [12] an average energy reduction of 28% was found based on an actual daylight-linked control systems generally utilizing photo sensors. However, large variations were exhibited between different case studies (standard deviation 11%). For instance, Galasiu et al. [256] found average energy reductions, during office hours, between 50% and 60% in four private offices, which is more in the range of the energy reductions found in this study. Moreover, for simulations, an average reduction of 48% was found [12]. Accounting for the relatively extreme conditions in this short-term study, the energy reductions do relate to earlier findings. In the long-term, slightly higher energy gains can be expected because the sunshine duration and global irradiation

were below, while the cloud cover was higher than the yearly average according to the KNMI. This study does not provide conclusive evidence that the luminance camera outperforms the photo-sensors that are generally applied, more research is required for this. However, this study shows the feasibility of a daylight-linked system using a luminance camera. It is expected that such a camera-based system is appropriate for environments with large window openings, resulting in large uniformities due to the high luminance gradients, because it contains spatially resolved data. However, direct sunlight might saturate the sensor when no neutral density filter is applied. Additionally, the control system, using a luminance camera, can easily be extended as there is a lot of spatially resolved data present. For instance, additional lighting quality aspects (Chapter 1) can be measured and added to the system, but also additional functionalities such as presence detection and video surveillance can be accounted for using the images gathered by the luminance camera.

9.4.1 Limitations

However, some limitations are expressed related to this research. Based on this study, it is not possible to directly relate the energy performance of the luminance-based lighting control systems to existing systems that use photo-sensors as these were not applied in this study. Moreover, the environmental conditions between different case studies, found in the literature, were significantly different resulting in large variations in energy reductions. Therefore, more research is required to relate these luminance-based systems to existing daylight-linked control systems, preferably under identical conditions.

Especially, algorithm 1 exhibited numerous artefacts that might have been prevented, if more extensive commissioning was applied. A controller gain of 1.0 was initially selected as this seemed appropriate. In theory, this gain would directly assign the correct dimming levels with a minimum settling time. Practice shows that measurement noise, environmental conditions (daylight) and delays necessitate a lower controller gain to prevent oscillations. More extensive commissioning might have led to algorithm 1 outperforming algorithm 2. Nevertheless, it remains sensible to apply an algorithm as simple as possible, among others because it is generally less susceptible to implementation errors.

Finally, the algorithms were implemented in a lab environment that did not accurately associate with authentic office environments. For instance, the desks were placed in the middle of a narrow space that suggested an office environment to indicate the feasibility of such luminance-based control systems. Moreover, the office environment was static. In a real case scenario, objects might be placed on the desk, or the luminance camera might be obstructed. Therefore, it is complicated to predict the environmental conditions that are suitable for these type of systems. Moreover, the desktop illuminance was only validated using two photometers. Consequently, the illuminance uniformity might have been overestimated because the minimum illuminance is expected to be found at the very end of the table. The Bee-Eye might have been able to indicate the desktop illuminance more accurately. However, it was chosen to use an completely independent measure.

The performance related to the visual performance was assessed indirectly based on recommendations. Visual comfort was not addressed explicitly in this research. For instance, in these conditions, it would have been appropriate that glare was as-

essed as well, especially for the 12th of November. Moreover, in a best case scenario, participants are present to directly assess the performance, based on aspects such as annoyance and reaction speed of such a system. However, an independent measure, in this case an approximation based on two sensor points, was deemed more acceptable. It was considered not fair to assess the performance of the lighting control system, which utilizes output from the Bee-Eye, based on the Bee-Eye.

The performance related to the visual performance was assessed indirectly based on recommendations. Visual comfort was not addressed explicitly in this research. For instance, in these conditions it would have been appropriate to assess glare as well, especially for the 12th of November. In a best case scenario, participants are present to directly assess the performance related to visual performance and visual comfort, based on aspects such as annoyance and reaction speed of such a system. However, this introduces additional issues such as complex long-term measurements and requires an accurate method to objectively quantify human responses.

9.5 Conclusion

This study aimed to test the feasibility of two basic luminance-based lighting control algorithms for daylight harvesting. The algorithms were applied in two identical mock-up offices for a period of three days.

The first algorithm aimed to apply proportional control to determine the appropriate dimming levels, while the second algorithm assigned the most suitable predefined scene to achieve the target illuminance. The algorithms were rated on the duration outside the targeted illuminance range, the time-weighted illuminance outside the targeted illuminance range, the average uniformity and the energy consumption. In all aspects, algorithm 2 performed better, while it was a more basic controller. For Algorithm 2, during office hours, 16.7% of the time the measured illuminance was outside the targeted illuminance range, the time-weighted illuminance (ΔTWE) outside the targeted range was $2,371 \text{ Eh}^{-1}$ while and average desktop uniformity of 0.85 was achieved during the measurement period. Moreover, the system required less energy, a reduction of 70% was achieved compared to steady-state lighting.

Algorithm 1 exhibited performance-reducing artefacts in the form of oscillations around the target illuminance. As a result, the under- and overshoots negatively affected all four assessment criteria. It was found that the set controller gain was not entirely fitting. Literature suggests that determining this gain, which is not always straightforward, is done actively during the commissioning phase. Based on this study, it seems that a relatively high complexity, as in algorithm 1, tends to be more susceptible to errors, hence an extensive commissioning process is required to compensate for this.

Nevertheless, this study shows that luminance-based daylight harvesting is feasible. However, just as with photo-sensor-based systems, an extensive commissioning is required. Further research is required to relate the performance of these luminance-based systems to already existing systems, although this study indicates that the performance is not worse. Moreover, one should take into account that luminance-based systems are much more versatile than photo-sensor-based systems due to their spatially resolved data. A luminance camera is able to address multiple relevant parameters (Chapter 8) such as the uniformity and wall luminance, which photo-

9.5. Conclusion

sensors cannot. Moreover, luminance cameras might be combined with alternative functionalities such as presence detection and video surveillance.

The recommendations for future work directly relate to the limitations of this study. When a luminance-based controller is applied, extensive commissioning should be applied in order to set a suitable controller gain. Alternatively, a universally applicable controller gain that has a relatively low gain, resulting in relative slow but accurate response, might be suitable as well from a users' perspective. Research dedicated to relating the performance of such systems to existing systems should be conducted in realistic conditions that include blind control.

General discussion

10.1 Introduction

In search of high quality office lighting, which will reduce costs and increase comfort, the scientific community faces two major challenges. First, there is the need for more insight into the complex and intangible subject that is lighting quality. Secondly, there is the technological challenge on how to provide high quality lighting for an office environment. In this thesis essential steps are made towards an improved understanding and implementation of lighting quality.

Chapter 1 proposed an approach on how to quantify lighting quality, based on a range of eleven different lighting quality aspects, because one cannot put a single number on "lighting that allows you to see what you need to see quickly and easily and does not cause visual discomfort but raises the human spirit" [8]. After all, measuring lighting quality is an essential component in bringing high quality lighting towards the office environment. Lighting control systems are essential due to the complex character of lighting quality. In addition, office workers have different preferences with respect to the various lighting quality aspects, adding an additional layer of complexity.

Currently, lighting control systems are not up to this task. They either have a limited focus (e.g. energy savings, desktop illuminance) or are often experienced as annoying, which is mainly caused by faulty sensors [21]. Consequently, there is a need for appropriate input for lighting control systems, on lighting quality. Chapter 1 indicated that the majority of relevant lighting quality aspects can be quantified in a continuous fashion based on the luminance distribution. This research aimed to develop a practical and validated luminance distribution measurement device to provide input for lighting control systems for high quality lighting.

This chapter discusses the key findings, strengths and weaknesses, and future research in relation to this topic. The key findings are also illustrated in Figure 10.1, which aims to provide a quick overview of the thesis. Moreover, some tips and tricks are proposed related to continuous luminance distributions measurements in real office scenarios, in addition to alternative applications for the luminance distribution.

10.2 Key findings

Lighting quality can be considered a construct [23]. Therefore, a literature review was conducted in Chapter 1 to find the different lighting quality aspects that, taken together, compose lighting quality. Table 1.1 indicates eleven aspects that were deemed to be relevant for lighting quality. Special attention was given to the variable lighting quality aspects, which could potentially be optimized in real-time by a lighting control system to provide high quality lighting. The distinct variable aspects are: quantity, distribution, glare, spectral power distribution (SPD), daylight, directionality and dynamics of light. As input to a lighting control system, continuous measurements of these aspects are required.

It turned out that the luminance distribution was able to quantify all variable lighting quality aspects (Figure 1.2), except the also highly relevant SPD and the associated CCT, making luminance distribution measurement devices a suitable tool for comprehensive measurements of the lit environment. However, some aspects are seldom measured using the luminance distribution. Moreover, commercially available

10.2. Key findings

	Topic	Reasoning	Type	Key Findings
 HDR	1 Comprehensive measurement of LQ 	<ul style="list-style-type: none"> No consensus about definition LQ Multidimensional concept Continuous measurements 	Literature Review 	<ul style="list-style-type: none"> 7 variable lighting quality aspects Luminance distribution suitable to continuously monitor LQ
	2 Measuring the luminance distribution 	<ul style="list-style-type: none"> Luminance distribution is suitable to monitor LQ No suitable available devices 	Prototyping 	<ul style="list-style-type: none"> Bee-Eye is able to measure practically and autonomously using HDR imaging Conventional method introduces measurement errors
	3 Spectral tuning of luminance cameras 	<ul style="list-style-type: none"> Methodological issues in conventional method to derive luminance 	Modelling + Lab study 	<ul style="list-style-type: none"> Validated models to improve spectral match of luminance camera Including spectral responsivity and SPD improves accuracy
	4 Spectral mismatch: cameras and SPDs 	<ul style="list-style-type: none"> Various cameras and SPDs Implementation alternative action spectra 	Modelling 	<ul style="list-style-type: none"> Large differences between cameras Mismatch is bounded by spectral responsivity Reasonable approximation melanopic radiance
 HDR	5 Spatial resolution of HDR images 	<ul style="list-style-type: none"> Limit privacy issues Prevent high computational costs Maintain accuracy 	Field + Lab study 	<ul style="list-style-type: none"> Resolution can be reduced (440 x 330) without compromising accuracy Glare measurements expected to require very high spatial resolutions
	6 Temporal resolution of HDR images 	<ul style="list-style-type: none"> Limit privacy issues Prevent high computational costs Maintain accuracy 	Data Analysis 	<ul style="list-style-type: none"> 5 minute interval does not seem to lose relevant information On average, variable conditions are normative
	7 Alternative measurement position for luminance cameras 	<ul style="list-style-type: none"> Prevent interference Maintain relevancy LQ aspects Maintain FOV 	Lab study 	<ul style="list-style-type: none"> Ceiling-based (20-degrees) position is feasible Only surface bound metrics were accurately approximated Correction model is required
 HDR	8 LQ measurements in real office environments 	<ul style="list-style-type: none"> Effect of user Effect of practical recommendations Long-term measurements of LQ aspects 	Lab + field study 	<ul style="list-style-type: none"> Not all LQ aspects are accurately measured User introduces random errors Methodology introduces systematic errors
	9 Luminance-based lighting control system 	<ul style="list-style-type: none"> Integration with DALI Daylight dimming 	Lab study + Prototyping 	<ul style="list-style-type: none"> Versatile sensor Commissioning is essential Adequate control

Figure 10.1: Overview of the thesis, shortly describing the reasoning, study type and the key findings of the different chapters (LQ = Lighting Quality).

luminance distribution measurement devices are not suitable for implementation in lighting control systems yet. Nevertheless, alternative measurement solutions generally have a lower applicability, as only a limited number of lighting quality aspects can be extracted.

10.2.1 Measuring the luminance distribution

Consequently, using a Raspberry Pi single-board computer [257], a low cost luminance camera was developed to be practical and autonomous in use (Chapter 2). The device, titled **the Bee-Eye**, was suitable for practical implementation in lighting control systems. The Bee-Eye makes use of the essential High Dynamic Range (HDR) technology [46], which allows the Bee-Eye to capture the luminance range occurring in the real world. The floating point Red-Green-Blue (RGB) values were, subsequently, utilized to calculate the luminance of each individual pixel. Using an equisolid-angle fisheye lens, the image projection can be used to map the luminance to the real world. By virtue of the Raspberry Pi, this process was completely automated into three distinct measurement tracks (Section 2.2.4), all requiring approximately 20 seconds, that yielded the raw HDR image, the luminance distribution according to Tregenza's subdivision [159], or a predefined luminance metric.

The accuracy of the conventional method to calculate the luminance was exposed as a research gap in Chapters 2 and 3. In the conventional method (Equation 2.3), assumptions regarding the spectral responsivity and SPD are made that seem not fitting, resulting in significant spectral mismatches. Nevertheless, using this conventional method a practical accuracy is still within reach, as long as a careful photometric calibration is conducted. In Chapter 3, two optimization criteria (Equations 3.5 and 3.7) were proposed to limit the spectral mismatch, using an alternative approach to calculate the luminance according to the floating point RGB values. Using two cameras, with different spectral responsivities, and three illuminants; LED, halogen and fluorescent, the validity of the proposed optimizations was tested both theoretically and practically. Although the results of the theoretical models and empirical data showed significantly different result, the results were considered promising. In the theoretical model, an increased performance was achieved for both camera types and all illuminants. The measurements only found an improved performance for the LEDs using both cameras and the fluorescent illuminant for one camera. However, the differences between the theoretical and practical work were attributed to methodological issues as extensively discussed in Section 3.5. Therefore, it was concluded that this alternative method to determine the luminance resulted in an improved spectral match.

It was hypothesized that the spectral mismatch of a luminance camera is largely dependent on the spectral responsivity and the SPD of the illuminant. Consequently, Chapter 4 assessed the performance of six alternative cameras relative to 205 SPDs using the theoretical model originating from Chapter 3. Using this model, the measurement errors were reduced to approximately 2% to 6%, relative to errors of 4% to 17% for the conventional method. The error ranges indicate that the spectral responsivity of the camera has a significant effect on the measurement error. Moreover, the effect of the SPD was assessed based on the Correlated Color Temperature (CCT) and the Full Spectrum Index (FSI). Using the conventional method, the CCT and FSI were largely impacting the accuracy, continuous SPDs with a CCT close to 6500

K generally performed the best. However, for the optimized luminance calculation this dependency was reduced to a large extent, as an benefit of the improved spectral match.

Alternatively, Chapter 4 applied the theoretical model to derive the melanopic radiance to assess the measurement performance for the Non-Image Forming (NIF) effects of light [184]. Some cameras were able to quantify the melanopic radiance relatively accurately. However, one of the cameras yielded average measurement errors exceeding 20%. Again, this indicates the large dependency on the spectral responsivity of the camera.

10.2.2 Recommendations for continuous luminance distribution measurements

Luminance cameras, such as the Bee-Eye, can be suitable for implementation in lighting control systems. However, one has to take into account some practical issues that might hamper the actual implementation. Interference, privacy, and high computational costs are issues that need to be considered carefully when applying a luminance camera in the office environment for longer periods of time. Three practical aspects were identified that relate to these issues: the spatial resolution, the temporal resolution and the measurement position.

The spatial resolution, researched in Chapter 5, represents the horizontal and vertical width of an HDR image, in pixels, and relates to privacy and computational costs. A sufficiently low spatial resolution prevents face recognition and limits the ability to track persons and monitor their behavior. Moreover, a low spatial resolution drastically reduces the computational costs. Luminance distribution measurements were conducted both in the lab and in the field with a high initial spatial resolution. Both the lab and field study recommended a spatial resolution of 440 x 330 pixels for mean luminance measurements. With this resolution automated facial recognition is practically prevented, while reducing the processing time, as indicator for the computational costs, to approximately 12 seconds. The maximum luminance, relevant for glare measurements, was not accurately measured using a reduced spatial resolution. It was estimated, in the lab, that a spatial resolution of approximately 3000 x 2250 was required, which indicates that extremely high spatial resolutions are required for accurate glare measurements. Consequently, privacy intrusion and high computational costs cannot be prevented when measuring the maximum luminance accurately. Overall a spatial resolution in the range of 440 x 330 is advised, as various luminance-based metrics are based on the mean luminance. However, high complexity of the measured scene, indicated by high luminance gradients, might argue for a higher spatial resolution as it was found to impact the required spatial resolution.

Analogous to the spatial resolution, the temporal resolution, representing the duration between two consecutive measurements, is relevant for privacy and the computational costs. Using Discrete Fourier Transforms (DFT), Chapter 6 aimed to propose a suitable temporal resolution for luminance distribution measurements. As a compromise between relevancy, privacy and computational costs the recommended temporal resolution contained 85% of the power of the original signal, which was considered affordable for lighting control applications. In all cases, a temporal resolution equal to or shorter than 5 minutes was required to maintain 85% of the power of the original signal. Outdoor measurements required the highest temporal resolution,

approximately 2 minutes, because the sensor was not shielded by the built environment. Moreover, the indoor measurements, with the electrical lighting switched on, required the lowest temporal resolution because the lighting added a constant component to the highly variable daylight. Naturally, the weather conditions were highly relevant. Intermediate sky conditions required the highest temporal resolution, while for overcast skies a temporal resolution greater than 1h generally sufficed.

At last, the most suitable measurement position for long-term luminance distribution measurements was determined in Chapter 7. According to best practice, the luminance distribution is best measured from eye position representing the Field of View (FOV) of the user, which is, unfortunately, not feasible for long-term measurements because this will cause interference. Consequently, an alternative position was required. A pilot study (Section 7.2) indicated that ceiling-based luminance distribution measurements were a feasible solution for desktop luminance measurements. Therefore, in the first phase of Chapter 7, the most suitable ceiling-based measurement position was determined for the Desktop Luminance, Monitor Luminance, 40° Luminance Band (B40 Luminance) and the Retinal Illuminance, representing visual performance (2x), visual comfort and NIF effects, respectively. On average, a ceiling-based position above the aisle with a 20° angle relative to the ceiling achieved the highest agreement with the eye level measurements because the FOV and the angle of view showed large similarities. In the second phase of Chapter 7, the performance of this position was assessed. Using very basic commissioning (linear correction model), the Desktop Luminance and the Monitor Luminance were approximated accurately with a Mean Absolute Percentage Error (MAPE) of 3.7% and 6.2%. The Retinal Illuminance required more extensive commissioning to achieve accurate results (MAPE of 12.5%), while the B40 Luminance was not approximated accurately (MAPE > 20%). The B40 Luminance is thus not a suitable indicator for visual comfort using ceiling-based measurements. Moreover, the uncertainty for each individual metric was illustrated as well for practical implementation. Preferably, surface-bound, non-transparent and predominantly diffuse, luminance-based metrics are used when applying a ceiling-based measurement position. In general, the correction model was essential to achieve accurate approximations. The translated luminance masks could be simplified, which is time saving, as long as they are corrected by these correction models.

10.2.3 Application of the luminance distribution

Chapter 8 describes an actual field study conducted using the recommendations of the previous chapters (e.g. a ceiling-based position). Two identical mock-up office environments, representing a lab and field condition, were monitored continuously for one week using the Bee-Eye with the objective to extract the relevant lighting quality aspects as proposed in Chapter 1. In the lab condition, state-of-the-art measurements were conducted, which provided a benchmark. The field condition was occupied by an office worker rendering high accuracy measurements unfeasible. The measurements showed that it is rather complex to approximate lighting quality using field measurements, relatively large differences were found compared to the benchmark. The Task Luminance and Daylight Ratio were measured with a substantial agreement according to Lin's Concordance Correlation Coefficient [176], moreover, the difference with the benchmark was not statistically significant. The Task/Adjacent/Background

10.3. Strengths and weaknesses

Ratio and the Daylight Variability achieved a moderate agreement with the benchmark. The remaining lighting quality aspects; Uniformity, Daylight Glare Probability (DGP) and, the Vector to Scalar Ratio generally performed poorly, having either a low precision or low accuracy (Table 8.7). Systematical errors were mainly introduced by the limitations of field measurements such as an alternative, ceiling-based, measurement position. However, there were also random errors, which were mainly caused by the office worker obstructing certain areas of the camera's FOV. Due to movements, the office worker adds a highly variable and irregular unknown component to the luminance distribution, which is not easily accounted for.

Finally, the Bee-Eye was implemented, as a proof of principle, in two alternative luminance-based lighting control systems using DALI, in Chapter 9. Both algorithms aimed to achieve a desktop illuminance between 750 and 1000 lx assuming a Lambertian desktop surface. The performance was assessed based on two Eltek photometers positioned on the desktop surface. The first algorithm applied proportional control to determine the appropriate dimming levels. The second algorithm administered the most suitable predefined scene. In general, the basic algorithm 2 outperformed the more complex algorithm 1, it exceeded the target illuminance less often, it provided a higher uniformity and saved more energy. Algorithm 1, theoretically more accurate than algorithm 2, exhibited oscillations around the target illuminance, a well known artefact of proportional control, which is only prevented by extensive commissioning. This proof of concept showed the feasibility of luminance-based lighting control, although extensive commissioning is required analogous to existing lighting control systems. However, the luminance camera is much more versatile than the commonly applied photo-sensor because of its spatially resolved data. Consequently, numerous lighting quality aspects can be extracted while other functionalities can be added as well (Section 10.5).

10.3 Strengths and weaknesses

10.3.1 Strengths

This thesis aimed to pave the road for practical application of luminance cameras for lighting quality control, which is a process covering multiple research directions, instead of a confined focus on a narrow research area. Consequently, a wide range of activities was conducted in this research, which is also illustrated in Figure 10.1. Already in Chapter 2, prototyping and programming was required to develop a luminance camera, which was subsequently tested using measurements. Moreover, theoretical models were applied to improve the spectral match in Chapters 3 and 4, which were validated by lab measurements. Lab measurements were extensively conducted for Chapters 5 to 8, while Chapter 5 and 8 also contained extensive field studies, which were analyzed using statistical tests, DFT and, estimation evaluations. Finally, a luminance-based lighting control system was employed that required prototyping and measurements as well.

As the research presented in this thesis was focused on practical implementation, a large part of the thesis can be applied directly to other research. For instance, the luminance camera developed in Chapter 2 can be used by research looking into human

factors in lighting. Or, the experiences and findings of the field study in Chapter 8 can help other researchers design their field studies more accurately. Additionally, the lab studies were designed such that they mimicked real office scenarios with the objective to be applicable for real office scenarios.

Often, research has a more fundamental approach, which is typically not directly applicable. Therefore, this thesis can be considered a valuable contribution as it really focuses on helping the scientific community to proceed research in the field of luminance measurements, lighting quality and lighting control. Nevertheless, the fundamental approach is relevant as well. Therefore, Chapters 3 and 4 were based on more fundamental research, mainly utilizing models instead of long-term measurements. Consequently, actual implementation of this knowledge is still slightly further away.

An important strength of this thesis is the amount of data on which this research is based. Due to the practical and automated Bee-Eyes, of which in total 6 were employed, we were able to conduct multiple measurements with relatively little effort. Over 15,000 luminance distribution measurements have been captured, and most of them have been analyzed as well. An advantage of a camera system like this is that it does not contain a mechanical shutter that breaks down after a certain number of clicks (typically in the order of 100,000). This mitigated the risk of conducting numerous measurements.

By using large data sets, we were able to account for variable conditions. Measurements have been conducted during different weather types, different seasons and different office types. However, even a higher number of conditions are, naturally, still lacking. Due to the high number of measurements, the focus in Chapter 5 and 8 was on the effect size instead of the p-value, as it tends to go to zero quickly for large sample sizes [206].

Following the previous point, interpretation of the results requires a careful attitude because there are no interpretation concepts that are simultaneously simple, intuitive, correct and foolproof [258]. Consequently, during our studies, we aimed to interpret the results using two interpretation concepts to achieve a robust assessment. For instance, in Chapter 3 the student t-test as well as Lin's Concordance Correlation Coefficient were utilized to assess whether the optimization criteria achieved an improved accuracy both for the theoretical models and the measurements. In Chapter 7, the MAPE was used to indicate the relevancy of ceiling-based measurements. However, the measurement uncertainty was employed as well, because this has a more practical application compared to the MAPE.

This thesis showed that it is feasible to develop a practical system that is capable of providing relevant input on lighting quality, which, subsequently can be used in lighting control systems based on components with a cost of approximately 100 Euros. Starting from Chapter 2, the objective was to maintain low costs in order to end up with a feasible system. Consequently, a Raspberry Pi camera was used instead of a probably more accurate DSLR camera. Additionally, the spectral match was digitally tuned instead of applying optical filters to improve the spectral match. Obviously, these considerations do have an effect, which we aimed to illustrate in Chapter 8. Chapter 8 concluded that not all lighting quality aspects can be measured accurately during a field study, which is not necessarily solved by applying

more expensive components. The limitations to it being a field study were mainly normative. Consequently, the quality of the components is expected to attribute only a minor improvement for these type of field studies.

10.3.2 Weaknesses

Based on the literature review conducted in Chapter 1, we proposed to quantify lighting quality using seven variable lighting quality aspects. Although these seven aspects were collected using a systematic approach, there is no guarantee that these aspects are complete or that they are all equally relevant. Using their occurrence in literature, we were able to put some weight on the individual lighting quality aspects but this does not necessarily align with their actual relevance. We believe that this indirect method, considering lighting quality a construct, is more suitable than a direct quantification of lighting quality which has already failed quite often (Section 1.4). Validation of quantifying lighting quality using these variable aspects was outside the scope of this thesis. Except the SPD and the associated CCT, which are also highly relevant, the variable lighting quality aspects were all measurable by the luminance distribution. This does not alter the fact that the luminance distribution is a very suitable tool for comprehensive measurements of the lit environment even though it is not able to extract the SPD.

The Bee-Eye was developed using a Raspberry Pi single-board computer, Raspberry Pi camera board and a miniature fisheye lens, which were all very suitable for prototyping but have their limitations. The approachable Raspberry Pi single-board computer, using a NOOBS operating system, was capable of carrying out the assigned task. However, a wide range of functionalities were present that were irrelevant for this specific application. Consequently, the device could have been more compact or quicker in processing.

The Raspberry Pi camera was easily connected to the Raspberry Pi single-board computer but had several limitations. Firstly, the spectral responsivity of the camera was not able to achieve a high spectral match (37%). For instance, Cam 6 in Chapter 4, which was also a miniature camera, might have been much more suitable as it could achieve a spectral mismatch of only 16%. Additionally, the focal length and aspect ratio were fixed, and the fisheye projection was not captured for the full 100% as was illustrated in Figure 2.7. Moreover, the highest exposure value ($EV = 18.8$) was not sufficient for this application, it still resulted in over-saturation for very bright conditions. Most likely, similar cameras will not (distinctively) exceed this exposure value. Consequently, a neutral density filter is likely to be required. However, the Raspberry Pi camera does not have a dedicated slot for such a filter like a DSLR camera. Alternatively highly specialized logarithmic response cameras might offer a, more expensive, solution as it does not exhibit any saturation like the integration sensors applied in this study.

The fisheye lens, currently not available anymore, provided a FOV slightly larger than 180° . A range of miniature fisheye lenses was assessed. Except for the applied fisheye lens, the performance in combination with the Raspberry Pi camera board was generally poor. Attaching the lens was only feasible with a make-do solution which might have introduced slight differences between cameras.

There is a wide range of alternative hardware components. For instance the

NVIDIA Jetson Nano [259] (\$100) is a powerful single-board computer especially designed for heavy image processing that would have been very suitable for the processing of the HDR images. As a cheaper (< \$10) and more compact alternative, the ESP32-CAM [260], which is a stand alone camera board, could have been considered. Additionally, Chapter 4 indicated that it is relevant to select the camera based on its spectral responsivity, which is likely decisive for the measurement capabilities.

This thesis mainly focused on the technological and practical challenges related to continuous luminance distribution measurements in office environments. However, the office worker is potentially standing in-between actual implementation. First, office workers might not tolerate such a camera-based system in their office environment. Moreover, office workers are an unpredictable, but essential, component of the office environment potentially inflicting the luminance distribution measurements, which was already mentioned in Chapter 8.

To assess the tolerance of office workers related to camera-based systems, such as the Bee-Eye, being implemented in the office environment a survey was conducted among 34 students at Eindhoven University of Technology. These students represent the next generation of office workers that might have to deal with these kind of high-tech systems actually being implemented in the office environment.

The survey addressed their sentiment towards a camera-based system in the office environment in relation to the often applied occupancy sensors (both indicated in Figure 10.2), but also in relation to potential (dis)comfort. Additionally, their general view on privacy was assessed.

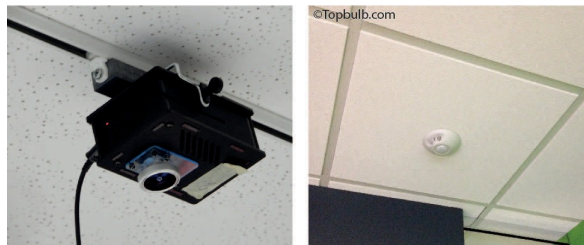


Figure 10.2: The camera based system and the occupancy sensor as referred to in the questionnaire.

The results showed that 50% of the students were either suspicious or uncomfortable due to an unknown camera sensor in their office environment, compared to only 6% that were suspicious about an occupancy sensor. 98% of the students had experienced annoyance due to automatic lighting or automatic blind systems, of which 46% experienced it on a regular basis. Consequently, only 18% of the students felt suspicious when the same camera sensor, that was given to provide high quality lighting in an automated fashion, was applied in their office environment. This corresponds to the fact that 85% of the students rate comfort above privacy, which, in fact, did not generally concern the majority (65%).

The results of the questionnaire show that awareness is essential. If a luminance camera is applied in an office environment without further feedback, office workers are inclined to not tolerate this, potentially even resulting in sabotage of the luminance camera [20]. A noticeable comfortably lit environment, due to the luminance

10.3. Strengths and weaknesses

camera, might already provide sufficient feedback, it gives a ‘return on investment’. Alternatively, when effects are very subtle, it is essential to inform the office worker about the characteristics and functionalities of the luminance camera.

These aforementioned measures do not dispense that the General Data Protection Regulation (GDPR) can be neglected. The HDR images potentially contain personal data which should be protected at all costs. Nevertheless, the solution is straightforward: First, the spatial resolution of the HDR images can be reduced to a point that no personal data is captured (Chapter 5), which is relevant mainly for research applications. Secondly, image processing can be executed locally at the camera sensor when applied in a lighting control system, which turns the luminance camera into a smart sensor. Consequently, only relevant luminance-based metrics, which do not contain any privacy sensitive data, need to be shared with other components within the system.

Empirical data, originating from Chapter 8, showed that the relevant lighting quality aspects were not all measured accurately in a simultaneous fashion. The Uniformity, DGP and Vector to Scalar Ratio representing the distribution of light, glare and the directionality of light, respectively, showed very limited agreement with the benchmark. Additionally, the Bee-Eye was not able to measure the SPD at all. Due to the ambiguity between monitoring relevant aspects and practical issues not all components can be satisfied during comprehensive lighting quality monitoring. For instance, the DGP and Vector to Scalar Ratio might benefit from a increased spatial resolution while the Uniformity might benefit from an alternative substitute position. However, this likely results in deterioration of other relevant aspects. Depending on the specific applications decisions might be different. Nevertheless, this thesis reveals a number of relevant considerations attributed to the luminance distribution and how they can be dealt with in context of lighting control systems for high quality lighting.

Alternatively, additional monitoring devices might offer a solution to perform more accurate monitoring. A small luminance mapping device dedicated to, for instance, DGP measurements might improve to overall accuracy of the lighting quality measurements. However, this negatively impacts the costs and complexity of such an control system.

It is feasible to control the electrical lighting based on input gathered by a luminance camera as indicated in Chapter 9. However, it is not straightforward. First, the luminance camera needs to be connected to the lighting control system. In Chapter 9, WiFi was used to connect the luminance camera to the control module, which, subsequently, translated the command to DALI. Preferably, a ‘plug and play’ like system is used, for instance based on Zigbee [261]. However, a considerable amount of effort is required to achieve this, which was outside the scope of this thesis as this is more a software technological challenge.

Another complexity related to implementation is the commissioning. Chapters 7, 8, and 9 indicate that commissioning is essential to achieve reliable results. Using a methodology analogous to Chapters 7 and 8 is time consuming as it contains mainly manual labor. Further development to automate the commissioning phase to a large extent is essential as well to make actual implementation feasible.

Overall, the Bee-Eye is able to provide relevant input on lighting quality. However, there are a number of lighting quality aspects that are not accurately measured yet, while the measurement plan utilized in Chapter 8 was carefully designed. Even with extensive commissioning and additional correction models significant errors were introduced. Consequently, one might argue whether the Bee-Eye is the solution to provide relevant input for lighting control systems. In theory, devices like the Bee-Eye are excellent for this application. Practice showed us, however, that it is not straightforward. These systems require significant effort to extract relevant information on a number of lighting quality aspects. Extra intelligence and automation is essential; without this there are still too many complications that prevent further market penetration. However, the versatility of the Bee-Eye should be emphasized, which is elaborated in Section 10.5. Other methods, such as person-bound measurements [3], location-bound estimations [3] or real-time simulations [140] might offer alternative solutions to extract relevant input for lighting control systems. However, multiple limitations are associated to these solutions as well. Consequently, to complete the journey towards high quality lighting, it is essential that research goes forward on all these potential measurement solutions.

10.4 Tips & tricks for luminance-based lighting control

10.4.1 Groundwork

Luminance-based lighting control can be a suitable means to achieve high quality lighting in the office environment. Before designing and implementing such a system, it is essential to assess the acceptance by the office workers that are occupying the respective office. If large objections are raised by certain office workers a lot of effort can be saved. During this assessment the ‘return on investment’ should be clear for the office workers.

Depending on the intended application the luminance-based metrics that need to be measured should be selected in advance. Except the SPD, all relevant lighting aspects, according to our literature review, can be quantified using the luminance distribution. However, the Uniformity, DGP and Vector to Scalar Ratio are not easily measured accurately in the field. Additional accommodations are required for these specific luminance-based metrics, which is further referred to in Sections 10.5 and 10.6. Moreover, it is advisable to use luminance-based metrics that are strictly bounded by a, preferably diffuse and non-transparent, surface such as the Desktop Luminance instead of, for instance, the more complex B40 Luminance.

10.4.2 The luminance camera

When developing a luminance camera, suitable hardware (Camera, Fisheye lens, and a computational unit) needs to be selected. Most important are the flexibility and the range of the system, which should all be programmable. HDR imaging to capture the luminance distribution requires different capabilities than making a beautiful picture. A Raspberry Pi based system is convenient, but not necessarily the most suitable. For instance, the NVIDIA Jetson Nano is expected to be very suitable. A logarithmic

10.4. Tips & tricks for luminance-based lighting control

response camera might also be suitable as it does not saturate under extremely bright conditions.

Subsequently, the luminance can be determined in multiple ways utilizing the floating point RGB values originating from the HDR image. The HDR images are preferably formed using *hdrgen* and contain a camera specific response curve [46]. One could apply the conventional method to determine the luminance (Equation 2.3), but dependent on the camera, this can lead to significant spectral mismatches. It is advised to optimize the luminance calculation depending on the spectral responsivity of the camera and the SPD of the light source. The spectral responsivity has the largest effect on the spectral match, and is preferably measured (by third parties). Alternatively, it can be extracted from data sheets. The SPD can be implemented as well to further improve the spectral match, however, it is less straightforward because the SPD is generally variable by nature.

Currently available cameras are able to capture a high spatial resolution, which is not necessarily required for luminance distribution measurements. If surface bound luminance-based metrics are measured, the spatial resolution can be reduced to approximately 440 x 330 pixels. Consequently, the privacy sensitive content and computational costs can be reduced drastically. However, if large luminance gradients are expected on the relevant surfaces, it is advised to increase the spatial resolution to a certain extent. Additionally, it should be prevented that luminance masks are comprised by only a few pixels. For glare measurements the spatial resolution is a complex issue. Chapter 5 showed that very high spatial resolutions are required for measurements of the maximum luminance, which is highly relevant for glare measurements, resulting in very high computational costs. On the other hand, the essential *evalglare* software requires a spatial resolution below 1200 x 1200 pixels to determine glare. For further assistance one could use the Spatial Resolution Toolbox originating from Chapter 5 [208].

The suitable temporal resolution is a bit more easy to determine. Chapter 6 showed that a very short interval is not necessarily required. With a temporal resolution of approximately 5 minutes most relevant data is still captured. Chapter 8 validated these findings. Nevertheless, if there are no constraints it can be sensible to increase the temporal resolution to achieve a quickly responding system.

An important consideration relates to where in the system the calculations are conducted. If the calculations are conducted locally on the camera system significant computational power is required. However, if all calculations are conducted in the cloud or on an external PC, the camera can be rather lightweight. Consequently, this consideration relates to the hardware that is required. Moreover, if calculations are conducted locally, privacy issues are largely prevented, which might allow a higher spatial and temporal resolution.

Finally, one could consider to add smart solutions to the camera system, which can add applications to the luminance camera and can improve the accuracy of the camera as well. A number of these smart solutions are elaborated in Sections 10.5 and 10.6.

10.4.3 Commissioning

During the commissioning phase, four distinct tasks can be distinguished:

- photometric calibration of the luminance camera;
- selection of the measurement position;
- development of the luminance masks;
- development of correction models for an alternative measurement position.

It is advised to always perform a photometric calibration when installing a luminance camera. This can either be a luminance-based or illuminance-based calibration [262]. Perform this calibration several times for conditions the luminance camera is to cover, at least make sure that different levels of brightness are captured.

After calibration, the most suitable position can be selected. Preferably, luminance distribution measurements are conducted from eye position, which is often not feasible as it will cause interference. This thesis suggested to use a ceiling-based position above the aisle with a 20° angle relative to the ceiling. Using this position, one to four workstations can be monitored at once.

Depending on the selected lighting quality aspects, luminance masks need to be developed. Make sure the camera is in the correct position, and capture a reference HDR image. Use software such as MATLAB or Photoshop to extract a luminance mask, which is a binary map in the spatial resolution of the reference HDR image. MATLAB provides a convenient point-and-click workflow using *impoly*.

Lastly, correction models are required, when using an alternative measurement position, to translate the luminance-based metrics to relevant quantities in relation to the user. In other words, the alternative measurement position has to be related to the relevant eye level position. Preferably, an additional, but identical, luminance camera is used to conduct the relative measurements at eye level. If no additional camera is available, grey cards should be used to account for the potentially variable conditions [89]. At least two reference measurements are required to establish either a linear (Chapter 7) or a quadratic (Chapter 8) relation. Be careful that the conditions during these reference measurements are realistic and not too extreme in order to achieve a reliable correction model. Obviously, more reference measurements result in an increased reliability. Individual correction models are required for all relevant luminance-based metrics. Luminance-based metrics that are comprised of multiple luminance masks, such as the Desktop/Background Ratio, require a model for each individual luminance mask, direct fitting to the luminance-based metric was shown to perform poorly in such cases.

10.4.4 Implementation

Actual implementation in control systems was not extensively researched in this thesis. Nevertheless, Chapter 9 performed a proof of concept study using DALI to control the electrical lighting based on luminance camera output, although blind control seems feasible as well. There is a wide range of communication protocols such as DALI and Zigbee that might be applicable for such systems. When an existing control system is available, it is advised to apply this to the luminance camera as well. Moreover, it is advised to have bidirectional communication between the lu-

10.5. Applications

minance camera and the control system because the luminance camera might behave differently under varying conditions.

10.4.5 Measuring

When the system is running correctly, it requires maintenance. Therefore, the system needs to be checked on a regular basis. Aspects that need a regular check up are: whether the luminance camera is still running without generating error messages, whether the luminance camera still has an unobstructed view and whether the office environment has undergone changes.

When error messages occur, it is advised to solve these directly, even when the system seems to be running normally. The errors might relate to a certain condition, such as extremely high luminance values compromising the performance, that might lead to a reduced performance at another time.

Additionally, the FOV of the luminance camera should be validated. Firstly, dust might change the luminance distribution that is captured by the imaging sensor and should therefore be prevented. Secondly, make sure that the FOV is not obstructed. Obstruction can happen knowingly when the luminance camera is sabotaged by a user, for instance due to privacy concerns or due to a non-functioning control system. Moreover, unknowing obstructions are likely to occur, for instance, in the form of decorations or due to added system walls.

Finally, if, for example, the office layout is altered following a re-organization, this needs to be taken into consideration by the luminance camera. One should prevent that too many workstations are monitored by a single luminance camera. Moreover, all luminance masks still need to cover the respective areas of interest. Misalignment between the relevant surfaces and luminance masks can have a severe impact on some luminance-based metrics such as the uniformity.

10.5 Applications

This thesis focused on extracting numerous relevant lighting quality aspects from the luminance distribution measured using the Bee-Eye luminance camera. Subsequently, the output on the lighting quality aspects can be used to control the lighting accurately. However, camera-based systems like the Bee-Eye are suitable for a wide range of applications that potentially can be combined with its current functionality, which can result in a highly versatile but also economic sensor.

10.5.1 OptiLight

This research was part of the multidisciplinary 'OptiLight' project, which aimed to develop a lighting control system that provides 'Human Centric Lighting' based on mathematical optimizations [22]. The general structure of the proposed system is illustrated in Figure 10.3. Image Forming (IF) as well as Non-Image Forming (NIF) effects of light are considered to determine the most suitable lighting scenario, however, their requirements do not necessarily align and might have complex interactions [263]. A digital sibling represents the central node of the system. It runs a particle filter-based model of the human circadian rhythm [264] based on sensory data

representing the lit environment but also human processes. In this case, the lit environment is monitored by a Bee-Eye. More specifically, the retinal illuminance, which was measured from the ceiling in Chapter 7, is extracted as main driver of the human circadian rhythm [265]. However, Chapter 7 showed that this metric is rather complex to measure using an alternative position. A neural network might be better able to extract reliable input on the retinal illuminance. Based on the sensory input, the digital sibling, representing a digital model of the real user, predicts the response of the user in real-time based on its internal clock. The viewing direction of the user is expected to be highly relevant [221], and is preferably integrated in the measurement as well. Additionally, alternative measurement solutions need to be developed to monitor the retinal illuminance, or alternative metrics, to drive the internal clock of the digital twin when the user is outside the office environment, for instance using smartwatches. According to the target response (e.g. alertness), the most suitable light setting is attributed to the lighting system. Obviously, these light scenarios should also provide a comfortably lit environment in addition to the target response.

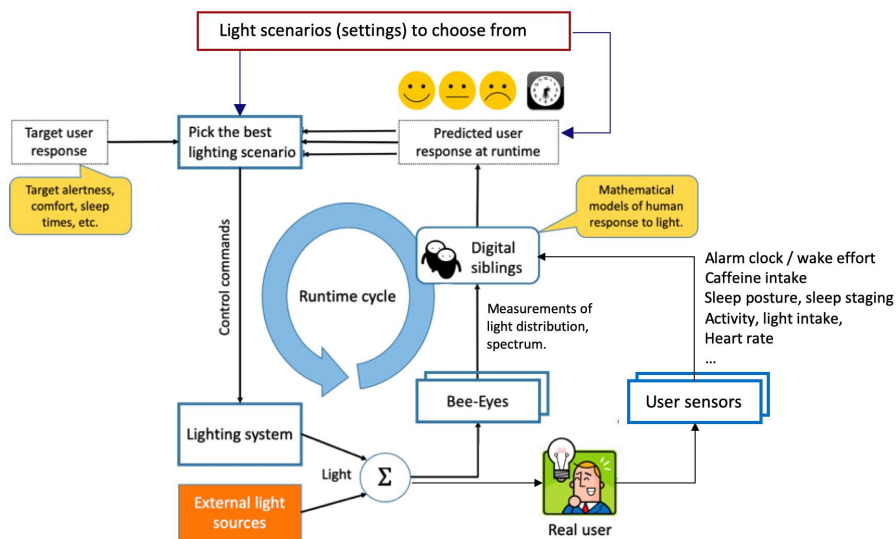


Figure 10.3: Schematic of the control system developed in the OptiLight project.

10.5.2 Office Applications

In addition to measuring lighting quality, there are multiple additional applications of the luminance camera that are suitable for office environments. A distinction can be made between applications using the image data and applications using the luminance data.

A first but basic application of the imaging device can be a surveillance camera. Chapter 6 showed that only once in the 5 minutes a measurement is required, which takes approximately 12 seconds (Chapter 5). Consequently, there is a lot of time to spare where the camera sensor can be utilized as a surveillance camera. Especially

10.5. Applications

when applied to the ceiling, it provides a good overview of the office environment. Such a surveillance system can be real-time as it does not require HDR imaging.

As an alternative, the camera can be utilized for occupancy sensing, which is generally required in a lighting control system. By combining two relevant applications, the relative costs of the sensor can be reduced drastically. The occupancy rate can, for instance, be extracted by image recognition using machine learning, which needs to be adapted to fish-eye projections. Consecutively, occupancy data can be translated to an occupancy heat map, which might be extremely relevant in the current 1.5 meter economy associated to the COVID-19 crisis. Depending on the application the response time needs to be determined. It is, however, expected that for office applications a response time of five minutes suffices.

Finally, the camera might be able to sense behavioral components, which could be relevant for lighting control systems. For instance, alertness of an office worker, roughly indicated by a camera system, might be very relevant for the system being developed in Section 10.5.1. It is feasible to extract posture of a person based on low resolution images. Posture might, subsequently, be related to behavioral components such as alertness. These applications that explicitly use image data, should carefully consider privacy.

Additionally, there are potential applications related to lighting control that could utilize the luminance distribution, measured with the camera system. These applications generally focus on specific components of the lit environment.

Automated blind systems are infamous due to their movements at strange and undesired moments [19]. This is caused by inadequate sensing, often caused by using single photometers in an open loop topology. Using a luminance camera, the blinds can be controlled accurately to avoid glare, as glare is often decisive in regard to blind use, such a system was already validated by [194]. Nevertheless, Chapters 5 and 8 showed difficulties measuring glare in real office scenarios while conducting comprehensive lighting quality measurements. A dedicated system might be able to overcome these issues. For instance, continuous glare estimations (e.g. simplified DGP [65]) can be calibrated by occasional (e.g. every 30 min) high resolution and high quality glare measurements. The occasional calibration is likely normative for the performance and it is largely impacted by the weather conditions. Additionally, more research is required related to the measurement position and spatial resolution in context to this specific use case. Moreover, some other potential applications are desktop illuminance control analogous to Chapter 9, wall luminance control [48], and directionality control related to NIF effects [229].

10.5.3 Home Applications

In addition to the office, home applications are feasible as well. However, broad application is not expected. Mainly appreciators of home automation might be attracted to a system such as the Bee-Eye. For instance, luminance cameras might be employed with a Philips Hue system to create an even more immersive gaming or TV experience. Home applications are a complete new use case for the Bee-Eye. Consequently, it requires a different approach. For home applications an appealing design, easy installation and compatibility are essential, which were outside the scope of this research.

10.5.4 Research Applications

The luminance camera developed in this thesis also has an application in research. The luminance is shown to be closely related to the visual perception of brightness [45]. Consequently, it is expected to be more suitable for research related to human factors in lighting than, for instance, the illuminance. The luminance distribution might be a means to finally find consensus regarding human preferences. Multiple studies already utilized the Bee-Eye to find preferred luminance ratios [266], to explore interaction of daylight and electrical light on subjective appraisals [233], train neural networks for daylight quality, and monitor the lit environment to assess spectral simulation software. Further research is required to find the most relevant luminance-based metrics in relation to human factors in lighting. Additionally, Chapters 5 to 7 need to be translated to the specific application that is aimed for.

Alternatively, Chapter 4 showed that besides the luminance the melanopic radiance can be measured as well, when the imaging system is spectrally tuned (e.g. Equation 3.5). Generally, it should be expected that the accuracy is lower compared to luminance measurements, as imaging devices aim to provide a visually pleasing image, which results in a high sensitivity in the range of the luminous sensitivity of the human eye. These findings still need to be validated by empirical data. In research related to NIF effects of light, the best practice is to measure all α -opic (ir)radiances [184] because it is not exactly clear yet how the human body is impacted by light. However, these individual measurements of the α -opics can be very time consuming. Using an HDR imaging device, the α -opics can be approximated in a spatially resolved fashion based on one single HDR image.

10.6 Recommendations for future work

This thesis utilized the luminance distribution as a means to provide input for lighting control systems and achieved significant progress. Nevertheless, there is still plenty of room for future work as already indicated in Section 10.3.2. Obviously, there is a need for conducting similar measurements, as conducted throughout this thesis, in different environments. For instance, an office environment with smaller windows and different orientation might be better able to approximate the lighting quality compared to the test case in Chapter 8. Additionally, human experience should be further accounted for. Firstly, to indicate the uncertainty caused by users during field measurements, should be elaborated more. Secondly, the sentiment of users towards such a luminance-based system should be assessed further.

The work in Chapters 3 and 4 refers to unmixed and pure SPDs. In practice, the SPD will be a combination of the different illuminants of the respective measurement location, most likely, a variable combination of daylight and electrical light. Consequently, it is beneficial to estimate the illuminant based on camera readings to improve the accuracy of the spectral mismatch optimizations proposed in Chapter 3. It is suggested to develop a predefined set of SPDs, and their mixtures, that might occur at the respective measurement location. Using a methodology analogous to Tominaga et al. [181], one might be able to pick the most likely SPD from a discrete set. This methodology was able to calculate color gamuts based on a range of Planckian radiators, subsequently, the color gamuts of the photographed scene were related to these predefined color gamuts to estimate the CCT. For this specific application,

10.7. Conclusion

the Planckian radiators would be replaced with the predefined set of SPDs. An estimation of the SPD suffices because only negligible differences are expected for the RGB weighting factors between similar SPDs (Chapter 4). Relevant differences are only expected to occur between distinctively different SPDs such as daylight and fluorescent illuminants. Moreover, utilizing HDR images in such a system might improve the reliability of such an estimation algorithm.

Chapter 8 showed that it is complex to approximate the lit environment according to the methodology proposed in this thesis. Photometric quantities are extracted from the luminance distribution, which, subsequently, are used to describe lighting quality. Performing a field study adds a considerable amount of uncertainty to the photometric quantities. It is suggested to directly relate the HDR image to lighting quality, by skipping a step the uncertainty might be reduced. A machine learning system is envisioned that links human input directly to the raw HDR image, for instance using a neural network [267, 268]. Using multiple inputs related to comfort, work performance and sleep quality, high quality lighting could be achieved after a certain training period. Nevertheless, a lot of training data is required to achieve a well functioning system.

Finally, there are numerous software related challenges left. Firstly, the software of the Bee-Eye can be improved, increasing efficiency and accuracy. Related to the recommendations in Part II, alternatives can be proposed that use additional intelligence. For instance, the temporal resolution might have a dynamic character, only measuring when change in the lit environment has occurred. Similar strategies, such as image obfuscation [269], can be composed for the spatial resolution. The relation between the ceiling-based and eye level measurements might be improved by more elaborate correction models or even neural networks. Finally, actual implementation was only considered in Chapter 9, commissioning and implementation to a functioning control system is not straightforward yet. A certain amount of automation is required to limit the manual labor during the commissioning phase. Moreover, translation of the luminance-based metrics to interpretable definitions according to often used communication protocols is essential to achieve a ‘plug and play’ sensor that is easy to implement.

10.7 Conclusion

In current practice, the quality of the lit environment is generally subordinate to reducing energy consumption. However, with wages representing the majority of operational costs, enhancing the user comfort can be considered a more efficient, and ethically correct, strategy. Due to the complex character and interaction effects of lighting, control systems are required. Nevertheless, these control systems are not up to this task yet because of faulty sensory input and inability to consider lighting quality holistically.

Consequently, accurate sensory input on lighting quality is required, which was subject to this research. Based on an extensive literature review, lighting quality was indirectly indicated based on seven individual and variable lighting quality aspects. Six out the seven lighting quality aspects were measurable, in a continuous fashion, using one single device, namely, a luminance distribution measurement device. Even though these systems can have severe spectral mismatches, which can be corrected to

a certain extent, relevant data on the luminous conditions can be extracted as long as a careful calibration is conducted.

During this research, the luminance distribution was measured using the Bee-Eye, a practical and autonomous luminance distribution measurement device. For application in real office conditions of such a sensor the best practice in luminance measurements can often not be executed because of interference, privacy and high computational costs. This thesis proposed recommendations to deal with these issues based on the spatial resolution, temporal resolution and the measurement position. Nevertheless, lighting quality measurements, using luminance distribution measurement devices, in living office environments remain difficult. Systematic errors will occur due to deviations of the best practice in addition to random errors caused by the office workers occupying the office environment.

Nevertheless, implementation of the Bee-Eye in lighting control systems is technologically feasible but extensive commissioning is required to wind up with an acceptable control system. However, photo sensors applied in existing control systems also require extensive commissioning but do not have the versatile character that the Bee-Eye has. Using software development, the Bee-Eye sensor can be made more efficient and accurate than tested in this thesis, which is essential if market penetration is persecuted. For instance, commissioning might be automated to a large extent. Hence, the hypothesis is partly met; the luminance distribution is suitable to provide input for lighting control systems aiming to provide high quality lighting. However, the application of the luminance distribution in practice is not straightforward and requires more research. Concluding, the first steps towards a lighting control system that provides high quality lighting are made, but the journey is not completed yet.

References

- [1] Buitelaar E, van den Berge M, van Dongen F, Weterings A, van Maarseveen R, Zwaneveld P. De toekomst van kantoren: Een scenariostudie naar de ruimtebehoefte. The Hague, Netherlands: Planbureau voor de Leefomgeving; 2017.
- [2] International WELL Building Institute. The WELL building standard; 2019. Available from: www.wellcertified.com/en/.
- [3] van Duijnhoven J. Personal lighting conditions of office workers: input for intelligent systems to optimize subjective alertness. Eindhoven University of Technology; 2019. Available from: <https://research.tue.nl/en/publications/personal-lighting-conditions-of-office-workers-input-for-intellig>.
- [4] Tom S. Managing Energy And Comfort. ASHRAE Journal. 2008; Available from: <http://www.buildpulse.com/wp-content/uploads/2017/01/tom-062008-feature.pdf>.
- [5] Rowbottom I. Improving Productivity with Light Controls. Lutron; 2009.
- [6] Veitch JA, Newsham GR. Determinants of Lighting Quality II: Research and Recommendations. In: 104th Annual Convention of the American Psychological Association. Toronto, Canada; 1996. p. 1–38. Available from: <https://pdfs.semanticscholar.org/53bc/e3783b32be6801ad7def7044c3f6564792eo.pdf>.
- [7] van Bommel WJM, van den Beld GJ. Lighting for work: a review of visual and biological effects. *Lighting Research and Technology*. 2004 12;36(4):255–269. Available from: <http://lrt.sagepub.com/cgi/doi/10.1191/1365782804li1220a>.
- [8] Boyce PR. *Human Factors in Lighting*. third edit ed. CRC Press; 2014. Available from: <https://www.taylorfrancis.com/books/9781439874899>.
- [9] Veitch JA, Newsham GR. Preferred luminous conditions in practice recommendations. *Lighting Research and Technology*. 2000;32(4):24–30.
- [10] Begemann SHA, van den Beld GJ, Tenner AD. Daylight, artificial light and people in an office environment, overview of visual and biological responses. *International Journal of Industrial Ergonomics*. 1997 9;20(3):231–239. Available from: <http://linkinghub.elsevier.com/retrieve/pii/S0169814196000534>.
- [11] Lashina T, Chraibi S, Despenic M, Shrubsole P, Rosemann A, van Loenen E. Sharing lighting control in an open office: Doing one’s best to avoid conflict. *Building and Environment*. 2019 1;148:1–10.
- [12] Williams A, Atkinson B, Garbesi K, Page E, Rubinstein F, Page Pe E. Lighting Controls in Commercial Buildings. *LEUKOS*. 2012;8(3):161–180. Available from: <https://www.tandfonline.com/action/journalInformation?journalCode=ulks20>.

References

- [13] Nagy Z, Yong FY, Schlueter A. Occupant centered lighting control: A user study on balancing comfort, acceptance, and energy consumption. *Energy and Buildings*. 2016;126:310–322.
- [14] Lee ES, Selkowitz SE. The New York Times Headquarters daylighting mockup: Monitored performance of the daylighting control system. *Energy and Buildings*. 2006 7;38(7):914–929. Available from: <http://www.sciencedirect.com/science/article/pii/S0378778806000739>.
- [15] Galasiu AD, Newsham GR, Suvagau C, Sander DM. Energy Saving Lighting Control Systems for Open-Plan Offices: A Field Study. *Leukos*. 2007;4(1):7–29. Available from: <http://www.tandfonline.com/doi/abs/10.1582/LEUKOS.2007.04.01.001>.
- [16] Ashibe M, Miki M, Hiroyasu T. Distributed optimization algorithm for lighting color control using chroma sensors. In: 2008 IEEE International Conference on Systems, Man and Cybernetics. IEEE; 2008. p. 174–178. Available from: http://ieeexplore.ieee.org/xpls/abs_all.jsp?arnumber=4811270.
- [17] Aarts MPJ, Aries MBC, Straathof J, van Hoof J. Dynamic lighting systems in psychogeriatric care facilities in the Netherlands: A quantitative and qualitative analysis of stakeholders' responses and applied technology. *Indoor and Built Environment*. 2015 8;24(5):617–630. Available from: <http://ibe.sagepub.com/cgi/doi/10.1177/1420326X14532387>.
- [18] Lucas RJ, Peirson SN, Berson DM, Brown TM, Cooper HM, Czeisler CA, et al. Measuring and using light in the melanopsin age. *Trends in Neurosciences*. 2014;37(1):1–9. Available from: <http://www.sciencedirect.com/science/article/pii/S0166223613001975>.
- [19] Meerbeek B, te Kulve M, Gritti T, Aarts MPJ, van Loenen EJ, Aarts E. Building automation and perceived control: A field study on motorized exterior blinds in Dutch offices. *Building and Environment*. 2014 9;79:66–77. Available from: <https://www.sciencedirect.com/science/article/pii/S0360132314001279>.
- [20] Loe DL. Energy efficiency in lighting - Considerations and possibilities. *Lighting Research and Technology*. 2009;41(3):209–218.
- [21] Pandharipande A, Newsham G. Lighting controls: Evolution and revolution. *Lighting Research and Technology*. 2018 1;50(1):115–128. Available from: <http://journals.sagepub.com/doi/10.1177/1477153517731909>.
- [22] Linnartz JPMG. New ILI project "OptiLight". Accessed on 22-08-2017; 2016. Available from: <https://www.tue.nl/onderzoek/instituten-groepen-scholen/toponderzoeksgroepen/intelligent-lighting-institute/news/12-02-2016-new-ili-project-optilight/>.
- [23] Veitch JA, Newsham GR. Determinants of Lighting Quality I: State of the Science. *Journal of the Illuminating Engineering Society*. 1998;27(1):92–106. Available from: <http://www.tandfonline.com/doi/pdf/10.1080/00994480.1998.10748215>.

References

- [24] Boyce PR. Lighting Quality for All. In: CISBE & SLL International Lighting Conference. Dublin; 2013. p. 1–5. Available from: <http://www.ilc2013.com/paper/Session3KeynotePBoyce.pdf>.
- [25] Veitch JA. Lighting Quality Contributions from Biopsychological Processes. *Journal of the Illuminating Engineering Society*. 2001;30(1):3–16. Available from: <http://ies.tandfonline.com/action/journalInformation?journalCode=uzie20http://dx.doi.org/10.1080/00994480.2001.10748329>.
- [26] Veitch JA, Newsham GR. Preferred luminous conditions in open-plan offices: Research and practice recommendations. *Lighting Research and Technology*. 2000;32(4).
- [27] Kruisselbrink TW, Dangol R, Rosemann ALP. Photometric measurements of lighting quality: An overview. *Building and Environment*. 2018 6;138:42–52. Available from: <http://linkinghub.elsevier.com/retrieve/pii/S0360132318302397>.
- [28] Levy AW. The CIE visual performance system. *Lighting Research and Technology*. 1978 3;10(1):19–27. Available from: <http://journals.sagepub.com/doi/10.1177/096032717801000103>.
- [29] Bean AR, Bell RI. The CSP index: A practical measure of office lighting quality as perceived by the office worker. *Lighting Research and Technology*. 1992;24(4):215–225.
- [30] Perry MJ, McFadden T. Validation of, and investigation of physical correlates with, the CSP lighting quality index. *CIE*. 1995;p. 188–191.
- [31] Petherbridge P, Hopkinson RG. Discomfort Glare and the Lighting of Buildings. *Lighting Research and Technology*. 1950 2;15(2 IEStrands):39–79. Available from: <http://lrt.sagepub.com/lookup/doi/10.1177/147715355001500201>.
- [32] Pop F, Beu D. Energy Efficiency in Interior Lighting - A Romanian Case Study. *Lighting engineering*. 2006;p. 11–26.
- [33] Pop F, Pop HF, Pop M. Lighting Quality - Component of Indoor Environment. In: *LUX Europa 2009*. Istanbul; 2009. p. 499–506.
- [34] Dehoff P. Lighting Quality and Energy Efficiency is Not a Contradiction. *Light & Engineering*. 2012;20(3):34–39.
- [35] Tralau B, Dehoff P. Examination: Ergonomic Lighting Indicator in practise. In: *Lux Europa*. Istanbul; 2009. p. 507–512.
- [36] Gentile N, Dubois MC, Osterhaus WKE, Stoffer S, Amorim CND, Geisler-Moroder D, et al. A toolbox to evaluate non-residential lighting and daylighting retrofit in practice. *Energy and Buildings*. 2016 7;123:151–161. Available from: <https://linkinghub.elsevier.com/retrieve/pii/S037877881630281X>.
- [37] Goodman TM. Measurement and specification of lighting: A look at the future. *Lighting Research and Technology*. 2009;41:229–243. Available from: <http://journals.sagepub.com/doi/pdf/10.1177/1477153509338881>.

References

- [38] Boyce PR, Cuttle C. Effect of correlated colour temperature on the perception of interiors and colour discrimination performance. *Lighting Research and Technology*. 1989;22(1):19–36.
- [39] Tregenza PR. The daylight factor and actual illuminance ratios. *Lighting Research and Technology*. 1980;12(2):64–68. Available from: <http://lrt.sagepub.com/cgi/doi/10.1177/096032718001200202%5Cnhttp://lrt.sagepub.com/cgi/content/abstract/12/2/64>.
- [40] Jay PA. Inter-relationship of the Design Criteria for Lighting Installations. *Lighting Research and Technology*. 1968;33(2):47–71.
- [41] Richman EE. Standard Measurement and Verification Plan for Lighting Retrofit Projects for Buildings and Building Sites. Richland: Pacific Northwest National Laboratory; 2012. Available from: [https://betterbuildingssolutioncenter.energy.gov/sites/default/files/attachments/lighting measurement evaluation protocol.pdf](https://betterbuildingssolutioncenter.energy.gov/sites/default/files/attachments/lighting%20measurement%20evaluation%20protocol.pdf).
- [42] European Committee For Standardization. NEN-EN 12464-1: Light and lighting - Lighting of work places - Part 1: Indoor work places. European Committee For Standardization; 2009.
- [43] Atif MR, Love JA, Littlefair PJ. Daylighting Monitoring Protocols & Procedures for Buildings; 1997. Available from: www.nrc.ca/irc/ircpubs.
- [44] Marty C, Fontoynt M, Christoffersen J, Dubois MC, Wienold J, Osterhaus WKE. User assessment of visual comfort: Review of existing methods; 2003. Available from: https://www.researchgate.net/profile/Jens_Christoffersen/publication/283497394_User_assessment_of_visual_comfort_Review_of_existing_methods/links/563b29af08ae337ef2988a61.pdf.
- [45] Van Den Wymelenberg KG. Evaluating Human Visual Preference and Performance in an Office Environment Using Luminance-based Metrics. University of Washington; 2012.
- [46] Reinhard E, Ward G, Pattanaik S, Debevec P. High Dynamic Range Imaging: Acquisition, Display, and Image-Based Lighting (The Morgan Kaufmann Series in Computer Graphics). San Fransisco: Morgan Kaufmann Publishers Inc.; 2006.
- [47] CIE. Guide to Protocols for Describing Lighting. Vienna, Austria; 2014.
- [48] Chraibi S, Crommentuijn L, van Loenen EJ, Rosemann ALP. Influence of wall luminance and uniformity on preferred task illuminance. *Building and Environment*. 2017 5;117:24–35. Available from: <https://linkinghub.elsevier.com/retrieve/pii/S0360132317300860>.
- [49] Inanici MN. Evaluation of high dynamic range photography as a luminance data acquisition system. *Lighting Research and Technology*. 2006 6;38(2):123–134. Available from: <http://journals.sagepub.com/doi/10.1191/1365782806li1640a>.

References

- [50] Van Den Wymelenberg KG, Inanici MN. A Critical Investigation of Common Lighting Design Metrics for Predicting Human Visual Comfort in Offices with Daylight. *LEUKOS*. 2014;10(3):145–164. Available from: <http://www.tandfonline.com/doi/pdf/10.1080/15502724.2014.881720?needAccess=true>.
- [51] Wienold J, Christoffersen J. Evaluation methods and development of a new glare prediction model for daylight environments with the use of CCD cameras. *Energy and Buildings*. 2006 7;38(7):743–757. Available from: <https://linkinghub.elsevier.com/retrieve/pii/S0378778806000715>.
- [52] Rea MS. *The IESNA lighting handbook*. New York :: Illuminating Engineering Society of North America; 2000.
- [53] Halonen L, Tetri E, Bhusal P. Lighting quality. In: Halonen L, Tetri E, Bhusal P, editors. - Annex 45 - Energy Efficient Electric Lighting for Buildings. Espoo: International Energy Agency; 2010. p. 45–56.
- [54] Carlucci S, Causone F, De Rosa F, Pagliano L. A review of indices for assessing visual comfort with a view to their use in optimization processes to support building integrated design. *Renewable and Sustainable Energy Reviews*. 2015 7;47:1016–1033. Available from: <https://linkinghub.elsevier.com/retrieve/pii/S1364032115002154>.
- [55] Osterhaus WKE. Discomfort glare assessment and prevention for daylight applications in office environments. *Solar Energy*. 2005 8;79(2):140–158. Available from: <https://linkinghub.elsevier.com/retrieve/pii/S0038092X04003536>.
- [56] Hirning MB, Isoardi GL, Cowling I. Discomfort glare in open plan green buildings. *Energy and Buildings*. 2014;70:427–440. Available from: <http://www.sciencedirect.com/science/article/pii/S0378778813007603>.
- [57] Hopkinson RG, Petherbridge P, Longmore J. *Daylighting*. London,: Heinemann; 1966.
- [58] CIE. Termlist — Electronic international light vocabulary. CIE; 2014. Available from: <http://eilv.cie.co.at/termlist>.
- [59] Clear RD. Discomfort glare: What do we actually know? *Lighting Research and Technology*. 2013;45:141–158. Available from: <http://journals.sagepub.com/doi/pdf/10.1177/1477153512444527>.
- [60] Pierson C. *Discomfort Glare Perception from Daylight : Influence of Socio-Environmental Context*. UC Louvain; 2019.
- [61] Bellia L, Spada G. Photometric characterisation of small sources with high dynamic range illuminance mapping. *Lighting Research and Technology*. 2013 2;46(3):329–340. Available from: <http://lrt.sagepub.com/cgi/doi/10.1177/1477153513476511>.
- [62] Eble-Hankins ML, Waters CE. VCP and UGR Glare Evaluation Systems: A Look Back and a Way Forward. *LEUKOS*. 2005 2;1(2):7–38. Available from: <https://www.tandfonline.com/doi/full/10.1582/leukos.2004.01.02.001>.

References

- [63] CIE. Discomfort glare in the interior working environment. Vienna, Austria; 1995.
- [64] Hopkinson RG. Glare from daylighting in buildings. *Applied Ergonomics*. 1972 12;3(4):206–215. Available from: <http://linkinghub.elsevier.com/retrieve/pii/0003687072901020>.
- [65] Wienold J. Dynamic daylight glare evaluation. In: Eleventh International IBPSA Conference. Glasgow, UK; 2009. p. 944–951. Available from: http://ibpsa.org/proceedings/BS2009/BS09_0944_951.pdf.
- [66] Luckiesh M, Guth SK. Brightnesses in Visual Field at Borderline Between Comfort and Discomfort. *Illuminating Engineering*. 1949;p. 650–670.
- [67] Iwata T, Tokura M. Position Index for a glare source located below the line of vision. *Lighting Research and Technology*. 1997 9;29(3):172–178. Available from: <http://lrt.sagepub.com/cgi/doi/10.1177/14771535970290030801>.
- [68] Wienold J. Evalglare V2.05. Accessed on 24-08-2020; 2016. Available from: <https://www.radiance-online.org/learning/documentation/manual-pages/pdfs/evalglare.pdf/view>.
- [69] Boyce PR, Slater AI. The application of CRF to office lighting design. *Lighting Research and Technology*. 1981;13(2):65–79. Available from: <http://lrt.sagepub.com/cgi/doi/10.1177/096032718101300203>.
- [70] Lighting Research Center. Spectral Power Distribution. Rensselaer Polytechnic Institute;. Available from: <http://www.lrc.rpi.edu/education/learning/terminology/spectralpowerdistribution.asp>.
- [71] Aries MBC, Aarts MPJ, van Hoof J. Daylight and health: A review of the evidence and consequences for the built environment. *Lighting Research and Technology*. 2015 2;47(1):6–27. Available from: <http://lrt.sagepub.com/cgi/doi/10.1177/1477153513509258>.
- [72] Rea MS, Freyssinier-Nova JP. Color rendering: A tale of two metrics. *Color Research and Application*. 2008;33(3):192–202.
- [73] Hunt RWG. Specifying colour appearance. *Lighting Research and Technology*. 1979;11(4):175–183.
- [74] Islam MS, Dangol R, Hyvarinen M, Bhusal P, Puolakka M, Halonen L. User acceptance studies for LED office lighting: Lamp spectrum, spatial brightness and illuminance. *Lighting Research and Technology*. 2015 2;47(1):54–79. Available from: <http://lrt.sagepub.com/cgi/doi/10.1177/1477153513514425>.
- [75] Wang Q, Xu H, Zhang F, Wang Z. Influence of Color Temperature on Comfort and Preference for LED Indoor Lighting. *Optik - International Journal for Light and Electron Optics*. 2016;.

References

- [76] Manav B. An experimental study on the appraisal of the visual environment at offices in relation to colour temperature and illuminance. *Building and Environment*. 2007 2;42(2):979–983. Available from: <https://linkinghub.elsevier.com/retrieve/pii/S036013230500452X>.
- [77] Wei M, Houser KW, Orland B, Lang DH, Ram N, Sliwinski MJ, et al. Field study of office worker responses to fluorescent lighting of different CCT and lumen output. *Journal of Environmental Psychology*. 2014 9;39:62–76. Available from: <https://linkinghub.elsevier.com/retrieve/pii/S0272494414000425>.
- [78] Li H, Luo MR, Liu X, Wang B, Liu H. Evaluation of colour appearance in a real lit room. *Lighting Research and Technology*. 2016;48:412–432. Available from: <http://journals.sagepub.com/doi/pdf/10.1177/1477153515571784>.
- [79] Fotios S. A Revised Kruithof Graph Based on Empirical Data. *LEUKOS*. 2017 1;13(1):3–17. Available from: <https://www.tandfonline.com/doi/full/10.1080/15502724.2016.1159137>.
- [80] Viénot F, Durand ML, Mahler E. Kruithof’s rule revisited using LED illumination. *Journal of Modern Optics*. 2009 7;56(13):1433–1446. Available from: <http://www.tandfonline.com/doi/abs/10.1080/09500340903151278>.
- [81] Dikel EE, Burns GJ, Veitch JA, Mancini S, Newsham GR. Preferred Chromaticity of Color-Tunable LED Lighting. *LEUKOS*. 2014 4;10(2):101–115. Available from: <http://www.tandfonline.com/doi/abs/10.1080/15502724.2013.855614>.
- [82] McCamy CS. Correlated color temperature as an explicit function of chromaticity coordinates. *Color Research & Application*. 1992 4;17(2):142–144. Available from: <http://doi.wiley.com/10.1002/col.5080170211>.
- [83] Robertson AR. Computation of Correlated Color Temperature and Distribution Temperature. *Journal of the Optical Society of America*. 1968 11;58(11):1528. Available from: <https://www.osapublishing.org/abstract.cfm?URI=josa-58-11-1528>.
- [84] Hernández-Andrés J, Lee RL, Romero J. Calculating correlated color temperatures across the entire gamut of daylight and skylight chromaticities. *Applied Optics*. 1999 9;38(27):5703. Available from: <https://www.osapublishing.org/abstract.cfm?URI=ao-38-27-5703>.
- [85] Gardner JL. Correlated colour temperature-uncertainty and estimation. *Metrologia*. 2000;37(5). Available from: <http://iopscience.iop.org/article/10.1088/0026-1394/37/5/8/meta>.
- [86] Li C, Cui G, Melgosa M, Ruan X, Zhang Y, Ma L, et al. Accurate method for computing correlated color temperature. *Optics Express*. 2016 6;24(13):14066. Available from: <https://www.osapublishing.org/abstract.cfm?URI=oe-24-13-14066>.

References

- [87] Konica Minolta. Chroma Meter CL -200A E; 2010. Available from: https://www.konicaminolta.com/instruments/download/catalog/light/pdf/cl200a_catalog_eng.pdf.
- [88] Tominaga S, Wandell BA. Natural scene-illuminant estimation using the sensor correlation. *Proceedings of the IEEE*. 2002;90(1):42–56. Available from: <http://ieeexplore.ieee.org/document/982404/>.
- [89] Dubois MC, Gentile N, Naves David Amorim C, Geisler-Moroder D, Jakobiak R, Matusiak B, et al. Monitoring protocol for lighting and daylighting retrofits: A Technical Report of Subtask D (Case Studies), T50.D3; 2016.
- [90] Bodrogi P, Brückner S, Khanh TQ. Dimensions of light source colour quality. In: *Conference on Colour in Graphics, Imaging, and Vision*; 2010. p. 155–159.
- [91] Davis W, Ohno Y. Color quality scale. *Optical Engineering*. 2010;49(3).
- [92] Guo X, Houser KW. A review of colour rendering indices and their application to commercial light sources. *Lighting Research and Technology*. 2004;36(3):183–199. Available from: <http://journals.sagepub.com/doi/pdf/10.1191/1365782804li1120a>.
- [93] Houser KW, Wei M, David A, Krames MR, Shen XS. Review of measures for light-source color rendition and considerations for a two-measure system for characterizing color rendition. *Optics Express*. 2013;21(8). Available from: https://www.osapublishing.org/DirectPDFAccess/2C63CBEB-B681-1C68-F5A66FF6DFB15922_252930/oe-21-8-10393.pdf?da=1&id=252930&seq=0&mobile=no.
- [94] CIE. Method of measuring and specifying color rendering properties of light sources. Vienna, Austria; 1995.
- [95] Judd DB. A Flattery Index for Artificial Illuminants. *Illuminating Engineering*. 1967;62(10).
- [96] Thornton WA. A Validation of the Color-Preference Index. *Journal of the Illuminating Engineering Society*. 1974 10;4(1):48–52. Available from: <http://www.tandfonline.com/doi/abs/10.1080/00994480.1974.10732288>.
- [97] Thornton WA. Color-Discrimination Index. *Journal of the Optical Society of America*. 1972 2;62(2):191. Available from: <https://www.osapublishing.org/abstract.cfm?URI=josa-62-2-191>.
- [98] Xu H. Colour rendering capacity and luminous efficiency of a spectrum. *Lighting Research and Technology*. 1993;25(3):131–132.
- [99] Pointer MR. Measuring colour rendering - A new approach. *Lighting Research and Technology*. 1986;18(4):175–184.
- [100] Hashimoto K, Yano T, Shimizu M, Nayatani Y. New Method for Specifying Color-Rendering Properties of Light Sources Based on Feeling of Contrast. *Color Research & Application*. 2007;32(5).

References

- [101] Smet KAG, Ryckaert WR, Pointer MR, Deconinck G, Hanselaer P. Memory colours and colour quality evaluation of conventional and solid-state lamps. *Optics Express*. 2010;18(25). Available from: <https://doi.org/10.1364/OE.18.026229>.
- [102] Szabó F, Bodrogi P, Schanda J. A colour harmony rendering index based on predictions of colour harmony impression. *Lighting Research and Technology*. 2009;41:165–182. Available from: <http://journals.sagepub.com/doi/pdf/10.1177/1477153509103067>.
- [103] Borisuit A, Linhart F, Scartezzini JL, Münch M. Effects of realistic office daylighting and electric lighting conditions on visual comfort, alertness and mood. *Lighting Research and Technology*. 2015 4;47(2):192–209. Available from: <http://lrt.sagepub.com/cgi/doi/10.1177/1477153514531518>.
- [104] Nabil A, Mardaljevic J. Useful daylight illuminances: A replacement for daylight factors. *Energy and Buildings*. 2006;38(7):905–913.
- [105] Beute F. Powered by nature: the psychological benefits of natural views and daylight. Eindhoven University of Technology; 2014. Available from: <https://pure.tue.nl/ws/files/3813377/780722.pdf>.
- [106] Lottrup L, Stigsdotter UK, Meilby H, Claudi AG. The Workplace Window View: A Determinant of Office Workers' Work Ability and Job Satisfaction. *Landscape Research*. 2015;40(1):57–75. Available from: <http://www.tandfonline.com/doi/pdf/10.1080/01426397.2013.829806?needAccess=true>.
- [107] Hellinga H. Daylight and View - The influence of windows on the visual quality of indoor spaces. Technische Universiteit Delft; 2013.
- [108] Galasiu AD, Veitch JA. Occupant preferences and satisfaction with the luminous environment and control systems in daylit offices: a literature review. *Energy and Buildings*. 2006;38(7):728–742.
- [109] Hellinga H, Hordijk T. The D&V analysis method: A method for the analysis of daylight access and view quality. *Building and Environment*. 2014 9;79:101–114. Available from: <https://linkinghub.elsevier.com/retrieve/pii/S036013231400136X>.
- [110] Inanici MN, Navvab M. The Virtual Lighting Laboratory: Per-pixel Luminance Data Analysis. *Leukos*. 2006;3(2):89–104. Available from: <http://ies.tandfonline.com/action/journalInformation?journalCode=ulks20>.
- [111] Cuttle C. Lighting patterns and the flow of light. *Lighting Research and Technology*. 1971 9;3(3):171–189. Available from: <http://journals.sagepub.com/doi/10.1177/096032717100300301>.
- [112] Khademagha P, Aries MBC, Rosemann ALP, van Loenen EJ. Implementing non-image-forming effects of light in the built environment: A review on what we need. *Building and Environment*. 2016;108:263–272.

References

- [113] Gershun A. The light field. *Journal of Mathematics and Physics*. 1936;18:51–151.
- [114] Ashdown I. The Virtual Photometer: Modeling the Flow of Light. In: IESNA 1998 Annual Conference Technical Papers; 1998. p. 1–16. Available from: https://www.researchgate.net/profile/Ian_Ashdown/publication/248393085_The_Virtual_Photometer_Modeling_the_Flow_of_Light/links/0c96051deea411072d000000.pdf.
- [115] Lynes JA, Burt W, Jackson GK, Cuttle C. The Flow of Light into Buildings. In: *Transactions of the Illuminating Engineering Society*. vol. 31; 1966. p. 65–91.
- [116] Hewitt H, Bridgers DJ, Simons RH. Lighting and the Environment. *Trans Illum Eng Soc (London)*. 1965;30(4):91.
- [117] Bean AR. Modelling indicators for combined side and overhead lighting systems. *Lighting Research and Technology*. 1978;10(4):199–202. Available from: <http://lrt.sagepub.com/cgi/doi/10.1177/096032717801000405>.
- [118] Love JA, Navvab M. The vertical-to-horizontal illuminance ratio: A new indicator of daylighting performance. *Journal of the Illuminating Engineering Society*. 1994;23(2):50–61.
- [119] Cuttle C. Cubic illumination. *Lighting Research and Technology*. 1997 3;29(1):1–14. Available from: <http://lrt.sagepub.com/cgi/doi/10.1177/14771535970290010601>.
- [120] Morgenstern Y, Geisler WS, Murray RF. Human vision is attuned to the diffuseness of natural light. *Journal of Vision*. 2014 8;14(9):1–18. Available from: <http://jov.arvojournals.org/article.aspx?doi=10.1167/14.9.15>.
- [121] Veitch JA. Lighting for high-quality workplaces. In: Clements-Croome D, editor. *Creating the Productive Workplace*. 2nd ed. Taylor & Francis; 2006. p. 206–222. Available from: http://nparc.cisti-icist.nrc-cnrc.gc.ca/npsi/jsp/nparc_cp.jsp?lang=fr.
- [122] Xia L, Pont SC, Heynderickx I. Light diffuseness metric Part 1: Theory. *Lighting Research and Technology*. 2017;49:411–427. Available from: <http://journals.sagepub.com/doi/pdf/10.1177/1477153516631391>.
- [123] Cuttle C. Research Note: A practical approach to cubic illuminance measurement. *Lighting Research and Technology*. 2014;46:31–34.
- [124] Howlett O, Heschong L, McHugh J. Scoping Study for Daylight Metrics from Luminance Maps Scoping Study for Daylight Metrics from Luminance Maps. *LEUKOS*. 2007;3(3):201–215. Available from: <http://www.tandfonline.com/action/journalInformation?journalCode=ulks20>.
- [125] Heschong Mahone Group Inc. Sidelighting Photocontrols Field Study; Scoping Study for Daylight Metrics from Luminance Maps; 2006. Available from: <http://neea.org/docs/reports/scopingstudydaylightmetricsluminancemaps91784a05ca85.pdf>.

References

- [126] Izsó L, Laufer L, Suplicz S. Effects of dynamic lighting on the visual performance of older adults. *Lighting Research and Technology*. 2009 12;41(4):361–370. Available from: <http://journals.sagepub.com/doi/10.1177/1477153509336802>.
- [127] Rockcastle S, Andersen M. Measuring the dynamics of contrast & daylight variability in architecture: A proof-of-concept methodology. *Building and Environment*. 2014 11;81:320–333. Available from: <https://linkinghub.elsevier.com/retrieve/pii/S036013231400198X>.
- [128] Kruithof AA. TUBULAR LUMINESCENCE LAMPS FOR GENERAL ILLUMINATION. *Philips Technical Review*. 1941;6(3):65–74.
- [129] Aries MBC, Zonneveldt L. Daylight variations in a moderate climate as input for lighting controls. In: *Velux Symposium*. Lausanne, Switzerland; 2011. p. 1–10.
- [130] CIE. CIE Standard General Sky Guide. Vienna, Austria; 2014.
- [131] Spasojević B, Mahdavi A. Calibrated Sky Luminance Maps for Advanced Daylight Simulation Applications. In: *Proceedings of the 10th International Building Performance Simulation Association Conference and Exhibition (BS2007)*. Beijing, China; 2007. p. 1205–1210.
- [132] NWO. OPTILIGHT: Mathematical Optimizations for Human Centric Lighting. Accessed on 20-04-2020; 2020. Available from: <https://www.nwo.nl/onderzoek-en-resultaten/onderzoeksprojecten/i/82/25982.html>.
- [133] Kruisselbrink TW, Dangol R, Rosemann ALP. Practical issues in field studies using luminance cameras. In: *CIE Expert Workshop on Research Methods for Human Factors in Lighting*. CIE; 2018. p. 14–15. Available from: www.tue.nl/tavernehttps://research.tue.nl/en/publications/practical-issues-in-field-studies-using-luminance-cameras.
- [134] Spasojević B, Mahdavi A. Sky Luminance Mapping for Computational Daylight Modelling. In: *Ninth International IBPSA Conference*. Montreal, Canada; 2005. p. 1163–1170.
- [135] Inanici MN. Evaluation of High Dynamic Range Image-Based Sky Models in Lighting Simulation. *LEUKOS*. 2010;7(2):69–84.
- [136] Chiou YS, Huang PC. An HDRi-based data acquisition system for the exterior luminous environment in the daylight simulation model. *Solar Energy*. 2015 1;111:104–117. Available from: <http://www.sciencedirect.com/science/article/pii/S0038092X14005192>.
- [137] Cai H. High dynamic range photogrammetry for synchronous luminance and geometry measurement. *Lighting Research and Technology*. 2013 4;45(2):230–257. Available from: <http://journals.sagepub.com/doi/10.1177/1477153512453273>.

References

- [138] Sarkar A, Mistrick RG. A Novel Lighting Control System Integrating High Dynamic Range Imaging and DALI. *LEUKOS*. 2006 4;2(4):307–322. Available from: <http://www.tandfonline.com/doi/abs/10.1080/15502724.2006.10747642>.
- [139] Tohsing K, Schrempf M, Riechelmann S, Schilke H, Seckmeyer G. Measuring high-resolution sky luminance distributions with a CCD camera. *Applied optics*. 2013 3;52(8):1564–73. Available from: <http://www.osapublishing.org/viewmedia.cfm?uri=ao-52-8-1564&seq=0&html=true>.
- [140] Wu Y, Kämpf JH, Scartezzini JL. Design and validation of a compact embedded photometric device for real-time daylighting computing in office buildings. *Building and Environment*. 2019 11;148:309–322. Available from: <https://www.sciencedirect.com/science/article/pii/S036013231830711X>.
- [141] Motamed A, Deschamps L, Scartezzini JL. On-site monitoring and subjective comfort assessment of a sun shadings and electric lighting controller based on novel High Dynamic Range vision sensors. *Energy and Buildings*. 2017 8;149:58–72. Available from: <https://www.sciencedirect.com/science/article/pii/S0378778816314384#bib0145>.
- [142] Moeck M, Anaokar S. Illuminance Analysis from High Dynamic Range Images. *LEUKOS*. 2006 9;2(3):211–228. Available from: <http://www.tandfonline.com/doi/abs/10.1582/LEUKOS.2006.02.03.005>.
- [143] Cai H, Chung TM. Improving the quality of high dynamic range images. *Lighting Research and Technology*. 2010;43(1):87–102.
- [144] Ward G. Anywhere Software. Accessed on 07-03-2016;. Available from: <http://www.anywhere.com/>.
- [145] Holzer B. High dynamic range image formats; 2006. Available from: http://www.cg.tuwien.ac.at/courses/Seminar/WS2006/hdri_formats.pdf.
- [146] Mead AR, Mosalam K. Ubiquitous luminance sensing using the Raspberry Pi and Camera Module system. *Lighting Research and Technology*. 2017 5;49:904–921. Available from: <http://lrt.sagepub.com/cgi/doi/10.1177/1477153516649229>.
- [147] Mitsunaga T, Nayar SK. Radiometric self calibration. In: *IEEE Computer Society Conference on Computer Vision and Pattern Recognition*, vol. 1. Fort Collins, USA: IEEE Comput. Soc; 1999. p. 374–380. Available from: <http://ieeexplore.ieee.org/lpdocs/epico3/wrapper.htm?arnumber=786966>.
- [148] Wüller D, Gabele H. The usage of digital cameras as luminance meters. *Electronic Imaging Conference*. 2007;6502:1–11. Available from: http://www.image-engineering.de/index.php?option=com_content&view=article&id=550&Itemid=145.
- [149] Schanda J, editor. *COLORIMETRY Understanding the CIE System*. John Wiley and Sons; 2007.

References

- [150] Roy GG, Hayman S, Julian W. Sky Modelling from Digital Imagery. ARC Project No. A89530177; 1998.
- [151] Judd DB, MacAdam DL, Wyszecki G, Budde HW, Condit HR, Henderson ST, et al. Spectral Distribution of Typical Daylight as a Function of Correlated Color Temperature. *Journal of the Optical Society of America*. 1964 8;54(8):1031. Available from: <https://www.osapublishing.org/abstract.cfm?URI=josa-54-8-1031>.
- [152] Cai H, Chung TM. Evaluating discomfort glare from non-uniform electric light sources. *Lighting Research and Technology*. 2012 8;45(3):267–294. Available from: <http://lrt.sagepub.com/cgi/doi/10.1177/1477153512453274>.
- [153] Cauwerts C, Bodart M, Deneyer A. Comparison of the Vignetting Effects of Two Identical Fisheye Lenses. *LEUKOS*. 2012 9;8(3):181–203. Available from: <http://www.tandfonline.com/doi/abs/10.1582/LEUKOS.2012.08.03.002>.
- [154] Inanici MN, Viswanathan K. Hdrscope : High Dynamic Range Image Processing Toolkit for Per-Pixel Lighting Analysis and Hdrscope : Lighting Analysis. In: 13th Conference of International Building Performance Simulation Association. Chambéry, France; 2013. p. 3400–3407.
- [155] Moore T, Graves H, Perry MJ, Carter DJ. Approximate field measurement of surface luminance using a digital camera. *Lighting Research and Technology*. 2000 3;32(1):1–11. Available from: <http://lrt.sagepub.com/content/32/1/1.abstract>.
- [156] Ulbricht R. *Das Kugelphotometer*. Berlin und Munchen: Verlag Oldenburg; 1920.
- [157] Stumpfel J, Jones A, Wenger A, Tchou C, Hawkins T, Debevec P. Direct HDR capture of the sun and sky. In: Proceedings of the 3rd international conference on Computer graphics, virtual reality, visualisation and interaction in Africa. Stellenbosch, South Africa; 2004. p. 145–149. Available from: <http://portal.acm.org/citation.cfm?doid=1185657.1185687>.
- [158] Schneider D, Schwalbe E, Maas HG. Validation of geometric models for fisheye lenses. *ISPRS Journal of Photogrammetry and Remote Sensing*. 2009 5;64(3):259–266. Available from: <http://www.sciencedirect.com/science/article/pii/S0924271609000045>.
- [159] Tregenza PR. Subdivision of the sky hemisphere for luminance measurements. *Lighting Research and Technology*. 1987 1;19:13–14. Available from: <http://lrt.sagepub.com/content/19/1/13.abstract>.
- [160] Baer R, Seifert D, Barfuß M. *Beleuchtungstechnik*. 4th ed. Berlin: HUSS-MEDIEN GmbH; 2016.
- [161] Moeck M. Accuracy of Luminance Maps Obtained from High Dynamic Range Images. *LEUKOS*. 2007 9;4(2):99–112. Available from: <http://www.tandfonline.com/doi/abs/10.1582/LEUKOS.2007.04.02.002>.

References

- [162] Coutelier B, Dumortier D. Luminance calibration of the Nikon Coolpix 990 digital camera. Application to glare evaluation. In: AIVC and EPIC Conference. 23. Lyon, France; 2002. p. 1–6.
- [163] Kobav MB, Bizjak G, Dumortier D. Characterization of sky scanner measurements based on CIE and ISO standard CIE S 011/2003. *Lighting Research and Technology*. 2013 10;45:504–512. Available from: <http://lrt.sagepub.com/content/45/4/504.abstract>.
- [164] Ineichen P, Molineaux B. Characterisation and Comparison of two Sky Scanners: PRC Krochmann & EKO Instruments. In: First draft, IEA Task XVII expert meeting. Geneva, Switzerland; 1993. p. 1–7.
- [165] Ramanath R, Snyder WE, Yoo Y, Drew MS. Color image processing pipeline. *IEEE Signal Processing Magazine*. 2005 1;22(1):34–43. Available from: <http://ieeexplore.ieee.org/document/1407713/>.
- [166] Jacobs A. High Dynamic Range Imaging and its Application in Building Research. *Advances in Building Energy Research*. 2007 1;1(1):177–202. Available from: <http://www.tandfonline.com/doi/abs/10.1080/17512549.2007.9687274>.
- [167] Lenseigne B, Jacobs VA, Withouck M, Hanselaer P, Jonker PP. Color sensitivity of the multi-exposure HDR imaging process. *Advanced Optical Technologies*. 2013;2(2):159–169.
- [168] CIE. Characterization of the performance of illuminance meters and luminance meters. Vienna, Austria: CIE; 2014.
- [169] Cai H. Camera Aided Luminance Measurement of the Luminous Surfaces of Different Light Sources. In: AEI 2011. Reston, USA: American Society of Civil Engineers; 2011. p. 272–279. Available from: <http://ascelibrary.org/doi/10.1061/41168%28399%2933>.
- [170] Borisuit A, Münch M, Deschamps L, Kämpf J, Scartezzini JL. A new device for dynamic luminance mapping and glare risk assessment in buildings. In: SPIE 8485, Nonimaging Optics: Efficient Design for Illumination and Solar Concentration IX. vol. 8485. San Diego, USA; 2012. .
- [171] Borisuit A, Deschamps L, Kämpf J, Scartezzini JL, Münch M. Assessment of circadian weighted radiance distribution using a camera-like light sensor. In: CISBAT 2013. Lausanne, Switzerland; 2013. p. 305–310. Available from: https://infoscience.epfl.ch/record/195695/files/4_borisuit.pdf?version=1.
- [172] Geisler-Moroder D, Dur A. Estimating Melatonin Suppression and Photosynthesis Activity in Real-World Scenes from Computer Generated Images. In: Conference on Colour in Graphics, Imaging, and Vision. Joensuu, Finland: Society for Imaging Science and Technology; 2010. p. 346–352.
- [173] Cauwerts C, Jost S, Deroisy B. COLORIMETRIC ACCURACY OF HIGH DYNAMIC RANGE IMAGES FOR LIGHTING RESEARCH. In: Proceedings of the 29th Quadrennial Session of the CIE. Washington D.C., USA; 2019. p. 622–628. Available from: http://files.cie.co.at/x046_2019/x046-OP89.pdf.

References

- [174] Fliegel K, Havlin J. Imaging photometer with a non-professional digital camera. In: Applications of Digital Image Processing XXXII. vol. 7443. San Diego, USA; 2009. p. 74431Q–74431Q–8. Available from: <https://proceedings.spiedigitallibrary.org/proceeding.aspx?doi=10.1117/12.825977>.
- [175] Hufkens K. Raspberry pi camera v2: spectral response curve. Accessed on 24-01-2018; 2016. Available from: <https://khufkens.com/2016/06/05/raspberry-pi-camera-v2-spectral-response-curve/>.
- [176] Lin L, Torbeck LD. Coefficient of accuracy and concordance correlation coefficient: new statistics for methods comparison. *PDA Journal of Pharmaceutical Science and Technology*. 1998;52(2):55–59.
- [177] DIN. DIN 5032 Photometry - Part 7: Classification of illuminance meters and luminance meters. Berlin, Germany: Deutsches Institut Fur Normung E.V.; 2017.
- [178] Pagnutti M, Ryan RE, Cazenavette G, Gold M, Harlan R, Leggett E, et al. Laying the foundation to use Raspberry Pi 3 V2 camera module imagery for scientific and engineering purposes. *Journal of Electronic Imaging*. 2017 2;26(1):013014. Available from: <http://electronicimaging.spiedigitallibrary.org/article.aspx?doi=10.1117/1.JEI.26.1.013014>.
- [179] Jung B, Inanici MN. Measuring circadian lighting through high dynamic range photography. *Lighting Research and Technology*. 2018;51(5):742–763. Available from: <https://journals.sagepub.com/doi/pdf/10.1177/1477153518792597>.
- [180] Jiang J, Liu D, Gu J, Susstrunk S. What is the space of spectral sensitivity functions for digital color cameras? In: Proceedings of IEEE Workshop on Applications of Computer Vision. Tampa, USA; 2013. p. 168–179. Available from: <http://www.gujinwei.org/research/camspec/camspec.pdf>.
- [181] Tominaga S, Ishida A, Wandell BA. Color temperature estimation of scene illumination by the sensor correlation method. *Systems and Computers in Japan*. 2007;38(8):95–108.
- [182] Berns RS, Taplin LA, Nezamabadi M, Mohammadi M, Zhao Y. Spectral imaging using a commercial colour-filter array digital camera. In: ICOM-CC 14th Triennial Meeting. vol. II. The Hague, Netherlands; 2005. p. 743–750. Available from: <http://art-si.org/>.
- [183] Shrestha R, Hardeberg JY, Mansouri A. One-shot multispectral color imaging with a stereo camera. In: Digital Photography VII. vol. 7876. San Francisco: SPIE; 2011. p. 787609. Available from: <http://proceedings.spiedigitallibrary.org/proceeding.aspx?doi=10.1117/12.872428>.
- [184] CIE. CIE System for Metrology of Optical Radiation for ipRGC-Influenced Responses to Light. Vienna, Austria: International Commission on Illumination; 2018. Available from: <http://www.cie.co.at/publications/cie-system-metrology-optical-radiation-iprgc-influenced-responses-light-o>.

References

- [185] Roby J, Aubé M. LSPDD — Light Spectral Power Distribution Database. Accessed on 30-11-2018; 2012. Available from: <http://galileo.graphyics.cegesherbrooke.qc.ca/app/en/lamps>.
- [186] Hohm W, Krochman J. ERMITTLUNG DER AEHNLICHSTEN FARBTEMPERATUR. FARBE. 1975;24(1-6):91–96.
- [187] Rea MS, Deng L, Wolsey R. Full-Spectrum Light Sources. *Lighting Answers*. 2005;7(5).
- [188] Newsham G, Arsenault C. A camera as a sensor for lighting and shading control. *Lighting Research and Technology*. 2009 6;41(2):143–163. Available from: <http://journals.sagepub.com/doi/10.1177/1477153508099889>.
- [189] Van Den Wymelenberg KG, Inanici MN, Johnson P. The Effect of Luminance Distribution Patterns on Occupant Preference in a Daylit Office Environment. *LEUKOS*. 2010;7(2):103–122. Available from: <http://ies.tandfonline.com/action/journalInformation?journalCode=ulks20>.
- [190] Painter B, Irvine KN, Waskett RK, Mardaljevic J. Evaluation of a Mixed Method Approach for Studying User Interaction with Novel Building Control Technology. *Energies*. 2016 3;9(3):215. Available from: <http://www.mdpi.com/1996-1073/9/3/215>.
- [191] Correia da Silva P, Leal V, Andersen M. Occupants interaction with electric lighting and shading systems in real single-occupied offices: Results from a monitoring campaign. *Building and Environment*. 2013 6;64:152–168. Available from: <https://www.sciencedirect.com/science/article/pii/S0360132313000954#bib38>.
- [192] Konis K. Evaluating daylighting effectiveness and occupant visual comfort in a side-lit open-plan office building in San Francisco, California. *Building and Environment*. 2013 1;59:662–677. Available from: <https://linkinghub.elsevier.com/retrieve/pii/S0360132312002594>.
- [193] Konis K, Lee ES. Measured daylighting potential of a static optical louver system under real sun and sky conditions. *Building and Environment*. 2015 10;92:347–359. Available from: <https://www.sciencedirect.com/science/article/pii/S0360132315001900#fig5>.
- [194] Goovaerts C, Descamps F, Jacobs VA. Shading control strategy to avoid visual discomfort by using a low-cost camera: A field study of two cases. *Building and Environment*. 2017 11;125:26–38. Available from: <https://linkinghub.elsevier.com/retrieve/pii/S0360132317303827>.
- [195] Lemieux A, Parizeau M. Experiments on eigenfaces robustness. In: *Object recognition supported by user interaction for service robots*. vol. 1. Quebec City, Canada: IEEE Comput. Soc; 2002. p. 421–424. Available from: <http://ieeexplore.ieee.org/document/1044743/>.

References

- [196] Wang J, Zhang C, Shum H. Face image resolution versus face recognition performance based on two global methods. In: Asia Conference on Computer Vision; 2004. p. 48–49. Available from: <http://citeseerx.ist.psu.edu/viewdoc/summary?doi=10.1.1.128.7445>.
- [197] Fookes C, Lin F, Chandran V, Sridharan S. Evaluation of image resolution and super-resolution on face recognition performance. *Journal of Visual Communication and Image Representation*. 2012 1;23(1):75–93. Available from: <https://www.sciencedirect.com/science/article/pii/S1047320311000721>.
- [198] Boom BJ, Beumer GM, Spreeuwers LJ, Veldhuis RNJ. The Effect of Image Resolution on the Performance of a Face Recognition System. In: 2006 9th International Conference on Control, Automation, Robotics and Vision. IEEE; 2006. p. 1–6. Available from: <http://ieeexplore.ieee.org/document/4150409/>.
- [199] Wang Z, Miao Z, Jonathan Wu QM, Wan Y, Tang Z. Low-resolution face recognition: A review. *Visual Computer*. 2014 4;30(4):359–386. Available from: <http://link.springer.com/10.1007/s00371-013-0861-x>.
- [200] Wen Yj, Bonnell J, Agogino AM. Energy Conservation Utilizing Wireless Dimmable Lighting Control in a Shared-Space Office. 2008 Annual Conference of the Illuminating Engineering Society. 2008; Available from: <https://citeseerx.ist.psu.edu/viewdoc/summary?doi=10.1.1.160.5248>.
- [201] Bai YW, Ku YT. Automatic room light intensity detection and control using a microprocessor and light sensors. *IEEE Transactions on Consumer Electronics*. 2008 8;54(3):1173–1176. Available from: <http://ieeexplore.ieee.org/document/4637603/>.
- [202] MathWorks. Resize image - MATLAB imresize. Accessed on 11-01-2019;. Available from: <https://nl.mathworks.com/help/images/ref/imresize.html>.
- [203] Bouguer P. *Traité d’optique sur la gradation de la lumière*. Guerin & Delatour; 1760.
- [204] Padgham CA, Saunders JE. Scales of Apparent Brightness. *Lighting Research and Technology*. 1966 12;31(4):122–149. Available from: <http://lrt.sagepub.com/lookup/doi/10.1177/147715356603100403>.
- [205] Pelli DG, Bex P. Measuring contrast sensitivity. *Vision Research*. 2013 9;90:10–14. Available from: <https://www.sciencedirect.com/science/article/pii/S0042698913001132>.
- [206] Lin M, Lucas HC, Shmueli G. Too Big to Fail: Large Samples and the p-Value Problem. *Information Systems Research*. 2013;24(4):906–917. Available from: <http://pubsonline.informs.orghttp://www.informs.org>.
- [207] Rosenthal R. Parametric measures of effect size. In: *The handbook of research synthesis*. New York, NY, US: Russell Sage Foundation; 1994. p. 231–244.

References

- [208] Kruisselbrink TW. Spatial Resolution Luminance Camera Toolbox. Accessed on 20-08-2020; 2019. Available from: <https://nl.mathworks.com/matlabcentral/fileexchange/73529-spatial-resolution-luminance-camera-toolbox>.
- [209] Yan D, O'Brien W, Hong T, Feng X, Burak Gunay H, Tahmasebi F, et al. Occupant behavior modeling for building performance simulation: Current state and future challenges. *Energy and Buildings*. 2015 11;107:264–278.
- [210] Vetterlí M, Kovačević J, Goyal VK. *Foundations of Signal Processing*. Cambridge University Press; 2014.
- [211] Valckenborg R. SolarBEAT Publiek Eindrapport. seac; 2018. Available from: <https://projecten.topsectorenergie.nl/storage/app/uploads/public/5ca/25c/f67/5ca25cf67f8ac864124603.pdf>.
- [212] Aries MBC, Rosemann ALP. Dynamic Daylight and Input for Intelligent (Day)lighting Control. In: *Proceedings 28th CIE Session*. Manchester, UK; 2015. p. 1099–1103. Available from: <https://www.researchgate.net/publication/305766706>.
- [213] Houtveen JH, Molenaar PC. Comparison between the Fourier and Wavelet methods of spectral analysis applied to stationary and nonstationary heart period data. *Psychophysiology*. 2001 9;38(5):729–35. Available from: <http://www.ncbi.nlm.nih.gov/pubmed/11577896>.
- [214] Harris FJ. On the Use of Windows for Harmonic Analysis. *Proceedings of the IEEE*. 1978;6(1):51–83.
- [215] Kontaxis PA, Bouroussis CA, Doulos LT, Topalis FV. APPLICATIONS OF CCD SENSORS IN PHOTOMETRY AND IN DAYLIGHT RESPONSIVE SYSTEMS. In: *Proceedings of the 5th Balkan Conference on Lighting (Balkan Light)*. Belgrade, Serbia; 2012. p. 3–6. Available from: <http://147.102.23.61/files/Publications/Proceedings/ApplicationsofCCDsensorsindaylightresponsivesystems.pdf>.
- [216] Doulos LT, Tsangrassoulis A, Bouroussis CA, Topalis FV. Reviewing drawbacks of conventional photosensors: are ccd/cmos sensors the next generation? In: *Lux Europa 2013, 12th European Lighting Conference*. Krakow, Poland; 2013. p. 1–6.
- [217] Konis K. Predicting visual comfort in side-lit open-plan core zones: Results of a field study pairing high dynamic range images with subjective responses. *Energy and Buildings*. 2014 7;77:67–79. Available from: <https://www.sciencedirect.com/science/article/pii/S0378778814002552>.
- [218] Motamed A, Deschamps L, Scartezzini JL. Validation and preliminary experiments of embedded discomfort glare assessment through a novel hdr vision sensor. In: *CISBAT 2015*. Lausanne, Switzerland; 2015. p. 235–240.

References

- [219] Fan D, Painter B, Mardaljevic J. A Data Collection Method for Long-Term Field Studies of Visual Comfort in Real-World Daylit Office Environments. In: 26th Conference on Passive and Low Energy Architecture. Quebec City, Canada; 2009. p. 251–256.
- [220] Kim M, Konstantzos I, Tzempelikos A. A New Control Framework For The Visual Environment Based On Low-Cost HDR Luminance Acquisition. In: International High Performance Buildings Conference; 2018. p. 1–11. Available from: <https://docs.lib.purdue.edu/ihpbc/328>.
- [221] Van Duijnhoven J, Aarts MPJ, Kort HSM. The importance of including position and viewing direction when measuring and assessing the lighting conditions of office workers. *Work*. 2019;64(4):877–895.
- [222] Leesman. The Next 250K. Leesman; 2018. Available from: <https://www.leesmanindex.com/our-research/>.
- [223] EIZO. EIZO Monitor Test. Accessed on 23-07-2019;. Available from: <https://www.eizo.be/monitor-test/>.
- [224] Loe DL, Mansfield KP, Rowlands E. Appearance of lit environment and its relevance in lighting design: Experimental study. *Lighting Research and Technology*. 1994 1;26(3):119–133. Available from: <http://lrt.sagepub.com/cgi/doi/10.1177/096032719402600301>.
- [225] Van Den Wymelenberg K, Inanici MN. Evaluating a New Suite of Luminance-Based Design Metrics for Predicting Human Visual Comfort in Offices with Daylight. *LEUKOS*. 2016;12:113–138. Available from: <https://www.tandfonline.com/doi/pdf/10.1080/15502724.2015.1062392?needAccess=true>.
- [226] Aries MBC, Begemann SHA, Zonneveldt L, Tenner AD, Eywo K. Retinal illuminance from vertical daylight openings in office spaces. In: *RIGHT LIGHT*. vol. 5. Nice, France; 2002. p. 75–80.
- [227] Van Derlofske JF, Bierman A, Rea MS, Maliyagoda N. Design and optimization of a retinal exposure detector. In: Sasian JM, editor. *Novel Optical Systems Design and Optimization III*. vol. 4092. International Society for Optics and Photonics; 2000. p. 60–70. Available from: <http://proceedings.spiedigitallibrary.org/proceeding.aspx?articleid=915788>.
- [228] Khademagha P, Aries MBC, Rosemann ALP, van Loenen EJ. New method for analyzing a luminous environment considering non-image-forming effects of light. In: *Proceedings of the PLEA 2017 Conference: Design to thrive*. vol. 2. Edinburgh, UK; 2017. p. 3245–3252. Available from: www.tue.nl/taverne.
- [229] Khademagha P, Aries MBC, Rosemann ALP, van Loenen EJ. Why Directionality Is a n Important Light Factor for Human Health to Consider in Lighting Design? *International Journal of Sustainable Lighting*. 2016;35:3–8.
- [230] de Bakker C, Aarts MPJ, Kort HSM, Rosemann ALP. The feasibility of highly granular lighting control in open-plan offices: Exploring the comfort and energy saving potential. *Building and Environment*. 2018 9;142:427–438.

References

- [231] Bellia L, Fragliasso F, Stefanizzi E. Daylit offices: A comparison between measured parameters assessing light quality and users' opinions. *Building and Environment*. 2017 2;113:92–106. Available from: <https://linkinghub.elsevier.com/retrieve/pii/S0360132316303092>.
- [232] Rea MS. *The IESNA LIGHTING HANDBOOK*. 9th ed. Illuminating Engineering Society of North America; 2000.
- [233] Peeters S, Kruisselbrink T, Smolders K, Dangol R, Vogels I, de Kort Y. Interaction of daylight and electric light on subjective light appraisals in office environments. In: *VELUX Daylight Symposium*; 2019. p. 1–2.
- [234] de Bakker C, Aarts MPJ, Kort H, Rosemann A. The feasibility of highly granular lighting control in open-plan offices: Exploring the comfort and energy saving potential. *Building and Environment*. 2018 9;142:427–438. Available from: <https://www.sciencedirect.com/science/article/pii/S036013231830386X>.
- [235] Roche L, Dewey E, Littlefair P. Occupant reactions to daylight in offices. *Lighting Research and Technology*. 2000;32(3):119–126.
- [236] Dong B, Lam KP. A real-time model predictive control for building heating and cooling systems based on the occupancy behavior pattern detection and local weather forecasting. *Building Simulation*. 2014;7(1):89–106.
- [237] Hyndman RJ, Koehler AB. Another look at measures of forecast accuracy. *International Journal of Forecasting*. 2006 10;22(4):679–688.
- [238] ISO. *ISO 5725-1:1994 Accuracy (trueness and precision) of measurement methods and results*; 1994. Available from: https://www.iso.org/obp/ui/#iso:std:iso:5725:-1:ed-1:v1:enhttp://www.iso.org/iso/iso_catalogue/catalogue_tc/catalogue_detail.htm?csnumber=11833.
- [239] McBride GB. A proposal for strength-of-agreement criteria for Lin's Concordance Correlation Coefficient; 2005.
- [240] Landis JR, Koch GG. The Measurement of Observer Agreement for Categorical Data. *Biometrics*. 1977 3;33(1):159. Available from: <https://www.jstor.org/stable/2529310?origin=crossref>.
- [241] Slater AI, Boyce PR. Illuminance uniformity on desks: Where is the limit? *Lighting Research and Technology*. 1990 12;22(4):165–174. Available from: <http://journals.sagepub.com/doi/10.1177/096032719002200401>.
- [242] Cantin F, Dubois MC. Daylighting metrics based on illuminance, distribution, glare and directivity. *Lighting Research and Technology*. 2011;43:291–307. Available from: <http://journals.sagepub.com/doi/pdf/10.1177/1477153510393319>.
- [243] Wang X, Tjalkens T, Linnartz JPMG. An Intelligent Lighting System: Learn User Preferences from Inconsistent Feedback. In: *UBICOMP/ISWC. HEIDELBERG, GERMANY*; 2016. p. 1620–1626. Available from: <http://dx.doi.org/10.1145/2968219.2968523>.

References

- [244] Papatsimpa C, Linnartz JPMG. Propagating sensor uncertainty to better infer office occupancy in smart building control. *Energy and Buildings*. 2018 11;179:73–82.
- [245] UN environment. *Accelerating the Global Adoption of Energy-Efficient Lighting*; 2017.
- [246] Sarkar A, Fairchild M, Salvaggio C. Integrated daylight harvesting and occupancy detection using digital imaging. In: Blouke MM, Bodegom E, editors. *Sensors, Cameras, and Systems for Industrial/Scientific Applications IX*. vol. 6816. International Society for Optics and Photonics; 2008. p. 68160F.
- [247] Granderson J, Gaddam V, DiBartolomeo D, Li X, Rubinstein F, Das S. Field-Measured Performance Evaluation of a Digital Daylighting System. *LEUKOS*. 2010 10;7(2):85–101. Available from: <https://www.tandfonline.com/doi/full/10.1582/LEUKOS.2010.07.02002>.
- [248] Bujdei C, Moraru SA. Ensuring comfort in office buildings: Designing a KNX monitoring and control system. In: *Proceedings of the 7th International Conference on Intelligent Environments*; 2011. p. 222–229.
- [249] Haas H, Yin L, Wang Y, Chen C. What is LiFi? *Journal of Lightwave Technology*. 2016 3;34(6):1533–1544.
- [250] Lim SK, Ruling KG, Kim I, Jang SI. Entertainment lighting control network standardization to support VLC services. *IEEE Communications Magazine*. 2013;51(12):42–48.
- [251] Aries MBC, Zonneveldt L. Architectural Aspects of Healthy Lighting. In: *Proceedings of the 21st Passive and Low Energy Architecture*; 2004. p. 1–5.
- [252] Foxtron. DALIconfig x64. Accessed on 17-01-2020;. Available from: <http://www.foxtron.cz/en/downloads/downloads/daliconfig>.
- [253] Hellerstein JL, Diao Y, Parekh S, Tilbury DM. Proportional Control. In: *Feedback Control of Computing Systems*. Hoboken, NJ, USA: John Wiley & Sons, Inc.; 2004. p. 243–291.
- [254] Ellis G. Delay in Digital Controllers. In: *Control System Design Guide*. Elsevier; 2012. p. 61–72.
- [255] Hellerstein JL, Diao Y, Parekh S, Tilbury DM. PID Controllers. In: *Feedback Control of Computing Systems*. Hoboken, NJ, USA: John Wiley & Sons, Inc.; 2004. p. 293–335. Available from: <http://doi.wiley.com/10.1002/047166880X.ch9>.
- [256] Galasiu AD, Atif MR, MacDonald RA. Impact of window blinds on daylight-linked dimming and automatic on/off lighting controls. *Solar Energy*. 2004 5;76(5):523–544.
- [257] Raspberry Pi Foundation. Raspberry Pi 3 Model B+. Accessed on 21-08-2020;. Available from: <https://www.raspberrypi.org/products/raspberry-pi-3-model-b-plus/>.

References

- [258] Greenland S, Senn SJ, Rothman KJ, Carlin JB, Poole C, Goodman SN, et al. Statistical tests, P values, confidence intervals, and power: a guide to misinterpretations. *European Journal of Epidemiology*. 2016 4;31(4):337–350.
- [259] NVIDIA. NVIDIA Jetson Nano Developer Kit — NVIDIA Developer. Accessed on 08-04-2020; 2019. Available from: <https://developer.nvidia.com/embedded/jetson-nano-developer-kit>.
- [260] Maker Advisor. ESP32-CAM. Accessed on 08-04-2020; 2020. Available from: <https://makeradvisor.com/tools/esp32-cam/>.
- [261] Zigbee Alliance. Home - Zigbee Alliance. Accessed on 20-04-2020; 2020. Available from: <https://zigbeealliance.org/>.
- [262] Pierson C, Cauwerts C, Bodart M, Wienold J. Tutorial: Luminance Maps for Daylighting Studies from High Dynamic Range Photography. *LEUKOS - Journal of Illuminating Engineering Society of North America*. 2019; Available from: <https://www.tandfonline.com/action/journalInformation?journalCode=ulks20>.
- [263] Peeters ST, Smolders KCHJ, Vogels IMCL, de Kort YAW. NIF and IF effects of different light scenarios in a real-life office setting. In: 31 Annual meeting of the The Society for Light Treatment and Biological Rhythms. Chicago, US; 2019. p. Poster.
- [264] Bonarius JH, Linnartz JPMG. Particle filter-based parameter estimation in a model of the human circadian rhythm. Enschede, Netherlands; 2018.
- [265] Kronauer RE, Czeisler CA, Pilato SF, Moore-Ede MC, Weitzman ED. Mathematical model of the human circadian system with two interacting oscillators. *The American journal of physiology*. 1982 1;242(1):3–17. Available from: <http://www.ncbi.nlm.nih.gov/pubmed/7058927>.
- [266] de Bakker C. Occupancy-based lighting control : developing an energy saving strategy that ensures office workers' comfort. Eindhoven University of Technology; 2019. Available from: <https://research.tue.nl/en/publications/occupancy-based-lighting-control-developing-an-energy-saving-stra>.
- [267] Sandhu JS, Agogino AM, Agogino AK. Wireless sensor networks for commercial lighting control: decision making with multi-agent systems. *AAAI workshop on sensor networks*. 2004;10:131–140.
- [268] Tran D, Tan YK. Sensorless illumination control of a networked LED-lighting system using feedforward neural network. In: *IEEE Transactions on Industrial Electronics*; 2014. p. 2113–2121. Available from: http://ieeexplore.ieee.org/xpls/abs_all.jsp?arnumber=6523127.
- [269] Subramaniam S, Hoffmann S. Image-obfuscation as a means for privacy-conscious visual data acquisition from building systems. In: *IOP Conference Series: Earth and Environmental Science*. vol. 323; 2019. p. 12125.

Curriculum Vitae

Thijs Kruisselbrink was born on 22-02-1993 in Winterswijk, the Netherlands. After finishing his pre-university education at Christelijk College Schaersvoorde in 2011, he enrolled his studies at Eindhoven University of Technology. After receiving his bachelor's degree in Architecture Building and Planning in 2014, he proceeded his master with the Building Physics and Services trajectory within Architecture Building and Planning. In 2016, Thijs graduated, within the Building Lighting group, on a methodology to measure the luminance distribution using low cost components.

After receiving his master's degree, he started his PhD in the Building Lighting group in September 2016 of which the results are presented in this dissertation. Thijs wrote a number of peer-reviewed journal and conference papers. His journal paper *'Photometric measurements of lighting quality: An overview'* published in Building and Environment has been among the most downloaded papers of this journal. Furthermore, he presented his work at several conferences, including CIE expert Workshop 2018 (Copenhagen), LICHT 2018 (Davos), and the CIE 2019 29th Quadrennial Session (Washington).

In addition to his research activities, Thijs was involved in a number of educational activities. Throughout his PhD Thijs has supervised many students both on BSc and MSc level, has been co-teaching BSc courses, and has occasionally given guest lectures.

Curriculum Vitae

List of Publications

Academic peer-reviewed publications

Kruisselbrink TW, Dangol R, van Loenen EJ. A comparative study between two algorithms for luminance-based lighting control. (Accepted for publication in *Energy and Buildings*).

Kruisselbrink TW, Dangol R, van Loenen EJ. Feasibility of ceiling-based luminance distribution measurements. *Building and Environment*. 2020 172;106699. <https://doi.org/10.1016/j.buildenv.2020.106699>

Kruisselbrink TW, Dangol R, van Loenen EJ. Recommendations for long-term luminance distribution measurements: The spatial resolution. *Building and Environment*. 2020 169;106538. <https://doi.org/10.1016/j.buildenv.2019.106538>.

Kruisselbrink TW, Dangol R, Rosemann ALP, van Loenen EJ. Spectral tuning of luminance cameras: A theoretical model and validation measurements. *Lighting Research & Technology*. 2019 52(5);654–674. <https://doi.org/10.1177/1477153519880231>

Kruisselbrink TW, Dangol R, Rosemann ALP. Photometric measurements of lighting quality: An overview. *Building and Environment*. 2018 6;138; 42–52. <https://doi.org/10.1016/j.buildenv.2018.04.028>

Dangol R, Kruisselbrink TW, Rosemann ALP(2017), Effect of Window Glazing on Colour Quality of Transmitted Daylight. *Journal of Daylighting*. 2017 4(2);37–47. <https://doi.org/10.15627/jd.2017.6>.

Kruisselbrink TW, Aries MBC, Rosemann ALP. A Practical Device for Measuring the Luminance Distribution. *International Journal of Sustainable Lighting*. 2017 19(1); 75–90. <https://doi.org/10.26607/ijsl.v19i1.76>

Proceedings and conference contributions

Kruisselbrink TW, Dangol R, van Loenen EJ. HDR IMAGING FOR LUMINANCE AND MELANOPIC RADIANCE: CAMERAS AND SPECTRAL POWER DISTRIBUTIONS. In: *Proceedings of the 5th CIE Symposium on Colour and Visual Appearance*. CIE; 2020. p. 1–12.

Peeters S, Kruisselbrink TW, Smolders K, Dangol R, Vogels I, de Kort Y. Interaction of daylight and electric light on subjective light appraisals in office environments. In: *VELUX Daylight Symposium*; 2019

List of Publications

Kruisselbrink TW, Dangol R, van Loenen EJ. CEILING-BASED LUMINANCE MEASUREMENTS: A FEASIBLE SOLUTION? In: Proceedings of the 29th Quadrennial Session of the CIE, Washington D.C., USA; International Commission on Illumination; 2019. pp. 1166–1174. <https://doi.org/10.25039/x46.2019.P0077>.

Kruisselbrink TW, van Duijnhoven J, Dangol R, Rosemann ALP. Improving lighting quality by practical measurements of the luminance distribution. In: Congress of the International Ergonomics Association vol. 827. Florence, Italy: Springer; 2019. p.190–198. https://doi.org/10.1007/978-3-319-96059-3_21

Kruisselbrink TW, Dangol R, Rosemann ALP. Practical issues in field studies using luminance cameras. In: CIE Expert Workshop on Research Methods for Human Factors in Lighting. Copenhagen, Denmark, CIE;2018. pp. 14–15.

Kruisselbrink, Dangol R, Rosemann ALP. The Bee-Eye: A practical device for measuring the luminance distribution. In LICHT 2018. Davos, Switzerland. 2018.

van Duijnhoven J, Kruisselbrink TW, Aarts MPJ, Rosemann ALP, Kort HSM. Guidance for office workers based on their real-life light exposure and alertness. In LICHT 2018. Davos, Switzerland. 2018

Kruisselbrink TW, Dangol R, Unobtrusive field measurements of the luminance distribution. In: 5th Data Science Summit (DSSE 2018). Eindhoven, The Netherlands. 2018

Kruisselbrink TW, Tang J, Bruggema HM, Zeiler W. The indoor environmental quality in a Dutch day care centre: the effects of ventilation on the conditions within the baby cots. In: 12th REHVA World Congress (CLIMA 2016); 2016. pp. 1–10.

Professional publications

Kruisselbrink TW, Optimizing lighting quality using the luminance distribution, IN-Side Information; 2018. pp. 30–32.

Acknowledgements

After almost a decade of Eindhoven University of Technology I have come to the very last part of my thesis. Who would have expected this when I moved to Eindhoven as an 18 year old chap. Especially, the last four years were very special and I could not have succeeded without the help and support of others.

First of all, I would like to thank my promoters. Alexander Rosemann, my first promoter, the guy who had confidence in me and hired me for this great job. Who would have known where I would be right now if you hadn't contacted me for a graduation project after I aced my Lighting Technology exam. You held, hypothetically, my hand during my first steps in the academical world. I strongly believe that it would not be such a success story without you. I will always remember your endless enthusiasm and your numerous anecdotes. Alex, you were, and still are, a great motivator, you should be proud of that! It was extremely meaningful that you managed to provide feedback on my thesis.

I am also extremely grateful for my second promoter, Evert van Loenen. You selflessly jumped in, when Alex was unavailable, despite your extremely busy agenda. I think all members of the building lighting group appreciate your effort to keep the group together. Personally, I highly valued your keen eye for details combined with your down to earth attitude. You really deserve your (part-time) retirement. Although I wonder whether you will actually work less hours.

My appreciation also goes to Rajendra Dangol, my co-promoter. It is very sad that your contract ended early and you were not able to stay. Thank you for your feedback during the last phase of my PhD while balancing a new job and renewed family life in Kathmandu. Throughout those extended three years you always made time for me. You helped me to achieve an academical level based on your own experiences and you were the perfect sounding board for my ideas.

Werner Osterhaus, Jean-Louis Scartezzini, Tanir Özçelebi and Mariëlle Aarts thank you for being my external committee members. I strongly believe that your feedback has further improved this thesis.

I could not have succeeded without the building lighting group. Mariëlle thank you for organizing the FABBLous (Friday Afternoon Borrel Building Lighting), during these difficult last 6 months, to keep the spirit in the building lighting group alive. Not to mention Juliëtte, Kars, Christel, Kazi, Sila, Yike, Sanae, Clotilde and Parisa. Thank you for the "gezellige" lunch-breaks at our exclusive spot at Vertigo Plaza, and for the various dinners and parties. Without you guys, this four years would have been a lot more boring. Hopefully, we can have a drink soon.

The intelligent lock-down occurred just before my last experiment. Thankfully, the faculty enabled me to continue just as planned by allowing me access to the lab. Jan en Wout, I am grateful for your willingness to help during this period that I spent in the lab. Although, I got the feeling that you were also glad to get out of the house. Wout, I would also like to thank you for assistance during these entire four year, but also for the fun chats we had.

This thesis was part of the multidisciplinary OptiLight project under supervision of

Acknowledgements

Jean-Paul Linnartz. As member of the Signal Processing Systems group your perspective was rather different, which resulted in difficult and unexpected questions that in the end had a meaningful contribution to this thesis. Throughout the four years of collaboration we have learned to communicate, regardless of our background, and to recognize each others strengths. Only that makes the OptiLight project already successful. It was my pleasure to work with all of you, Samantha, Jochem, Chara and Qinhzi. I would like to mention Samantha specifically, I enjoyed the time we spent at the coffee machine, in the car and at Kropman. I am already looking forward to your defense!

I strongly believe that a healthy work-life balance is essential to prevent suffocation in the bubble that a PhD sometime is. Consequently, I am grateful for my friends. Life would be different without the (special) beers, board-games, city-trips and "carbid schieten". Also the long Sundays on the pitch and in the canteen at Pusphaira should not be forgotten. Coming season P4 (#NeverForget) has to pronounce its championship aspirations without this mediocre defender.

Frank en Jannie, ook al ken ik jullie niet langer dan twee jaar. Ik ben dankbaar voor jullie interesse en niet aflatende gastvrijheid. Daarnaast waren de 3 weken die wij doorgebracht hebben in jullie huis een fijne onderbreking van de sleur.

Pap en Mam, bedankt voor jullie steun, ook al was mijn promoveren misschien een ver-van-jullie-bed-show, letterlijk en figuurlijk. Pap, voor de duidelijkheid, een thesis is dat wat je nu in je handen houdt. Desalniettemin, weet ik dat jullie hartstikke trots op mij zijn, het doet me namelijk elke keer weer goed als ik mijn eerste artikel aan de binnenkant van het keukenkastje zie hangen. Naast het feit dat ik mij nu doctor mag noemen hoeven jullie vanaf vandaag niemand meer uit te leggen dat jullie zoon aan het promoveren is in iets met lampjes. Ik ben blij dat jullie van dit leed verlost zijn.

Ik moet jullie wel teleurstellen, ik vermoed dat ik voorlopig niet terugkeer naar de Achterhoek (ik zal proberen in Nederland te blijven), maar ik zal proberen jullie, en Banjer niet te vergeten, vaker op te zoeken.

Lieve Else,

door jouw had ik iets om vooruit te kijken tijdens die eindeloze dagen van thuis werken. Je hebt mij daardoor dan ook echt door deze laatste maanden geholpen. Ik kan dan ook niet wachten om nog meer tijd samen door te brengen in ons eigen huisje. Lets grow old together!

Bouwstenen

Bouwstenen is een publicatiereeks van de Faculteit Bouwkunde, Technische Universiteit Eindhoven. Zij presenteert resultaten van onderzoek en andere activiteiten op het vakgebied der Bouwkunde, uitgevoerd in het kader van deze Faculteit.

Bouwstenen en andere proefschriften van de TU/e zijn online beschikbaar via:
<https://research.tue.nl/>

Bouwstenen

Reeds verschenen in de serie

Bouwstenen

nr 1

Elan: A Computer Model for Building Energy Design: Theory and Validation

Martin H. de Wit

H.H. Driessen

R.M.M. van der Velden

nr 2

Kwaliteit, Keuzevrijheid en Kosten: Evaluatie van Experiment Klarendal, Arnhem

J. Smeets

C. le Nobel

M. Broos

J. Frenken

A. v.d. Sanden

nr 3

Crooswijk: Van 'Bijzonder' naar 'Gewoon'

Vincent Smit

Kees Noort

nr 4

Staal in de Woningbouw

Edwin J.F. Delsing

nr 5

Mathematical Theory of Stressed Skin Action in Profiled Sheeting with Various Edge Conditions

Andre W.A.M.J. van den Bogaard

nr 6

Hoe Berekenbaar en Betrouwbaar is de Coëfficiënt k in x -ksigma en x -ks?

K.B. Lub

A.J. Bosch

nr 7

Het Typologisch Gereedschap: Een Verkennende Studie Omtrent Typologie en Omtrent de Aanpak van Typologisch Onderzoek

J.H. Luiten

nr 8

Informatievoorziening en Beheerprocessen

A. Nauta

Jos Smeets (red.)

Helga Fassbinder (projectleider)

Adrie Proveniers

J. v.d. Moosdijk

nr 9

Strukturering en Verwerking van Tijdgegevens voor de Uitvoering van Bouwwerken

ir. W.F. Schaefer

P.A. Erkelens

nr 10

Stedebouw en de Vorming van een Speciale Wetenschap

K. Doevendans

nr 11

Informatica en Ondersteuning van Ruimtelijke Besluitvorming

G.G. van der Meulen

nr 12

Staal in de Woningbouw, Korrosie-Bescherming van de Begane Grondvloer

Edwin J.F. Delsing

nr 13

Een Thermisch Model voor de Berekening van Staalplaatbetonvloeren onder Brandomstandigheden

A.F. Hamerlinck

nr 14

De Wijkgedachte in Nederland: Gemeenschapsstreven in een Stedebouwkundige Context

K. Doevendans

R. Stolzenburg

nr 15

Diaphragm Effect of Trapezoidally Profiled Steel Sheets:

Experimental Research into the Influence of Force Application

Andre W.A.M.J. van den Bogaard

nr 16

Versterken met Smit-Ferrocement: Het Mechanische Gedrag van met Smit-Ferrocement Versterkte

Gewapend Betonbalken

K.B. Lubir

M.C.G. van Wanroy

Bouwstenen

- nr 17
De Tractaten van
Jean Nicolas Louis Durand
G. van Zeyl
- nr 18
Wonen onder een Plat Dak:
Drie Opstellen over Enkele
Vooronderstellingen van de
Stedebouw
K. Doevendans
- nr 19
Supporting Decision Making Processes:
A Graphical and Interactive Analysis of
Multivariate Data
W. Adams
- nr 20
Self-Help Building Productivity:
A Method for Improving House Building
by Low-Income Groups Applied to Kenya
1990-2000
P. A. Erkelens
- nr 21
De Verdeling van Woningen:
Een Kwestie van Onderhandelen
Vincent Smit
- nr 22
Flexibiliteit en Kosten in het Ontwerpproces:
Een Besluitvormingondersteunend Model
M. Prins
- nr 23
Spontane Nederzettingen Begeleid:
Voorwaarden en Criteria in Sri Lanka
Po Hin Thung
- nr 24
Fundamentals of the Design of
Bamboo Structures
Oscar Arce-Villalobos
- nr 25
Concepten van de Bouwkunde
M.F.Th. Bax (red.)
H.M.G.J. Trum (red.)
- nr 26
Meaning of the Site
Xiaodong Li
- nr 27
Het Woonmilieu op Begrip Gebracht:
Een Speurtocht naar de Betekenis van het
Begrip 'Woonmilieu'
Jaap Ketelaar
- nr 28
Urban Environment in Developing Countries
editors: Peter A. Erkelens
George G. van der Meulen (red.)
- nr 29
Stategische Plannen voor de Stad:
Onderzoek en Planning in Drie Steden
prof.dr. H. Fassbinder (red.)
H. Rikhof (red.)
- nr 30
Stedebouwkunde en Stadsbestuur
Piet Beekman
- nr 31
De Architectuur van Djenné:
Een Onderzoek naar de Historische Stad
P.C.M. Maas
- nr 32
Conjoint Experiments and Retail Planning
Harmen Oppewal
- nr 33
Strukturformen Indonesischer Bautechnik:
Entwicklung Methodischer Grundlagen
für eine 'Konstruktive Pattern Language'
in Indonesien
Heinz Frick arch. SIA
- nr 34
Styles of Architectural Designing:
Empirical Research on Working Styles
and Personality Dispositions
Anton P.M. van Bakel
- nr 35
Conjoint Choice Models for Urban
Tourism Planning and Marketing
Benedict Dellaert
- nr 36
Stedelijke Planvorming als Co-Productie
Helga Fassbinder (red.)

Bouwstenen

nr 37

Design Research in the Netherlands

editors: R.M. Oxman
M.F.Th. Bax
H.H. Achten

nr 38

Communication in the Building Industry

Bauke de Vries

nr 39

Optimaal Dimensioneren van Gelaste Plaatliggers

J.B.W. Stark
F. van Pelt
L.F.M. van Gorp
B.W.E.M. van Hove

nr 40

Huisvesting en Overwinning van Armoede

P.H. Thung
P. Beekman (red.)

nr 41

Urban Habitat: The Environment of Tomorrow

George G. van der Meulen
Peter A. Erkelens

nr 42

A Typology of Joints

John C.M. Olie

nr 43

Modeling Constraints-Based Choices for Leisure Mobility Planning

Marcus P. Stemerding

nr 44

Activity-Based Travel Demand Modeling

Dick Ettema

nr 45

Wind-Induced Pressure Fluctuations on Building Facades

Chris Geurts

nr 46

Generic Representations

Henri Achten

nr 47

Johann Santini Aichel: Architectuur en Ambiguiteit

Dirk De Meyer

nr 48

Concrete Behaviour in Multiaxial Compression

Erik van Geel

nr 49

Modelling Site Selection

Frank Witlox

nr 50

Ecolemma Model

Ferdinand Beetstra

nr 51

Conjoint Approaches to Developing Activity-Based Models

Donggen Wang

nr 52

On the Effectiveness of Ventilation

Ad Roos

nr 53

Conjoint Modeling Approaches for Residential Group preferences

Eric Molin

nr 54

Modelling Architectural Design Information by Features

Jos van Leeuwen

nr 55

A Spatial Decision Support System for the Planning of Retail and Service Facilities

Theo Arentze

nr 56

Integrated Lighting System Assistant

Ellie de Groot

nr 57

Ontwerpend Leren, Leren Ontwerpen

J.T. Boekholt

nr 58

Temporal Aspects of Theme Park Choice Behavior

Astrid Kemperman

nr 59

Ontwerp van een Geïndustrialiseerde Funderingswijze

Faas Moonen

Bouwstenen

nr 60

**Merlin: A Decision Support System
for Outdoor Leisure Planning**

Manon van Middelkoop

nr 61

The Aura of Modernity

Jos Bosman

nr 62

Urban Form and Activity-Travel Patterns

Daniëlle Snellen

nr 63

Design Research in the Netherlands 2000

Henri Achten

nr 64

**Computer Aided Dimensional Control in
Building Construction**

Rui Wu

nr 65

Beyond Sustainable Building

editors: Peter A. Erkelens
Sander de Jonge
August A.M. van Vliet

co-editor: Ruth J.G. Verhagen

nr 66

Das Globalrecyclingfähige Haus

Hans Löfflad

nr 67

Cool Schools for Hot Suburbs

René J. Dierkx

nr 68

**A Bamboo Building Design Decision
Support Tool**

Fitri Mardjono

nr 69

Driving Rain on Building Envelopes

Fabien van Mook

nr 70

Heating Monumental Churches

Henk Schellen

nr 71

**Van Woningverhuurder naar
Aanbieder van Woongenot**

Patrick Dogge

nr 72

**Moisture Transfer Properties of
Coated Gypsum**

Emile Goossens

nr 73

Plybamboo Wall-Panels for Housing

Guillermo E. González-Beltrán

nr 74

The Future Site-Proceedings

Ger Maas

Frans van Gassel

nr 75

**Radon transport in
Autoclaved Aerated Concrete**

Michel van der Pal

nr 76

**The Reliability and Validity of Interactive
Virtual Reality Computer Experiments**

Amy Tan

nr 77

**Measuring Housing Preferences Using
Virtual Reality and Belief Networks**

Maciej A. Orzechowski

nr 78

**Computational Representations of Words
and Associations in Architectural Design**

Nicole Segers

nr 79

**Measuring and Predicting Adaptation in
Multidimensional Activity-Travel Patterns**

Chang-Hyeon Joh

nr 80

Strategic Briefing

Fayez Al Hassan

nr 81

Well Being in Hospitals

Simona Di Cicco

nr 82

**Solares Bauen:
Implementierungs- und Umsetzungs-
Aspekte in der Hochschulausbildung
in Österreich**

Gerhard Schuster

Bouwstenen

nr 83

Supporting Strategic Design of Workplace Environments with Case-Based Reasoning

Shauna Mallory-Hill

nr 84

ACCEL: A Tool for Supporting Concept Generation in the Early Design Phase

Maxim Ivashkov

nr 85

Brick-Mortar Interaction in Masonry under Compression

Ad Vermeltfoort

nr 86

Zelfredzaam Wonen

Guus van Vliet

nr 87

Een Ensemble met Grootstedelijke Allure

Jos Bosman

Hans Schippers

nr 88

On the Computation of Well-Structured Graphic Representations in Architectural Design

Henri Achten

nr 89

De Evolutie van een West-Afrikaanse Vernaculaire Architectuur

Wolf Schijns

nr 90

ROMBO Tactiek

Christoph Maria Ravesloot

nr 91

External Coupling between Building Energy Simulation and Computational Fluid Dynamics

Ery Djunaedy

nr 92

Design Research in the Netherlands 2005

editors: Henri Achten

Kees Dorst

Pieter Jan Stappers

Bauke de Vries

nr 93

Ein Modell zur Baulichen Transformation

Jalil H. Saber Zaimian

nr 94

Human Lighting Demands: Healthy Lighting in an Office Environment

Myriam Aries

nr 95

A Spatial Decision Support System for the Provision and Monitoring of Urban Greenspace

Claudia Pelizaro

nr 96

Leren Creëren

Adri Proveniers

nr 97

Simlandscape

Rob de Waard

nr 98

Design Team Communication

Ad den Otter

nr 99

Humaan-Ecologisch Georiënteerde Woningbouw

Juri Czabanowski

nr 100

Hambase

Martin de Wit

nr 101

Sound Transmission through Pipe Systems and into Building Structures

Susanne Bron-van der Jagt

nr 102

Het Bouwkundig Contrapunt

Jan Francis Boelen

nr 103

A Framework for a Multi-Agent Planning Support System

Dick Saarloos

nr 104

Bracing Steel Frames with Calcium Silicate Element Walls

Bright Mweene Ng'andu

nr 105

Naar een Nieuwe Houtskeletbouw

F.N.G. De Medts

Bouwstenen

nr 106 and 107
Niet gepubliceerd

nr 108
Geborgenheid
T.E.L. van Pinxteren

nr 109
Modelling Strategic Behaviour in Anticipation of Congestion
Qi Han

nr 110
Reflecties op het Woondomein
Fred Sanders

nr 111
On Assessment of Wind Comfort by Sand Erosion
Gábor Dezsö

nr 112
Bench Heating in Monumental Churches
Dionne Limpens-Neilen

nr 113
RE. Architecture
Ana Pereira Roders

nr 114
Toward Applicable Green Architecture
Usama El Fiky

nr 115
Knowledge Representation under Inherent Uncertainty in a Multi-Agent System for Land Use Planning
Liyang Ma

nr 116
Integrated Heat Air and Moisture Modeling and Simulation
Jos van Schijndel

nr 117
Concrete Behaviour in Multiaxial Compression
J.P.W. Bongers

nr 118
The Image of the Urban Landscape
Ana Moya Pellitero

nr 119
The Self-Organizing City in Vietnam
Stephanie Geertman

nr 120
A Multi-Agent Planning Support System for Assessing Externalities of Urban Form Scenarios
Rachel Katoshevski-Cavari

nr 121
Den Schulbau Neu Denken, Fühlen und Wollen
Urs Christian Maurer-Dietrich

nr 122
Peter Eisenman Theories and Practices
Bernhard Kormoss

nr 123
User Simulation of Space Utilisation
Vincent Tabak

nr 125
In Search of a Complex System Model
Oswald Devisch

nr 126
Lighting at Work: Environmental Study of Direct Effects of Lighting Level and Spectrum on Psycho-Physiological Variables
Grazyna Górnicka

nr 127
Flanking Sound Transmission through Lightweight Framed Double Leaf Walls
Stefan Schoenwald

nr 128
Bounded Rationality and Spatio-Temporal Pedestrian Shopping Behavior
Wei Zhu

nr 129
Travel Information: Impact on Activity Travel Pattern
Zhongwei Sun

nr 130
Co-Simulation for Performance Prediction of Innovative Integrated Mechanical Energy Systems in Buildings
Marija Trcinka

nr 131
Niet gepubliceerd

Bouwstenen

- nr 132
Architectural Cue Model in Evacuation Simulation for Underground Space Design
Chengyu Sun
- nr 133
Uncertainty and Sensitivity Analysis in Building Performance Simulation for Decision Support and Design Optimization
Christina Hopfe
- nr 134
Facilitating Distributed Collaboration in the AEC/FM Sector Using Semantic Web Technologies
Jacob Beetz
- nr 135
Circumferentially Adhesive Bonded Glass Panes for Bracing Steel Frame in Façades
Edwin Huveners
- nr 136
Influence of Temperature on Concrete Beams Strengthened in Flexure with CFRP
Ernst-Lucas Klamer
- nr 137
Sturen op Klantwaarde
Jos Smeets
- nr 139
Lateral Behavior of Steel Frames with Discretely Connected Precast Concrete Infill Panels
Paul Teewen
- nr 140
Integral Design Method in the Context of Sustainable Building Design
Perica Savanovic´
- nr 141
Household Activity-Travel Behavior: Implementation of Within-Household Interactions
Renni Anggraini
- nr 142
Design Research in the Netherlands 2010
Henri Achten
- nr 143
Modelling Life Trajectories and Transport Mode Choice Using Bayesian Belief Networks
Marloes Verhoeven
- nr 144
Assessing Construction Project Performance in Ghana
William Gyadu-Asiedu
- nr 145
Empowering Seniors through Domotic Homes
Masi Mohammadi
- nr 146
An Integral Design Concept for Ecological Self-Compacting Concrete
Martin Hunger
- nr 147
Governing Multi-Actor Decision Processes in Dutch Industrial Area Redevelopment
Erik Blokhuis
- nr 148
A Multifunctional Design Approach for Sustainable Concrete
Götz Hüsken
- nr 149
Quality Monitoring in Infrastructural Design-Build Projects
Ruben Favié
- nr 150
Assessment Matrix for Conservation of Valuable Timber Structures
Michael Abels
- nr 151
Co-simulation of Building Energy Simulation and Computational Fluid Dynamics for Whole-Building Heat, Air and Moisture Engineering
Mohammad Mirsadeghi
- nr 152
External Coupling of Building Energy Simulation and Building Element Heat, Air and Moisture Simulation
Daniel Cóstola

Bouwstenen

nr 153

**Adaptive Decision Making In
Multi-Stakeholder Retail Planning**

Ingrid Janssen

nr 154

Landscape Generator

Kymo Slager

nr 155

Constraint Specification in Architecture

Remco Niemeijer

nr 156

**A Need-Based Approach to
Dynamic Activity Generation**

Linda Nijland

nr 157

**Modeling Office Firm Dynamics in an
Agent-Based Micro Simulation Framework**

Gustavo Garcia Manzato

nr 158

**Lightweight Floor System for
Vibration Comfort**

Sander Zegers

nr 159

Aanpasbaarheid van de Draagstructuur

Roel Gijsbers

nr 160

'Village in the City' in Guangzhou, China

Yanliu Lin

nr 161

Climate Risk Assessment in Museums

Marco Martens

nr 162

Social Activity-Travel Patterns

Pauline van den Berg

nr 163

**Sound Concentration Caused by
Curved Surfaces**

Martijn Vercammen

nr 164

**Design of Environmentally Friendly
Calcium Sulfate-Based Building Materials:
Towards an Improved Indoor Air Quality**

Qingliang Yu

nr 165

**Beyond Uniform Thermal Comfort
on the Effects of Non-Uniformity and
Individual Physiology**

Lisje Schellen

nr 166

Sustainable Residential Districts

Gaby Abdalla

nr 167

**Towards a Performance Assessment
Methodology using Computational
Simulation for Air Distribution System
Designs in Operating Rooms**

Mônica do Amaral Melhado

nr 168

**Strategic Decision Modeling in
Brownfield Redevelopment**

Brano Glumac

nr 169

**Pamela: A Parking Analysis Model
for Predicting Effects in Local Areas**

Peter van der Waerden

nr 170

**A Vision Driven Wayfinding Simulation-System
Based on the Architectural Features Perceived
in the Office Environment**

Qunli Chen

nr 171

**Measuring Mental Representations
Underlying Activity-Travel Choices**

Oliver Horeni

nr 172

**Modelling the Effects of Social Networks
on Activity and Travel Behaviour**

Nicole Ronald

nr 173

**Uncertainty Propagation and Sensitivity
Analysis Techniques in Building Performance
Simulation to Support Conceptual Building
and System Design**

Christian Struck

nr 174

**Numerical Modeling of Micro-Scale
Wind-Induced Pollutant Dispersion
in the Built Environment**

Pierre Gousseau

Bouwstenen

nr 175

Modeling Recreation Choices over the Family Lifecycle

Anna Beatriz Grigolon

nr 176

Experimental and Numerical Analysis of Mixing Ventilation at Laminar, Transitional and Turbulent Slot Reynolds Numbers

Twan van Hooff

nr 177

Collaborative Design Support: Workshops to Stimulate Interaction and Knowledge Exchange Between Practitioners

Emile M.C.J. Quanjel

nr 178

Future-Proof Platforms for Aging-in-Place

Michiel Brink

nr 179

Motivate: A Context-Aware Mobile Application for Physical Activity Promotion

Yuzhong Lin

nr 180

Experience the City: Analysis of Space-Time Behaviour and Spatial Learning

Anastasia Moiseeva

nr 181

Unbonded Post-Tensioned Shear Walls of Calcium Silicate Element Masonry

Lex van der Meer

nr 182

Construction and Demolition Waste Recycling into Innovative Building Materials for Sustainable Construction in Tanzania

Mwita M. Sabai

nr 183

Durability of Concrete with Emphasis on Chloride Migration

Przemysław Spiesz

nr 184

Computational Modeling of Urban Wind Flow and Natural Ventilation Potential of Buildings

Rubina Ramponi

nr 185

A Distributed Dynamic Simulation Mechanism for Buildings Automation and Control Systems

Azzedine Yahiaoui

nr 186

Modeling Cognitive Learning of Urban Networks in Daily Activity-Travel Behavior

Şehnaz Cenani Durmazoglu

nr 187

Functionality and Adaptability of Design Solutions for Public Apartment Buildings in Ghana

Stephen Agyefi-Mensah

nr 188

A Construction Waste Generation Model for Developing Countries

Lilliana Abarca-Guerrero

nr 189

Synchronizing Networks: The Modeling of Supernetworks for Activity-Travel Behavior

Feixiong Liao

nr 190

Time and Money Allocation Decisions in Out-of-Home Leisure Activity Choices

Gamze Zeynep Dane

nr 191

How to Measure Added Value of CRE and Building Design

Rianne Appel-Meulenbroek

nr 192

Secondary Materials in Cement-Based Products: Treatment, Modeling and Environmental Interaction

Miruna Florea

nr 193

Concepts for the Robustness Improvement of Self-Compacting Concrete: Effects of Admixtures and Mixture

Components on the Rheology and Early Hydration at Varying Temperatures

Wolfram Schmidt

Bouwstenen

nr 194

Modelling and Simulation of Virtual Natural Lighting Solutions in Buildings

Rizki A. Mangkuto

nr 195

Nano-Silica Production at Low Temperatures from the Dissolution of Olivine - Synthesis, Tailoring and Modelling

Alberto Lazaro Garcia

nr 196

Building Energy Simulation Based Assessment of Industrial Halls for Design Support

Bruno Lee

nr 197

Computational Performance Prediction of the Potential of Hybrid Adaptable Thermal Storage Concepts for Lightweight Low-Energy Houses

Pieter-Jan Hoes

nr 198

Application of Nano-Silica in Concrete

George Quercia Bianchi

nr 199

Dynamics of Social Networks and Activity Travel Behaviour

Fariya Sharmeen

nr 200

Building Structural Design Generation and Optimisation including Spatial Modification

Juan Manuel Davila Delgado

nr 201

Hydration and Thermal Decomposition of Cement/Calcium-Sulphate Based Materials

Ariën de Korte

nr 202

Republiek van Beelden: De Politieke Werkingen van het Ontwerp in Regionale Planvorming

Bart de Zwart

nr 203

Effects of Energy Price Increases on Individual Activity-Travel Repertoires and Energy Consumption

Dujuan Yang

nr 204

Geometry and Ventilation: Evaluation of the Leeward Sawtooth Roof Potential in the Natural Ventilation of Buildings

Jorge Isaac Perén Montero

nr 205

Computational Modelling of Evaporative Cooling as a Climate Change Adaptation Measure at the Spatial Scale of Buildings and Streets

Hamid Montazeri

nr 206

Local Buckling of Aluminium Beams in Fire Conditions

Ronald van der Meulen

nr 207

Historic Urban Landscapes: Framing the Integration of Urban and Heritage Planning in Multilevel Governance

Loes Veldpaus

nr 208

Sustainable Transformation of the Cities: Urban Design Pragmatics to Achieve a Sustainable City

Ernesto Antonio Zumelzu Scheel

nr 209

Development of Sustainable Protective Ultra-High Performance Fibre Reinforced Concrete (UHPRFC):

Design, Assessment and Modeling

Rui Yu

nr 210

Uncertainty in Modeling Activity-Travel Demand in Complex Urban Systems

Soora Rasouli

nr 211

Simulation-based Performance Assessment of Climate Adaptive Greenhouse Shells

Chul-sung Lee

nr 212

Green Cities: Modelling the Spatial Transformation of the Urban Environment using Renewable Energy Technologies

Saleh Mohammadi

Bouwstenen

nr 213

A Bounded Rationality Model of Short and Long-Term Dynamics of Activity-Travel Behavior

Ifigeneia Psarra

nr 214

Effects of Pricing Strategies on Dynamic Repertoires of Activity-Travel Behaviour

Elaheh Khademi

nr 215

Handstorm Principles for Creative and Collaborative Working

Frans van Gassel

nr 216

Light Conditions in Nursing Homes: Visual Comfort and Visual Functioning of Residents

Marianne M. Sinoo

nr 217

Woonsporen:

De Sociale en Ruimtelijke Biografie van een Stedelijk Bouwblok in de Amsterdamse Transvaalbuurt

Hüseyin Hüsni Yegenoglu

nr 218

Studies on User Control in Ambient Intelligent Systems

Berent Willem Meerbeek

nr 219

Daily Livings in a Smart Home: Users' Living Preference Modeling of Smart Homes

Erfaneh Allameh

nr 220

Smart Home Design: Spatial Preference Modeling of Smart Homes

Mohammadali Heidari Jozam

nr 221

Wonen:

Discoursen, Praktijken, Perspectieven

Jos Smeets

nr 222

Personal Control over Indoor Climate in Offices:

Impact on Comfort, Health and Productivity

Atze Christiaan Boerstra

nr 223

Personalized Route Finding in Multimodal Transportation Networks

Jianwe Zhang

nr 224

The Design of an Adaptive Healing Room for Stroke Patients

Elke Daemen

nr 225

Experimental and Numerical Analysis of Climate Change Induced Risks to Historic Buildings and Collections

Zara Huijbregts

nr 226

Wind Flow Modeling in Urban Areas Through Experimental and Numerical Techniques

Alessio Ricci

nr 227

Clever Climate Control for Culture: Energy Efficient Indoor Climate Control Strategies for Museums Respecting Collection Preservation and Thermal Comfort of Visitors

Rick Kramer

nr 228

Fatigue Life Estimation of Metal Structures Based on Damage Modeling

Sarmediran Silitonga

nr 229

A multi-agents and occupancy based strategy for energy management and process control on the room-level

Timilehin Moses Labeodan

nr 230

Environmental assessment of Building Integrated Photovoltaics: Numerical and Experimental Carrying Capacity Based Approach

Michiel Ritzen

nr 231

Performance of Admixture and Secondary Minerals in Alkali Activated Concrete: Sustaining a Concrete Future

Arno Keulen

Bouwstenen

nr 232

World Heritage Cities and Sustainable Urban Development: Bridging Global and Local Levels in Monitoring the Sustainable Urban Development of World Heritage Cities

Paloma C. Guzman Molina

nr 233

Stage Acoustics and Sound Exposure in Performance and Rehearsal Spaces for Orchestras: Methods for Physical Measurements

Remy Wenmaekers

nr 234

Municipal Solid Waste Incineration (MSWI) Bottom Ash: From Waste to Value Characterization, Treatments and Application

Pei Tang

nr 235

Large Eddy Simulations Applied to Wind Loading and Pollutant Dispersion

Mattia Ricci

nr 236

Alkali Activated Slag-Fly Ash Binders: Design, Modeling and Application

Xu Gao

nr 237

Sodium Carbonate Activated Slag: Reaction Analysis, Microstructural Modification & Engineering Application

Bo Yuan

nr 238

Shopping Behavior in Malls

Widiyani

nr 239

Smart Grid-Building Energy Interactions: Demand Side Power Flexibility in Office Buildings

Kennedy Otieno Aduda

nr 240

Modeling Taxis Dynamic Behavior in Uncertain Urban Environments

Zheng Zhong

nr 241

Gap-Theoretical Analyses of Residential Satisfaction and Intention to Move

Wen Jiang

nr 242

Travel Satisfaction and Subjective Well-Being: A Behavioral Modeling Perspective

Yanan Gao

nr 243

Building Energy Modelling to Support the Commissioning of Holistic Data Centre Operation

Vojtech Zavrel

nr 244

Regret-Based Travel Behavior Modeling: An Extended Framework

Sunghoon Jang

nr 245

Towards Robust Low-Energy Houses: A Computational Approach for Performance Robustness Assessment using Scenario Analysis

Rajesh Reddy Kotireddy

nr 246

Development of sustainable and functionalized inorganic binder-biofiber composites

Guillaume Doudart de la Grée

nr 247

A Multiscale Analysis of the Urban Heat Island Effect: From City Averaged Temperatures to the Energy Demand of Individual Buildings

Yasin Toparlar

nr 248

Design Method for Adaptive Daylight Systems for buildings covered by large (span) roofs

Florian Heinzlmann

nr 249

Hardening, high-temperature resistance and acid resistance of one-part geopolymers

Patrick Sturm

Bouwstenen

nr 250

Effects of the built environment on dynamic repertoires of activity-travel behaviour

Aida Pontes de Aquino

nr 251

Modeling for auralization of urban environments: Incorporation of directivity in sound propagation and analysis of a framework for auralizing a car pass-by

Fotis Georgiou

nr 252

Wind Loads on Heliostats and Photovoltaic Trackers

Andreas Pfahl

nr 253

Approaches for computational performance optimization of innovative adaptive façade concepts

Roel Loonen

nr 254

Multi-scale FEM-DEM Model for Granular Materials: Micro-scale boundary conditions, Statics, and Dynamics

Jiadun Liu

nr 255

Bending Moment - Shear Force Interaction of Rolled I-Shaped Steel Sections

Rianne Willie Adriana Dekker

nr 256

Paralympic tandem cycling and hand-cycling: Computational and wind tunnel analysis of aerodynamic performance

Paul Fionn Mannion

nr 257

Experimental characterization and numerical modelling of 3D printed concrete: Controlling structural behaviour in the fresh and hardened state

Robert Johannes Maria Wolfs

nr 258

Requirement checking in the building industry: Enabling modularized and extensible requirement checking systems based on semantic web technologies

Chi Zhang

nr 259

A Sustainable Industrial Site Redevelopment Planning Support System

Tong Wang

nr 260

Efficient storage and retrieval of detailed building models: Multi-disciplinary and long-term use of geometric and semantic construction information

Thomas Ferdinand Krijnen

nr 261

The users' value of business center concepts for knowledge sharing and networking behavior within and between organizations

Minou Weijs-Perrée

nr 262

Characterization and improvement of aerodynamic performance of vertical axis wind turbines using computational fluid dynamics (CFD)

Abdolrahim Rezaeiha

nr 263

In-situ characterization of the acoustic impedance of vegetated roofs

Chang Liu

nr 264

Occupancy-based lighting control: Developing an energy saving strategy that ensures office workers' comfort

Christel de Bakker

nr 265

Stakeholders-Oriented Spatial Decision Support System

Cahyono Susetyo

nr 266

Climate-induced damage in oak museum objects

Rianne Aleida Luimes

nr 267

Towards individual thermal comfort: Model predictive personalized control of heating systems

Katarina Katic

Bouwstenen

nr 268

Modelling and Measuring Quality of Urban Life: Housing, Neighborhood, Transport and Job

Lida Aminian

nr 269

Optimization of an aquifer thermal energy storage system through integrated modeling of aquifer, HVAC systems and building

Basar Bozkaya

nr 270

Numerical modeling for urban sound propagation: developments in wave-based and energy-based methods

Raúl Pagán Muñoz

nr 271

Lighting in multi-user office environments: improving employee wellbeing through personal control

Sanae van der Vleuten-Chraibi

nr 272

A strategy for fit-for-purpose occupant behavior modelling in building energy and comfort performance simulation

Isabella I. Gaetani dell'Aquila d'Aragona

nr 273

Een architectuurhistorische waardestelling van naorlogse woonwijken in Nederland: Het voorbeeld van de Westelijke Tuinsteden in Amsterdam

Eleonore Henriette Marie Mens

nr 274

Job-Housing Co-Dependent Mobility Decisions in Life Trajectories

Jia Guo

nr 275

A user-oriented focus to create healthcare facilities: decision making on strategic values

Emilia Rosalia Catharina Maria Huisman

nr 276

Dynamics of plane impinging jets at moderate Reynolds numbers – with applications to air curtains

Adelya Khayrullina

nr 277

Valorization of Municipal Solid Waste Incineration Bottom Ash - Chemical Nature, Leachability and Treatments of Hazardous Elements

Qadeer Alam

nr 278

Treatments and valorization of MSWI bottom ash - application in cement-based materials

Veronica Caprai

nr 279

Personal lighting conditions of office workers - input for intelligent systems to optimize subjective alertness

Juliëtte van Duijnhoven

nr 280

Social influence effects in tourism travel: air trip itinerary and destination choices

Xiaofeng Pan

nr 281

Advancing Post-War Housing: Integrating Heritage Impact, Environmental Impact, Hygrothermal Risk and Costs in Renovation Design Decisions

Lisanne Claartje Havinga

nr 282

Impact resistant ultra-high performance fibre reinforced concrete: materials, components and properties

Peipeng Li

nr 283

Demand-driven Science Parks: The Perceived Benefits and Trade-offs of Tenant Firms with regard to Science Park Attributes

Wei Keat Benny Ng

nr 284

Raise the lantern; how light can help to maintain a healthy and safe hospital environment focusing on nurses

Maria Petronella Johanna Aarts

nr 285

Modelling Learning and Dynamic Route and Parking Choice Behaviour under Uncertainty

Elaine Cristina Schneider de Carvalho

Bouwstenen

nr 286

Identifying indoor local microclimates for safekeeping of cultural heritage

Karin Kompatscher

nr 287

Probabilistic modeling of fatigue resistance for welded and riveted bridge details. Resistance models and estimation of uncertainty.

Davide Leonetti

nr 288

Performance of Layered UHPFRC under Static and Dynamic Loads: Effects of steel fibers, coarse aggregates and layered structures

Yangyueye Cao

nr 289

Photocatalytic abatement of the nitrogen oxide pollution: synthesis, application and long-term evaluation of titania-silica composites

Yuri Hendrix

nr 290

Assessing knowledge adoption in post-disaster reconstruction: Understanding the impact of hazard-resistant construction knowledge on reconstruction processes of self-recovering communities in Nepal and the Philippines

Eefje Hendriks

nr 291

Locating electric vehicle charging stations: A multi-agent based dynamic simulation

Seheon Kim

nr 292

De invloed van Lean Management op de beheersing van het bouwproces

Wim van den Bouwhuisen

nr 293

Neighborhood Environment and Physical Activity of Older Adults

Zhengying Liu

In this thesis, a luminance camera, called the Bee-Eye, was developed using low cost components utilizing the High Dynamic Range technology. This practical device was able to autonomously measure a range of variable lighting quality aspects in a continuous fashion, which is essential for lighting control systems that aim to provide high quality lighting. Additionally, the Bee-Eye can be considered a versatile sensor that is able to combine multiple functionalities.

A practical accuracy was achieved for the Bee-Eye, when the luminance was determined according to the conventional method. The accuracy was improved by limiting the spectral mismatch, which includes the spectral responsivity and the spectral power distribution of the illuminant in the calculation.

Additionally it is a complex task to measure the luminance distribution continuously in real office environments. Comparative measurements showed that some lighting quality aspects were not accurately measured in a real office environment, both methodological and random errors were introduced compared to the benchmark. The methodological errors were mainly caused by a reduced spatial and temporal resolution in combination with an alternative, ceiling-based, measurement position, which were validated measures applied to prevent privacy intrusion, high computational cost and interference with office activities. Additionally, the presence of users adds a highly irregular component by occasionally obstructing certain areas of the luminance distribution, resulting in random errors.

DEPARTMENT OF THE BUILT ENVIRONMENT

Requirements, Criteria

Excellence

Originality of the research:

The thesis investigates the feasibility of developing and applying a **novel sensor**, capable of measuring the key parameters needed to control and optimize lighting quality in smart lighting systems. Today's adaptive lighting systems merely switch lights on or off to save energy, using motion sensors as indicators for presence of people. Automatically optimizing lighting quality would be much more relevant for the wellbeing of office workers, but requires measuring a much broader set of 7 quantities, including quantity, distribution, glare, spectral power distribution, daylight, directionality, and the dynamics of light, received on users' eyes

Significance of the results:

However, such sensor would still need to be very low cost, capable of measuring continuously and avoid privacy issues or interference with office work. Thijs has successfully managed to develop such a low-cost sensor (named Bee-Eye), using HDR luminance distribution measurement principles. He optimized its performance using smart algorithms, to a sufficiently high level for practical application. He also demonstrated the feasibility of integrating his Bee-Eye with an actual lighting control system into a first quality controlled smart lighting system.

Complexity of the work conducted:

The thesis itself is also of high quality, excellently structured and with great eye for detail. Prof. W. Osterhaus from Aarhus University, one of the independent external committee members, spontaneously remarked in his evaluation: "The thesis is very well structured, and I would like to say that it is one of the best I have seen in recent years", while Prof. J.L. Scartezini from EPFL wrote: "The different chapters of the report are very detailed showing a systematic and rigorous scientific approach".

He also managed to complete his final experiments in the lab despite the complex Covid19 challenges and completed the full PhD trajectory well within schedule and following his own clear planning.

Impact

Publication impact:

His work has resulted in a patent application for the innovative sensor, next to 15 publications (6 journal papers and 9 peer reviewed conference papers). His journal paper 'Photometric measurements of lighting quality: An overview' published in Building and Environment is already ranked among the most downloaded papers of this journal. Furthermore, he presented his work at several conferences, including CIE expert Workshop 2018 (Copenhagen), LICHT 2018 (Davos), and the CIE 2019 29th Quadrennial Session (Washington).

Societal impact of the work:

By enabling the continuous sensing of a far broader range of lighting parameters than used today, the work of Thijs opens up a new domain in smart lighting, aimed at improving performance as well as health and wellbeing of office workers and others. His work forms a solid basis for follow-up research.

Outreach impact:

The work of Thijs has already drawn significant interest from 3rd parties such as Signify (formerly Philips Lighting), who considered his invention disclosure of high relevance, sufficient to support filing of a patent application. The results are already being used in the broader ILLI Optilight project, aiming to develop a smart lighting control system.

Readability of the thesis, in particular also its introduction, conclusions and summary:

The thesis was considered of excellent quality by the committee, well structured, and written in excellent English. It deals with many aspects. All analysis, design, prototyping, testing, integration and evaluation activities were executed by himself. His work forms a solid basis for follow-up research.

Thijs Kruisselbrink was born on 22-02-1993 in Winterswijk, the Netherlands. After finishing his pre-university education at Christelijk College Schaersvoorde in 2011, he enrolled his studies at Eindhoven University of Technology. After receiving his bachelor's degree in Architecture Building and Planning in 2014, he proceeded his master with the Building Physics and Services trajectory within Architecture, Building and Planning. In 2016, Thijs graduated, within the Building Lighting group, on a methodology to measure the luminance distribution using low cost components.

After receiving his master's degree, he started his PhD in the Building Lighting group in September 2016. Thijs successfully defended his dissertation in October 2020 and obtained his degree of doctor with honors. During his PhD Thijs wrote a number of peer-reviewed journal and conference papers. His journal paper '*Photometric measurements of lighting quality: An overview*' published in Building and Environment has been among the most downloaded papers of this journal. Furthermore, he presented his work at several conferences, including CIE expert Workshop 2018 (Copenhagen), LICHT 2018 (Davos), and the CIE 2019 29th Quadrennial Session (Washington).

In addition to his research activities, Thijs was involved in a number of educational activities. Throughout his PhD Thijs has supervised many students both on BSc and MSc level, has been co-teaching BSc courses, and has occasionally given guest lectures.

After his PhD, Thijs continued his career as a junior consultant building physics at Peutz. At Peutz he conducts calculations, simulations and measurements, in the field and in the laboratory, related to lighting, heat and moisture transfer and energy performance. Additionally, he has been involved in the supervision of interns and has taken up a role in the CIE Technical Committee for Glare Measurement by Imaging Luminance Measurement Device (ILMD).

List of Publications

Academic peer-reviewed publications

Kruisselbrink, TW, Dangol, R, & van Loenen, EJ (2020). A comparative study between two algorithms for luminance-based lighting control. *Energy and Buildings*, 228, 110429.

Kruisselbrink TW, Dangol R, van Loenen EJ. Feasibility of ceiling-based luminance distribution measurements. *Building and Environment*. 2020 172;106699.

Kruisselbrink TW, Dangol R, van Loenen EJ. Recommendations for long-term luminance distribution measurements: The spatial resolution. *Building and Environment*. 2020 169;106538.

Kruisselbrink TW, Dangol R, Rosemann ALP, van Loenen EJ. Spectral tuning of luminance cameras: A theoretical model and validation measurements. *Lighting Research & Technology*. 2019 52(5);654–674.

Kruisselbrink TW, Dangol R, Rosemann ALP. Photometric measurements of lighting quality: An overview. *Building and Environment*. 2018 6;138; 42–52.

Dangol R, Kruisselbrink TW, Rosemann ALP(2017), Effect of Window Glazing on Colour Quality of Transmitted Daylight. *Journal of Daylighting*. 2017 4(2);37–47.

Kruisselbrink TW, Aries MBC, Rosemann ALP. A Practical Device for Measuring the Luminance Distribution. *International Journal of Sustainable Lighting*. 2017 19(1); 75–90.

Proceedings and conference contributions

Kruisselbrink TW, Dangol R, van Loenen EJ. HDR IMAGING FOR LUMI-NANCE AND

MELANOPIC RADIANCE: CAMERAS AND SPECTRAL POWER DISTRIBUTIONS. In: Proceedings of the 5th CIE Symposium on Colour and Visual Appearance. CIE; 2020. p. 1–12. Peeters S, Kruisselbrink TW, Smolders K, Dangol R, Vogels I, de Kort Y. Interaction of daylight and electric light on subjective light appraisals in office environments. In: VELUX Daylight Symposium; 2019

Kruisselbrink TW, Dangol R, van Loenen EJ. CEILING-BASED LUMINANCE MEASUREMENTS: A FEASIBLE SOLUTION? In: Proceedings of the 29th Quadrennial Session of the CIE, Washington D.C., USA; International Commission on Illumination; 2019. pp. 1166–1174.

Kruisselbrink TW, van Duijnhoven J, Dangol R, Rosemann ALP. Improving lighting quality by practical measurements of the luminance distribution. In: Congress of the International Ergonomics Association vol. 827. Florence, Italy: Springer; 2019. p.190–198.

Kruisselbrink TW, Dangol R, Rosemann ALP. Practical issues in field studies using luminance cameras. In: CIE Expert Workshop on Research Methods for Human Factors in Lighting. Copenhagen, Denmark, CIE;2018. pp. 14–15.

Kruisselbrink, Dangol R, Rosemann ALP. The Bee-Eye: A practical device for measuring the luminance distribution. In LICHT 2018. Davos, Switzerland. 2018.

van Duijnhoven J, Kruisselbrink TW, Aarts MPJ, Rosemann ALP, Kort HSM. Guidance for office workers based on their real-life light exposure and alertness. In LICHT 2018. Davos, Switzerland. 2018

Kruisselbrink TW, Dangol R, Unobtrusive field measurements of the luminance distribution. In: 5th Data Science Summit (DSSE 2018). Eindhoven, The Netherlands. 2018

Kruisselbrink TW, Tang J, Bruggema HM, Zeiler W. The indoor environmental quality in a Dutch day care centre: the effects of ventilation on the conditions within the baby cots. In: 12th REHVA World Congress (CLIMA 2016); 2016. pp. 1–10.